LEACHING OF CHALCOPYRITE

by

R.C.H. FERREIRA

Eng. Químico Industrial (I.S.T) - Lisbon

A thesis submitted for the degree of Doctor of Philosopy of the University of London

April, 1972

ABSTRACT

Two forms of chalcopyrite were synthesized. A β-form, cubic, of composition $CuFeS_{1.83}$, and an α-form, apparently tetragonal and with composition near to $Cu_{1.12}Fe_{1.09}S_2$, having about 10.7% excess copper and 8.3% excess iron over the stoichiometric $CuFeS_2$.

Samples of the two synthetic materials were crushed and sieved, and the fractions obtained were leached with acidic ferric sulphate solutions. Leaching with hydrogen peroxide was also used on the β-form, and the effect of chloride ion on the leaching rate of the α-form was studied.

The effects of some leach variables, for example, temperature and ferric ion concentration, were investigated.

β-chalcopyrite was leached in three stages, the first and second being mainly diffusion controlled and the third chemically controlled.

α-chalcopyrite was found to be metastable, changing with age. The dissolution rate-curves altered as this change took place, until a stable form was reached. This form was leached in two stages, the first corresponding to the removal of the 10.7% excess copper over the stoichiometric $CuFeS_2$, and the second the straightforward dissolution of the remaining, nearly stoichiometric, residue to produce elemental sulphur. Natural chalcopyrite is leached in a manner very similar to this second stage, involving nearly stoichiometric chalcopyrite. The change in both α- and β- form leach residues were studied using X-ray powder diffraction techniques, electron probe microanalysis and microscopic examination.

Finally the use of E-pH diagrams for temperatures other than 298°K was studied for the systems sulphur-water, copper oxides and sulphides-water, iron oxides and sulphides-water, and special attention was paid to the use of half-cell reactions and the thermodynamic properties of the electron, in the calculations.

CONTENTS

		Page
ABSTRACT		2
INTRODUCTION		7
SECTION 1 -	LITERATURE SURVEY	8
1.1	Previous Work on the Leaching of Chalcopyrite	8
1.2	Chalcopyrite Structures	33
1.3	Phase Relations in the Cu-Fe-S System	55
1.4	Previous Work on the Synthesis of Chalcopyrite	64
1.5	Sulphur Vapour Pressure	66
1.6	Thermal Behaviour of Chalcopyrite. Thermodynamic Properties	71
1.7	Complexing of the Ferric Ion in the Leach Solution. Jarosite-type Species.	83
SECTION 2 -	EXPERIMENTAL PROCEDURES.	88
2.1	Synthesis of Chalcopyrite	88
2.1.1	β-Chalcopyrite	92
2.1.2	α-Chalcopyrite	96
2.2	Leaching Apparatus and Experimental Procedure	100
2.3	Analytical Methods	104
2.3.1	Atomic Absorption	104
2.3.2	Nephelometry	106
2.3.3	UV Spectrophotometer. Elemental Sulphur Determinations.	107
2.3.4	X-ray Powder Diffraction	108
2.3.4.1	Choice of Radiation	108
2.3.4.2	Measurement of Line Positions	109
2.3.4.3	Measurement and Calculation of the Intensities of X-ray Reflections.	109
2.3.5	Other Methods	112
2.4	Purity of Materials	113

Page

SECTION 3 - β-CHALCOPYRITE. RESULTS AND DISCUSSION 117

3.1 Ferric Sulphate Leaching. Kinetic Rate-Curves. Effect of the Leach Variables on the Rate of Reaction. 117

3.1.1 Temperature 117

3.1.2 Particle Size and Sample Weight 127

3.1.3 Ferric Ion Concentration 131

3.2 X-ray Powder Diffraction Study of the Leach Residues 134

3.3 Electron Probe Microanalysis 141

3.4 Change of Colour 143

3.5 Leaching with Hydrogen Peroxide 144

3.6 Microscope Examination 149

SECTION 4 - α-CHALCOPYRITE. RESULTS AND DISCUSSION 151

4.1 Ferric Sulphate Leaching. Kinetic Rate-Curves. 151

4.1.1 Effect of Storage Time 151

4.1.2 Effect of Ferric Ion Concentration 156

4.2 Electron Probe Microanalysis 158

4.3 Leaching with Hydrochloric Acid. Effect of Chloride Ion on the Leaching Rate. 161

4.4 X-ray Powder Diffraction Study of the Leach-Residues 167

4.5 Microscope Examination 169

SECTION 5 - CONCLUSIONS 170

5.1 Summary of Results 170

5.2 Comparison of the Present Investigation with Previous Work 173

APPENDIX A - HIGH TEMPERATURE POTENTIAL -pH DIAGRAMS FOR THE SULPHUR-WATER, COPPER OXIDES AND SULPHIDES-WATER AND IRON OXIDES AND SULPHIDES-WATER SYSTEMS 178

		Page
A-1.	Introduction	179
A-2.	Relations Used	180
	A-2.1 Non-Redox Reactions	180
	A-2.2 Redox Reactions	180
	A-2.3 Calculation of ΔG_T^o	180
	A-2.4 Use of Half-Cell Reactions - Thermodynamic Properties of the Electron	182
	A-2.5 Variation of Activity Coefficients and pH with Temperature	185
A-3.	Simplified Relations for Each Temperature	188
	A-3.1 t = 25°C T = 298°K	188
	A-3.2 t = 100°C T = 373°K	188
	A-3.3 t = 150°C T = 423°K	188
A-4	Sulphur-Water System	190
	A-4.1 Reactions	190
	A-4.2 Potential-pH Relationships	192
	A-4.2.1 t = 25°C T = 298°K	192
	A-4.2.2 t = 100°C T = 373°K	193
	A-4.2.3 t = 150°C T = 423°K	194
	A-4.3 Discussion on the Sulphur-Water System	195
A-5	Copper Oxides and Sulphides-Water System	201
	A-5.1 Reactions	201
	A-5.2 Potential-pH Relationships	203
	A-5.2.1 t = 25°C T = 298°K	203
	A-5.2.2 t = 100°C T = 373°K	204
	A-5.2.3 t = 150°C T = 423°K	205
	A-5.3 Conclusions on Copper Oxides and Sulphides-Water System	206
A-6	Iron Oxides and Sulphides-Water System.	213
	A-6.1 Reactions	213
	A-6.2 Potential-pH Relationships	215
	A-6.2.1 t = 25°C T = 298°K	215
	A-6.2.2 t = 100°C T = 373°K	216
	A-6.2.3 t = 150°C T = 423°K	217
	A-6.3 Conclusions on Iron Oxides and Sulphides-Water System	218

Page

A-7 Some Comparisons with Results of Other Authors 223

A-8 Auxiliary Thermodynamic Data 227

APPENDIX B - EXPERIMENTAL RESULTS FROM THE LEACHING RUNS 231

B-1 Leach Liquor 232

B-1.1 β-Chalcopyrite 232

B-1.2 α-Chalcopyrite 248

B-2 Solid Residues 256

B-2.1 Atomic Absorption and Electron Probe Analyses 256

B-2.2 X-ray Powder Diffraction Analyses 258

B-2.3 X-ray Powder Photographs 293

B-2.4 Photomicrographs of the Residues. 302

APPENDIX C - OPEN FURNACE AND PRESSURE FURNACE DESIGN 316

C-1 Basic Relations 317

C-2 Open Furnace 319

C-2.1 Calculations of the External Surface Temperature 319

C-2.2 Determination of the Number of Turns in the Winding 321

C-3 Pressure Furnace 322

C-3.1 Calculation of the Thickness of the Insulating Layer 322

C-3.2 Calculation of the Wall and Cover Plates Thickness for the Pressure Vessel 324

C-3.3 Design of Welded Connections and Fittings 325

C-4 Workshop Drawings 327

ACKNOWLEDGEMENTS 332

REFERENCES 333

INTRODUCTION

Copper sulphide minerals are the largest source of copper in the worldand chalcopyrite is one of the most important of them.

Smelting of the ores containing these minerals contributes to the pollution of the atmosphere due to the production of sulphur dioxide. With the introduction of increasing restrictions on the permitted pollution level, hydrometallurgy became a short term solution of the problem.

However, chalcopyrite is the copper sulphide which presents the greatest resistance to dissolution, and even drastic processes using high temperatures and pressures are still relatively slow.

A process normally used for low grade ores is dump leaching, and in the case of chalcopyrite the use of ferric sulphate as an oxidising agent is quite common, although having the disadvantage of being a very lengthy recovery method.

Most of these dissolution processes are based on an old fashion empiricism of successive trial of conditions, some of them leading to expensive technological solutions.

The aim of this work is to try and clarify some points in the mechanism of leaching of chalcopyrite and obtain information that will allow the handling of the recovery process in such a way to increase yields and reduce prices.

Thus, attempts were made to obtain pure chalcopyrite by synthetic methods, since the natural ores seem to be affected by the impurities they normally contain, changing the reactivity and masking the true mechanism.

Ferric sulphate was found to be a suitable oxidizing agent, since it led to a very slow dissolution process, and allowed the transformation of the solid to be followed in relative detail.

SECTION I

LITERATURE SURVEY

1.1 Previous work on the Leaching of Chalcopyrite

The leaching of chalcopyrite has been the subject of many investigations[1-20] covering the three main points normally known as

- Atmospheric leaching
- Pressure leaching
- Bacterial leaching

The first major contribution was given by WARREN[1] in 1958. He studied in detail the acid pressure leaching of the -100 + 200 mesh fraction of a chalcopyrite concentrate containing approximately 20 per cent of pyrite, and reported the influence of temperature, acidity, oxygen partial pressure and surface area on the oxidation rate of that concentrate. The ranges of acidity considered were described by Warren as "moderate" - between pH 1.0 and 1.5 - and "high" - below pH 1.0. The effect on the rate of leaching copper, and oxidation of sulphur to sulphate by increasing the temperature from 120°C to 180°C is shown in Fig. 1 . As can be seen, this effect is more pronounced at "moderate" acidity (pH 1.0 - 1.5). The lower values at "high" acidity were due to the formation of a coating of molten elemental sulphur* (less sulphur oxidized to sulphate) at the temperatures used (M.P. 112.8°C), slowing down the process.

The activation energy for the process controlling the rate of oxidation of chalcopyrite concentrate at "moderate" acidity was found to be 23kcal $mole^{-1}$. This rate of oxidation at 180°C was independent of oxygen partial pressure for values above 150 p.s.i., both for "moderate" and "high" acidities. Lowering this pressure to 100 p.s.i. or less in conditions of

* Small quantities of sulphur were always observed to be present in the reactor after the "high" acidity runs.

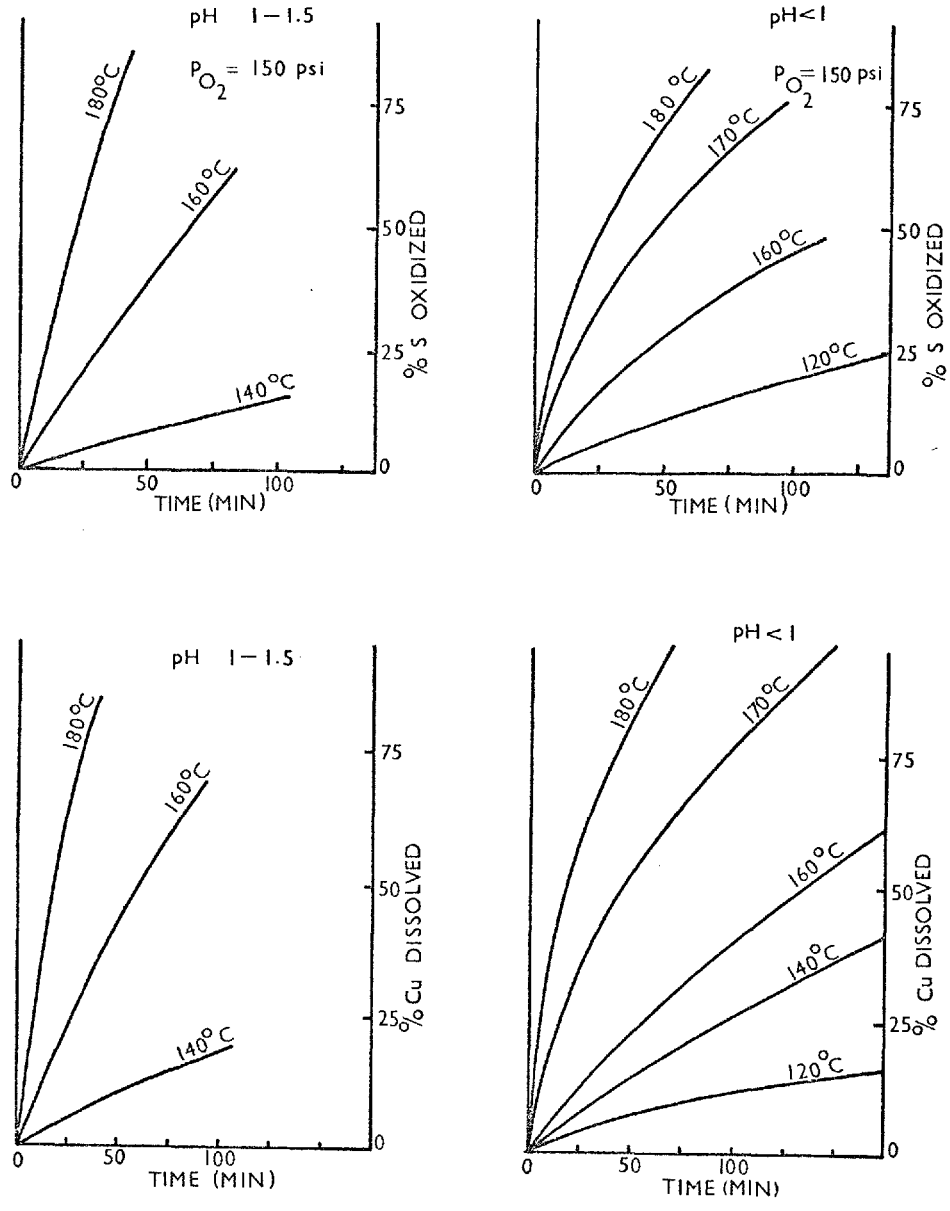

Fig. 1. Variation of the rate of copper dissolution and of oxidation of sulphur with temperature during the acid pressure leaching of chalcopyrite - Warren(1).

"high" acidity (pH<1) led to the evolution of hydrogen sulphide and severe corrosion of the reactor body. The results obtained by Warren on the effect of surface area at "moderate" acidity on the leaching rates of copper are shown in Fig. 2 and Warren suggested that once the process was not controlled by diffusion (high value for the apparent activation energy), there was a rate-controlling heterogeneous process at the surface for the pressure dissolution of chalcopyrite.

From the results obtained the suitable conditions of pressure leaching were found to correspond to pH values between 1.0 and 2.1, depending on the oxygen partial pressure, and corresponding also to conditions of low corrosiveness within the reactor.

The characteristic parabolic rate-time plots obtained by Warren, similar to the graphs obtained by SERAPHIM and SAMIS (1956)[2] for lead sulphide, were explained as the result of a sulphur coating. Warren pointed out the distinction between production of elemental sulphur, when pH<1.5 and temperatures below melting point (112.8°C) and a coating of sulphur when this temperature was exceeded.

Finally, Warren explained the interaction between oxygen partial pressure and acidity in determining the rate of leaching of chalcopyrite, by an increase of oxygen oxidation potential with acidity. When the heat of oxidation was small - resulting from a low oxygen oxidation potential - the products of the reaction did not leave the surface of the mineral before they were activated by collisions with solvent molecules in a relatively slow process. Therefore if this was the slowest step, the leaching would be "desorption" controlled. When the heat of oxidation was large - due to high oxygen oxidation potential (high acidity) - the products of the reaction had sufficient energy to leave the mineral surface rapidly and the rate controlling step was probably the oxidation reaction itself. The fact that for a given oxygen pressure the rate of leaching became independent of pH for "moderate" acidities

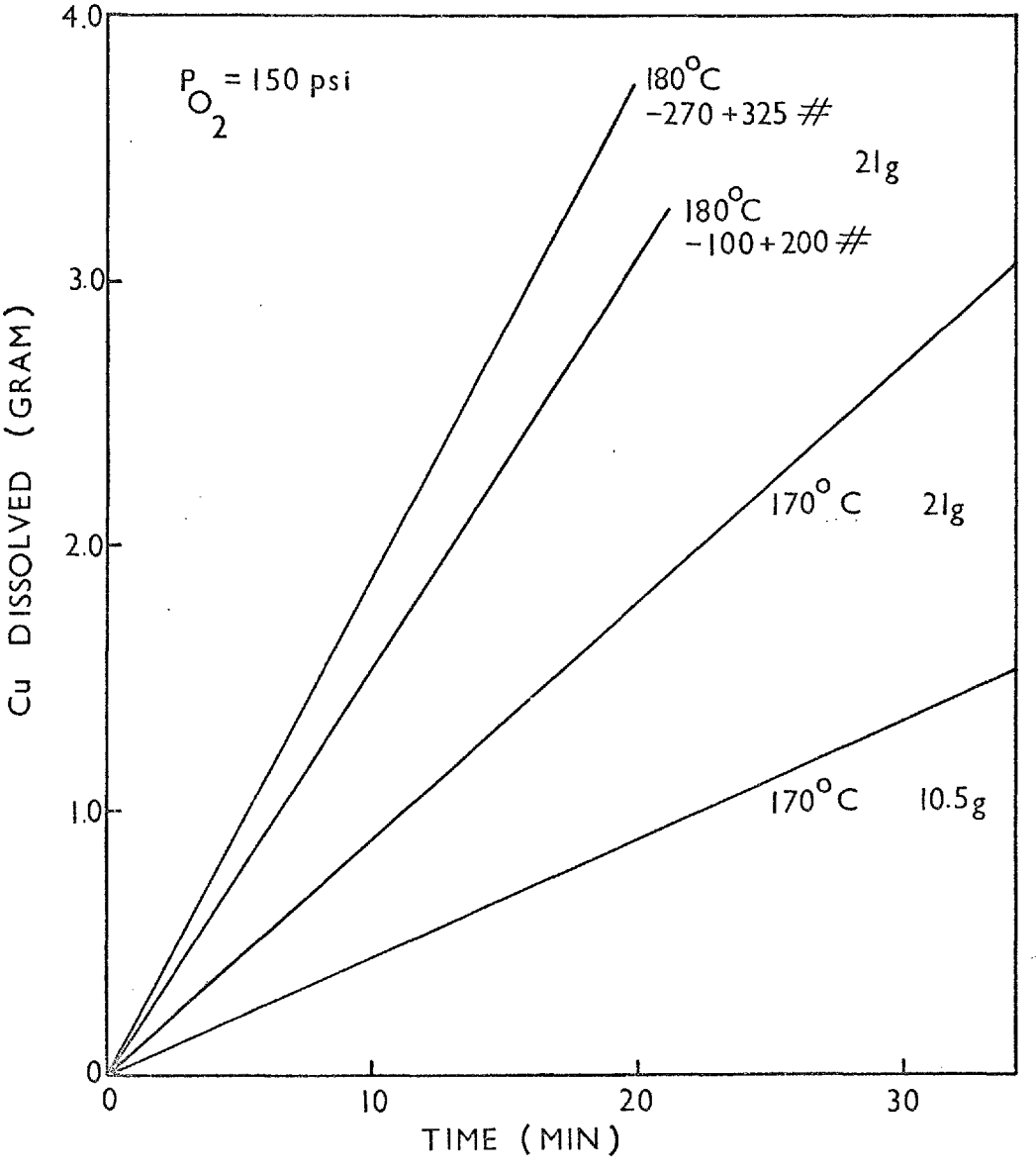

Fig. 2. Variation of the rate of acid pressure leaching of chalcopyrite with surface area at "moderate" acidity - Warren(1).

suggests a transition in the type of controlling step.

JACKSON and STRICKLAND in 1958[3] studied the dissolution of sulphide ores in acid chlorine solutions. They determined the rate of reaction and the products of reaction for the more common sulphide minerals, and found that, with the exception of galena, the kinetics were transport controlled. Experiments were made with a chalcopyrite ore 99% pure, at pH 1, temperatures varying between 25-50°C. The initial concentration of Cl_2 varied from 14.5×10^{-3} to 38.4×10^{-3} M in Cl_2. Stirring rate was kept at 300 r.p.m. and all starting solutions were 0.5M with respect to chloride. The cations present were H^+ and Na^+.

From the results obtained they were able to calculate a value of about 5kcal for the apparent activation energy. Although polarographic analysis of copper in presence of an equal quantity of iron were not too satisfactory, it was possible to see that the behaviour of chalcopyrite, under the mentioned conditions, was similar to sphalerite where the ore surface becomes coated with a layer of sulphur-sulphur monochloride mixture. Part of this sulphur was oxidized by chlorine to $SO_4^=$. Jackson and Strickland concluded that the reaction must be at the surface of the coating as no abnormal slowing of the reaction was observed.

In 1962 a work by DOBROKHOTOV and MAIOROVA[4] was published on the kinetics of autoclave leaching of chalcopyrite concentrate containing about 2-25% of pyrite and 5-20% of bornite. Rotating discs of known area were used in an autoclave with stirring facilities, the hydrodynamics of the system being known [5]. The temperature was varied between 125°C and 175°C, the oxygen pressure between 2.5 and 10 atm, initial acidity between 0.0464 and 0.515 mole $liter^{-1}$ (H_2SO_4), and stirring rate, expressed in Reynolds number, between 2900 and 55000.

They found that the amount of copper dissolved increased linearly with time, while Fe^{2+} concentration in solution rose, passing through a maximum and decreasing, this maximum increasing with the acidity of the solution. The amount of Fe^{3+} also increased linearly with time. To explain the shape of the Fe^{2+} concentration-time diagram, Dobrokhotov and Maiorova mentioned that the oxidation rate of Fe^{2+} was proportional to its concentration and to the concentration of Cu^{2+}, which acted as a catalyst. Initially both Fe^{2+} and Cu^{2+} concentrations in solution were small and oxidation was limited. Once the concentration of these ions increased, the oxidation process accelerated and Fe^{2+} concentration decreased.

They also found that the rate of iron dissolution was higher than the rate of copper dissolution, probably due to the selective dissolution of the accompanying minerals (e.g. pyrite). Also different selections of specimens gave different rate constants, but similar results were obtained for the same selection.

From Dobrokhotov and Maiorova findings it is interesting to note that no surface films were formed and the reaction rate was independent of the rate of stirring. The kinetic relationships obtained show that the rate of copper dissolution was directly proportional to the solution acidity, and to the oxygen partial pressure to the power 0.5. The activation energy, in the acidity range 0.04 - 0.2M, was found to be 7.17kcal/mole.

The results obtained were said to indicate that the leaching process consisted of the following consecutive stages.

1) Dissolution of gaseous oxygen (rapid)

$$O_2 \text{ gas} \rightleftarrows O_2 \text{ solution}$$

2) Activated adsorption of oxygen by the chalcopyrite surface (rapid)

$$CuFeS_2 + mO_2 \text{ solution} \quad [\text{Active complex}_{CuFeS_2} - 2mO]$$

3) Chemical reaction at the surface (slow)

$$[^{\text{Active complex}}_{CuFeS_2 - 2mO}] + 4mH^+ \rightarrow [CuSO_4 + FeSO_4 + 2mH_2O] .$$

4) Diffusion of the reaction products into the main bulk of the solution (rapid), and chemical reaction within the solution (slow).

$$4FeSO_4 + O_2 \text{ solution} + 2H_2SO_4 \rightarrow Fe_2(SO_4)_3 + 2H_2O$$

The over-all reaction being:

$$4CuFeS_2 + 17O_2 + 2H_2SO_4 = 4CuSO_4 + 2Fe_2(SO_4)_3 + 2H_2O$$

STANCZYK and RAMPACEK (1963)[6] studied the acid leaching of impure commercial copper sulphide flotation concentrates, and specimen-grade hand-picked copper sulphide minerals at elevated temperatures and pressures. Copper extractions of 97-99% were obtained by leaching chalcopyrite and flotation concentration with water under oxidizing conditions at 200°C for 30 to 60 minutes and therefore no acid was used, while in tests with bornite, chalcocite and cement Cu was necessary the addition of H_2SO_4 or pyrite to obtain similar extractions of Cu.

BJORLING and KOLTA[7] presented the results of oxidizing leach of sulphide concentrates and other materials catalysed by nitric acid, to the VII International Mineral Processing Congress in 1964.

They reported the findings on leaching of chalcopyrite concentrate from Boliden Mining Company after being decomposed, by heating in the absence of air.

This heating was done in a small rotating furnace at 550°C and the authors assumed that the products obtained had the composition of $Cu_2S.2FeS$.

Samples of the decomposed material were leached in both an open vessel and autoclave to determine the rate of leaching with nitric acid at different pH values, at 90°C.

In the open vessel the best conditions for formation of elemental sulphur (88% against 10.6% sulphate sulphur) were

found at pH 0.8 after 180 min. reacting time.

In the autoclave leaching runs, the yield of elemental sulphur was found to depend on pH and oxygen pressure, the best conditions being obtained at pH 0.8 and oxygen pressure of 0.5 atm. (87.2% S^o against 11.8% as sulphate sulphur), the sulphate formation being favoured at high acidities and pressures.

It must be pointed out that the aim of these experiments was to find a leaching method which will directly separate sulphur and iron from each other and will allow the metals to be easily recovered.

In 1966 KLETS and LIOPO(8) used a sample containing about 70% of chalcopyrite, 20-30% of covellite and less than 5% of cubanite to study the behaviour of chalcopyrite in salt leaching.

For this purpose they used a ferric chloride solution and they assumed that the following reactions take place:

$$CuFeS_2 + 4FeCl_3 = CuCl_2 + 5FeCl_2 + 2S^o$$

$$8S + 6H_2O = H_2S_3O_6 + 5H_2S$$

$$CuCl_2 + H_2S = CuS + 2HCl$$

$$CuCl_2 + FeCl_2 + 2H_2S = (CuS.FeS) + 4HCl$$

They suggested an industrial system of leaching for this type of ore with continuous removal of sulphur from the particle surfaces and a regulation of acidity to prevent or reduce sulphur hydrolysis.

Another work by STANCZYK and RAMPACEK(9) was published in 1966, this time concerning the oxidation leaching of copper sulphide minerals and a composite of impure flotation concentrates at elevated temperature and pressure with ammoniacal solutions.

Copper extractions of 96% were obtained by leaching

chalcopyrite (apparently with the same composition already referred in the other work by the same authors[6]), at 75°C under oxidizing conditions, for 60 minutes.

Although ammonium sulphate was not required when digesting chalcopyrite, copper extractions were enhanced and less ammonia was required when it was added.

In 1966 a paper was presented by NAKAHIRO[10] which related the amount of leached copper with the degree of oxidation of chalcopyrite. Experimental results were claimed to show that sulphide ores were oxidized rapidly when the atmospheric moisture was increased to 80% and temperature raised to 40°C. This is surprising.

MAJIMA and PETERS (1966)[11] studied the oxidation rates of sulphide minerals by aqueous oxidation at elevated temperatures. They used high-grade minerals crushed and screened to -150 + 200 mesh size.

The experiments were performed in a shaking autoclave and the starting conditions were 124 psi of oxygen pressure, temperature 120°C and $pH_{120°C}$ varying from 2.7 to 14, (it is not clear what was meant by $pH_{120°C}$ - see Appendix A).

The results were obtained through oxygen absorption (pressure drop) curves for each type of initial condition and are discussed below with Majima and Peters' conclusions.

At pH_{120} 2.7 in phosphate buffered solutions, the chalcopyrite and other copper minerals as well as pyrite showed an almost linear oxidation rate. Under the conditions of this experiment they did not produce elemental sulphur quantitatively, most of the sulphur being oxidized to sulphate. At pH_{120} 7, also buffered with phosphate salts, and assumed by the authors as neutral solutions, sulphur does not have a range of stability (Appendix A) and it is unlikely that any would form during the reaction. However, as in the previous runs it was difficult to determine the stoichiometry of the system, because the sulphate and polythionates may have formed during the early stages of oxidation. Chalcopyrite as well as other sulphides (ZnS,

PbS, and FeS) remained relatively inert for ½ to 1 hour before oxidation commenced, but after this the rates were constant and similar for the different sulphides. Majima and Peters assumed therefore that the structures of the mineral do not play a role in the oxidation mechanism except during the initial period. Experiments at pH_{120} 11.2 showed that the sulphur rich minerals, such as chalcopyrite, were more easily oxidized, the sulphur to metal ratio for the different sulphides seeming to be more important than the properties of the constituents, as far as oxidation rates in basic solutions are concerned.

Although the authors had not checked the presence of thiosulphate and polythionates, they assumed that they were present in view of earlier work on ammonia leaching.

In caustic solutions pH_{120} 14 (1 M Na OH), sulphur rich minerals, such as chalcopyrite (and Sb_2S_3, FeS_2, CuS) were again the most rapidly reacting.

In ammonia (NH_3-1M) - ammonium sulphate (0.5M) buffered solution (pH_{25}~8.7) the copper minerals showed greatly enhanced oxidation rates when compared with the other sulphides, due to the presence of a complexing agent for the metal cation.

A study of the recovery of copper and elemental sulphur from chalcopyrite concentrate by pressure leaching appeared in 1967. The authors VIZSOLYI et al.[12] outlined a process for direct pressure oxidation of chalcopyrite concentrate in an aqueous sulphuric acid medium, resulting in the production of a copper sulphate solution suitable for copper recovery by almost all known means (e.g. electrowinning, hydrogen reduction, solvent extraction combined with electrolysis) and pure elemental sulphur as by-product.

They divided the mechanism of the pressure leaching process into two main simultaneous reactions.

The first one corresponds to the oxidation of sulphide sulphur to elemental sulphur and formation of cupric and ferrous sulphates.

The second is the oxidation of ferrous to ferric sulphate, hydrolysis of the iron with release of acid which in turn reacts with more chalcopyrite. From the experimental results obtained by VIZSOLYI et al. the principal reactions were expressed in a somewhat idealized form (as they point out) as follows:

$$CuFeS_2 + 2H_2SO_4 + O_2 \rightarrow CuSO_4 + FeSO_4 + S^o + 2H_2O$$

$$FeSO_4 + 1/2\ H_2SO_4 + 1/4O_2 \rightarrow 1/2\ Fe_2(SO_4)_3 + 1/2\ H_2O$$

$$1/2\ Fe_2(SO_4)_3 + 3H_2O \rightarrow Fe(OH)_3 + 1\ 1/2\ H_2SO_4$$

Eventually the reaction reached the equilibrium when all the sulphuric acid had been consumed by the formation of cupric sulphate.

Finally an idealized overall reaction can be written as:

$$CuFeS_2 + H_2SO_4 + 1\ 1/4\ O_2 + 1/2H_2O \rightarrow CuSO_4 + Fe(OH)_3 + 2S^o$$

However, in fact the complete equilibrium state was not reached within normal retention times, nor did the oxidation of $S^=$ go to S^o quantitatively. This oxidation depends, as they say, on the type of concentrate and the leaching conditions, and an eventual oxidation of $S^=$ to $SO_4^=$ can occur, part of the $SO_4^=$ going into solution and part hydrolysing with iron to basic ferric sulphate [$Fe(SO_4)OH$], producing an impure ferric hydroxide precipitate.

Describing the experiments and determinations of optimum leaching conditions they mentioned the composition of chalcopyrite concentrate as being 91% of chalcopyrite, 4.5% of pyrrhotite and the balance gangue, pentlandite and pyrite.

The starting experimental conditions were a slurry consisting of 6000 ml of leach solution containing 95 g/l H_2SO_4 1800 g or 300 g of concentrate for litre of leach solution. The authors studied the following parameters:

a) oxygen partial pressure (between 30 and 500 psi)
b) particle size (52.6 to 99.5% - 325 mesh)

c) quantity of excess concentrate (0 to 100% excess)
d) temperature (99°to 149°C)

From the study of the parameters the authors found that the best conditions for the pressure leaching of chalcopyrite concentrate should lie between the following ranges for an average 2-3 hours retention time.

a) oxygen partial pressure 200 to 500 psi. No further significant rate increase was expected above 500 psi,
b) particle size 95 to 99.5% - 325 mesh. Finest grind with a larger surface area giving higher rate of oxidation,
c) quantity of excess concentrate 25 to 50%. This is not very critical providing that there is more than 25% excess concentrate, allowing also for a more easy adjustment of pH (excess of acid would prevent hydrolysis of iron to the value desired),
d) temperature 110 to 118°C. Above that temperature the melting of elemental sulphur occurs - 120°C(*) coating the unreacted solid and preventing further oxidation.

In the same year a Japanese work was published by UCHIDA et al.[13] on the leaching of copper and copper-bearing ores with a dilute solution of sulphuric acid and ferric sulphate.

They found that copper in chalcopyrite was hardly extracted by leaching with dilute acidic ferric sulphate solutions, whereas from bornite it was easily leached under the same conditions. No appreciable effect of particle size on the rates of leaching was observed, and only a slight increase with increase of Fe^{3+} concentration.. It is interesting to note that an experiment with a leaching solution containing 0,01N sulphuric acid and 0.4% Fe^{3+}

(*) The authors seem to have considered sulphur in amorphous state.

leached out about 40% of the copper from bornite and 4-5% of the copper from chalcopyrite in two weeks leaching. In the abstract referring to this paper no mention was made about the temperature or other parameter of this run.

In 1968 WARREN et al[14] studied the behaviour of a chalcopyrite concentrate previously subject to two types of heat treatment. The first, calcination of the mineral at 825°C for two hours in the absence of oxygen inducing a sulphur loss by volatilization of about 6% producing a material with an X-ray pattern where the merging of lines 1.57 and 1.59 and 1.85 and 1.86 Å were interpreted by the authors as suggesting the creation of some disorder in the mineral lattice. The second, treatment of the mineral with elemental sulphur at 475°C leading to a sulphur uptake of about 8% producing a mixture of covellite and pyrite confirmed by X-ray.

The chemical analysis of the untreated concentrate shows that apart from the amount of insoluble material (about 3%), the copper iron and sulphur content indicates that the concentrate contains iron sulphide minerals in addition to chalcopyrite, however, these were not detected by X-ray.

They assumed that the sulphur lost from the calcined concentrate was unlikely to have come from the small adulteration of iron sulphide. Pyrite was present in an amount less than 2%, since no lines for this mineral appeared in the X-ray diffraction pattern of the chalcopyrite concentrate.

However, the authors suggested the need for studies with samples of chalcopyrite with composition closer to the ideal in order to confirm that the sulphur lost came from the chalcopyrite itself.

The three samples, untreated, calcined and sulphidized concentrate ware submitted by Warren et al. to pressure leaching experiments, using an acid solution containing 1 mole of sulphuric acid per mole of copper, oxygen pressure of

70 psi and temperature of 90°C. The results they obtained over a period of 10 hours are shown in Fig. 3-a and it can be seen that the extraction of copper from the sulphidized material was both more rapid and greater than that from either the calcined product or the original chalcopyrite concentrate.

The percentage of iron in solution dissolved from the solid was parallel to that of copper in both untreated and calcined concentrate but much slower for the sulphidized (CuS + FeS_2) concentrate. However, at about 95% of extraction of copper from the sulphidized material the iron extraction increased rapidly. Fig. 3-b

All three samples produced sulphur. However, for the untreated and calcined materials the production was proportional to the sulphuric acid consumed in solubilizing copper and iron, while the sulphidized material produced both elemental sulphur proportional to the copper dissolution, and sulphate proportional to the iron dissolution.

Finally, they explained the increased leaching rate observed for the calcined material compared to the untreated concentrate by the apparently slightly disordered structure of the former.

A study on the kinetics of dissolution of synthetic chalcopyrite in aqueous acidic ferric sulphate solutions by DUTRIZAC et al.[15] appeared in 1969.

They synthesized CuS and $FeS_{1.002}$ from stoichiometric quantities of the elements and X-ray analysis confirmed that the copper sulphide was covellite and the iron sulphide was troilite. The two ground (-100 mesh) sulphides were mixed in equimolar amounts, pressed into pellets at 80 000 psi , placed into a vacuum-sealed pyrex vessel and sintered for 3 days at 550°C. X-ray analysis showed the product to be $CuFeS_2$.

The only impurity they found in the material thus prepared was 0.5 volume percent of pyrite, and according to their findings this did not interfere with the amount of copper dissolved during the runs.

a)

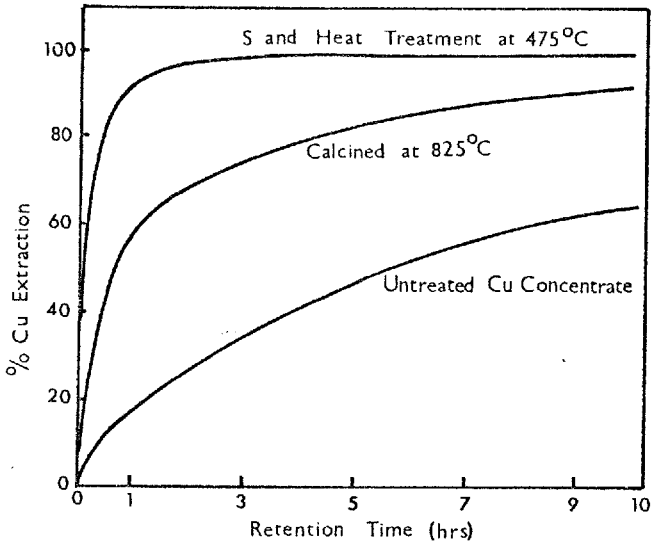

b)

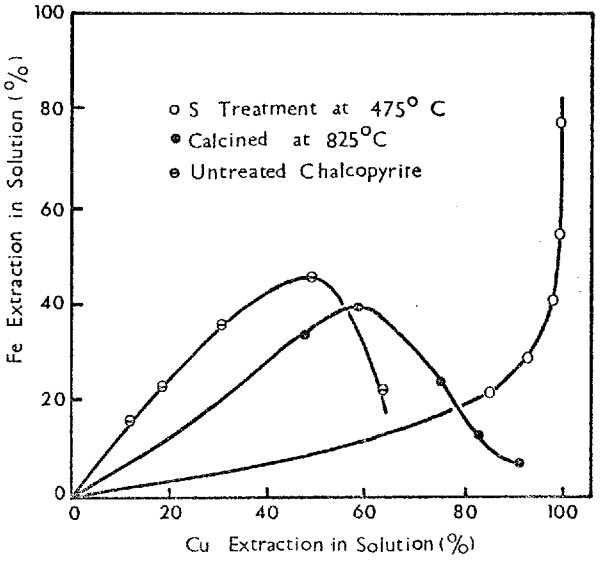

Fig. 3. Acid pressure leaching of untreated calcined and sulphidized chalcopyrite concentrate - Warren[14]

a) Extraction of copper
b) The copper/iron extraction ratios.

The sintered disks of synthetic chalcopyrite were 80% of theoretical density and they explained this fact assuming that the true area of the disks was larger than the measured one.

The disks were cemented to lucite cylinders and only a polished face was exposed to the solution.

Experiments at 80°C in acidified ferric sulphate solution in an atmosphere of nitrogen allowed the authors to determine the stoichiometry of the leaching reaction. For this purpose they determined the amount of copper in solution, the elemental sulphur formed (extracted with CS_2 in a Soxhlet extraction apparatus), and the ratio of these elements. Also they calculated the ratio of ferrous ion to cupric ions in solution, giving the final equation

$$CuFeS_2 + 2Fe_2(SO_4)_3 \rightleftharpoons CuSO_4 + 5FeSO_4 + 2S$$

The authors stated that the residue obtained after the extraction of elemental sulphur, consisted of unreacted chalcopyrite only.

An experiment at 70°C in 0.11 molar Fe^{+3} and 0.1 molar H_2SO_4 was done on a synthetic and a natural chalcopyrite and the results obtained by Dutrizac et al. are shown in Fig. 4 . From the linearity of the same square root plot they assumed that the dissolution kinetics were parabolic. The authors explained the difference in magnitude of the two leaching rates by the possibility of variations in the ratio of true to apparent surfaces (the porous synthetic material having the larger true area) and also the existence of impurities in the natural material that may alter the rate of the diffusion process indicated by the parabolic kinetics. The effect of temperature on the rate of reaction was determined and a value of 17 ± 3 kcal per mole was found for the activation energy. According to the authors, this value is consistent with rate control by a diffusion process, and they related this fact with the layer of sulphur on the surface of the partly leached sample, which they had detected by X-ray diffraction.

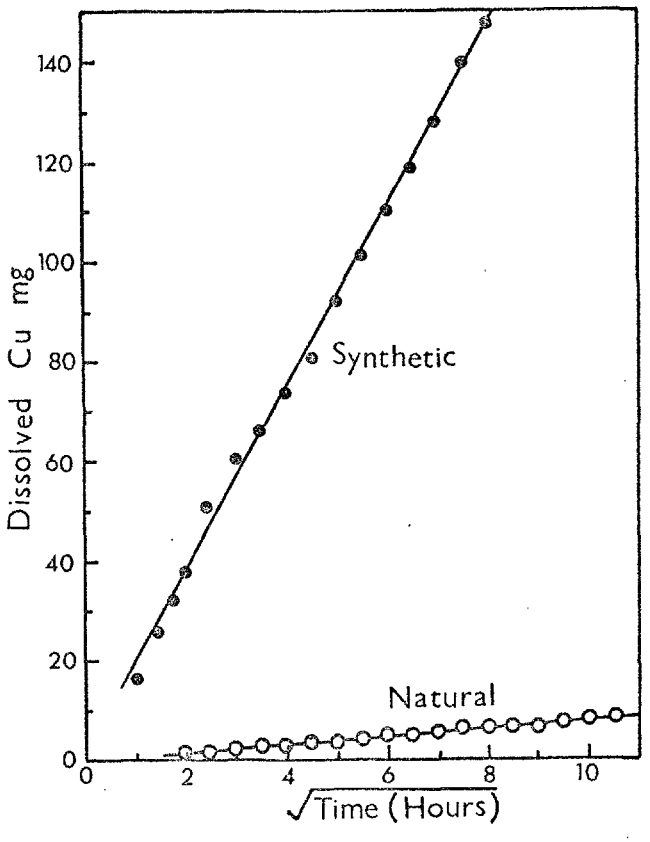

Fig. 4. Dissolution of synthetic and natural chalcopyrite disks at 70°C and 250 rpm in 0.11 M Fe^{+++} and 0.1M H_2SO_4 solutions - Dutrizac et al. (15)

Further experiments showed that neither acid concentration nor the speed of rotation of the disk had any effect on the leaching rate, confirming the hypothesis of diffusion of either the reactants or products through the sulphur film.

They also found that there was no effect on the rate due to variation of Fe^{3+} above 0.01 molar. A study of the variation of the rate constant below this value, permitted the authors to conclude that the rate controlling step was the diffusion of Fe^{3+} inwards through the layer of sulphur formed. Experiments with ferric iron concentrations above 0.01 molar and variable amounts of ferrous sulphate showed, according to these authors, that the rate of controlling step was the outward diffusion of ferrous sulphate through the sulphur layer. Finally, they checked that acid alone did not attack chalcopyrite, the only reason for its presence was to prevent the hydrolysis of the iron salts.

In 1968, BJÖRLING and LESIDRENSKI(16) studied the pressure leaching of chalcopyrite activated by heating with metallic copper (scrap) to about 450°C, with exclusion of air.

The activation was quick and could be represented by

$$Cu + CuFeS_2 \rightarrow Cu_2S + FeS$$

According to the authors the important characteristics of this leaching procedure were the "continuous operation under constant conditions, the choice of suitable pH and presence of nitric acid". With continuous operation the retention time of free sulphur was minimized, reducing the probability of its being oxidized (see Appendix A , Diagrams E-pH) in view of its slow kinetics.

Bjorling and Lesidrenski also found that a suitable pH should allow sufficient free nitric acid to be present to promote oxidation of the sulphide sulphur to elemental sulphur, without promoting the oxidation of the iron to Fe^{3+}. Dilute nitric acid (≈20g/l maximum) acted as mild

oxidizing agent, reacting according to

$$3MeS + 2HNO_3 + 6H^+ \rightarrow 3Me^{2+} + 3S^o + 2NO + 4H_2O$$

the NO reacting with free oxygen and water

$$2NO + 3/2\ O_2 + H_2O \rightarrow 2HNO_3$$

The authors mentioned that too high temperatures should be avoided because they promote the oxidation of sulphur to sulphate (Appendix A) although they speed up the reaction.

For their experiments, they used samples of natural chalcopyrite containing more iron and sulphur than required for the stoichiometry $CuFeS_2$, probably due to other iron sulphides, and also containing impurities such as 2.75% of Zn, 1.40% of Pb, and 12.6% of others non specified.

According to their findings very good recoveries were obtained - 99% of copper and 79% of sulphur globules - at 110°C, retention times of about one hour, and 2 to 3 atm of air pressure. The authors, however, suggested the need of further experiments for complete elucidation of the rate of oxidation.

In 1970, PRATER et al.[17] studied the sulphation of copper sulphide flotation concentrate as well as copper-iron sulphide minerals with hot concentrated sulphuric acid. These minerals were natural specimens of chalcopyrite, covellite, chalcocite, digenite, bornite and pyrite, containing only quartz and pyrite as impurities.

A large excess of sulphuric acid (concentration varying between 75 and 96%) was used to prevent substantial dilution of this reactant with water produced during the reaction. The other factors considered were the temperature, varying between 180° and 260°C, reaction times between 0.3 and 4 hours and oxygen partial pressure varying from 0 to 1 atm. The degree of "rabbling" was also one of the variables considered.

The technique described by Prater et al., involved the removal of sulphur dioxide produced during the reaction, by

either an oxygen or a nitrogen flow and absorption by iodine solution. Elemental sulphur was recovered by extraction with carbon disulphide.

After the sulphation, copper and iron sulphates were extracted from the roasted residues by leaching for 15 minutes with a solution described by the authors as pH 1.5 water at 60°C. With the results obtained, they formulated the basic reactions for the sulphation of chalcopyrite as

$$CuFeS_2 + 2H_2SO_4 \rightarrow CuSO_4 + FeSO_4 + 2H_2S$$
$$2FeSO_4 + 2H_2SO_4 \rightarrow Fe_2(SO_4)_3 + SO_2 + 2H_2O$$
$$H_2S + H_2SO_4 \rightarrow S^o + SO_2 + 2H_2O$$
$$S^o + 2H_2SO_4 \rightarrow 3SO_2 + 2H_2O$$

Solid roasted residues were analysed by X-ray diffraction and chalcopyrite as well as covellite and pyrite gave no apparent intermediate sulphide reaction products; only metal sulphates and elemental sulphur were obtained in the residues. However, the authors envisaged the possibility of a more complex decomposition for chalcopyrite and pyrite. They suggested as probable, the formation of elemental sulphur and hydrogen sulphide from the sulphide ions present in the minerals. Formations of most of the sulphur dioxide and all of the water vapour was from the decomposition of sulphuric acid, some of the sulphur dioxide being produced by the oxidation of elemental sulphur.

The results of the experiments obtained by Prater et al. showed that while chalcopyrite (and covellite) was the most resistant of the copper sulphides in normal hydro-metallurgical processes, in an acid roast system it was the most reactive one. They also found that chalcopyrite could be selectively sulphated in presence of pyrite if no digenite and chalcocite were present.

The best conditions of roasting were found to be the minimization of the sulphide particle size, maximum sulphuric acid concentration (experiments showed that acid below 92% in concentration resulted in reduced sulphation of chalcopyrite),

agitation of the mixture and temperature high enough to drive off the steam produced, but low enough to prevent both acid fuming and substantial pyrite oxidation (when present). The authors mentioned that if maximum recovery of sulphur is desired, an inert atmosphere should be used. Over 99% of copper sulphation was obtained after 1 hour at 190°C, by baking chalcopyrite under the best mentioned conditions.

In a communication to the "Conférence de la Société Française de Minéralogie et de Cristallographie, 1969" WYCKOFF[18](1970) presented part of a study on bacterial leaching of chalcopyrite. This work involved experiments with ferrobacillus or thiobacillus and the results enabled Wyckoff to classify the sulphides in two groups, according to their resistence to the bacteria. Those strongly attacked, transforming to sulphates, were nickel, zinc and iron sulphides (pyrite as well as pyrrhotite), and several sulphides of copper (chalcocite, covellite, bornite and digenite). At the other extreme some minerals were inert in the presence of bacteria, as for example molybdenum sulphide.

According to Wyckoff, natural chalcopyrite may be leached bacterially very readily, or to an intermediate degree, or not at all, depending on the sample. Purity seemed to play no part in this anomaly; once samples with different behaviour had the same chemical composition and identical positions and reflection intensities for the X-ray diffraction diagrams.

No relation was found between surface properties of the mineral (e.g. particle size) and the susceptibility for the attack. Based on this evidence, Wyckoff proposed the existence of two types of natural chalcopyrite, in which the metal atoms had different valencies, varying between the two extremes of a series, $Cu^{1+}Fe^{3+}S_2$ and $Cu^{2+}Fe^{2+}S_2$, most of chalcopyrites being intermediates between the two. He presumed that it was $Cu^{2+}Fe^{2+}S_2$ which dissolved more readily, due to the oxidation of divalent iron.

Synthetic samples, prepared by the author, were partly soluble under bacterial attack, suggesting a mixture of the two chalcopyrites. However, work was still in progress to obtain more information. Wyckoff's experiments also involved studies on two types of bacteria, one oxidizing the iron but not attacking the sulphur, the other digesting the sulphur as well as the divalent iron. Some behaved differently from others in the same conditions of pH, temperature and chemical elements.

A more complete study of microbiological leaching of sulphide concentrates by BRUYNESTEYN and DUNCAN appeared in 1971[19], with a special reference to chalcopyrite.

The bacteria used was Thiobacillus Ferrooxidans, which gets energy from the oxidation of reduced sulphur and ferrous iron.

The authors mentioned as the most important factors influencing bacterial leaching, the availability of substrate such as a mineral sulphide, an electron acceptor (in this case oxygen) during the oxidation process, a carbon source for the microorganism (supply of carbon dioxide), ammonia and phosphate as nutrients for the metabolic systems of the organism, the acidity of the environment (pH 1.5 to 3.5), optimum temperature (about 35°C) a solvent to transport the nutrient and remove the metal sulphate produced (water), and particle size of the substrate to be oxidized.

Fast techniques were devised for bacterial leaching, allowing the study of the different variables in a matter of days or weeks compared with the old two years column-type studies.

In Fig. 5-a is reproduced the diagram that presents the improvement of leaching rates obtained since 1962 by the introduction of these faster techniques. Also reproduced are a series of leaching tests carried out at 35°C using a chalcopyrite concentrate containing about 28% copper. (Fig. 5-b,c,d)

It can be seen that the rate of the linear part (after the exponential growth phase of the bacteria) augmented by

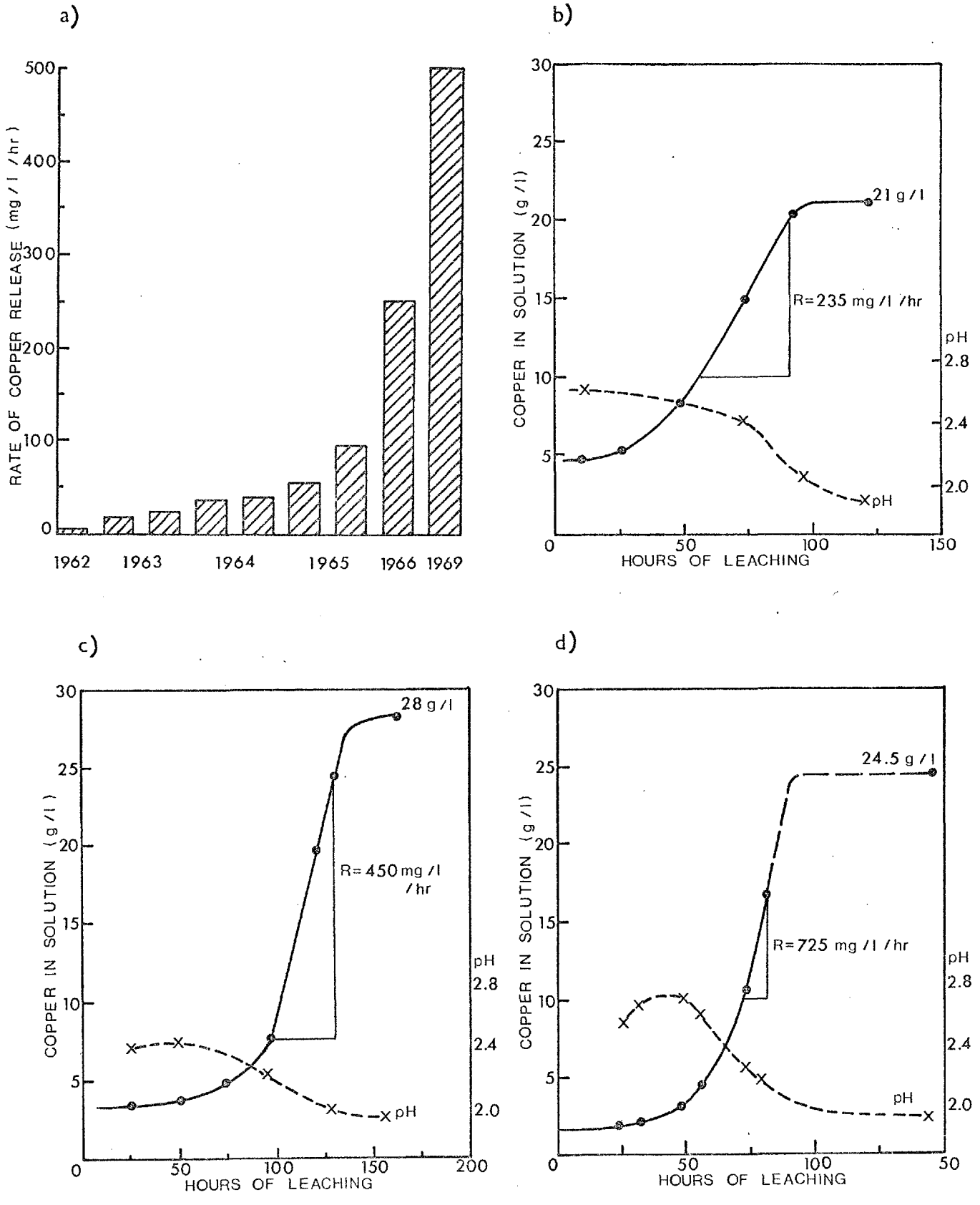

Fig. 5. Microbiological leaching of chalcopyrite concentrate - Bruynesteyn and Duncan (19)

a) Improvement in microbiological rate of release of copper from chalcopyrite.

b) Leaching of chalcopyrite concentrate at 35°C. Turbine agitated. V=21.8 litres; 10% pulp density.

c) Leaching of chalcopyrite concentrate at 35°C, in an atmosphere containing ∿ 0.1% carbon dioxide. Propellor agitated. V=5 litres; 20% pulp density.

d) Leaching of chalcopyrite concentrate at 35°C. Surface areator. V=50 litres; 20% pulp density.

the use of 0.1% carbon dioxide and increase of pulp density, (giving more area for the bacteria), and final concentrations of 28g/l were obtained. Fig. 5.d shows the result of using a surface aerator.

With these experiments Bruynesteyn and Duncan confirmed that high leaching rates in shake flasks could be obtained with even better results in stored tanks. However, there was no improvement in the extraction above 50 to 60 per cent of the copper removed from chalcopyrite. Regrinding the unreacted chalcopyrite in the leach residue resulted in further extraction. Finally, they found that the rate and extent of extraction were function of particle size, and that some iron was going into solution, always in ferric form, and staying in the range of 5 to 13 gram per litre, depending on the conditions of the leach.

In 1971 HAVER and WONG(20) studied the recovery of copper, iron and sulphur from chalcopyrite concentrate using a ferric chloride leach. Experiments were performed with a chalcopyrite flotation concentrate, and X-ray diffraction showed that this consisted of about 75% chalcopyrite, 15% pyrite and 5%of quartz, small amounts of silver; gold as well as traces of calcium,magnesium and lead were detected by chemical analysis. The variables investigated were reaction time, particle size, $FeCl_3/CuFeS_2$ weight ratio and temperature. The ferric chloride solutions for the leaching experiments had a concentration of 212g Fe^{3+}/l (about 3.8M Fe^{3+}) and dilute HCl to prevent hydrolysis of iron salts.

To determine the effect of particle size all slurries were held at the boiling point (106°C) and stirred at 250 rpm. At the end of the experiment elemental sulphur was removed from the residue with CS_2. As a result of these experiments the authors found that the finest grind gave the fastest rate of reaction, with about 100% of the copper removed from 100% -325 mesh material in 2 hours. They also found that 2.7 was the minimum $FeCl_3/CuFeS_2$ weight ratio for optimum extraction of copper, iron and sulphur, most of the copper in solution being present as Cu^+.

They assumed therefore the equation of the reaction to be

$$CuFeS_2 + 3FeCl_3 \rightarrow CuCl + 4FeCl_2 + 2S$$

As far as temperature is concerned the best results were obtained at the highest temperature of the experiments (106°C).

Under the optimum conditions mentioned above 99% of the copper, 73.7% of the iron, and 70.5% of the sulphur were recovered by a two hour leach.

Finally, the authors mentioned a parabolic reaction rate which they explained by a progressive thickening of sulphur film on the surface of the particles, and a value of 12.3kcal/mole for the apparent activation energy found in the literature[21].

1.2 Chalcopyrite Structures

The crystal structure of chalcopyrite has been the subject of several investigations.

The major first contribution was that of BURDICK and ELLIS[22] (1917), who measured the angles and intensities of reflections on a sphenoidal-type crystal from French Creek, Pennsylvania, using a highly purified palladium target. Reflections observed were from planes with unmixed indices (no odd-order reflections except from planes with all indices odd) typical of a face-centered lattice, and the atomic arrangement was determined regarding the crystal as isometric, since the a/c ratio was nearly unity (1:0.985).

The results showed that the structure could be derived from that of sphalerite (ZnS) Fig. 6-a by replacing half the zinc atoms by copper, and the other half by iron, the atomic positions being:

2 Cu at 000, $\frac{1}{2}$ $\frac{1}{2}$ 0
2 Fe at $\frac{1}{2}$ 0 $\frac{1}{2}$, 0 $\frac{1}{2}$ $\frac{1}{2}$
4 S at $\frac{1}{4}$ $\frac{1}{4}$ z, $\frac{3}{4}$ $\frac{3}{4}$ z, $\frac{3}{4}$ $\frac{1}{4}$ $\bar{z}$, $\frac{1}{4}$ $\frac{3}{4}$ $\bar{z}$.

with z = 0.25

This means that the iron and copper atoms were located so that together they would form a face-centered tetragonal lattice, "the planes perpendicular to the tetragonal axis being made up alternately of copper atoms alone and iron atoms alone". The sulphur atoms were also in a face centered tetragonal lattice, lying halfway between the iron and copper atoms planes, in all three axial direction, Fig. 6-b

According to this scheme the unit cell contained two $CuFeS_2$ "molecules", and from the angles of reflections the cell dimensions were calculated as a = 5.24 Å and c = 5.15 Å.

In 1923 GROSS and GROSS[23] using data from Laue patterns obtained ona crystal from Arakawa, (JAPAN), derived a structure entirely similar to the Burdick-Ellis structure but they changed the z value to 0.21 and cell dimensions to a = 5.270 Å, c = 5.194 Å

a)

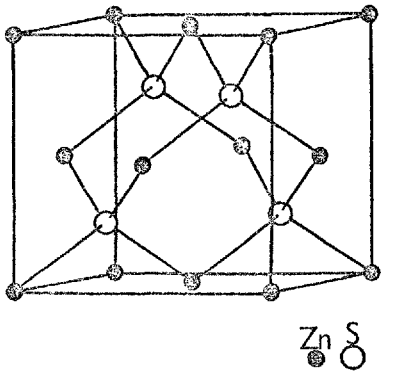

b)

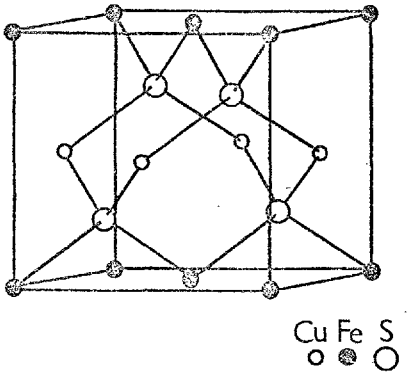

Fig. 6. A comparison of the chalcopyrite and zinc blende structures

a) Zinc-blende structure
b) Chalcopyrite structure according to Burdick and Ellis (22).

The next attempt was made by PAULING and BROCKWAY (1932)[24], based on the values of interatomic distances in chalcopyrite crystals from Joplin, Missouri. Using mainly Laue diagrams and a few oscillation diagrams with Mo radiation, they were able to describe a completely different structure, rejecting the pseudo-cubic unit described above and presenting one, twice as large, with a completely different distribution of copper and iron atoms.

Using an incident beam parallel to the c-axis of a crystal, Pauling and Brockway were able to confirm, through Laue photographs, the existence of a four-fold axis and four symmetry planes this together with the sphenoidal development of the crystals allowedthemto describe the point-group symmetry as a D_{2d}-$\bar{4}2m$. Reflections obtained on Laue photographs eliminated the possibilit of a cell with c=5.15Å. However, they could be explained assuming a unit cell with a=5.24Å, c=10.30Å, leading to a cell twiceas big.

This cell would contain $4CuFeS_2$ corresponding to a density of 4.28, while the density recorded in the literature lies between 4.1 and 4.3.

On assigning indices and calculating $n\lambda$ values for this new unit, forms like ((431)) gave first-order reflections, therefore eliminating the face-centered type lattices. This fact associated with the non-existence of reflections from forms with $h+k+\ell$ odd, indicated a body-centered lattice. From the two possible space groups based on this lattice and isomorphous with the group D_{2d}, the D_{2a}^{12} - $I\bar{4}2d$ was chosen since the other, D_{2d}^{11} - $I\bar{4}2m$, allows reflections from forms ((hℓk)) with $\frac{1}{2}(2h+\ell)$ odd and no such reflections were observed by Pauling and Brockway.

The low intensity found for all reflections except those corresponding to a face-centered pseudo-cubic arrangement should be noted.

Based on the intensity of reflections a proper set of equipoints was determined(*)

(000; $\frac{1}{2}$ $\frac{1}{2}$ $\frac{1}{2}$) +

4Cu: 000; 0 $\frac{1}{2}$ $\frac{1}{4}$ cont/..

(*) the values presented here were obtained choosing a set of coordinates enabling the use of the atomic positions as they are listed in the International Tables. As mentioned by Donnay et al. (25), a matrix 0$\bar{1}$0/100/001 can be used for the transformation. Using the new set of axes, the z value equal to 0.27 for sulphur calculated by Pauling and Brockway became x = -z = 0.73.

$$4Fe:\ 00\ \tfrac{1}{2};\ 0\ \tfrac{1}{2}\ \tfrac{3}{4}$$

$$8S:\ x\ \tfrac{1}{4}\ \tfrac{1}{8};\ \bar{x}\ \tfrac{3}{4}\ \tfrac{1}{8};\ \tfrac{3}{4}\ x\ \tfrac{7}{8};\ \tfrac{1}{4}\ \bar{x}\ \tfrac{7}{8}$$

with $x = 0.73 \pm 0.01$.

The structure found by Pauling and Brockway is essentially a supperlattice on that of zinc blende, Fig. 7-a . Each sulphur atom is surrounded by four metal atoms, two copper and two iron, at the corners of a nearly regular tetrahedron, while each metal atom is similarly surrounded by four sulphur atoms. The sulphur displacement from the center of its metal coordination tetrahedron was later determined by Donnay et al.[25] using neutron diffraction. The value found, $\varepsilon = 0.02$, confirmed the PB structure.

The results found by Pauling and Brockway led to the following interatomic distances:

$$Cu\text{-}S = 2.32\text{Å}\ ,\quad Fe\text{-}S = 2.20\text{Å}\ ,\quad S\text{-}S = 3.56\text{Å}\ .$$

Assuming that the values for the tetrahedral electron-pair bond radii effective for these elements[26-27] in other crystals could be applied to chalcopyrite:

S- 1.04Å, Cu^{I} - 1.35 Å, Fe^{II} - 1.19Å, Fe^{III} - 1.13Å, with no value for Cu^{II}; the radius sums:

$$Cu^{I}\text{-}S = 2.39\text{Å} \quad \text{and} \quad Fe^{III}\text{-}S = 2.17\text{Å}$$

were not in good agreement with the results above.

Hence, they assumed that the atoms had no fixed valence and were fluctuating between the two states

$$Cu^{I}\ Fe^{III}S_2 \quad \text{and} \quad Cu^{II}Fe^{II}S_2$$

In 1934, BUERGER and BUERGER[28] established the existence of a second form of chalcopyrite, which they designated as high-temperature chalcopyrite. According to their findings, it was a disordered structure when compared with the ordered normal or low-temperature chalcopyrite.

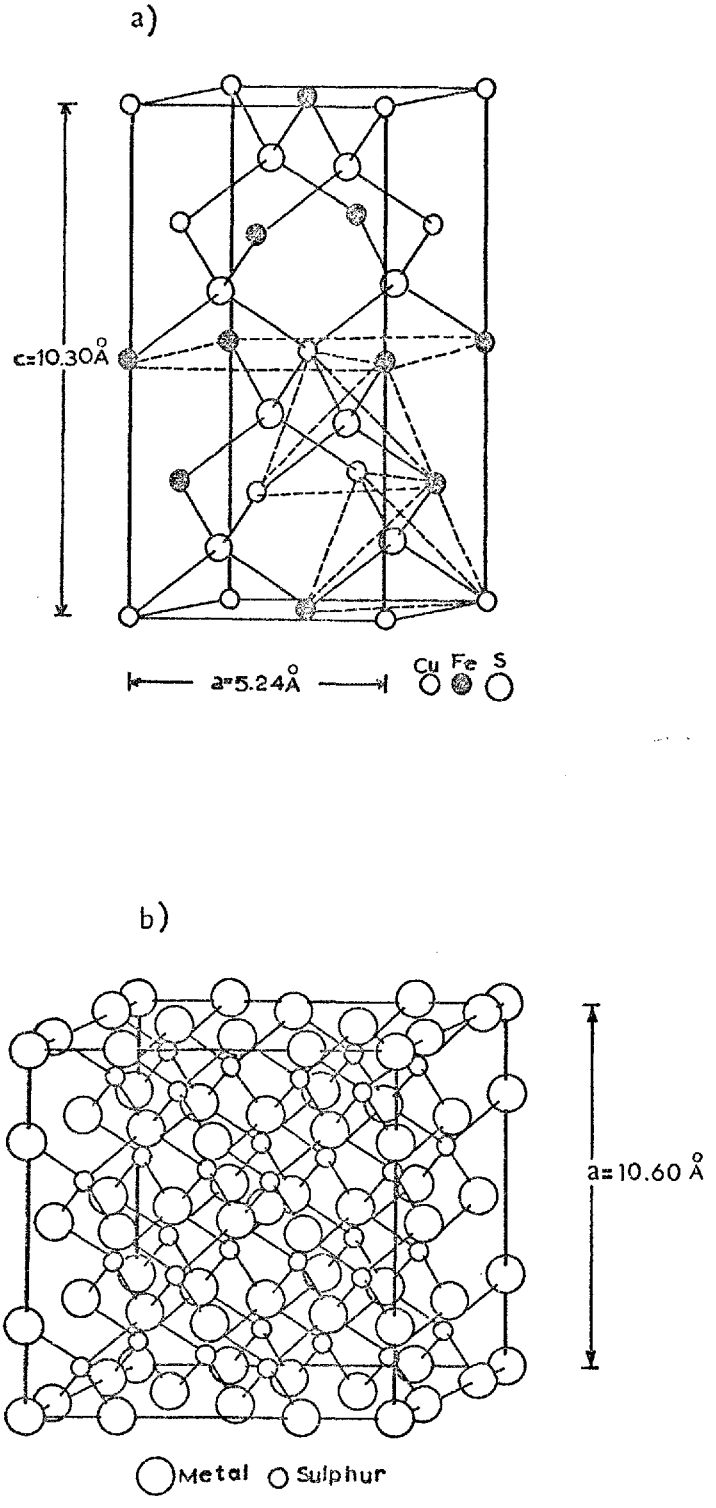

Fig. 7. Low and high-temperature chalcopyrite

a) Low temperature chalcopyrite (α) according to Pauling and Brockway(24).

b) High-temperature chalcopyrite (β) according to Hiller and Probsthain (34)

In the same year, KÔZU and TAKANÉ[29] studied chalcopyrite from Arakawa (JAPAN) using Cu and Mo radiations to take Laue, oscillation and rotation patterns. They found the same structure reported by Burdick and Ellis. The cell dimensions and the axial ratio obtained were

$$a = 5.28\ \text{Å},\quad c = 5.22\ \text{Å} \text{ and } c/a = 0.989$$

Results obtained form experiments with rotation and Laue photographs could be explained satisfactorily using these parameters.

From the same rotation photographs values of sin θ were obtained, and using reciprocal lattices, the corresponding indices were determined, showing that the values of h, k and l were wholly even or wholly odd. Identical results were obtained with Laue photographs, with unmixed indices of the spots, indicating a face-centered-like lattice.

The above results, morphological studies and reflections measurements led Kôzu and Takané to conclude that chalcopyrite belonged to the tetragonal sphenoidal class, space group D_{2d}^{5} - $P\bar{4}m2$, cell dimensions as mentioned with two "molecules" of $CuFeS_2$ contained in the unit cell and atomic positions:

$(000;\ \frac{1}{2}\ \frac{1}{2}\ 0)$ +

2Cu at 000

2Fe at $\frac{1}{2}\ 0\ \frac{1}{2}$

4S at $\frac{1}{4}\ \frac{1}{4}\ z,\ \frac{1}{4}\ \frac{3}{4}\ \bar{z}$

with $z = 0.25 - 0.26$.

In 1944 BOON[30] investigated the structure of chalcopyrite from an undisclosed locality. In order to increase the effective difference in the scattering powers of copper and iron he used a radiation close to the K absorption edge of Fe (in fact CoK radiation), the scattering factor of Fe diminishing and the Cu scattering factor remaining constant without secondary blackening resulting (See also Section 2.3.4). Using rotation methods Boon confirmed the structure described by Pauling and Brockway.

CHERITON[31] in 1953 claimed the existence of a cubic synthetic high-temperature modification (inversion temperature at 540°C) later confirmed by other authors.

In 1954 FRUEH[32] applied the use of zone theory to chalcopyrite, giving a new approach to the explanation of its structure. He criticized the excessive attention given to the covalent nature and partial ionic character of the bonds compared with the almost neglected possibility of a metallic type bond. He mentioned the importance of the structures of the individual atoms in determining bond type. The covalent bond approach to the chalcopyrite structure assumes that copper forms tetrahedral sp^3 bonds, and that iron, being capable of great flexibility in the use of its outer orbitals , is very likely to form sp^3 bonds.

Frueh then, while making an analysis of the ternary diagram Cu-Fe-S, pointed out the factor which determines the limit of solubility and the appearance of a different phase. This is the formation of the "electron compounds" (Hume-Rothery), these corresponding to definite ratios of free electrons to atoms. For the application of zone theory to the sulphide system, Frueh pointed out that these minerals exhibit the properties of intrinsic semi-conductors and therefore he assumed that free electron states exactly filled one of the zones, with an energy gap between the filled zone and the next higher zone. The value of this energy gap 0.53 eV was determined later (1956) by Austin et al.[33] and corresponds to that of a normal semi-conductor. Frueh then gave the principal Brillouin zones of the minerals of the copper-rich side of the Cu-Fe-S system and the electron-to-atom ratios necessary to fill these zones, listed below for the case of chalcopyrite

	Indices of forms determining principal zones	Electron-to-atom ratio of filled zone
a)	((112)) ((200)) ((004))	1
b)	((204)) ((220))	4

These values were determined knowing that each Brillouin zone has a volume which is a measure of ½ the number of electron states comprising the zone (the Pauli exclusion principle allows each energy state to be occupied by two electrons of opposite spin). This means that the electron-to-atom ratio necessary to fill a zone will be equal to twice the volume of the zone multiplied by the atomic volume (volume of the unit cell divided by the total number of atoms).

For the two forms given above and using integral expressions Frueh worked out:

a) $V_{zone} = \frac{4}{a^3}$ $\qquad V_{atomic} = \frac{a^3}{8}$ (assuming axial ratio $\frac{a}{c} = \frac{1}{2}$)

b) $V_{zone} = \frac{16}{a^3}$ $\qquad V_{atomic} = \frac{a^3}{8}$

Assuming that all the electrons of the outer shell of the elements contributed to the free electrons, he stated that chalcopyrite will have 4 electrons per atom (three from the iron, one from copper and six from sulphur). These 4 electrons will fill exactly one of the important Brillouin zones.

It is interesting to quote his conclusions:

"In sulphide minerals, where the cohesive forces appear to be metallic in nature, an important part of the energy is due to the energy states of the free electrons. The periodic structure of the mineral determines bonds or zones of energy levels that can be occupied by the electrons. A structural type is maintained despite changes in composition when the electron-to-atom ratio necessary to fill one of its Brillouin zones is maintained. To accomplish this, vacancies are created in certain positions. These vacancies increase the energy of the crystal in varying degrees, depending upon the importance of the original position in maintaining the structure".

Two years later (1956) an extensive work by HILLER and PROBSTHAIN[34] appeared on thermal and x-ray investigations on chalcopyrite. They found three possible types for chalcopyrite that they designated as α, β and γ, but without implying any statement about eventual polymorphic relations between them:

$CuFeS_2$ - normal or α-chalcopyrite

$Cu_{17+x}Fe_{17+x}S_{32}$ (with x = 0.6) β-chalcopyrite ($\simeq CuFeS_{1.82}$)

$CuFeS_{2-x}$ (x having a wide range) γ-chalcoprite

As can be seen, β and γ are sulphur deficient forms of normal α-chalcopyrite.

Hiller and Probsthain observed that when normal α-chalcopyrite was heated in a nitrogen filled oven, it changed to a high-temperature mixed-crystal phase (γ) at 550°C, the sulphur content decreasing with increasing temperature up to about 720°C when an end product with the lowest content in sulphur was found (β). They also showed that α appeared together with β on cooling, whenever the heating was interrupted between 550° and 720°C, the percentage of α decreasing with increasing temperature until β was obtained alone.

The results of a thermogram traced by these authors were:

Temperature °C	Loss of weight %	X-ray results
434	0	α
500	0.4	α
586	0.9	α + β
620	2.0	α + β
650	2.3	α + β
700	2.5	traces of α + β
750	3.0	β

Apparently the metastable form γ was retained at room temperature by quenching sealed vessels previously heated between 550° and 720°C. It transformed, however, to the stable β form, which on reheating changed back to γ at 230°C. Hiller and Probsthain's tests showed that after 4 hours the γ-phase could still be recognized besides β , disappearing completely after about 3 days.

The analysis of the table presented above shows the need of a total weight loss of 3% corresponding to a sulphur deficit of about 9% for the formation of the β-phase.

From their findings, that between α and β on the one hand, and between β and γ on the other, no intermediate products were observed, it follows that α, β and γ were three independent phases and not the end products of a region with a continuous change of lattice constants.

It is also clear that at room temperature the two phase region α + β extends approximately from $CuFeS_{1.82}$ to $CuFeS_{1.95}$, while the region $CuFeS_{1.95}$ - $CuFeS_2$ can be considered as natural chalcopyrite.

An interesting point in their experiment was that α and γ were never observed together.

When determining the structure of β they were unable, using Debye-Scherrer photographs, to decide if there was an order-disorder relationship between α and β. However, using rotating crystal photographs they obtained weak but clear superstructure reflections which made necessary a doubling of the a-axis whilst the c-axis remained unchanged. Thus, it excluded an ordered distribution of metal atoms in the zinc positions of the zinc blende base lattice, that would lead to a smaller cell volume, and also a primitive cubic lattice that would give different intensities of reflection.

According to Hiller and Probsthain, the superstructure of the β-phase is therefore not originated by an ordering of the metal atoms, confirming with limitations the existence of a disordered form of chalcopyrite proposed by Buerger and Buerger[28].

For the determination of the true structure Hiller and Probsthain assumed that the zinc-blende-like ground structure remained, and the superstructure could only be due to deviations from the simple rational relation of metal to sulphur. From the results obtained with x-rays and picnometric density measurements ($D=4.35 \pm 0.05 g\ cm^{-3}$) they concluded that there was excess metal atoms incorporated in interstitial positions. In this case the theoretical value for the density would be $4.40 g\ cm^{-3}$, in agreement with the experimental value.

Finally, they assumed the space group $I\bar{4}3m$, a = 10.60Å, and based in the total formula $Cu_{17.6}\ Fe_{17.6}\ S_{32}$ the equipoint-set:

2 Me at (a)
0.9 Me at (b)

cont/....

8 Me	at (c)	with $x = \frac{1}{4}$
10.71Me	at (d)	
10.71Me	at (e)	with $x = \frac{1}{4}$
2.81Me	at (g)	with $x = \frac{1}{4}$, $z = 0$
35.2 Me	(17.6 Cu + 17.6 Fe)	

8 S	S at (c)	with $x = \frac{1}{8}$
24 S	S at (g)	with $x = \frac{3}{8}$, $z = \frac{1}{8}$
32 S		

On Fig. 7-b only the main positions are shown, so as to give a better view. The remaining tetrahedral gaps which can still accept metal atoms lie in the middle of the edges and surfaces, or at the center of the faces of the octahedron.

As can be seen the structure of the β-phase represents a transition from zinc-blende to antifluorite type. However, essentially, the zinc-blende structure remains.

Microscope examination of the cubic β-phase did not show the weak anisotropy effect of the α-form confirming therefore the x-ray results.

Hiller and Probsthain did not elucidate completely the structure of the γ-phase but they were able to define it as a tetragonal superstructure cell with a = 10.58Å and c = 5.37Å.

DONNAY and KULLERUD[35] in 1957-58 confirmed the existence of a cubic, high-temperature modification of chalcopyrite with a=5.264 ± 0.003Å and diffraction aspect F***. However, their conclusions did not entirely agree with the peculiar behaviour of chalcopyrite which they had observed.

In 1958 a detailed study of the magnetic structure of natural chalcopyrite was published by DONNAY et al.[25] and the results strongly suggest the existence of antiferromagnetism. For the crystal structure determination they used a sample from Japan, the same ore used by Kôzu and Takané, and a specimen from Joplin (U.S.A.), both giving diffraction aspect I** d. The results of structure analysis indicated a magnetic moment of zero for copper (or at most 0.2μB), suggesting valence I for Cu

and III for Fe, and a moment for iron of 3.85 μB, values consistent with a covalent model and sp^3 hybrid orbitals, providing that further participation of 3d electrons of iron in the covalent bond occurs, decreasing the iron moment(*), and making Fe-S bonds stronger. This idea is supported by the fact that sulphur atoms are displaced from the centre of the metal tetrahedra towards the Fe-Fe atom pair.

FRUEH in 1958[36] considered that the transition to cubic form that occurs at about 550°C in chalcopyrite is of the order-disorder type, involving the interchange of cations among the cationic positions. He assumed that above 550°C Fe and Cu atoms are randomly arranged in the positions of tetrahedral co-ordination of a face-centered cubic sulphur structure, but unlike Hiller and Probsthain, he determined a value of a = 5.29Å. Frueh discussed the effect of thermal treatment on chalcopyrite, and concluded that the low temperature form of chalcopyrite (tetragonal - c<2a) transforms to the high-temperature form (cubic) upon heating, a change occurring not only in the relative positions of the cations but also in the dimensions of the sulphur framework.

The thermal transformation between 200° and 1000°C of chalcopyrite in argon atmosphere was studied by SHIMA in 1962[37]. Thermogravimetry, X-ray and reflecting microscopic examinations were used to follow this transformation. Both the thermogravimetry and differential-thermal analysis curves suggested some endothermic reaction or transformation at 540-550°C, corresponding to the change of tetragonal α-chalcopyrite into cubic β-chalcopyrite.

SHIMA also found that chalcopyrite dissociates into bornite and pyrrhotite at about 850°C.

YUND and KULLERUD in 1966[38] confirmed that the stable form of chalcopyrite at 700°C was isometric. Cooling, even at the most rapid rate possible, with a ratio Cu:Fe near one and Me:S also near one (maximum sulphur content) the inversion to the tetragonal form took place at 547±5°C. With Me:S near maximum (minimum sulphur content) no inversion occurred and the isometric form was retained at room temperature. Over periods of 5 years these authors did not observe any change in the isometric form.

(*) $\mu_{Cu^+} = 0\mu B$ $\mu_{Fe^{++}} = 4\mu B$

$\mu_{Cu^{++}} = 1\mu B$ $\mu_{Fe^{+++}} = 5\mu B$

However, compositions between the two extremes considered, gradually inverted to the tetragonal form, on storage for extended periods of time at room temperature.

ARAMU and BRESSANI[39] (1967) studied the Mössbauer effect of chalcopyrite, the samples being powdered ore from "Funtana Raminosa" mine (Sardinia).

From the spectra obtained and analysis of the results, they considered that the relative probability of the presence of electrons at iron nuclei in chalcopyrite ($CuFeS_2$) is greater than that assuming the iron to be in the pure ionic state Fe^{3+}. This fact associated with the semiconducting properties of chalcopyrite, which can occur with covalent bonding, led Aramu and Bressani to suggest a resonance between the limiting formulae:

$$\underset{\text{(ionic)}}{Cu^{+}\ Fe^{+++}\ S_2^{--}} \leftrightarrow \underset{\text{(covalent)}}{Cu^{---}\ Fe^{-}\ S_2^{++}}$$

corresponding to the following configuration:

$$3d^{10}\ (Cu^{+})\ 3d^{5}\ (Fe^{+++})\ 2\ [3s^2p^6]\ (S^{--})_2 \leftrightarrow$$

$$\leftrightarrow 3d^{10}/4sp^3\ (Cu^{---})\ 3d^5/4sp^3\ (Fe^{-})\ 2\ [3sp^3]\ (S^{++})_2$$

This hypothesis is consistent with the crystallographic data of Pauling and Brockway[24] and neutron diffraction experiments of Donnay et al.[25].

(40)

In the same year (1967), a paper by MARFUNIN and MKRTCHYAN appeared on the Mössbauer spectra in sulphides. After general considerations they start by dividing the sulphides in the following categories:

a) sulphides with complex radicals, covalent

$[S_2]^{2-}$ — pyrite, marcasite

$[AsS]^{3-}$ — arsenopyrite

$[As_2]^{2-}$ — loellingite

b) sulphides with complex radicals, ionic

$[SbS_2]^-$ — berthierite

$[SnS_4]^{4-}$ — stannite

c) sulphides without complex radicals

Fe_4^{3+} — chalcopyrite, bornite

Fe_4^{2+} — cubanite, sphalerite, pentlandite

Fe_6^{2+} — troilite, pyrrhotite

and using existing date as well as their experimental results obtained from Mössbauer spectroscopy measurements, Marfunin and Mkrtchyan analysed each of the above mentioned groups.

For the chalcopyrite measurements these authors used a sample of tetragonal ore from Talnakh and an "isometric" chalcopyrite sample from the same locality. From their findings and comparison with other data they concluded that in tetragonal chalcopyrite, iron occurs in the Fe^{3+} state. However, the spectrum for "isometric" chalcopyrite, although similar to the tetragonal previously obtained, was found to be not very clear and any conclusions about the oxidation state of the iron in this form should be taken with reserve.

In 1967, ZUEV[41] established empirical rules on maximum and minimum parameters, permitting the determination of valence-equilibrium states of atoms in complex compounds. For this purpose he used the example of tetragonal chalcopyrite in the two possible variants $Cu^{I}\ Fe^{III}\ S_2$ and $Cu^{II}\ Fe^{II}\ S_2$.

According to Zuev the most stable form, $Cu^{I}\ Fe^{III}S_2$, had the following maximum parameters (Table 1):

i) maximum energy of the crystal lattice (U),

ii) maximum difference ($\Delta E = E_a - \bar{E}_k$) of electronegativity of anionic part (E_a) and average electronegativity of

cationic part ($\bar{E}_k = \frac{E_{Cu} + E_{Fe}}{2}$) of the compound, and average value for the amount of ionic character, and effective charge of the atoms,

iii) maximum completion of the electron shells of metal atoms;

and the minimum parameters

i) minimum total magnetic moment of atoms in the limiting ionic form of the compound
ii) minimum average electronegativity of the cationic part of the compound ($\bar{E}_k$),
iii) minimum difference (ΔE_k) of electronegativity in the cationic part of the compound.

TABLE 1

A - Maximum Parameters

	$Cu^{I}\ Fe^{III}\ S_2$	$Cu^{II}\ Fe^{II}\ S_2$
U, (Kcal $mole^{-1}$)	1950	1700
$\Delta E = E_a - \bar{E}_k$, (eV)	0.8	0.75
Configuration Cu	$3d^{10}$	$3d^{9}$
Configuration Fe	$3d^{5}$	$3d^{6}$
Effective cationic charge	+ 1.28	+ 1.20
Average value for i	0.66	0.65

B - Minimum Parameters

	$Cu^{I}\ Fe^{III}\ S_2$	$Cu^{II}\ Fe^{II}\ S_2$
Total magnetic moment, (μ,B)	5.92	6.63
$\bar{E}_k$, (eV)	1.8	1.85
ΔE_k, (eV)	0	0.3

For the computation of the electronegativities Zuev presented

the equation

$$E = \frac{\sum_{n=1}^{n=n} \frac{I_n}{n}}{n} + A$$

where the first term of the second member is the average potential of ionization of an atom to the n-charge state and A the electron affinity.

Electronegativities for an extensive group of atoms for the various valence-states were calculated by this author using existing data on the potentials of ionization and electron affinities.

Applying this method for the chalcopyrite atoms he derived:

E_S = 2.6 eV (2.6 by thermochemical calculations)

E_{Cu^I} = 1.7 eV (1.8 by t.c)

$E_{Cu^{II}}$ = 1.9 eV (2.0 by t.c)

$E_{Fe^{II}}$ = 1.5 eV (1.7 by t.c)

$E_{Fe^{III}}$ = 1.7 eV (1.8 by t.c)

Zuev analysed in detail the two basic opinions concerning the valence of copper and iron in chalcopyrite. Thus, according to Pauling and Brockway's[24] view, a fluctuation takes place between $Cu^{I}Fe^{III}S_2$ and $Cu^{II}Fe^{II}S_2$, and according to the theory developed in terms of the physics of semiconductors and crystal chemistry, $Cu^{I}Fe^{III}S_2$ describes chalcopyrite. Besides the results already mentioned in the present report on the magnetic properties of chalcopyrite (Donnay et al.[25]), he quoted criteria of interatomic distances and energetic considerations.

Bearing in mind that in a stable system the energy tends towards a minimum, Zuev showed that, Table 1, $Cu^{I}Fe^{III}S_2$ with ΔE_k=0 described chalcopyrite whereas $Cu^{II}Fe^{II}S_2$, ΔE_k=0.3, could be considered as a non-equilibrium system.

Also, the greater the difference between the electronegativities of combining atoms the more stable is the compound

($\Delta E_{Cu^{I}Fe^{III}S_2} = 0.8$, $\Delta E_{Cu^{II}Fe^{II}S_2} = 0.75$)

Calculations of crystal lattice energy using existing data showed that $U(Cu^{+1}Fe^{+3}S_2^{-2}) > U(Cu^{+2}Fe^{+2}S_2^{-2})$ and the first variant is therefore the more stable. Consequently, he concluded that from the point of view of energy, fluctuation of the two structures is unlikely and chalcopyrite apparently is described by $Cu^{I}Fe^{III}S_2$.

Referring to the covalent bond approach constructed on the basis of ordinary σ-bonds of the sp^3 hybrid orbitals, Zuev presented the configurations of the two variants for the limiting covalent and limiting ionic forms

A) $Cu^{I}\ Fe^{III}\ S_2$

i) Limiting ionic $Cu^{+}\ Fe^{+++}\ S_2^{--}$

ii) Limiting covalent $Cu^{\downarrow\downarrow\downarrow\downarrow---}\ Fe^{\downarrow\downarrow\downarrow\downarrow-}\ S_2^{\uparrow\uparrow\uparrow\uparrow++}$

where

Cu^{---} activated [Ar] [↑↓I↑↓I↑↓I↑↓I↑↓] [↓] [↓I↓I↓]
$3d^{10}$ $4sp^3$

Fe^{-} activated [Ar] [↓I↓I↓I↓I] [↓] [↓I↓I↓]
$3d^{5}$ $4sp^3$

S^{++} activated [Ne] [↑] [↑I↑I↑]
$3sp^3$

B)= $Cu^{II}\ Fe^{II}\ S_2$

i) Limiting ionic $Cu^{++}\ Fe^{++}\ S_2^{--}$

ii) Limiting covalent $Cu^{\downarrow\downarrow\downarrow\downarrow--}\ Fe^{\downarrow\downarrow\downarrow\downarrow--}\ S_2^{\uparrow\uparrow\uparrow\uparrow++}$

The redistribution of electrons in neutral atoms for the hypothetical limiting covalent formula provides formal charges, and sulphur atoms being more electronegative try to attract bonding pairs of electrons.

In order to determine the partial ionic character (i), Zuev used the relation

$$Q = (1-i)\ Q_k + i\ Q_I$$

where Q is the effective charge of the atoms, Q_k the limiting covalent charge and Q_I the limiting ionic charge. Assuming that the difference of electronegativity ΔE must determine the degree of transition of the valence electrons from one atom to the other he presented the relation

$$\Delta E = \frac{Q}{Q_I},$$

obtaining by simple proportions the following effective charges.

$Cu^{I}\ Fe^{III} S_2$ $\qquad$ $Cu^{+0.32}\ Fe^{+0.96}\ S_2^{-0.64}$

and

$Cu^{II}\ Fe^{II}\ S_2$ $\qquad$ $Cu^{+0.48}\ Fe^{+0.72}\ S_2^{-0.60}$

With the Q values so obtained and using the relation Q = f(i) mentioned above, Zuev determined the average value for the amount of ionic character, as shown in Table 1 .

He also referred to the tendency towards maximum completion of the electron shell of metal atoms, illustrated by the copper atom ($d^{10}s^2p^6$) only in the case of the $Cu^{I}\ Fe^{III} S_2$ variant.

Quoting work of Donnay et al.[25] on the problem of low magnetic moment for iron atoms, (already mentioned in the present report), Zuev suggested that, out of five uncoupled, two Fe^{III} electrons are "free", meaning by this that they take part in the metal bond and are statistically compensated by two corresponding uncoupled electrons of other atoms of iron. Thus, with these delocalized bonds Fe-Fe, he explained the "metallic" properties such as colour, lustre and conductivity.

Finally, he referred to the general valence of the iron in chalcopyrite as being equal to 5, as 3 electrons participate in Fe-S bonds while 2 electrons participate in the bonds Fe-Fe. It is difficult to see what is meant by this conclusion.

In 1968, BORSHAGOVSKII et al.[42] confirmed the presence of Fe^{3+} in tetragonal chalcopyrite, and several other authors[43-44] directed their attention to this problem.

From this literature survey on the crystal structure of chalcopyrite it is evident that there is no unanimity of opinion, although the general consensus is to consider the low temperature natural form of chalcopyrite as tetragonal.

A brief survey of the results obtained by the above mentioned workers, summarized in Table 2 shows that there are a number of questions which remain unanswered.

An important factor that affects the number and intensity of the reflections, and consequent determination of the structure, is the suitable choice of radiation for X-ray analysis (see Section 2.3.4).

Another aspect that should be taken into consideration is the purity of the natural ores used by these investigators, although an effort was made by them to select specimens as pure as possible. Apparently, the location where the samples were taken from also plays an important part in the results obtained.

The few suggestions of the existence of a cubic low temperature natural chalcopyrite(*) from Noril'sk (Siberia) as mentioned by Bud'ko and Kulagov[45], and GenKin et al.[46], were subsequently shown to be doubtful, (Cabri[47]), and Marfunin and Mkrtchyan's[40] report of an isometric sample from Talnakh must be looked upon with reserve.

The chemical structure for the low temperature tetragonal chalcopyrite suggested by Pauling and Brockway[24], $Cu^{I}Fe^{III}S_2 \leftrightarrow Cu^{II}Fe^{II}S_2$, and the resonance between hypothetical limiting ionic and covalent configurations suggested by Aramu and Bressani[39] and by Zuev[41] seem to be incorrect, although they explain some properties (even structural) of this double sulphide.

(*) The very first results obtained by Burdick and Ellis and Gross and Gross, due to the analytical limitations of the equipment used, are normally considered as having only an historical value.

They must be considered as a useful tool in, for example, describing certain behaviour assuming a partial ionic character, or the use of covalent bonding, but not as a definitive description of the structure.

Freuh's[32] approach in terms of zone theory is perhaps the most elegant and the one that suits best the known properties and behaviour of low temperature tetragonal chalcopyrite.

TABLE 2

Low Temperature Chalcopyrite

Worker	Location	Target used	Tetragonal Structure (a,c in Å)	Pseudo Cubic Structure (a,c in Å)
Burdick & Ellis (22)	Pennsylvania (USA)	Pd		FCC {a= 5.24, c= 5.15
Gross & Gross (23)	Arakawa (Japan)	?		FCC {a= 5.270, c= 5.194
Pauling & Brockway (24)	Joplin-Missouri (USA)	Mo	$I\bar{4}2d$ {a= 5.24, c=10.30	
Kôzu & Takané (29)	Arakawa (Japan)	Cu&Mo	$P\bar{4}m2$ {a=5.28, c=5.22	
Boon (30)	?	Co	$I\bar{4}2d$ {a= 5.24, c=10.30	
Donnay et al. (25)	Arakawa (Japan)	?	I**d	
Donnay et al. (25)	Joplin-Missouri (USA)	?	I**d	

High Temperature Chalcopyrite

Worker	Transition Temperature, °C	Structure (a,c in Å)
Buerger & Buerger[28]		Disordered
Cheriton[31]	540	Cubic
Hiller & Probsthain[34]	550(?)	β-cubic, $I\bar{4}3m$ {a= 10.60
Hiller & Probsthain[34]		γ-Tetragonal(?) {a= 10.58, {c= 5.37
Donnay & Kullerud[35]		Cubic, F*** {a= 5.264±0.003
Frueh[36]	550	Cubic, disordered {a=5.29
Shima[37]	540-550	Cubic
Yund & Kullerud[38]	547±5	Cubic

1.3 Phase Relations in the Cu - Fe - S System

The Cu-Fe-S system has been extensively investigated from temperatures as low as 25°C to temperatures up to 1100°C [48-52]. However, there are still many uncertainties specially at low temperatures and the phase relations for this complex system are far from being solved.

MERWIN and LOMBARD[50] produced the first detailed study of this system at 455 mm pressure of sulphur vapour and variable temperature, and from then on several important contributions to this investigation were published. In Fig. 8-a and 8-b are represented two phase diagrams for the relation in the Cu-Fe-S system at 25°C by two different authors and the discrepancy between them is clear.

Fig. 9 to 13 were taken from YUND and KULLERUD[38-49] and they show isothermal sections at 200°-500°-900°-1000° and 1100°C, and a detail of chalcopyrite solid solution at 700°C.

According to the findings of these authors there are three main areas to be considered at high temperatures. As shown in Fig. 8-b and 11 the first solid solution field is that of pyrrhotite and is quite limited except at high temperatures. The second one, the large single-phase area including Cu_2S (chalcocite), $Cu_{1.8}S$ (digenite) and Cu_5FeS_4 (bornite) is normally designated as bornite solid solution, becoming at lower temperatures two one-phase areas, the larger area including stoichiometric bornite. Finally, the third is the chalcopyrite solid solution and occurs at temperatures above 550°C. It is a one-phase field extending at 700°C from a Cu/Fe atomic ratio of approximately 1.5 to a composition near to cubanite ($CuFe_2S_3$) with a Cu/Fe atomic ratio slightly greater than 0.5, the metal to sulphur ratio varying from slightly over 1 to at least 1.17. It is interesting to note that this solid solution does not include the stoichiometric compositions $CuFeS_2$, $CuFe_2S_3$ or $Cu_3Fe_4S_6$.

On isothermal sections below 550°C the chalcopyrite solid solution becomes two one-phase areas, the chalcopyrite and the cubanite phases.

In the range of higher temperatures the detailed study by KULLERUD[49] covers from 700°C to temperatures above 1100°C. He has showed previously[51] that apart from the field of liquid immiscibility for the join Cu-Cu_2S above 1105°C determined by SCHLEGEL and SCHULLER[52], a second liquid immiscibility field covers the sulphur-rich portion of the system above 1083°C, these two fields being separated by a field of homogeneous liquid. At temperatures of about 1400°C the only solid phase in the system was metallic iron which melts at 1534°C. On cooling at 1192°C a pyrrhotite solid phase ($Fe_{1-x}S$) crystallized from the homogeneous liquid, followed at 1129°C by the crystallization of a chalcocite type (Cu_2S) solid phase. At 1067°C out of the Cu liquid crystallized the Cu-S binary join, and metallic Cu coexisted with bornite solid solution near Cu_2S composition, and with Fe solid solution.

At about 960°C the crystallization of chalcopyrite phase occurring from the ternary homogeneous liquid, appearing with a content of 35 wt% Fe, 32.5 wt% Cu and 31.5 wt% S, corresponding to a metal-to-sulphur ratio of about 2:1.75. According to Kullerud, on cooling the sulphur content of the chalcopyrite phase increased quickly, and at the same time larger variations in the Cu-Fe ratio were tolerated.

At about 935°C, tie lines between chalcopyrite phase and pyrrhotite were established where a maximum solid solution of chalcopyrite in pyrrhotite existed. Chalcopyrite phase on the other hand contains a maximum of about 37.5 wt% Fe.

Cooling below this temperature, Kullerud found next that bornite and chalcopyrite solid solutions became stable together at 930°C.

At 900°C the stoichiometric composition $CuFeS_2$ still remained within the homogeneous ternary liquid field.

At 860°C the tie lines between ternary liquid and pyrrhotite can be replaced by chalcopyrite-liquid sulphur tie lines, once the liquid composition has moved toward the Cu-S join.

Pyrite appeared on the Fe-S join at about 743°C and finally tie lines were established between this phase and the chalcopyrite solid solution at 739°C.

Abbreviations used in this Section(*)

Phase	Abbreviation	Composition	Crystallography
Chalcocite	cc_o	Cu_2S	Orthorhombic
Chalcocite	cc_h	Cu_2S	Hexagonal
Chalcocite	cc	Cu_2S	Isometric
Djurleite	djur	$Cu_{1.96}S$	Low symmetry
Digenite	dig	$Cu_{1.8}S$	Isometric
Covellite	cov	CuS	Hexagonal
Pyrrhotite	po	FeS	Hexagonal
Marcasite	mar	FeS_2	Orthorhombic
Pyrite	py	FeS_2	Isometric
Bornite	bn_t	Cu_5FeS_4	Tetragonal
Bornite	bn	Cu_5FeS_4	Isometric
Idaite	id	$Cu_{5.5}FeS_{6.5}$	Hexagonal
Chalcopyrite	cp_t	$CuFeS_2$	Tetragonal
Chalcopyrite	cp	$CuFeS_2$(?)	Isometric
Cubanite	cb_o	$CuFe_2S_3$	Orthorhombic
Cubanite	cb_t	$CuFe_2S_3$	Tetragonal
Cubanite	cb	$CuFe_2S_3$	Isometric

and also:

2- Assemblage consisting of two condensed phases

S_L- Liquid sulphur

(*) According to those adopted by Yund and Kullerud[38].

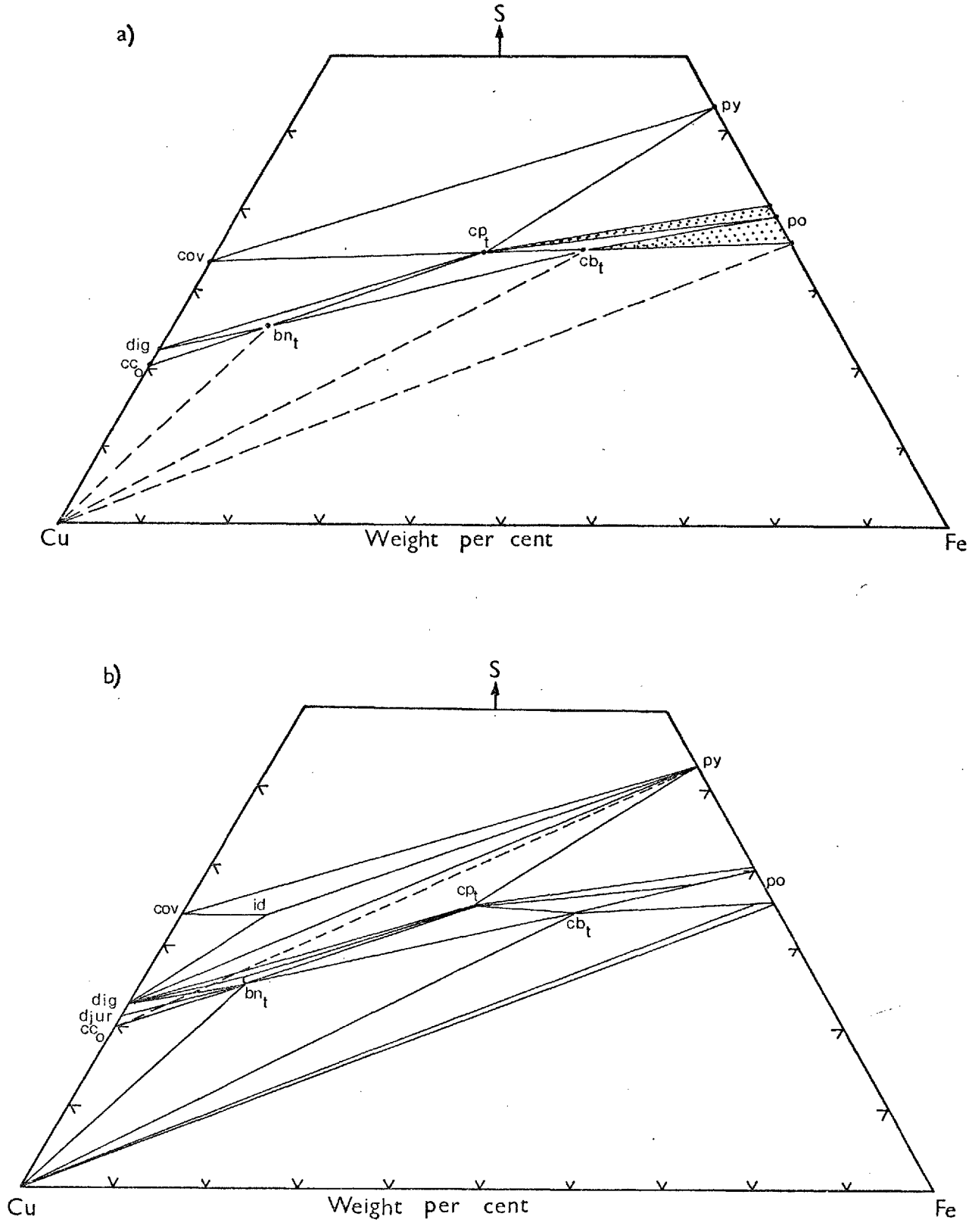

Fig. 8. Phase relations in the Cu-Fe-S system at 25°C

a) According to Bartholomé[48]

b) According to Barnes[48-a]

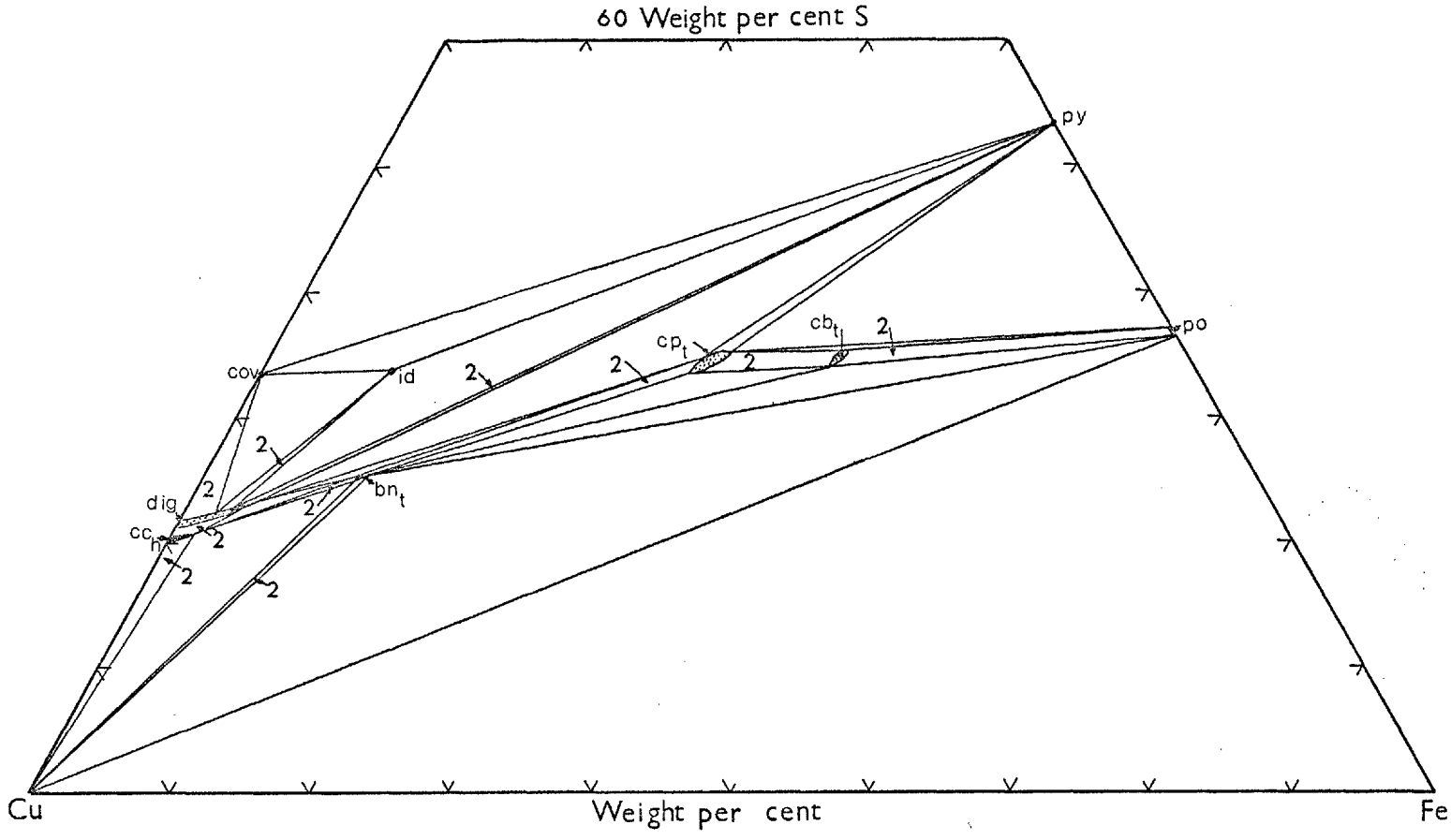

Fig. 9. Phase relations in the Cu-Fe-S system at 200°C - Yund and Kullerud(38)

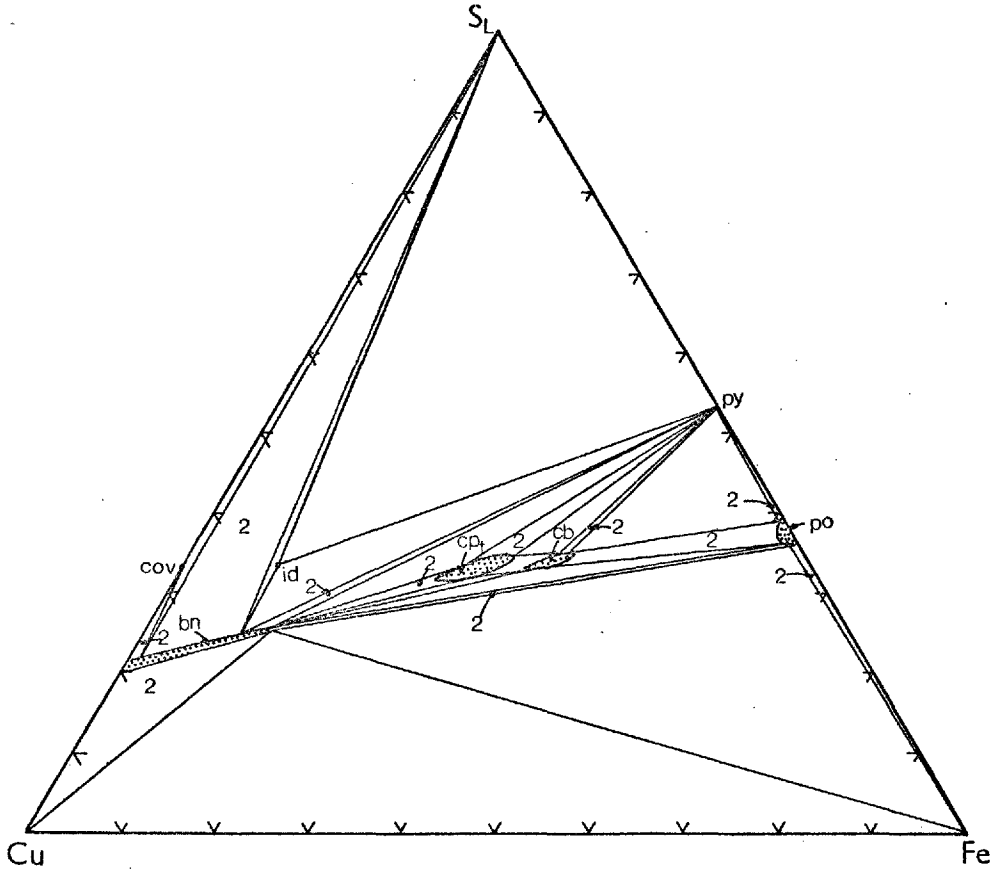

Fig. 10. Phase relations in the Cu-Fe-S system at 500°C - Yund and Kullerud(38)

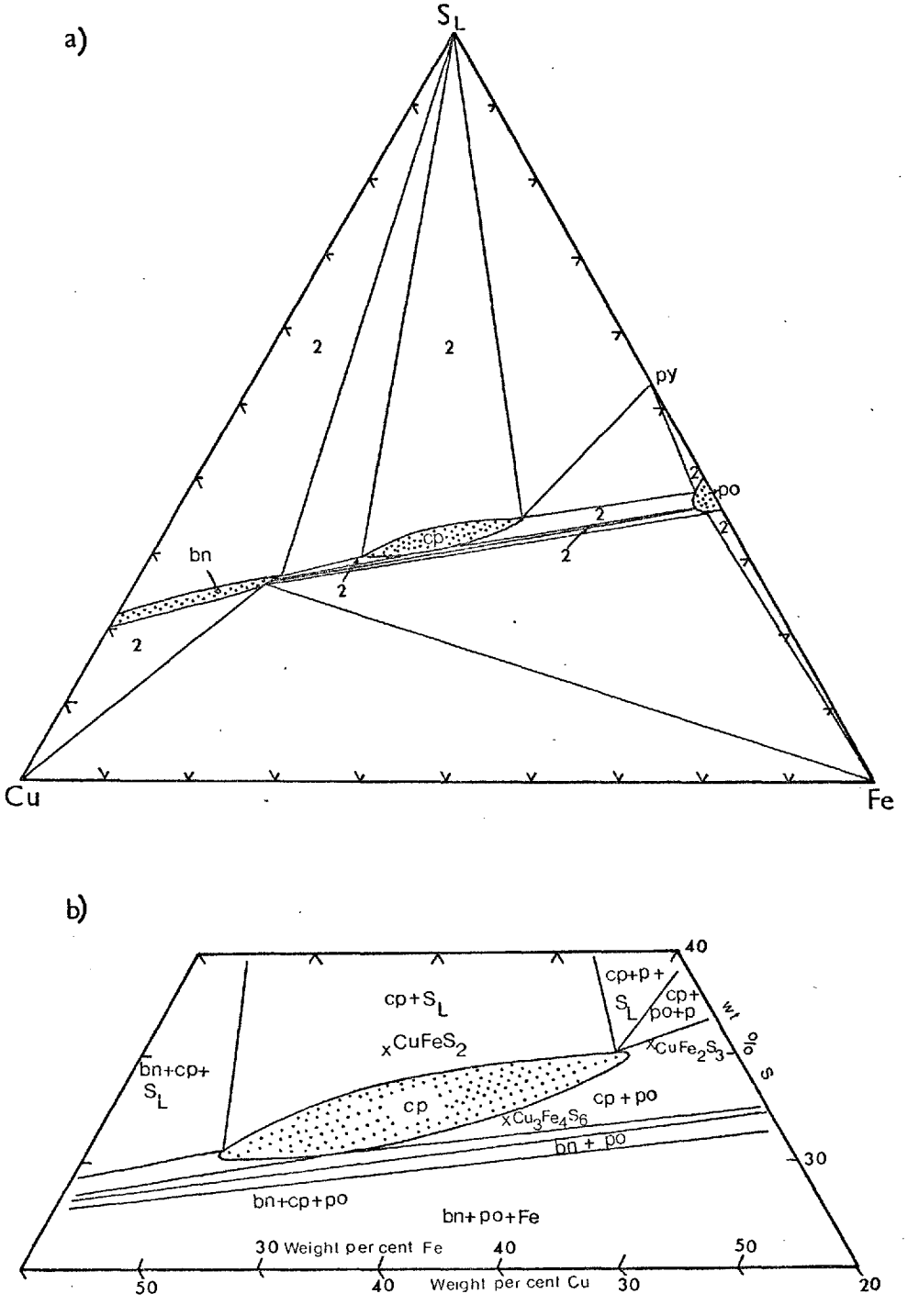

Fig. 11. Phase relations in the Cu-Fe-S system at 700°C - Yund and Kullerud(38).

a) 700°C isothermal section

b) Chalcopyrite solid solution at 700°C

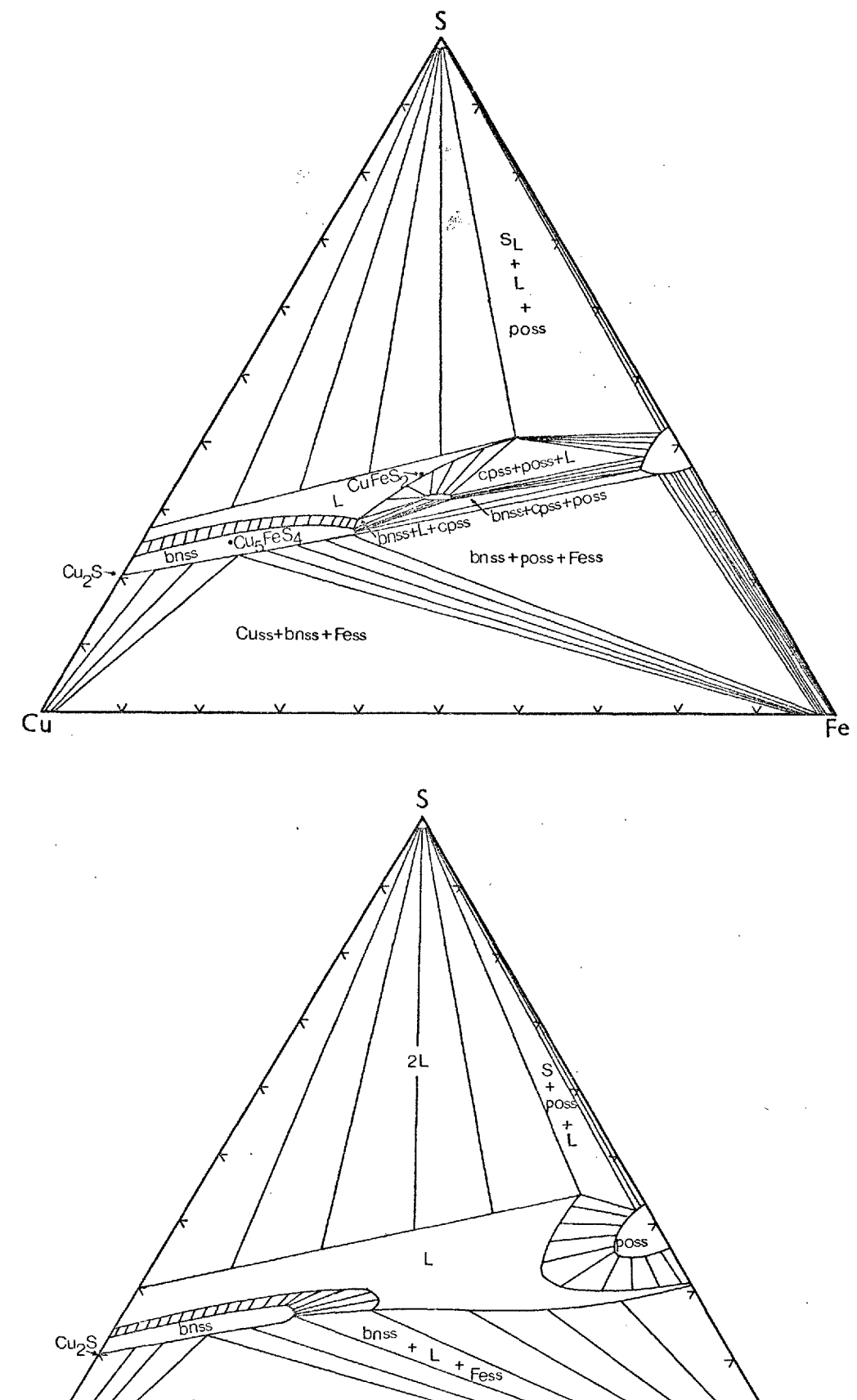

Fig. 12. Phase relations in the Cu-Fe-S system - Kullerud(49)

a) 900°C isothermal section

b) 1000°C isothermal section

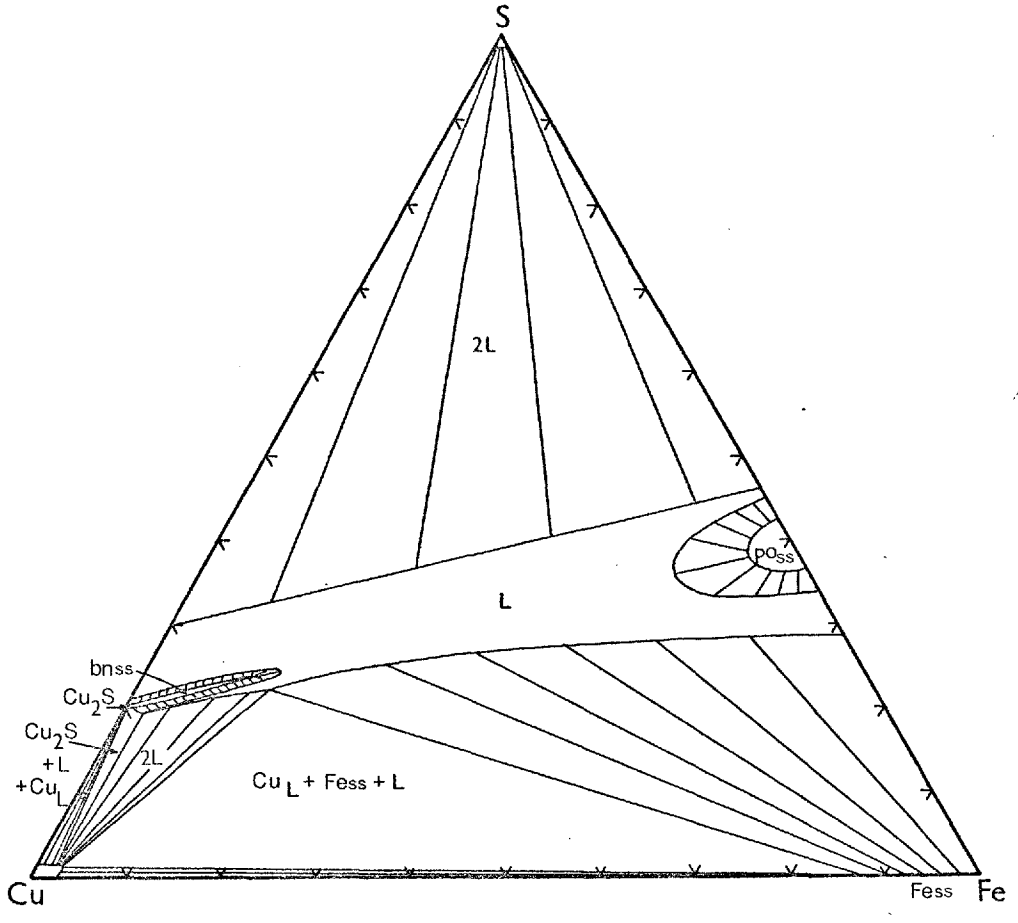

Fig. 13. Phase relations in the Cu-Fe-S system at 1100°C - Kullerud(49)

1.4 Previous Work on the Synthesis of Chalcopyrite

Generally both α- and β-chalcopyrites are prepared using stoichiometric amounts of copper, iron and sulphur required for the formula $CuFeS_2$.

HILLER and PROBSTHAIN[34] mentioned that synthetic samples of chalcopyrite were prepared in small sealed quartz tubes (used as melting vessels), by weighing the components in the required amounts. Sulphur deficient forms were obtained by allowing the small sealed tubes to explode at high temperatures, so that the excess sulphur could evaporate (section 1.2). The final products were checked by X-ray diffraction.

This process using stoichiometric amounts was apparently successfully used by DONOVAN and REICHEMBAUM[53] by melting the elements together in a sealed silica tube which fitted exactly a stainless steel bomb, and keeping the temperature in the range 900-1100°C for a period of 8-10 hours. No X-ray or other analysis of the final product obtained were made by these authors, apart from an electron microscope examination. They claimed no evidence of any free copper, iron or sulphur and assumed that the departures from stoichiometry were extremely small.

BRETT[54] in his work on experimental data from the system Cu-Fe-S, mentioned that elemental iron, sulphur and copper of high purity were used as starting materials for the synthesis of double sulphides.

KULLERUD[51] in his study of the Cu-Fe-S system, prepared gram batches of $CuFeS_{2-x}$ from the elements at 700°C. However, no details are given about the experimental conditions.

YUND and KULLERUD[38] used also the required proportion of the elements to synthesize double sulphides and in some cases, to increase the reaction rate, they first prepared mixture of copper and iron of the required composition, heating

the mixture in sealed silica-glass tubes at 1450°C to produce a homogeneous melt.

In the chalcopyrite case, for compositions with a Cu/Fe ratio of 1 and a maximum or near maximum sulphur content (metal to sulphur ratio near 1) gold tubes at 700°C were used with a total pressure of about 200 bars, obtaining a final product with 1.20 ± 0.25 weight per cent less sulphur than that of the stoichiometric $CuFeS_2$. X-ray and other analysis confirmed the wet chemical analysis. Using this method they were able to prepare samples with variable composition (section 1.2 - Crystal Structures), and therefore α tetragonal or β cubic forms alone or mixtures in different proportions.

DUTRIZAC et al.[15] prepared synthetic chalcopyrite using a method already described in section 1.1 . They started with the synthesis of CuS and $FeS_{1.002}$ from the elements, followed by sintering in a sealed silica tube, at 550°C for three days, of equimolar amounts of these sulphides, previously ground to -100 mesh, mixed and pressed at 80000 psi. The final product was found to be $CuFeS_2$ by X-ray diffraction.

More recently PANKRATZ and KING[55] used a rather complicated method for the synthesis of chalcopyrite, dissolving separately, copper and iron in HNO_3, dehydrating the solutions and igniting the residues to oxides. After a partial reduction of the iron oxide by H_2 this product was mixed in stoichiometric amounts with CuO and the mixture reduced in a H_2 stream. The sulphur was then added to the mixture in silica bulbs, placed in an ice bath as some reaction started occurring even at room temperature. The sealed bulbs were placed in a steel bomb and after an initial heating to 300°C overnight, they were kept at 650°-680°C for 3 days. Final adjustments in the stoichiometry were carried out after cooling, grinding and mixing in N_2 atmosphere.

The material was then reheated in the same way and finally checked by X-ray diffraction. The analysis gave the tetragonal α-chalcopyrite pattern.

With the information available from these previous workers a study was carried out to find the best conditions for the synthesis of chalcopyrite.

1.5 Sulphur Vapour pressure

The first important factor to be considered for the synthesis was the sulphur vapour pressure that will build up inside the sealed vessel upon heating, before the reaction goes to completion.

Table 3 is the compilation of the more reliable values for the relation of vapour pressure of sulphur to temperature. For very low temperatures the values were determined by RUFF and GRAF[56] and for the range 183.8°C to 444.6°C is presented the result of an exhaustive compilation by STULL[57]. However, Stull's compilation did not include the results of WEST and MENZIES[58], the most accurate study on this field at the time of the experimental work carried out and described in the present report.

West and Menzies equationed

$$\log P = a + b^{\alpha t} + c^{\beta t}$$

for the range 270°C to 550°C with the following constants

$$\begin{aligned} a &= 6.109689 \\ \log b &= 1.0229544 \text{ (neg.)} \\ \log c &= 1.9198970 \text{ (neg.)} \\ \log \alpha &= \bar{1}.9992626992 \\ \log \beta &= \bar{1}.995996284 \end{aligned}$$

and they found that the agreement with the experimental results was within a few tenths of one per cent.

For higher temperatures an extension by J.R. West[59] was used. This extrapolated West and Menzies results to 1040°, the critical temperature (RASSOW[60]) corresponding to the critical pressure of 116 atm(*).

West J.R. established

$$\log P = 4.57579 - \frac{3288.5}{T} \qquad \text{(bar)}$$

(*) This value is the arithmetic average taken by West. J.R. from the values obtained by different workers.

and this expression was used in the present work with 1 atm = 0.986923 bar.

The results so obtained agree with the values reported by LOEBEL[61] for pressures above 1 atm up to temperatures of 720°C.

They also agree reasonably up to 800°C with the quite recent experimental results obtained by BAKER [62]. Above this temperature Baker's results gave higher pressures.

The tabulated values were obtained by this author using the expression

$$\log P_{atm} = 6.00282 - \frac{3584.42}{T} - 2.23934 \times 10^{-3} T + 1.14662 \times 10^{-6} T^2$$

with 1.2 per cent mean deviation between the calculated and his observed values.

From Rassow's value of 1040°C for the critical temperature the corresponding critical pressure obtained from this expression becomes 204 atm.

TABLE 3

Vapour Pressure - Temperature Relation
for Sulphur up to the Critical Point

Temperature °C	Ruff & Graf (56)	Stull (57)	West & Menzies (58)	J.R. West (59) extrapolation	Loebel (61)	Baker (62)
49.7	0.00034 mm Hg					
78.3	0.0023					
89.0	0.0057					
99.3	0.0089					
104.0	0.0115					
110.8	0.0200					
114.5	0.0285					
123.8	0.0535					
131.9	0.081					
132.2	0.079					
133.1	0.088					
141.0	0.131					
147.0	0.192					
157.0	0.332					
162.0	0.403					
172.0	0.629					
183.8		1 mm Hg				
189.5	1.38					
211.3	3.14					
223.0		5				
243.8		10				
264.7		20				
270			229 mm Hg			
280			30.2			

Temperature °C	Ruff & Graf (56)	Stull (57)	West & Menzies (58)	J.R. West (59) extrapolation	Loebel (61)	Baker (62)
300			50.4			
305.5		60				
320			80.7			
327.2		100				
340			124.3			
340.5						0.166atm
359.7		200				
360			185.4			
380			268.5			
388						0.400
399.6		400				
400			379.5			
420			524.4			
432						0.814
440			710.7			
444.5						0.981
444.6		760				
460			946.5			
480			1241			
493					2 atm	
498						2.04
500			1605			
520			2048			
540			2583			
550			2870			
552.5						3.93
554						4.00
574					5	
600				6.4 atm		
608.5						7.15
640					10	

Temperature °C	Ruff & Graf (56)	Stull (57)	West & Menzies (58)	J.R. West (59) extrapolation	Loebel (61)	Baker (62)
643						10.03
650				10.2		
672						13.13
700				15.5		
717						19.48
720					20	
722						20.32
750				22.7		
773						30.82
800				32.1		
810						41.05
833						48.79
850				43.9		
873.5						65.57
888						72.72
900				58.5		
915.5						88.22
936						101.6
940						104.5
950				76.2		
967						125.6
971						129.0
987						143.7
1000				97.1		
1003						159.8
1022						181.3
1039						202.8
1040				116.5		

1.6 Thermal Behaviour of Chalcopyrite. Thermodynamic Properties

There is no consensus of opinion about the thermal behaviour of chalcopyrite either under atmospheric pressure or in vacuum. Some workers found high-temperature modifications of chalcopyrite, others bornite and a third group single sulphides as the decomposition products, but in every case the reaction proceeded with the isolation of elemental sulphur.

According to ISAKOVA et al. (1968)[63], the decomposition of chalcopyrite may therefore be represented in a general way by

$$A = B + \text{gas}.$$

MAYER (1937)[64] used the experimental observations of JOLY (1913)[65] who gave 743°K for the decomposition temperature of $CuFeS_2$ compared with 713°K for marcasite, and assigned a value for the decomposition pressure at 743°K of log P=-4.15 assuming that marcasite has about the same decomposition pressure as pyrite.

Representing the decomposition by the reaction

$$2CuFeS_2 = Cu_2S + 2FeS + \frac{1}{x} S_x$$

where x was the average molecular complexity of sulphur gas, Mayer was able to make an approximate calculation

$$Cu(s) + Fe_\alpha(s) + 2\,S_{rh}(s) = CuFeS_2(s)$$

$$\Delta G^\circ_{298} = -41.33 \text{ Kcal mole}^{-1}$$

$$\Delta H^\circ_{298} = -41.59 \text{ Kcal mole}^{-1}$$

MERWIN and LOMBARD (1937)[50] established a dissociation pressure curve for $CuFeS_{1.95}$ for the range 547° to 627°C with a variation from 10-16mmHg to 610mmHg. They also found chalcopyrite to melt at 875° ± 10°C.

VOLSKY and AGRATCHEVA (1945)[66] considered the dissociation of chalcopyrite to follow the equation:

$$4CuFeS_2 = 2Cu_2S + 4FeS + S_2$$

and they presented the results of experimental determinations of sulphur vapour pressure over chalcopyrite in the range 500° to 700°C.

In the work of Volsky and Agratcheva the chalcopyrite samples were heated in a neutral atmosphere for the decomposition of pyrites present. ISAKOVA et al (1969)[67] suggested that due to this fact a certain decomposition of chalcopyrite had probably taken place and the vapour pressure was determined over a sulphide which contained less sulphur than chalcopyrite.

In the recent work by ISAKOVA et al. (1968)[63] on the thermal behaviour of chalcopyrite in vacuum they referred to the findings of several authors:

"According to CHIZHIKOV (1948)[68] chalcopyrite when heated to 400° dissociated into single sulphides

$$CuFeS_2 \rightarrow Cu_2S + FeS."$$

However, HILLER and PROBSTHAIN (1956)[34], as mentioned in section 1.2 found that the tetragonal chalcopyrite turns into cubic when heated to 550°C with a decrease in sulphur content as the temperature increases.

Still quoting the compilation of ISAKOVA et al.(1968)[63], "SVETROV (1958)[69] found a change at 560°C, and in the end the mineral dissociated into bornite (Cu_3FeS_4 ?) and troilite (FeS).

However, in the opinion of POPOUKINA and OKUNEV (1958)[70] dissociation of chalcopyrite begins at 350°C and the rate increases little as the temperature increases."

BARTHOLOME (1958)[48], using the diagram shown in Fig.8-a (Section 1.3), and available date on partial pressures of sulphur over the assemblages (at 25°C) calculated for $CuFeS_2$ a value of

$$\Delta G^{\circ}_{298} \simeq -45 \text{ Kcal mole}^{-1}$$

Nevertheless, the diagram used by him is probably not correct and data values employed not very reliable.

Again quoting ISAKOVA et al. (1968)[63], "MARGULIS and PONOMAREV (1959)[71] concluded that during the decomposition of $CuFeS_2$ in a flow of nitrogen, elemental sulphur is produced and bornite is formed.

In 1962 SHIMA[37] found a transformation to cubic chalcopyrite at 540-550°C and a dissociation into bornite and pyrrhotite at about 850°C.

GOLOMZIK (1964)[72] established a general equation

$$\log P_{S_2} = \frac{A}{T} + B$$

and using the two limit values at 500° and 700°C found by VOLSKII and AGRATCHEVA[66] for the sulphur vapour pressure over $CuFeS_2$, was able to calculate

$$A = - 14393$$
$$B = + 10$$

Assuming the decomposition

$$4CuFeS_2 = 2Cu_2S + 4FeS + S_2$$

extrapolating the general equation to 25°C and using

$$\Delta G^{o}_{298} = - RT \ln P$$

Golomzick found for $CuFeS_2$:

$$\Delta G^{o}_{298} = - 51.49 \text{ Kcal mole}^{-1} .$$

Using the value:[73-74]

$$\Delta H^{o}_{298} = - 40.94 \text{ Kcal mole}^{-1}$$

he determined:

$$\Delta S^{o}_{298} = + 35.4 \text{ cal mole}^{-1} {}^{o}K^{-1} .$$

Golomzick's report did not justify, or mention the limitations, of such extrapolation and he did not consider the heat of transformation, specific heat changes, or the pressure of molecular forms of sulphur vapour other than the diatomic. His values must therefore be regarded as being in considerable error.

TKACHENKO et al. (1965)[75] in their studies detected the tetragonal-cubic transformation at 550°-650°C and found single sulphides of copper and iron at temperatures above 700°C.

Calculations for the ΔG^{o}_{298} of chalcopyrite and other copper-iron sulphides were made by YOUNG (1967)[76] using MERWIN and

LOMBARD's [50] values for the sulphur vapour pressures over $CuFeS_{1.95}$, and based on the low-temperature assemblages by BARTHOLOMÉ[48], high-temperature assemblages by YUND and KULLERUD[38] and mineral assemblages alone. Establishing the different possible equilibrium reactions for chalcopyrite, (each reaction being written with one mole of S_2):

(I) $9CuFeS_2(s) \rightarrow Cu_5FeS_4(s) + 4CuFe_2S_3(s) + S_2(g)$ — Based on the Bartholomé's diagram at 25°C

(II) $5CuFeS_2(s) \rightarrow Cu_5FeS_4(s) + 4FeS(s) + S_2(g)$ — Based on the Yund and Kullerud's diagrams.

(III) $4CuFeS_2(s) \rightarrow 2Cu_2S(s) + 4FeS(s) + S_2(g)$

and using data from dissociation pressures they obtained the ΔG°_{298} for chalcopyrite. These values were converted to Kcal per mole of chalcopyrite giving for each of the three cases presented

(I) $\Delta G^{\circ}_{298} = -60.094$ Kcal mole^{-1}

(II) $\Delta G^{\circ}_{298} = -58.816$ Kcal mole^{-1}

(III) $\Delta G^{\circ}_{298} = -59.100$ Kcal mole^{-1}

Using mineral assemblages alone and assuming that "natural assemblages of sulphides minerals are likely to represent low-temperature equilibria" the author proceeded to "determine the magnitude of the sulphur pressures over the relevant ternary associations on the grounds that at constant temperature, the higher the sulphur content of the solid phases, the higher the equilibrium pressure", and finally obtained a value for the free energy of formation of chalcopyrite which he considered highly reliable,

$$\Delta G^{\circ}_{298} \simeq -64.661 \text{ Kcal mole}^{-1}$$

when compared with the previous values. Young criticized his own calculations involving dissociation pressures because he assumed diatomic sulphur vapour.

Fig. 14 reproduces Young's diagram of the molecular aggregation of sulphur vapour.

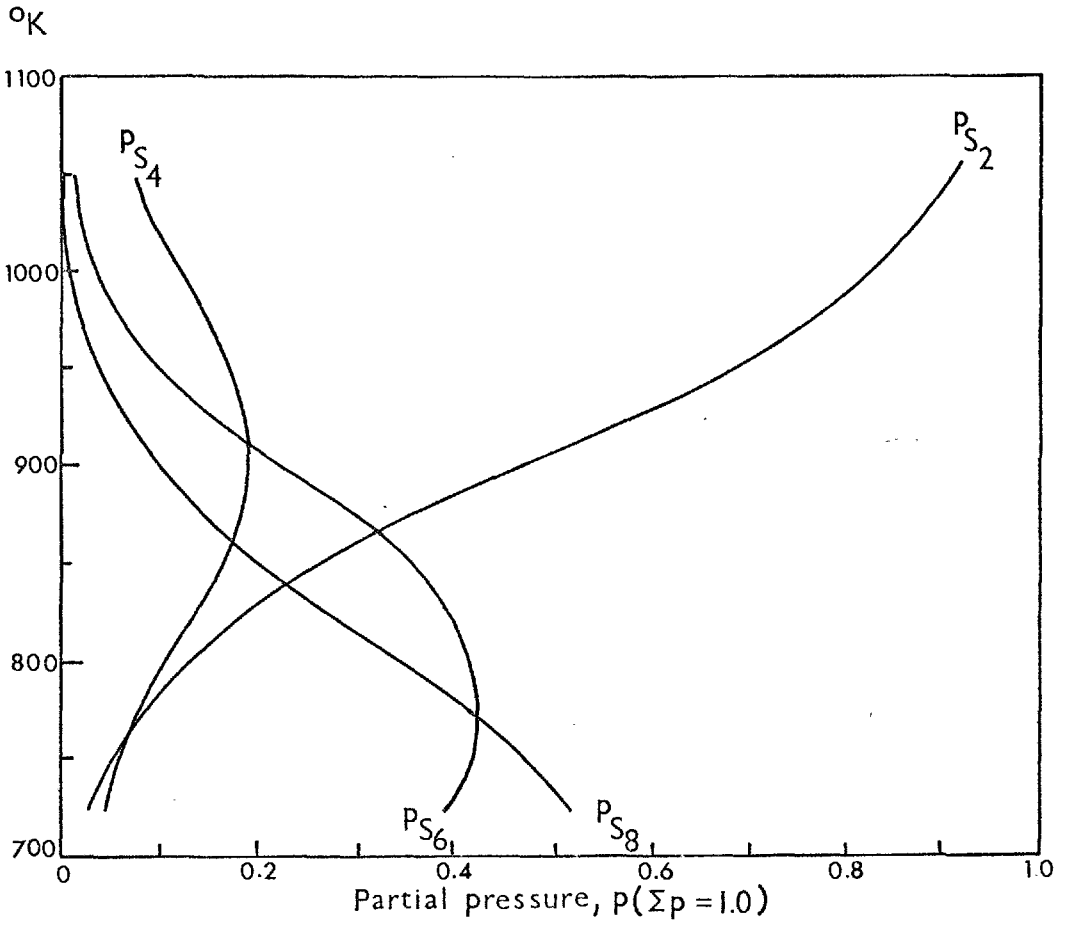

Fig. 14. Molecular aggregation of sulphur vapour - Young(76)

ISAKOVA et al. (1968[63]) studied the kinetics of decomposition of chalcopyrite in vacuum. They found that in a vacuum of 0.1mmHg when heating chalcopyrite at a constant rate of 10°C per minute the formation of sulphur began at 300°C (Fig. 15a and b). With an increase in temperature to 600°C, the rate and degree of sulphur distillation increased, but subsequently the rate fell. These authors assumed that, in theory, during full decomposition 9% of the sulphur in $CuFeS_2$ must be given off (HILLER and PROBSTHAIN[34] - see Section 1.2).

With a subsequent increase in temperature from 700° to 1000°C the decomposition process was very slow and practically stopped at 1000°C when the degree of sulphur distillation was about 90%. A complete kinetic analysis was carried out by these authors, and finally the residues were subjected to X-ray analysis. They found that, between 550°C and 620°C, chalcopyrite changed from tetragonal to cubic, and in the interval 620-750°C, bornite was formed. At 850°C and above, pyrrhotite appeared with a sulphur content which fluctuated from 51.4 to 51.8 atomic percent However, the bornite X-ray lines shifted to the side of the larger angles and the authors assumed that this was probably due to the formation of a solution of chalcocite in bornite. They suggested that the decomposition of $CuFeS_2$ takes place in stages, with a multiplicity of intermediate phases. First a change of α tetragonal to β cubic with separation of sulphur, then the appearance of bornite, or a bornite chalcocite solid solution, followed by single sulphides of copper and iron and metallic copper.

In 1969 ISAKOVA et al.[67] presented a study of the dissociation pressure of chalcopyrite and bornite. On the basis of the composition of the chalcopyrite and of the residue after decomposition, the authors of the article suggested the following overall reaction

$$4CuFeS_2 = 2Cu_2S + 4FeS + S_2.$$

A sample of natural ore, carefully selected by means of a magnifying glass was used by ISAKOVA et al. for their determinations. The analysis of this sample gave 35.11% Cu, 30.6% Fe and 34.86% S (against 34.624% Cu, 30.432% Fe and 34.944% S in $CuFeS_2$), 0.1% calcium, and small amounts of silver and zinc. X-ray analysis showed that chalcopyrite contained single particles of silicates.

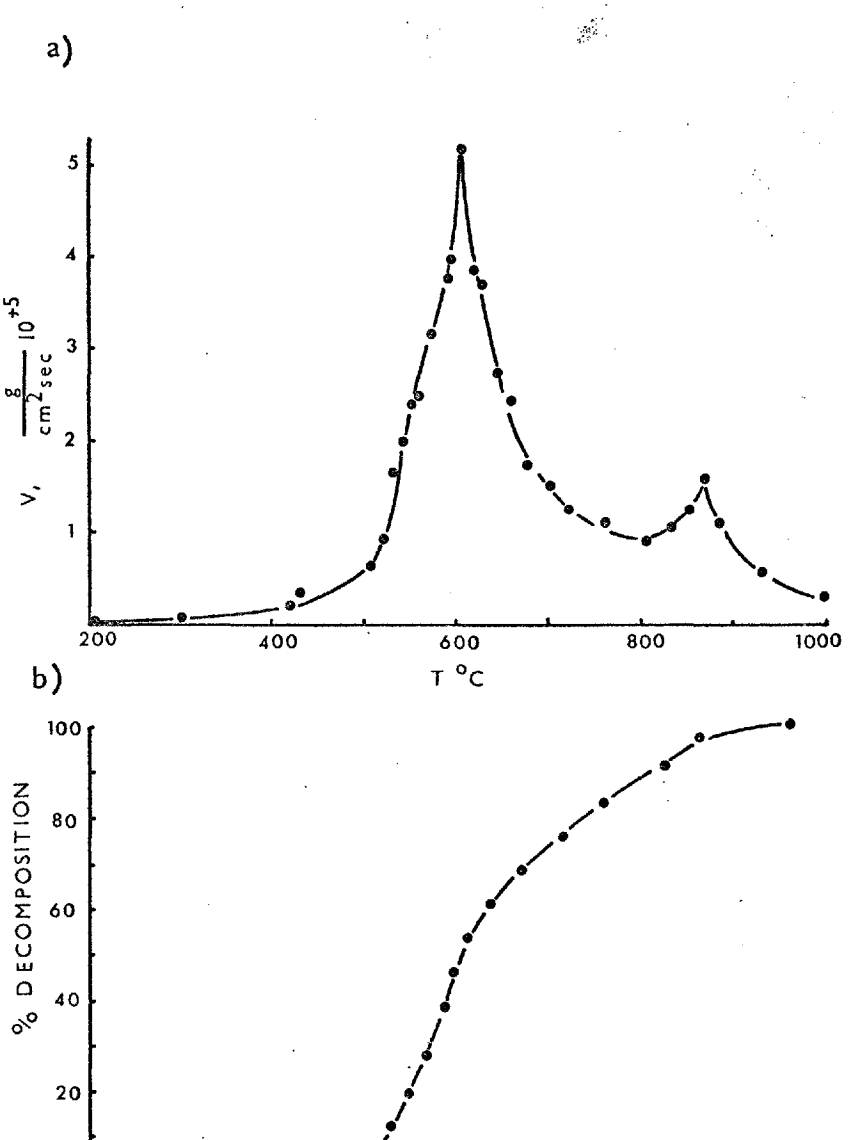

Fig. 15. Kinetics of decomposition of chalcopyrite in vacuum - Isakova et al.(63)

a) Dependence of the rate of decomposition of $CuFeS_2$ on temperature
b) Dependence of the degree of decomposition of $CuFeS_2$ on temperature.

The dissociation pressure of chalcopyrite was determined by the transfer method in a stream of argon, the amount of sulphur condensed being determined analytically. During the calculations allowance was made for the fact that the composition of the gas phase, depended on the temperature (Fig. 14). The results of the experiments are reproduced below in Table 4 and the corresponding diagram, where a comparison is made with the values of MERWIN and LOMBARD[50], and VOLSKII and AGRATCHEVA[66] in Fig. 16.

The analysis of these results shows that chalcopyrite dissociates at relatively low temperatures.

ISAKOVA et al. established an expression relating the sulphur vapour pressure to the temperature

$$\log P_{S_2\ (\text{over chalcopyrite})} = -\frac{17997.32}{T} + 21.9 \ (\text{mmHg})$$

and they found the heat of dissociation for chalcopyrite to be 82.3 Kcal $mole^{-1}$

TABLE 4 (ISAKOVA et al.[67])

Temperature, ^{o}C	Pressure of sulphur vapour over chalcopyrite, mm Hg	
	Experimental	Calculated
500	0.03	0.04
550	1.06	1.08
575	5.83	4.75
600	38.40	19.28
600	34.50	19.28
650	127.5	251.20

As can be seen the agreement between experimental determinations and calculated values using the expression mentioned above is not very satisfactory at higher temperatures.

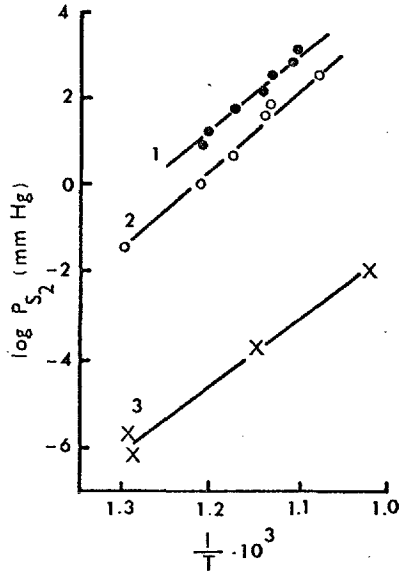

Fig. 16. Dissociation pressure of chalcopyrite.
1- According to Merwin and Lombard[50]
2- According to Isakova et al.[67]
3- According to Volskii and Agratcheva[66]

In a recent paper by PANKRATZ and KING (1970)[55] the results were published of enthalpies determinations above 298°K on synthetic chalcopyrite (See Section 1.4). In order to use the data in algebraic form he applied the equations recommended by MAYER and KELLEY (1932)[77] and quoted by KELLEY (1960)[78]

$$H_T - H_{298.15} = aT + bT^2 + cT^{-1} + d \text{ (calories mole}^{-1}\text{)}$$

obtaining the following final expressions:

$$H_T - H_{298.15} = 20.79T + 6.40 \times 10^{-3} T^2 + 1.34 \times 10^5 T^{-1} - 7\,217$$

(0.4 per cent; 298° - 830°K)

$$H_T - H_{298.15} = -141.40T + 105.00 \times 10^{-3} T^2 + 62\,043$$

(0.3 per cent; 830° - 930°K)

$$H_T - H_{298.15} = 41.22T - 16\,979$$

(0.1 per cent; 930° - 1 200°K),

the corresponding molal heat-capacities taking the form

$$Cp = a + 2bT - cT^{-2}$$

Table 5 , (below) reproduced Pankratz and King values at a number of temperatures for the enthalpy increments, and derived heat capacities and entropy increments, between 298.15 and 1200°K.

In their experiments they found two transitions for chalcopyrite, the first one at 830°K with an isothermal heat of transition of 2.405 Kcal mole^{-1}, corresponding to the low-temperature tetragonal to high-temperature cubic structure. A second transition was found at 930°K with no change in phase involved, and the authors suggest it to be the antiferromagnetic transition temperature.

Worth mentioning is the value for the heat of formation ΔH^o_{298} = + 34.3 Kcal mole^{-1} found by SONGINA et al.[79] (1966) for chalcopyrite, in agreement with ZEUV's value[41] (1967) of ΔH^o_{298} = + 35 Kcal mole^{-1} taken from LETNIKOV[80] (1965).

A compilation of the thermodynamic values mentioned here is presented in Table 6

TABLE 5 - Thermodynamic functions at even temperatures for chalcopyrite ($CuFeS_2$)
(PANKRATZ and KING (55))

T, °K	Cp, cal/deg mole	$S_T - S_{298.15}$, cal/deg mole	$H_T - H_{298.15}$, cal/mole
298.15	22.89	0	0
350	24.26	3.79	1,225
400	25.29	7.10	2,465
450	26.10	10.12	3,750
500	26.69	12.91	5,070
550	27.11	15.47	6,420
600	27.46	17.85	7,780
650	27.89	20.06	9,165
700	28.64	22.15	10,575
750	30.05	24.17	12,040
800	32.56	26.18	13,600
830(α)	34.83	27.42	14,610
830(β)	36.21	30.32	17,015
850	34.29	31.15	17,715
900	46.21	33.29	19,590
930	75.07	35.22	21,355
930	41.22	35.22	21,355
950	41.22	36.10	22,180
1,000	41.22	38.21	24,240
1,050	41.22	40.22	26,300
[1]1,100	(41.22)	(42.14)	(28,360)
[1]1,150	(41.22)	(43.97)	(30,425)
[1]1,200	(41.22)	(45.73)	(32.485)

[1] Values in parenthesis are extrapolations.

TABLE 6

MAYER-JOLY (64-65)	MERWIN and LOMBARD (50)	VOLSKII and AGRATCHEVA GOLOMZIK (72) (66)	(48) BARTHOLOMÉ	(76) YOUNG	ISAKOVA et al. (67)	SONGINA et al. (79) ZUEV (41)
Decompos. temp. = 743°K p_{S_2} (743°K) = 7.079 x 10^{-5} atm ($CuFeS_2$)	M.P. = 875° ± 10°C p_{S_2} ($CuFeS_{1.95}$) mm Hg — °C 10-16 — 547 25 — 560 58 — 575 150 — 597 250 — 606 400 — 619 455 — 620 610 — 627 Starting material: synthetic	p_{S_2} ($CuFeS_2$) atm — °C 2.4×10^{-9} — 500 3.3×10^{-7} — 600 1.6×10^{-5} — 700 $\log p_{S_2} = -\frac{14393}{T} + 10$ (atm) Starting product: Natural ore			p_{S_2} ($CuFeS_2$) mm Hg — °C 0.03 — 500 5.83 — 575 127.5 — 650 $\log p_{S_2} = -\frac{17997.32}{T} + 21.9$ (mmHg) Starting product: Natural ore	
$\Delta G^\circ_{298} = -41.33$ Kcal mole^{-1} $\Delta H^\circ_{298} = -41.59$ Kcal mole^{-1}		$\Delta G^\circ_{298} = 51.49$ Kcal mole^{-1} (-70.8 Kcal mole^{-1}) $\Delta H^\circ_{298} = -40.94$ Kcal mole^{-1} $S^\circ_{298} = +65.09$ cal mole^{-1} °K^{-1} (A)	$\Delta G^\circ_{298} \simeq -45$ Kcal mole^{-1}	$\Delta G^\circ_{298} \simeq -64.661$ Kcal mole^{-1}		ΔH°_{298} 35 Kcal mole^{-1}
Decomp. products considered: Cu_2S, FeS, S_x		Decomp. products considered: Cu_2S, FeS, S_2. A-correction by Young.			Decomp. products considered: Cu_2S, FeS, S_2.	

1.7 Complexing of the Ferric Ion in the Leach Solution. Jarosite-type species

The pale purple hexaquo ferric ion in aqueous solution shows great tendency to hydrolyse and form complexes.

The stages of hydrolysis normally considered, where the aquo ion loses protons to form the mono- and dihydroxo species are:

$$[Fe(H_2O)_6]^{3+} = [Fe(H_2O)_5(OH)]^{2+} + H^+ \qquad K_1$$

$$[Fe(H_2O)_5(OH)]^{2+} = [Fe(H_2O)_4(OH)_2]^{+} + H^+ \qquad K_2$$

and also the dimer formation

$$2[Fe(H_2O)_6]^{3+} = [Fe(H_2O)_4(OH)_2 Fe(H_2O)_4]^{4+} + H^+ \qquad K^+$$

A survey by King[81] showed from the results found that the first hydrolysis equilibrium constant K_1 varied with the ionic strength (I) following the equation

$$\log K_1 \underset{(25^oC)}{} = -2.172 - \frac{2.04\, I^{\frac{1}{2}}}{1 + 2.4 I^{\frac{1}{2}}} - 0.01I$$

The more recent value $K_1 = 10^{-3.05}$ presented by Cotton and Wilkinson[82] corresponds on this equation to an ionic strength near to 2.

King's compilation showed that $K_2 = 5 \times 10^{-4}$ seemed representative of the experimentally determined values while Cotton and Wilkinson presented $K_2 = 10^{-3.26}$.

The dimer formation equilibrium constant, according to King's survey, could also be expressed as a function of the ionic strength

$$\log K^+ \underset{(25^oC)}{} = 1.46 + \frac{4.08 I^{\frac{1}{2}}}{1+2.1 I^{\frac{1}{2}}} + 0.075I$$

This equation leads, for an ionic strength of 1, to a value near to the Cotton and Wilkinson's $K^+ = 10^{-2.91}$.

Taking the set of values presented by these two authors

$$K_1 = 10^{-3.05}$$

$$K_2 = 10^{-3.26}$$

$$K^+ = 10^{-2.91}$$

it can be seen that values as high as 99% for the ferric hexaquo ion are only achieved at pH near to zero while extensive hydrolysis occurs even at rather acid pH's of 2-3.

At higher pH other polynuclear species are formed with appearance of colloidal gels, and finally the hydrous ferric oxide is precipitated.

According to Cotton and Wilkinson this precipitate is better represented by $Fe_2O_3 . nH_2O$ than by the $Fe(OH)_3$ hydroxide, part of it being in fact FeO(OH), which can have at least two crystalline forms.

It also should be noted that the hydroxy species in solution are yellow and this colour becomes stronger with an increase in temperature.

Iron (III) at low pH (<3) and in presence of sulphate tends to form iron (III) hydroxide sulphate hydrate species, which have an extensive range.

Some examples are for example:

$$Fe(OH)\ SO_4,\ nH_2O\ (n=2,3,5)$$

and the jarosite type compounds, having the general formula

$$MFe_3(SO_4)_2\ (OH)_6$$

where M can be Na^+, K^+, Rb^+, NH_4^+, Ag^+; Pb^{2+} or H_3O^+.

The hydronium jarosite,

$$(H_3O)\ Fe_3\ (SO_4)_2\ (OH)_6$$

is normally known as carphosiderite and is very often represented as

$$(H_2O)\ Fe_3(SO_4)_2\ (OH)_5,\ H_2O$$

or

$$Fe_3\ (SO_4)_2\ (OH)_5,\ 2H_2O.$$

Jarosite itself is in fact

$$K\ Fe_3\ (SO_4)_2\ (OH)_6.$$

where the hydronium group was substituted by potassium.

Brown (1970)[83] studied the equilibrium of synthetic potassium-hydronium jarosites at 25°C and 1 atmosphere, and found that "the incorporation of potassium in the jarosite structure was consistently greater than that of hydronium even for a ratio a_{K+}/a_{H_3O+} in solution as low as 0.3", whereas at high temperatures (up to 170°C) the results showed the formation of hydronium-rich jarosites from alkali defficient solutions. According to Brown this confirmed the tendency of H_3O^+ to be replaced by K^+ in the jarosite structure at low temperatures.

His experimental determinations led to a value of $\Delta G^{\circ}_{298^{\circ}K}$ = - 794 Kcal $mole^{-1}$ for the potassium-rich jarosite .

He also found that variations in the lattice parameters, determined using X-ray powder diffraction methods (FeK_{α}) on different synthetic jarosites samples, had no relation with the hydronium-potassium composition.

The general consensus is to accept that jarosite is stable under highly acid and oxidizing conditions and this topic was also discussed by Brown (1971)[84] for the jarosite-goethite (Fe OOH) stabilities at 25°C and 1 atm, using three-dimensional E-pH-log $a_{Fe^{2+,3+}}$ (or log a_{K+}) diagrams. The calculations implied the use of his previously determined $\Delta G^{\circ}_{298^{\circ}K}$(jarosite) = -794.0 Kcal $mole^{-1}$ and Berner's[85] value $\Delta G^{\circ}_{298^{\circ}K}$(goethite)= -116.878 Kcal $mole^{-1}$. Brown mentioned that the error involved in the experimental determinations of the free energy for jarosite will result in a variation in the size of the jarosite stability field but the slopes of the boundaries will remain constant.

By expressing the equilibrium jarosite-goethite as

$$3Fe\ OOH + K^+ + 2SO_4^{2-} + 3H^+ = KFe_3(SO_4)_2(OH)_6$$

he concluded that the reaction would proceed spontaneously since $\Delta G_{reaction}$ = -19.7 Kcal $mole^{-1}$.

The variables considered by Brown for the drawing of the three-dimensional diagrams were E, pH, activity of total sulphur species and activity of potassium.

It is worth quoting his conclusions from the analysis of the diagrams obtained:

"1) jarosite is stable at low pH and moderately oxidizing E values as predicted.

2) as the activity of dissolved iron or potassium increases, the stability field of jarosite moves to increasingly lower E values (jarosite may form if the activity of ferrous iron is greater than the activity of ferric iron).

3) the jarosite field completely eliminates the Fe^{3+} stability field for high activities of Fe^{3+} and SO_4^{2-}.

4) the activities of H^+ and SO_4^{2-} (and/or HSO_4^-) are critical to jarosite precipitation or solution.

In Fig. 17 , is reproduced an E-pH diagram drawn by Brown and showing the stability fields of jarosite and goethite for activities of sulphur species $\approx 10^{-2}$M and iron species 10^{-4}M at 25°C and 1 atm.

It can be seen that jarosite isshown to be stable in an acid medium (pH<3) in moderate to high oxidizing conditions, and goethite stable at pH greater than 3.

Brown suggested that the persistence of jarosite occurring outside its stability field was due to the slow kinetics of the reaction jarosite→goethite.

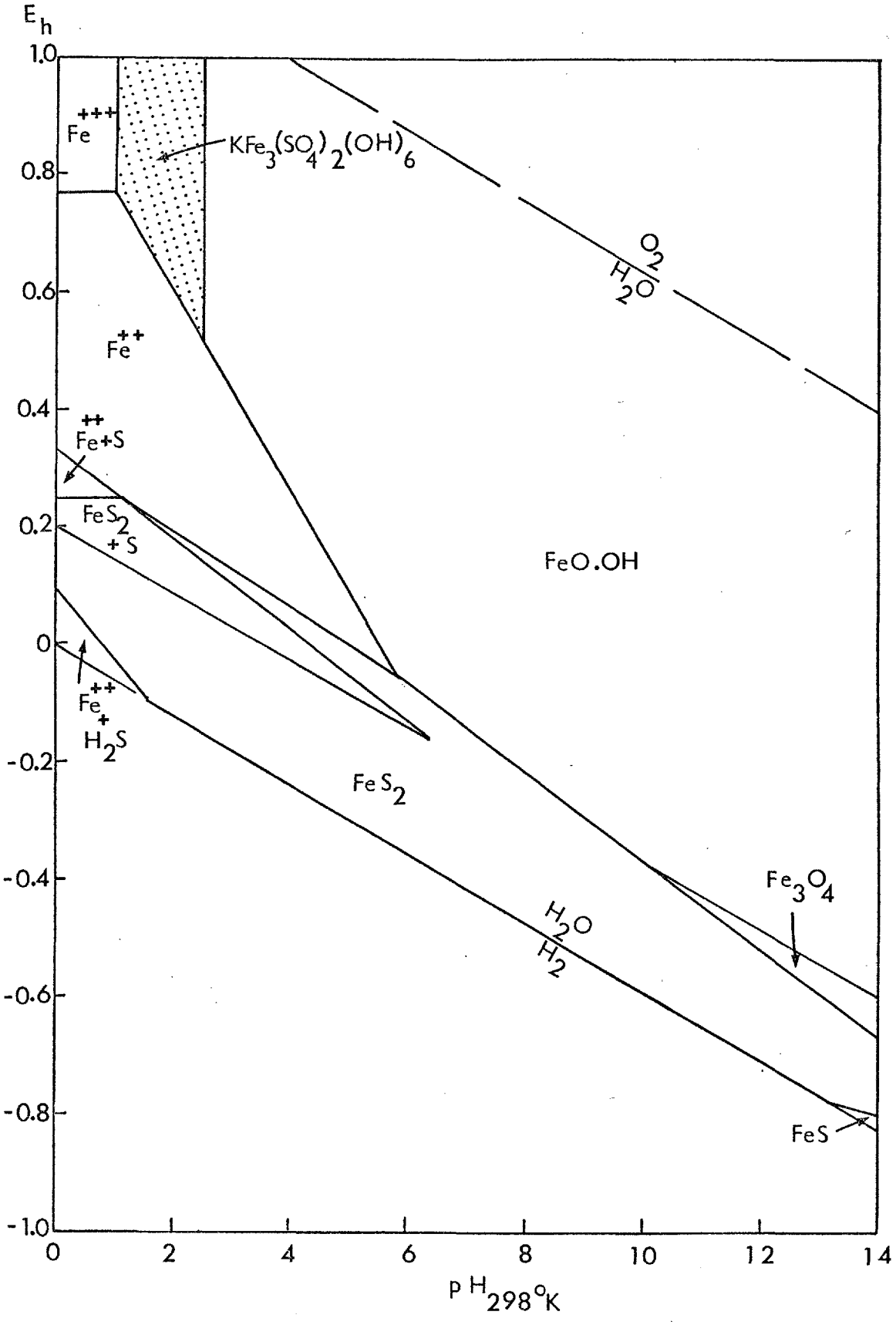

Fig. 17. Stability regions of jarosite and goethite for activities of sulphur species ~ 10^{-2} M and iron species 10^{-4}M at 25°C and 1 atm - Brown(84)

SECTION 2

EXPERIMENTAL PROCEDURES

2.1 Synthesis of Chalcopyrite

Similar methods were used for the first step of preparation of both α- and β-chalcopyrite starting from the stoichiometric amounts of the elements for the formula $CuFeS_2$.

The synthesis was carried out in vacuum, at temperatures of 900°C for about ten days, in a two compartment silica-vessel, similar to the glass vessels used by King (1966)[81]. This type of arrangement avoided the direct contact of molten sulphur with the iron sponge and copper rod used, therefore preventing a very fast, if not explosive, reaction as the temperature increased.

Spectrographically pure copper rods, sulphur powder and reduced iron sponge (Section 2.4) were used in both α- and β-chalcopyrite preparations. The iron sponge was previously reduced in a stream of hydrogen at 500°C using the furnace described in Appendix C . To achieve this reduction, temperatures of 500°C proved to be as effective as the reductions of iron sponge at 900°C described by Yund and Kullerud[38], without the inconvenience of obtaining a sintered product.

The problem of filling the silica vessel with the elements was solved by keeping the vessel vertical while transferring the sulphur to the smaller compartment, and positioning the vessel horizontally for the insertion of the copper rod and iron sponge. The reduced iron sponge was introduced through a specially designed funnel with the help of a magnet.

The open end of the silica tube was then connected to an oil diffusion pump and the vessel evacuated. Only then was the system sealed, with an oxygen torch, the neck having been previously constricted to a diameter just big enough to allow the copper rod through.

The system was then placed within the constant temperature zone of a horizontal electric tube furnace designed to reach 1100°C (Appendix C), the heating being controlled by a transitol electronic controller and the temperature of the silica vessel checked with a 13% Pt-Pt/Rh thermocouple connected to a potentiometer with compensating wire. With this system, a control of ± 2°C was possible.

For three days the temperature was kept just below 600°C to allow the reaction to proceed without a build up of sulphur vapour pressure and eventual explosion of the vessel. The pressure corresponding to 600°C was found to be 6.4 atm using West J.R.[59] extrapolation, later confirmed (6.55 atm) using Baker's[62] equation (Section 1.5, Table 3).

After this initial heating period the tube became clear (no trace of sulphur vapour), due to the reaction of sulphur with both copper and iron, and the temperature was slowly increased during two days up to 900°C and kept there for 10 days. X-ray analysis using the powder method were made for a sample kept at about 700°C for 10 days. The resulting pattern (TableB-22.1) shows that a mixture of α-chalcopyrite, bornite and pyrite was obtained at that temperature.

No data was found in the literature concerning the sulphur vapour pressure over chalcopyrite in this range of temperature. An extrapolation of Merwin and Lombard's[50] values for sulphur pressure over $CuFeS_{1.95}$ (Section 1.6) showed that 1 atm was reached at 632°C. However, Golomzik's[72] equation, based on Volskii and Agratcheva's[66] results, extrapolated for temperatures above 650°C gave the following set of values,

Temperature, °C.	Sulphur Pressure over $CuFeS_2$, atm
700	1.6×10^{-5}
800	3.9×10^{-4}
845	1.3×10^{-3}
900	5.4×10^{-3}
1000	4.9×10^{-2}
1100	3.3×10^{-1}
1166	1

On the other hand extrapolation of measurements of Isakova et al.[69] to higher temperatures produced the following results:

Temperatures °C	Sulphur Pressure over $CuFeS_2$, atm
700	3.3
800	17.6
845	834.1

Although, as already mentioned, the agreement between experimentaland calculated values using the equation of Isakova et al. was not particularly good the experimental data are, so far, the most reasonable results published. Decomposition of chalcopyrite occurs at temperatures above 800°C and near to 845°C, as reported by Shima[37] and Isakova et al.[63] (Section 1.6). This seems to justify the deviation between the calculated values and the real pressures in this range. In fact, sealed silica vessels containing the elements in proportions for $CuFeS_2$ were held at about 1000°C, occasionally without explosions.

In order to evaluate sulphur vapour pressures for the range 727°-927°C, calculations for the free energy of the reaction

$$4CuFeS_2 = 2Cu_2S + 4FeS + S_2$$

were made using the relation

$$\Delta G^\circ_T = - RT \ln P_{S_2}$$

and (Appendix A)

$$\Delta G^\circ_T = \Delta G^\circ_{298} - \Delta S^\circ_{298} (T-298) + \overline{\Delta C^\circ_p}]^T_{298} (T-298) - 2.303T\overline{\Delta C^\circ_p}]^T_{298} \log \frac{T}{298}$$

where $\overline{\Delta C^\circ_p}]^T_{298}$ is the mean ΔC°_p for the reaction, between 298°K and the temperature T considered.

ΔG°_{298} and ΔS°_{298} for Cu_2S and FeS were taken from Latimer[86] and for S_2, from Kelley[87].

Using Golomzik's value $\Delta G^\circ_{298} = - 51.49$ Kcal mole^{-1} jointly with $\Delta H^\circ_{298} = - 40.94$ Kcal mole^{-1} from Gerasimov et al.[73] and Karapet'yants[74] a value of $\Delta S^\circ_{298} = + 35.4$ cal mole^{-1} °K^{-1} was determined for $CuFeS_2$(*).

$\overline{\Delta C^\circ_p}]^T_{298}$ were calculated using Kubaschewski and Evans relation[88]

$$C_{pT} = a + bT + cT^{-2}$$

applied to S_2, Cu_2S and FeS with the following constants:

(*) A more recent value for the heat of formation, corresponding to 35 Kcal mole^{-1} was found in a report by Letnikov[80].

	S_2 (298-2000°K)	Cu_2S (623°-1400°K)	FeS (598°-1195°K)
a	8.54	20.32	12.20
b	0.28×10^{-3}	-	2.38×10^{-3}
c	-0.79×10^{5}	-	-

Heat capacity values for $CuFeS_2$ were taken from Pankratz and King's[55] data (Section 1.6).

Absurd values were obtained by the use of this method for the range of temperatures considered (727°-927°C), when compared with the experimental determinations mentioned above.

An error in Pankratz and King'svalues is not likely, since they used a quite straightforward method for the determination of enthalpy data and derived heat capacities. A back calculation shows that in order to have 1 atm pressure at 927°C the heat capacity at that temperature for $CuFeS_2$ should be 146.6 cal $mole^{-1}$ $°K^{-1}$ against 41.22 cal $mole^{-1}$ $°K^{-1}$.

It seems more likely that there is an error in Golomzik's free energy of formation for $CuFeS_2$

$$\Delta G^{o}_{298} = -51.49 \text{ Kcal mole}^{-1}$$

which was evaluated by extrapolation to 298°K ignoring heats of transformation and changes in specific heat. Also the heat of formation $\Delta H^{o}_{298} = -40.94$ Kcal $mole^{-1}$ given by Gerasimov et al.[73] and Karapet'yants[74] must be considered with a certain reserve.

After the tenth day at 900°C the silica reactor vessel was allowed to cool slowly to about 540°C and kept at this temperature for 24 hours. The power supply to the furnace was then slowly reduced until the temperature had fallen to about 200°C, when the tube was removed.

The final product obtained was not completely homogeneous, as could be seen through the transparent vessel.

It was possible to break the incipiently melted material

without opening the silica tube, and to confirm that the copper had diffused through the sulphides to the solid sulphur-gas interface, from the hole left by the copper rod, as already reported by King[81] for the case of chalcocite and Ugarte-Alvarez[89] for bornite.

From this point on, different procedures were used to obtain β and α-chalcopyrites, so they are described in different sections.

2.1.1 β-Chalcopyrite

One of the products obtained during the first stage of preparation outlined above was remelted in the same sealed vessel, using the same electrical furnace placed vertically. The tube was lowered from the top of it at a rate of 0.79 inches per hour.

Once the hot zone, kept at 990°C, was crossed, the solidification of the melted material in a narrower part of the silica vessel caused it to crack, allowing some of the sulphur to distil off, and conferring an approximate composition $CuFeS_{1.83}$ to the solid. This corresponded to a weight loss of about 3% or a sulphur deficit of 9% in agreement with the findings of Hiller and Probsthain[34] described in Section 1.2. In fact, when these authors heated $CuFeS_2$ to 750°C in a nitrogen filled furnace they found, upon cooling, a solid with the composition $CuFeS_{1.82}$. Also, according to their thermograms the sulphur loss depended on the temperature and therefore it seems likely that the cracking of the vessel in the present work occurred around 750°C.

The final product obtained was compact, and a recent uneven fracture presented a brass-yellow colour and metallic lustre, typical of normal tetragonal chalcopyrite, but tarnishing rapidly in contact with air.

Under polarized light no anisotropy was observed, even under oil and with intense illumination. Polished sections showed no heterogeneity and only a negligible number of pores, and when over-polished, these sections turned into a brighter pinkish colour.

A lamellae type structure Fig.B-9 , Appendix B , could be seen quite clearly after exposing a polished section to the air for some time.

Electron probe microanalysis confirmed the homogeneity of the material, the sample being suitable for a standard after chemical analysis. No variation of composition was detected under the probe for the lamellae reported above.

The outside layer of the synthetic block was removed and not used in subsequent leaching experiments since it showed a certain degree of oxidation and traces of impurities.

An interesting feature worth mentioning concerns the determination of the melting point of this synthetic material, showing under 800 psi melting beginning at 891°C and a complete melting at 931°C; upon cooling , solidification started at 926°C, and was complete at 901°C.

These values do not agree with the 800°C reported by Dana-Hurlbut[90] for the melting point of normal chalcopyrite. However, they approach those found by Merwin and Lombard[50] for their synthetic $CuFeS_{1.95}$ and are near to the range 860°C to 895°±3°C determined by Kullerud[51]. The variation of results obtained seems to be a function of the sulphur content in the samples.

Analyses by X-ray powder diffraction were made using samples representative of the bulk of the product prepared(*). The pattern obtained is shown on Fig. B-1 and interplanar spacing and intensities of the lines in Table B-2.2, together with the results of Cabri[47] and Hiller and Probsthain[34]. The agreement between the data obtained here and Cabri's values for the interplanar spacings of a new copper-sulphide is excellent. On the other hand, the intensities of the reflections approach the values observed by either Cabri or Hiller and Probsthain, with the exception of the lines corresponding to the d-spacings 2.651 and 1.186Å, which approach the theoretical values calculated by Hiller and Probsthain.

Lines 3.07, 2.264 and 1.612Å are of doubtful existence, and most of the weaker lines were detected with the help of a magnifying glass.

The results obtained for the synthetic material confirm, due to the absence of indices $h+k+\ell \neq 2n$, the existence of a body centered cubic lattice, in agreement with the findings by the above mentioned authors. The superstructure lines reported here for the synthetic material, though their intensities were calculated by Hiller and Probsthain, were not detected by these two authors. Also they do not mention the conditions or even type of radiation used in their X-ray determinations.

(*) Not considering the outside layer.

Cabri's work involved the study of a new-copper-iron sulphide, he described as $Cu_{18}(Fe,Ni)_{18}S_{32}$. This author rejected the so called β-chalcopyrite of Hiller and Probsthain as a high temperature cubic form with space group $I\bar{4}3m$ and cell parameter a = 10.60 Å. He adopted instead the smaller cell (a = 5.29 Å) face centered cubic, obtained by Donnay and Kullerud[35] and also by Frueh[36], for a high temperature synthetic chalcopyrite.

In Cabri's report, samples from Noril'sk (Western Siberia) were crushed and run through a magnetic separator. Point counting showed a variation of chalcopyrite from 95.5% (area per cent) for the fraction -65 + 100 mesh, to 87.0% for the fraction -100+200 mesh, the remainder being cubanite and pentlandite. Electron probe analysis reported by this author on the -65 + 100 mesh fraction presented the following results:

Cu	36.1%	±	0.5
Fe	31.6%	±	0.5
S	31.9%	±	0.5
Ni	0.7%	±	0.1

X-ray diffraction techniques employed by Cabri involved the same conditions as used in the present work(*) (114.6 mm Debye-Scherrer camera, CoK_α radiation) except for the time of the exposures. In fact, he used between 30 to 70 hours against 3 to 10 hours in the present work. These long exposures of Cabri's work were not used here, to avoid excessive blackening of the powder photographs, which could lead to wrong measurements of the relative intensities of reflections (see Section 2.3.4).

Electron probe microanalyses were made here on the synthetic material obtained, and nickel was checked by spectrum tracing at maximum sensitivity. None was detected using this method, and it can be said that the nickel level in the bulk material was below 300 ppm, this value (≈0.03%) being smaller than the error on Cabri's determinations. All samples were also traced across, including edges and cracks, to check for nickel contamination, and where necessary, the nickel trace was repeated at Ni background setting, to ensure that any

(*) In the present work, the values of about 40Kv, 20mA were generally used.

detected at the edge was not merely a topographic effect on the background. With the exception of one of the external edges of the sample, where a value slightly above the background was obtained (doubtful, however, due to the very noisy signal), no nickel was detected.

X-ray fluorescence techniques were also used and the results were consistent with those obtained by the method described above. Comparison with a standard alloy containing 0.35% nickel, confirmed that this element, if present, would be below 0.035%. The existence of any nickel in the samples can therefore be related to the purity of the starting elements used for the synthesis (see Section 2.4).

However, the X-ray pattern for this synthetic material (TableB-22.2) shows the existence of more reflections than were found by Hiller and Probsthain for their β-chalcopyrite, and is very similar to Cabri's pattern for his $Cu_{18.0}Fe_{17.7}Ni_{0.3}S_{32}$. Also the X-ray data presented here for the synthetic material, obtained by using approximately ten times less exposure than Cabri's results(*) seem to indicate a cubic cell with an approximate a = 10.60_7 Å, similar to a = 10.60 Å for Hiller and Probsthain's β-body centered cubic cell and smaller than Cabri's body centered cubic cell, a = 10.64_8 Å, for his $Cu_{18.0}Fe_{17.7}Ni_{0.3}S_{32}$.

The analyses obtained by standard atomic absorption techniques gave the following results:

35.69% Cu
31.36% Fe
32.95% S (by difference)

corresponding to the approximate formula:

$$CuFeS_{1.83}$$

in good agreement with the $CuFeS_{1.82}$ (or $Cu_{17.6}Fe_{17.6}S_{32}$) for the Hiller and Probsthain's β-form.

A final test was made, consisting of a staining technique, described by Yund and Kullerud[38], to distinguish isometric cubanite from cubic chalcopyrite. It involved the use of a staining solution, 400mg $(NH_4)_2Cr_2O_7$ in 25ml of a 10 per cent HCl, that stains brown the isometric cubanite and leaves chalcopyrite unaltered. The synthetic material prepared here

(*) Cabri did not mention the KV and mAused in his analysis.

did not react to this test, remaining unaffected.

Upon all this evidence, it seems possible to assume, with reasonable confidence, that the sample obtained was a body centered cubic chalcopyrite, and the terminology β- for $CuFeS_{1.83}$ will be used from now on for this material.

No effort was made to prepare single crystals in view of the difficulties found by Austin et al.[91] in their attempts to grow large crack-free crystals of chalcopyrite and chalcopyrite-type structure compounds. Methods used by these authors, like directional freezing, zone-melting or pulling techniques, proved to be quite unsuccessful and they relate this fact with the "small distortion of the lattice in all chalcopyrite type compounds, originating a small degree of anisotropy and with it a differential thermal expansion".

2.1.2 α-Chalcopyrite

After the first step of preparation described in Section 2.1 the sealed silica tube was broken and the material ground in an agate mortar under acetone (AnalaR) to avoid oxidation. The wet product was then introduced into a single compartment silica vessel, evacuated and at the same time heated to about 150° to expel any traces of acetone and water. As the sulphur vapour pressures at this temperature for all possible sulphides existing in this material are very low[50-92] the sulphur losses were negligible. After about 5 hours of pumping, the vessel was sealed and then passed twice through the vertical furnace at a rate of 3¼ inches per hour, the hot zone being kept at about 1000°C.

The reason for the method described above was to allow a complete homogeneisation of the product reducing the risk of explosion when remelting.

However, the process is not recommended and was only employed because the pressure furnace, described in Appendix C, was not yet available. The use of this furnace will reduce the risks and will allow the recrystallization to be made in the same silica vessel in which the first step of the synthesis takes place. The end of a long thin capillary connected to this vessel will be broken during recrystallization and an external pressure of argon will balance the sulphur pressure inside. Thus, losses by diffusion will be minimised.

The final recrystallized product obtained was subjected to the same type of analysis and examinations described for the β-form in Section 2.1.1. Microscopic analysis showed the homogeneity of the final product.

A lamellae type structure, Fig. B-18, Appendix B, was clearly visible after exposing a polished section for some time to the air. This structure is quite similar to the "Oleander-leaf" lamellae of a former high-temperature chalcopyrite reported by Ramdohr,[93], and did not present any noticeable variation of composition under the probe.

Fresh cleavage showed the characteristic brass yellow colour of chalcopyrite, soon turning to a dark golden yellow tone in contact with the atmosphere.

Polished sections were light yellow with metallic lustre and under polarized light it was possible to observe, although with difficulty, a very weak anisotropy.

The outside layer of the synthetic material was also rejected (as for β-chalcopyrite) and the remaining part stored under nitrogen atmosphere, to reduce oxidation.

X-ray analysis results using the powder method and both Cu_α and CoK_α radiations are presented on Table B-22.11. Photographs obtained with CuK_α radiation showed the fluorescence effect submerging the weaker lines detected when using CoK_α radiation (see Section 2.3.4). On the same table are also reported the interplanar spacings found by Frueh[32], using a Guinier camera and CoK_α radiation, from a non-specified sample of chalcopyrite. Also presented are the A.S.T.M. data by Berry and Thompson[94] the X-ray patterns of a Tilt Cove chalcopyrite[95] associated with some pyrite (pyrite lines are not presented on this tabulation), and a Temagami chalcopyrite[95]. Besides pyrite, the Tilt Cove ore is reported to contain several other small impurities.

The lines described by Berry and Thompson for the tetragonal chalcopyrite were also found for the synthetic material prepared here, with the exception of the reflections corresponding to 1.518Å (I/I_1=5) also not reported for the Tilt Cove chalcopyrite.

The most noticeable difference between the X-ray pattern obtained for the synthetic product and the A.S.T.M. data was the reverse of intensities for the lines corresponding to the d-spacings 1.869 and 1.854Å and also for 1.214 and 1.205Å, Fig. B-7, Appendix B.

Superstructure lines were found for the synthetic sample, under CoK_α radiation, although they were not visible (as already mentioned) using CuK_α radiation. It can be seen, by comparison with the results of the other authors, that these superstructure lines are not exclusive to this synthetic material, but no attempts were made to solve the structure due to the uncertainty involving the measurements of the very weak reflections.

The small number of lines reported by Berry and Thompson is probably due to the use by these authors of FeK_α radiation limiting the number of reflections recorded (See Section 2.3.4).

The composition of the synthetic material was determined by atomic absorption spectrophotometric techniques and the results obtained were

36.28% Cu
31.03% Fe
32.69% S (by difference)

corresponding to the formula

$$Cu_{1.12}\ Fe_{1.09}\ S_{2.00}$$

The synthetic sample is similar in composition to one of those prepared by Yund and Kullerud[38] (36.19% Cu, 31.81% Fe, 32.00%S) and reported as tetragonal chalcopyrite at room temperature. These authors also found that the reflections $d_{116,\ 033}$ varied with the composition, and from the results obtained they suggested that "d values and therefore the cell parameters appear to be affected more by a change in the metal to sulphur ratio than by a variation in the Cu to Fe ratio".

It is worth noting that the formula for the synthetic material prepared here, $Cu_{1.12}\ Fe_{1.09}\ S_2$ corresponds to an excess of 10.7% of Cu and 8.3% of Fe over the stoichiometric $CuFeS_2$.

Since this material is within the range of composition, metal to sulphur ratio, 1 to about 1.17, and copper to iron ratio, 0.5 to 1.5 (Section 1.2) which according to Yund and Kullerud, produces tetragonal low temperature chalcopyrite, it will be referred to, from now on as α-chalcopyrite.

In conclusion it is likely that the excess of Cu and Fe over the stoichiometric $CuFeS_2$ which is present in the synthetic $Cu_{1.12}Fe_{1.09}S_2$ is responsible for some of the extra reflections not reported by Berry and Thompson[94]. But it is also likely that the use by these authors of a FeK radiation, as already mentioned, is the reason for the apparent failure to detect the other extra reflections, found for example by Frueh[32] and also in the ores of Tilt Cove and Temagami[95].

2.2 Leaching Apparatus and Experimental Procedure

The very simple leaching apparatus used for the leaching experiments is shown in Fig. 18 . It consisted of a 250ml vessel and a five neck lid, this system being imersed in a paraffin-oil bath, thermostatically controlled by a fail-safe unit, capable of $\pm$ 0.01°C precision and a range 60 to 130°C. With this unit it was possible to control the temperature of the solution in the vessel within $\pm$ 0.05°C.

The degree of stirring required was maintained with the help of a two bladed glass propeller, the shaft passing through the central neck in the lid and being connected to a variable (170 to 1700 r.p.m.) constant speed stirrer (checked by stroboscopic means). A mercury seal was used.

In the other four necks of the lid were a condenser to avoid evaporation , a baffle to provide turbulent regime in the solution and keep the particles in suspension, a thermometer to check the temperature of the solution, and the fourth neck was connected either to an automatically operated sampling device, or to a tube for direct pipetting of the solution. The automatic sampler consisted of a small peristaltic pump attached to a synchronous 10 r.p.m. motor, allowing a flow of 2.0 ml min^{-1}, and another synchronous motor and gearbox unit, with a final drive of 1 rev per 24 hours, which was connected to a circular holder for 24 small flasks.

The movement of the peristaltic pump was interconnected with that of the stirring unit by means of a double action relay. A start-stop electrical switch was adapted to give sampling intervals from 10 minutes to 3 hours and to energize the double action relay for 5 to 75 seconds, during which time the stirrer was stopped and the peristaltic pump put into action.

The leaching procedure was carried out as follows:

200 ml of leaching solutions were kept overnight in the 250 ml vessel which was immersed in the thermostatically controlled paraffin-oil bath, thus allowing thermal equilibrium to be established. The freshly crushed and sieved (to the required particle size) synthetic material was then injected into the solution.



Fig. 18 Leaching apparatus

Previous runs showed that turbulent regime was achieved above 700 r.p.m., the amount of solids in suspension depending however, on the particle size in use. 950 r.p.m. was found to be a suitable speed for all sizes considered, and this value was used through all the experiments conducted, thus preventing the rate being controlled by the access of reactants or products to the surface of the solid.

Samples of the leach liquor were extracted periodically as described, and diluted with sulphuric acid solutions (pH≈1), whenever $Fe_2(SO_4)_3$ was used as the oxidizing agent, or diluted with HCl (pH≈1) for both H_2O_2 and HCl runs. The liquor samples were then analysed for copper and eventually for iron and sulphate.

Whenever samples were taken using a calibrated pipette, the same volume of fresh leaching solution, kept at the temperature of the run, was injected back into the reaction vessel. Thus it was possible to maintain a constant volume as well as an approximately constant amount of oxidising agent. Calculations involving the determination of final concentrations took into account the dilution factor of the products.

On the other hand, when the automatic sampling device was used, there was no replacement by fresh solution and the calculations were referred to the initial volume of solution. The volume of leach liquor contained in the sampling tube and pump was taken into account by calibrating the system for each temperature used, and drawing histograms instead of plotting points for the rate curves.

Occasionally small samples of the solid residue were taken, and again this was considered in the calculations. These samples were normally used for X-ray diffraction and electron-probe microanalysis, as well as for microscopic examination.

At the end of the run the final residue, whenever there was one, was washed, after filtering off the leach liquor, with the same solution (pH≈1) used for diluting the aliquots taken during the run, then with water and finally with acetone*, and was dried.

(*) Washing with acetone did not affect the structure or properties of the solids in any way.

The pipettes used to extract samples of leach liquor were calibrated at each temperature, T, by filling them up to the mark with distilled water kept at the temperature $T \pm 2^{\circ}C$ and weighing the delivered volume in a stoppered bottle. Knowing the density d_T of water for each temperature, $V_T = \frac{m_T}{d_T}$, and the equivalent volume at $20^{\circ}C$, $V_{20} = \frac{m_T}{d_{20}}$ were obtained.

A similar procedure was used with the peristaltic pump for both volume delivered for a set number of seconds of pumping, and the volume of leach liquor existing in the pumping system.

For each run the suitable particle size was chosen by collecting the crushed material between two consecutive sieves. The following table is presented for an easy relation between the nominal apperture and the sieve series used:

British Standard Sieve Series B.S. 410: 1962

Mesh Number	Nominal Width of Apperture (micron)
25	600
36	420
100	150
120	125
150	105
170	90
200	75
240	63
300	53
350	45

2.3 Analytical Methods

2.3.1 Atomic Absorption

Colorimetric methods for copper and iron determinations in solutions were found to be very lengthy and not very accurate. After some initial attempts this method was given up in favour of Atomic Absorption Spectrophotometry. A standard technique was adopted for both copper and iron, using solutions diluted to within the range of the apparatus used, a single beam Perkin Elmer 290B model.

The wavelengths used were 3247Å for copper and 2483Å for iron. Whenever required, and for quick checking of very concentrated solutions, other less sensitive lines were used, as listed in the Perkin Elmer Analytical Methods Manual[96]. Both multielement and single element hollow cathode lamps were used and no significant difference was found. For both lamps the possible interferences of the other ions existing in solution were studied, and none was found.

A 2" burner was normally used associated to a 2Å slit for the multielement lamp and 7Å slit when using the copper single element lamp. Fuel and oxidant were adjusted to obtain an oxidizing (lean, blue) flame, and the deflections obtained by passing the solutions through were recorded graphically.

Calibration curves were drawn, using standards prepared from 1000 p.p.m. stock solutions, and whenever possible, the same diluent was used for both these solutions and the aliquots of the leach liquor.

For the analysis of copper and iron in the residues by Atomic Absorption a technique based in a method by Pantony[97] was used:

A sample of the solid was first attacked with hot concentrated nitric acid(*) until complete dissolution of the solid had occurred, and the heating was continued until a substantial reduction of the volume was obtained, without taking it to the dryness. The remaining solution was then allowed to cool and only then was added to it a small volume of carbon tetrachloride and bromine, for complete oxidation of the sulphur, the tetrachloride acting as a solvent. It was found that 5 ml

(*) The use of aqua-regia mixture was not so effective for these specific synthetic materials.

of CCl_4 and 3ml of bromine were enough for up to 0.5g of solid residues.

While agitating the flask (Kjeldahl) the solution was heated gently until complete removal of bromine and carbon tetrachloride. It was then diluted with dilute sulphuric acid solution (pH=1) to within the range desired for direct determination by atomic absorption. A blank was prepared using the same procedure.

2.3.2 Nephelometry

A nephelometric method was used for the determination of sulphate in the leach liquor. The technique employed, based on the precipitation of barium sulphate, is described by Vogel[98]. Great care was taken to follow his experimental procedure, since the turbidity of a dilute barium sulphate suspension is difficult to reproduce, the rate of dissolution of barium chloride controlling the reaction. The only difference from Vogel's method was the use of the sieved fraction -25 + 36 mesh of barium chloride, instead of the recommended -20 + 30 mesh, but it seemed to have no major effect on the results. In fact excellent results were obtained by the use of this method.

2.3.3 UV Spectrophotometer - Elemental Sulphur Determinations

Elemental sulphur determinations were made with the help of a Unicam SP 800 spectrophotometer. Any free sulphur existing in the residue was extracted in a Soxhlet extractor using either carbon disulphide (CS_2)(*) or carbon tetrachloride (CCl_4).

However, it was found that carbon disulphide interfered with the sulphur maximum absorbance wavelength and carbon tetrachloride was used instead, with quartz 2cm light-path cells at 275 nm wavelength.

(*) The solubility of sulphur depends on the crystalline form as can be seen from the following data for CS_2(99):

Rhombic Sulphur	-	23g per 100 ml
Monoclinic Sulphur	-	70g per 100 ml
Amorphous Sulphur	-	Insoluble

According to Seidell(100) the treatment of "insoluble" sulphur (amorphous) with CS_2 or CCl_4 extracts a small amount that varies with time of contact, temperature and nature of the solvent, but not with the relative amount of solvent. He explains this fact by assuming a partial transformation of amorphous sulphur to soluble orthorhombic form.

2.3.4 X-ray Powder Diffraction

2.3.4.1 Choice of Radiation

Both unleached starting materials and residues of the leach reaction were analysed using the method of X-ray powder diffraction.

A 114.6mm Debye-Scherrer camera was used and the solids, crushed and sieved to -350 mesh, were introduced in small 0.2mm glass-capillary sample holders.

At the beginning of the experiments, and for a few samples, a Cu target with a Ni filter was used, since no other was available. Due to the intense fluorescent radiation a very heavy background was produced, and the photographs obtained did not show the weaker lines later observed using a Co target.

Most samples were analysed using CoK_α radiation, 40 KV and 20 mA, and exposures times from 3 to 10 hours. Using this incident radiation, fluorescent effects were minimised, since the corresponding wavelength, $Co\lambda_{K\alpha 1} = 1.78892\,\text{Å}$, is longer than the absorption edge of copper, $Cu\lambda_K = 1.38043\,\text{Å}$, and iron $Fe\lambda_K = 1.74334\,\text{Å}$, while $Cu\lambda_{K\alpha 1} = 1.54051\,\text{Å}$ is shorter than the K absorption edge of iron.

The use of FeK_α radiation with even longer wavelength, $Fe\lambda_{K\alpha 1} = 1.93597$, would spread the diffraction pattern over a wider range of diffraction angles, giving more accurate readings but limiting the number of reflections recorded. Also, as found by Bradley and Hope[101], and Glocker and Schäfer[102], and reported by Boon[30], the atomic scattering factor of Cu being only slightly greater than that of Fe, it will be possible to increase this difference by using a radiation which wavelength lies near to the K absorption edge of Fe, diminishing the atomic scattering factor of Fe, while the atomic scattering factor of Cu remained constant as found by Rusterholz[103]. This difference in the scattering powers of copper and iron enhances the intensities of the reflections to which copper and iron atoms contribute with opposite phases. For the present case, the best radiation would be CoK_α since the other possibility, NiK_α radiation, has a wavelength $Ni\lambda_{K\alpha 1} = 1.65784$, below the K absorption edge of Fe. This fact is specially important when dealing with single-crystal techniques.

2.3.4.2 Measurement of line positions

A film-measuring device was used and as a 114.6mm camera was employed the distance in mm between the centre of two symmetrical lines and each line was nummerically equal to 2θ. Calculations of d interplanar spacings involved the use of Bragg's relation:

$$\lambda = 2d \sin\theta,$$

and the values for the radiations wavelength were taken from the International Tables for X-ray Crystallography, Vol. III.

A calibration curve was obtained by using NaCl as standard (Table B-22.14 Appendix B) giving the error for each Bragg angle, as shown in Fig. 19 . All values presented in this report are consistent with this calibration.

In the case of a 114.6mm camera the distance between the centres of the incident and transmited beams should be 360mm, since the angle between them is 180°C. Therefore, the unsymmetrical or Straumanis method of film loading was used, facilitating corrections for film shrinkage.

2.3.4.3 Measurement and Calculation of the Intensities of X-ray Reflections

A Densitometer connected to a recorder provided with integrating facilities was used to determine the degree of blackening of each powder photograph diffraction line. The curve obtained for the intensity versus 2θ, was used to calculate the integrated intensity for each reflection above the general background blackening.

The blackening or photographic density D is given by the relation

$$D = \log_{10} \frac{I_o}{I}$$

where I_o is the intensity of the incident beam and I is the intensity of the transmitted beam.

Normally the density is directly proportional to the exposure (being defined by the relation: exposure = intensity of X-ray beam x time) up to densities values of about 1.0, corresponding

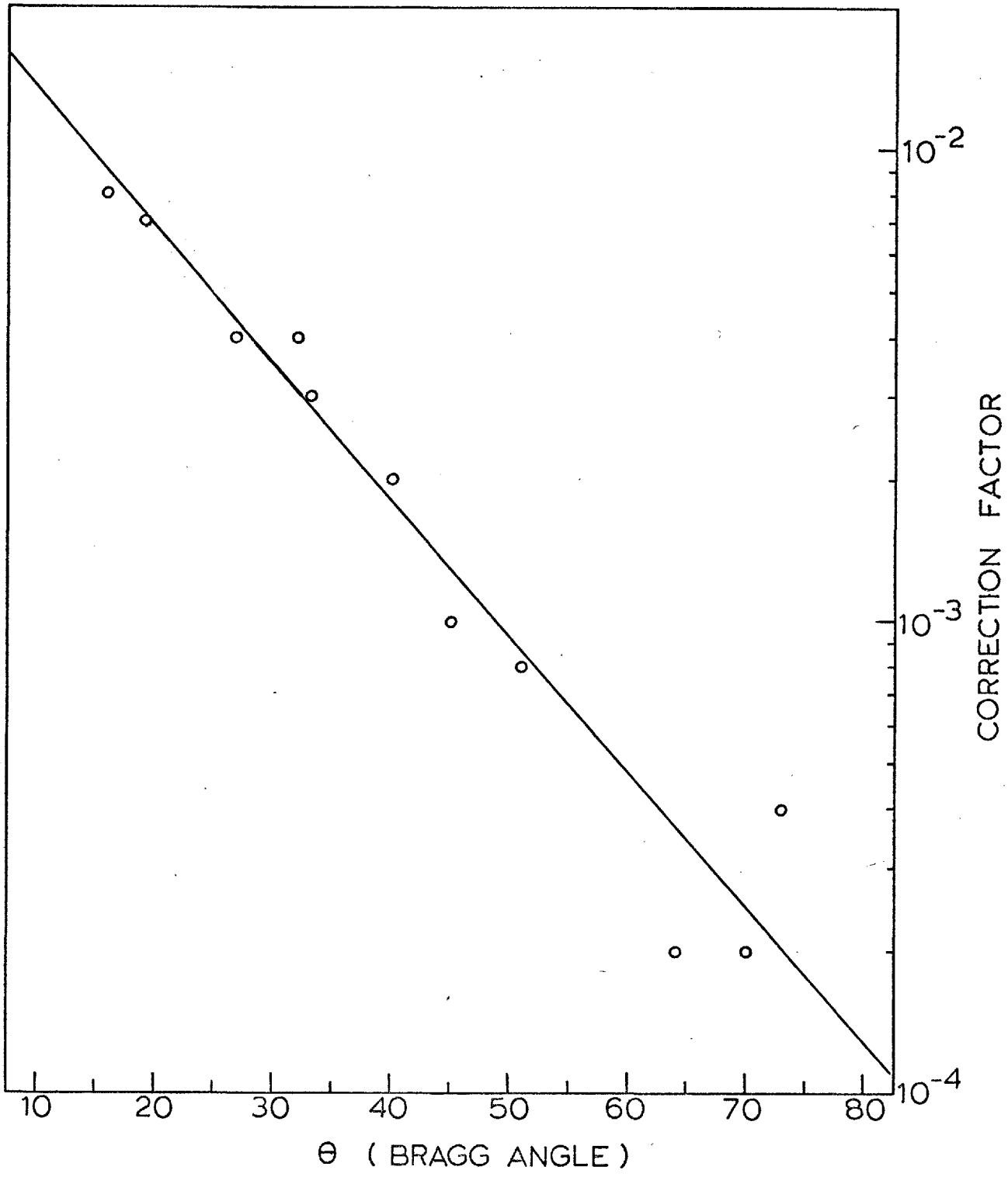

Fig. 19. Calibration curve using NaCl as a standard for the measurement of X-ray line positions

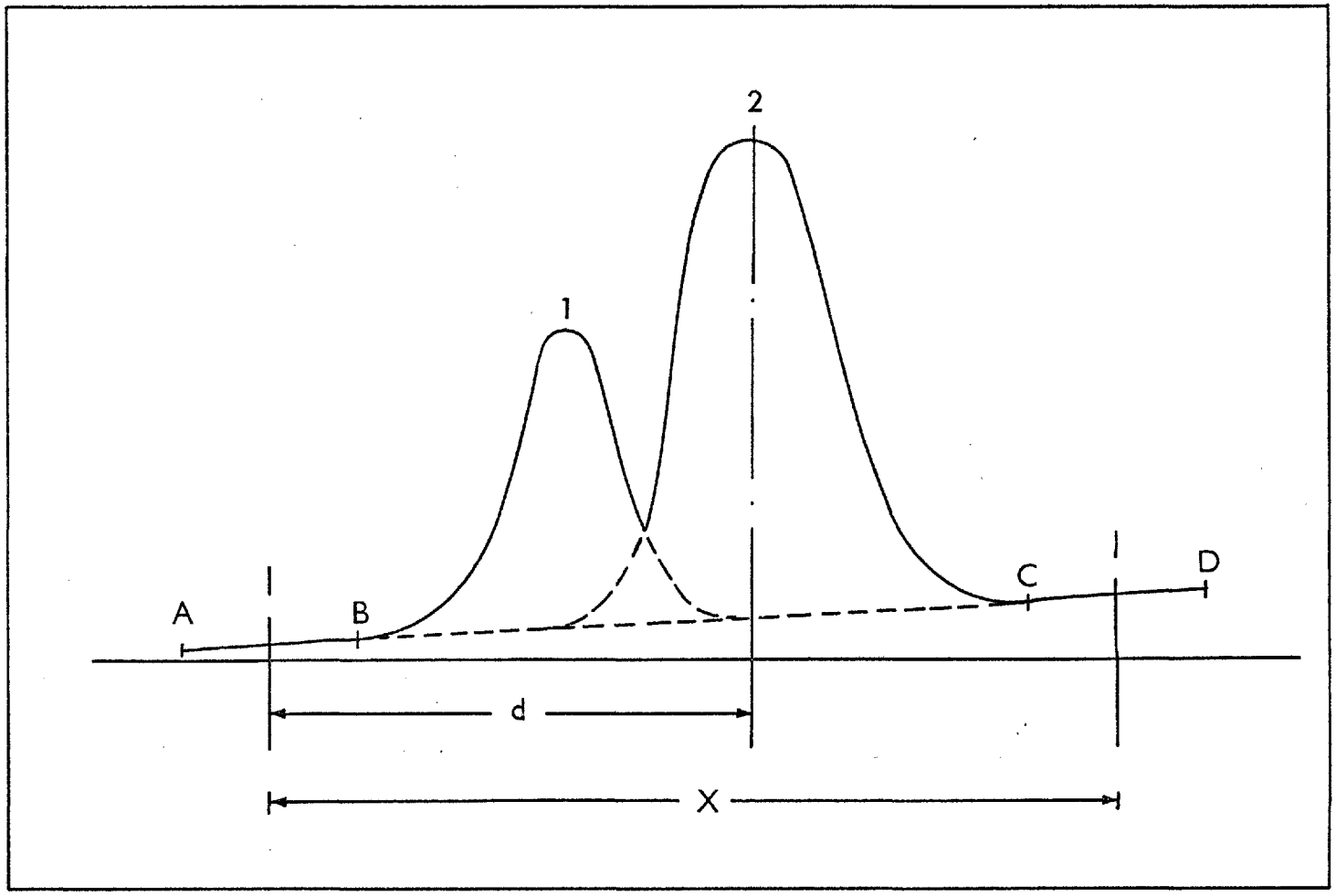

Fig. 20 Correction for the peak areas for two very close lines (104)

to 10% transmission of the incident beam. Great care was taken to observe this values, specially to give about the same exposure to all the films.

The integration of the areas was obtained by the number of counts given by the integrator.

When two peaks were not completely separate, due to two lines being very close together, determination of the corrected peak areas (whenever possible) involved the following relations[104] based in Fig. 20 .:

$$\text{corrected peak area} = T - W\,(k \pm c \times d),$$

where T is the total area counts for peak, W is the peak width (estimated), k is the first measured slope, d the distance from centre of peak to centre of first measured slope and c the rate of change (counts per unit of length).

The value of c is given by the relation

$$c = \frac{\ell - k}{X},$$

where ℓ is the slope of trace C-D, k the slope of trace A-B and X the distance between the centers of the traces A-B and C-D.

For superimposition of doublets α_1 and α_2, the correction suggested by Rachinger[105] can be used.

2.3.5 Other Methods

Among other methods used here it is worth while mentioning the microscopic examination of the polished samples of both unleached and leached samples, and observations under polarized light; electron probe microanalysis using a 1μ probe diameter and resolution usually better than 1μ, as well as X-ray fluorescence.

2.4 Purity of Materials

a) Copper Rod - Spectrographically Pure
(Johnson Matthey)

Spectrographic examination:

Element	Estimate of quantity present (ppm)
Silver	5
Lead	3
Nickel	1
Silicon	1
Bismuth, Cadmium, Iron, Magnesium	each less than 1

b) Iron Sponge - Spectrographically Pure
(Johnson Matthey)

Spectrographic examination:

Element	Estimate of quantity present (ppm)
Silicon	3
Magnesium	2
Manganese	2
Nickel	2
Copper, Silver	each less than 1

c) Sulphur Powder - Spectrographically Pure
(Johnson Matthey)

Spectrographic examination:

Element	Estimate of quantity present (ppm)
Aluminium	0.5
Sodium	0.2

c) cont..

Element	Estimate of quantity present (ppm)
Zinc	0.2
Barium	0.1
Nickel	0.1
Copper	0.05
Titanium	0.05
Magnesium	0.03
Manganese	0.03
Silver	0.03
Boron	0.01
Calcium)	
Iron) each less than	1
Silicon)	

d) Acetone - Analytical Reagent
(BDH Chemicals)

Distillation Range	Not less than 95% distils between 56.0° and 56.5°C
Acidity ($CH_3.COOH$)	0.002%
Alkalinity	0.03ml N/1%
Non-volatile matter	0.0005%
Aldehyde (H.CHO)	0.002%
Methanol ($CH_3.OH$)	0.05%
Substances reducing Permanganate(O)	0.0002%
Water	0.2%

e) Ferric Sulphate - General Purpose Reagent (low in Nitrate)
(Hopkin & Williams)

Specification

Chloride (Cl)	0.04% max.
Nitrate (NO_3)	0.003% max.
Ferrous iron (Fe)	0.028% max.
$Fe_2(SO_4)_3$, $9H_2O$	97% minimum

f) Sulphuric Acid - General Purpose Reagent
(Hopkin & Williams)

Specification

Non-volatile matter	0.015% max.
Chloride (Cl)	0.004% max.
Nitrate(NO_3)	0.0005% max.
Heavy metals (Fe)	0.0025% max.

About 98% w/w H_2SO_4

g) Hydrochloric Acid - General Purpose Reagent
(Hopkin & Williams)

Non-volatile matter	0.005% max.
Sulphate (SO_4)	0.01% max.
Heavy metals and iron (Fe)	0.001% max.

About 32% w/w HCl

h) Nitric Acid - Research Reagent
(May & Baker)

Specification

Assay	69-71% w/w
Chloride	Not more than 0.005% (Cl)
Sulphate	" 0.01% (SO_4)
Iron	" 0.002% (Fe)
Arsenic	" 0.0001% (As)
Lead	" 0.0002% (Pb)
Non-volatile Residue	" 0.01%

i) Hydrogen Peroxide - General Purpose Reagent (20 volumes)
(Hopkin & Williams)
Specification

Chloride	0.0015% max.
Non-volatile matter	0.2% max.

6% w/v H_2O_2 minimum

j) Sodium Chloride - Analytical Reagent
(Hopkin & Williams)

Specification

NaCl (after ignition) not less than	99.9%
Insoluble Matter	0.003%
Free Acid (HCl)	0.0018%
Free Alkali	0.05 ml N/1
Bromide and Iodide (Br)	0.005%
Nitrate (NO_3)	0.0005%
Phosphate (PO_4)	0.0005%
Sulphate (SO_4)	0.002%
Ammonium (NH_4)	0.00004%
Barium (Ba)	0.001%
Calcium and Magnesium (Ca)	0.004%
Iron (Fe)	0.0003%
Heavy Metals (Pb)	0.0005%
Potassium (K)	0.01%

k) REMKO Pure Iron Rod
(Ernst B. Westman)

Specification

	(%)
Carbon	0.03
Silicon	0.01
Manganese	0.12
Phosphorus	0.005
Sulphur	0.01
Chromium	0.005
Nickel	0.005
Copper	0.01
Tin	0.002
Total	0.197

SECTION 3

β-CHALCOPYRITE, RESULTS AND DISCUSSION

3.1 Ferric Sulphate Leaching. Kinetic Rate-Curves. Effect of the Leach Variables on the Rate of Reaction.

Kinetic rate-curves were obtained for the leaching of β-chalcopyrite with acidified ferric sulphate solutions, using the apparatus described in Section 2.2.

The influence of some variables on the rate was studied, and the results obtained suggested a possible mechanism for the leaching reaction.

Some extrapolations were necessary since the process of dissolution of β-chalcopyrite was very lengthy, with copper recoveries of about 26% after 26 days at 50°C. Even at 95°C extractions of up to 80% were only obtained after 7 days of leaching.

3.1.1 Temperature

The effect of the temperature on the leaching rate of β-chalcopyrite was investigated and the results found are shown in Table B-11.1 to B-11.4 (Appendix B) and Fig. 21

According to the rate-curves the leaching reaction seems to be characterised by a three-stage process, the first covering from 0% to slightly below 20% of copper removed, the second from this point to somewhere between 30% and 35% and the third stage from this value upwards.

The first part of the rate curves (0 to about 20% of Cu removed) showed that, in this range, the leaching reaction was sensitive to temperature. Attempts were made to calculate the critical increment of energy by extrapolation of the rate constants to the origin. This method, however, proved to be unsuccessful due to the fast initial removal of copper, and it was possible to obtain almost any value for the apparent activation energy. Also the slight oxidation of the surface of the particles is expected to affect the initial rate and contribute to inaccurate results. Attempts were made to obtain

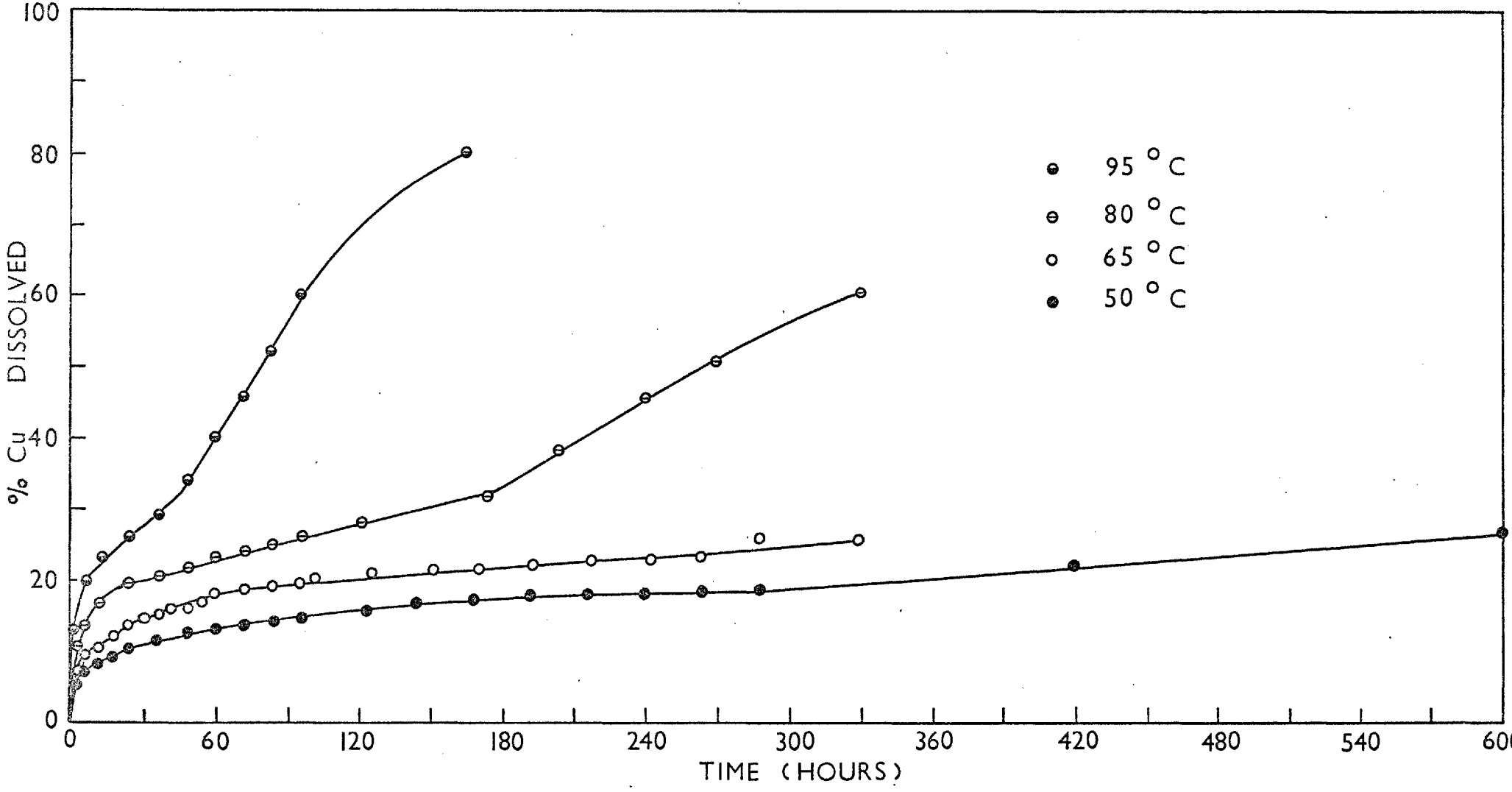

Fig. 21. Effect of temperature on the rate of leaching of β-chalcopyrite

a rate equation to fit the experimental curves, but were unsuccessful. The curves do not seem to appear to indicate simple order for the reaction at this stage. Very inaccurate approximations gave 7±3 Kcal mole^{-1} for the apparent activation energy. This critical increment of energy is too low for a chemically controlled reaction and slightly above the values normally considered when a reaction is entirely transport controlled (∿4Kcal mole^{-1}, Burkin[106]). It therefore seems to indicate an intermediate process where the rate is mainly controlled by a transport mechanism.

It was later found (Section 3.5) that some iron as well as sulphur (in sulphate form) passed into solution during this first stage of the leaching reaction.

During this stage, no elemental sulphur was detected by X-ray powder diffraction, but in residues above 14.5% of copper removed, traces were visible under the microscope. This examination also showed that the particles contained an appreciable number of pores and a few cracks, although retaining their initial shape (see Section 3.6)

The results obtained from the X-ray photographs of the leach residues (Section 3.2) indicated a variation in β-chalcopyrite lattice parameters, as well as a disordered variation in the intensities of some reflections, and a slight broadening of others.

Quantitative electron-probe determinations, obtained by point counting across the grains, showed no appreciable variation of composition, even near the edges, up to 6.5% of Cu removal. Above this value the results were not consistent (Section 3.3).

It seemed possible to explain the mechanism for this first stage as a process mainly controlled by the diffusion of copper to the surface ofthe particles, simultaneous with the oxidation of S^{--} and electron transference within the solid structure.

X-ray results on the residues (Section 3.2) and atomic absorption analyses of both residues and leach solutions (Tables B-21.1, B-11.9, Appendix B) indicated that the structure of β-chalcopyrite was maintained while copper was removed, and the relative proportions of the elements present in the solid altered. The unit cell showed a degree of contraction, responsible for the reduction of the rate of dissolution of copper during this stage, and also accounting for the few cracks observed.

However, with around 17.5% of copper removed, the interplanar d-spacings showed an abrupt variation and some broad lines appeared. This corresponded to the finding under the microscope of severely attacked particles and wide dissemination of cracks (See Section 3.6). Therefore, this point (17.5%) seems to be the limit between the first and second stage of leaching.

The second stage of the leaching reaction lies in the range 20% to somewhere between 30% and 35% of copper removed, and the corresponding rate-curves approach linearity.

The Arrhenius plot for the apparent activation energy, clearly shows two distinct lines, Fig. 22 , suggesting the presence of two competing reactions with different apparent activation energies, characteristic of a reaction occuring both homogeneously and heterogeneously. The homogeneous reaction, having the higher activation energy, is favoured at high temperatures, while the heterogeneous predominates at low temperatures. The respective values for the two branches of the curve were about 20Kcal $mole^{-1}$ and 1.5Kcal $mole^{-1}$.

This seems to indicate that at higher temperatures, above 65°C, the mechanism of dissolution is entirely different, specially when temperatures as high as 95°C are reached.

Attempts were made to find whether at high temperatures (above 65°C), the rate of this second stage of leaching was dependent on the concentration of the reactants. However, due to the extensive iron hydrolysis, the results obtained were not significant (see Section 3.1.3).

Results from X-ray powder diffraction analysis of the residues for this second stage showed, up to about 31.5% of copper removed, a reasonable constancy of interplanar d-spacings, although the values were slightly below the values found in the next stage for the final residues of the leaching reaction. The observed intensities were also reasonably constant.

As in the first stage, no elemental sulphur was detected by X-ray diffraction, but microscopic examination showed the existence of small amounts in pores and cracks.

Also, the number of pores and cracks did not increase significantly.

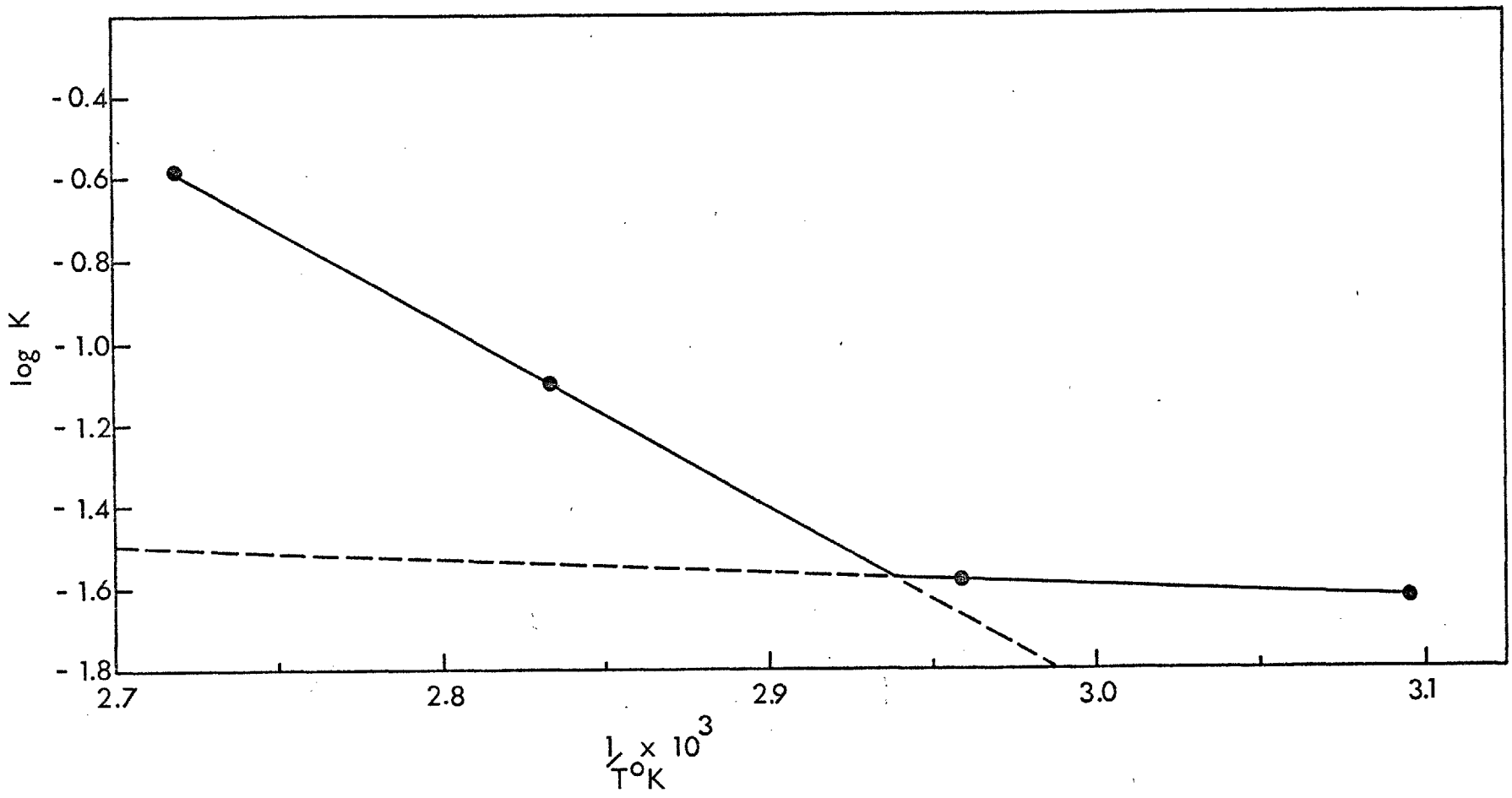

Fig. 22. Arrhenius plot for second stage of the dissolution of β-chalcopyrite

The apparent constancy of the rate, although the particles were reduced in size, could be explained by an increase in surface area due to the severe pitting and extensive number of cracks. This is further confirmed by the fact that both first and second stages of leaching were affected by the particle size (Section 3.1.2).

The X-ray results for the final residues of this stage showed values near to the typical α-chalcopyrite structure. However, analytical determinations for the composition of both residues (Table B-21.1) and leaching solutions (Section 3.5) led to the approximate formula $CuFe_{1.2}S_{2.3}$, with a Me:S atom ratio near to 1 (in fact 0.96) and Cu:Fe ratio equal to 0.82, in agreement with the findings of Yund and Kullerud[38] for the zone of existence of α-chalcopyrite structure (see Section 1.2).

The possibility of formation of iron sulphides during the leaching of β-chalcopyrite was considered. However, it can be seen from the E-pH diagrams (Appendix A), that under the conditions of the experiments (presence of oxidant at pH~1) ferrous sulphide is not stable and according to Kuzminykh and Yakhontova and reported by Habashi[107] the reaction

$$FeS + Fe_2(SO_4)_3 \rightarrow 3FeSO_4 + S$$

takes place quantitatively.

Thermodynamically, pyrite is not stable under the oxidising conditions used, but due to its slow rate of dissolution it should be detected by X-ray measurements, if formed during the leaching of β-chalcopyrite. However, neither ferric nor ferrous sulphides were found (Section 3.2).

On the other hand, copper sulphides are unstable under these conditions (see E-pH diagrams, Appendix A) and the dissolution reaction proceeds fairly quickly (King[81]).

Besides the α-chalcopyrite lines found in the X-ray photographs, a few other extremely faint lines were found and apparently they correspond to jarosite type compounds (see Section 3.2). However, they seem to be present in the solid in very small amounts and the interference with the atomic absorption determinations of the residue should be minimal. It seems reasonable to adopt for the final residue composition the formula $CuFe_{1.2}S_{2.3}$.

During the leaching process the colour of the solid changes progressively. It is initially a light copper, passing through a metallic yellow to a yellow grey similar to the dark golden yellow of α-chalcopyrite in contact with the atmosphere (Section 3.4).

For the third stage of dissolution of β-chalcopyrite, no rate-curves were determined at temperatures below 80°C since the reaction proceeded very slowly(*).

However, from the results obtained at 80° and 95°C (Fig. 21) it is evident that an abrupt change in the rate of dissolution occurred after 30 to 35% of the copper was removed. From this value upwards the rate-curves approached linearity and at about 60% of copper dissolution the rate slowly dropped. At the same time the solution became turbid, flakes of a solid looking like iron hydroxide covered the walls of the reaction vessel above the liquid level and appreciable amounts of what was later found to be elemental sulphur, floated in the leach liquor.

Microscopic examination (Section 3.6) showed the existence of small amounts of elemental sulphur on the edges, cracks and pores. This agrees with the common knowledge that in an oxidising medium, (see Appendix A), when leaching is conducted below 120°C (melting point of amorphous sulphur) the oxidation of sulphur to sulphate is very slow. The direct extraction of sulphur from the residues using carbon tetrachloride or carbon disulphide in a Soxhlet extractor proved almost unsuccessful with only a small percentage going into solution. However, some of the sulphur on the walls of the reaction vessel was extracted (CCl_4) and detected using an UV spectrophotometer at 275nm, Fig. 23.

This, with the constancy of composition of the residues found by analysis, seems to prove that, during this third stage of the leaching reaction, dissolution of the product with the α-chalcopyrite type structure led directly to the formation of elemental sulphur, most of this floating away from the solid residue.

An approximate value of 16Kcal was determined for the critical increment of energy in the range 80° to 95°C, excluding a transport controlled mechanism. However, this relatively low

(*) As already mentioned, 26% of Cu was removed after 25 days at 50°C.

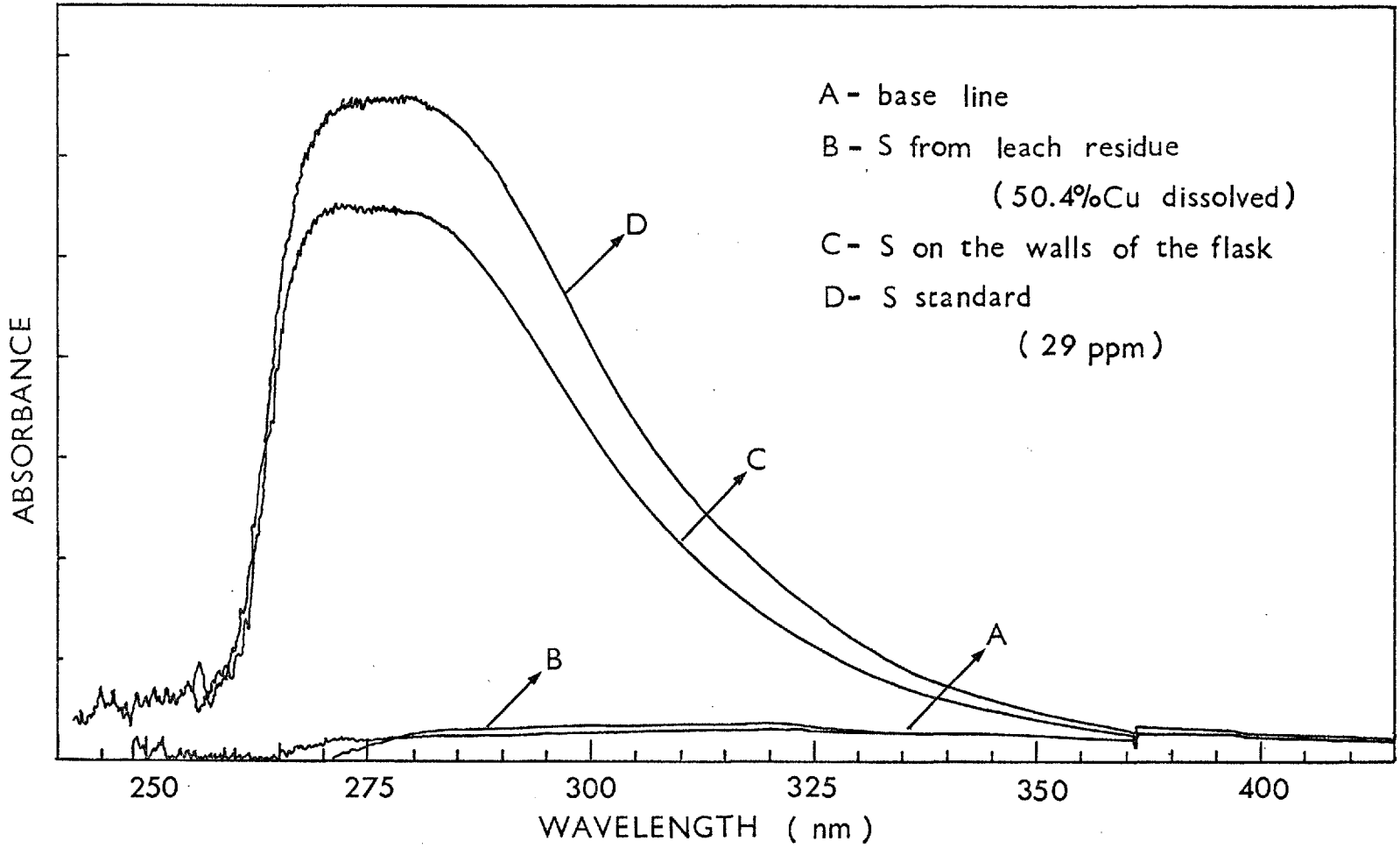

Fig. 23. The spectrum of sulphur extracted with CCl_4 from the β-leach residues and walls of the reaction vessel

apparent activation energy is believed to be due to the formation of a sulphur coating on the surface of the residue, making access to the surface of reactants and removal of the products formed, difficult.

The apparent drop in rate towards the end of the third stage of the reaction is probably due in part to the presence of a sulphur coating, and in part to the fact that the percentage of copper dissolved, determined by analyses of the solutions, was slightly too low.

Samples of the flakes mentioned above were collected from the wall and after careful washing they were redissolved. The solutions so obtained were analysed by atomic absorption spectrophotometry and showed the presence of considerable quantities of iron and small amounts of copper.

All of this agrees with the findings on the effect of the weight of the sample (Section 3.1.2) where the use of a smaller amount of β-chalcopyrite resulted in less iron being precipitated, and so less copper being entrained, resulting in a smaller drop in the leaching rate Fig. 25.

X-ray analysis of several residues obtained during this stage showed a constancy of the α-chalcopyrite d-spacings, and both composition ($\sim CuFe_{1.2}S_{2.3}$) and colour (dark yellow grey) remained approximately the same until disappearance of the solid. It was also observed by microscopic examination that the grains broke up to form very small porous particles of undefined shape.

A suitable mechanism for the dissolution of β-chalcopyrite can be devised in terms of charge balance if we consider the following hypothetical oxidation states for the elements in $CuFeS_{1.83}$:

$$Cu^{+} \; Fe^{++}_{0.34} \; Fe^{+++}_{0.66} \; S^{--}_{1.83}.$$

This is equivalent to assuming that 34% of the iron is in the form of Fe^{++}

During the first and second stage of leaching, about 34% of copper was removed before the sudden change of rate occured.

If no iron and sulphur were removed this would just correspond to the idealised oxidation of all the ferrous iron to ferric, in order to keep the charge neutrality. In fact it was found later, Section 3.5, that this copper removal was accompanied by about 19% of iron and the corresponding approximately 15% of sulphur, to maintain charge balance.

Schematically this can be represented,

$$\underset{34\%\ \text{removed}\ \downarrow}{Cu^{+}} \qquad Fe^{++}_{0.34} \xrightarrow[34\%]{} Fe^{+++}_{0.66} \qquad \underset{\downarrow 19\%\ \text{removed}}{S^{--}_{1.83}} \qquad \downarrow 15.6\%\ \text{removed}$$

leading to the final theoretical composition

$$Cu^{+} \quad Fe^{+++}_{1.227} \quad S^{--}_{2.3405}.$$

The results of atomic absorption analysis of the leach residue , Table B-21.1, Appendix B, showed for the solids obtained after 34% of copper removed a composition near to

$$Cu \quad Fe_{1.2} \quad S_{2.3}$$

in reasonable agreement with the hypothetical explanation given above.

This mechanism can be represented in an idealised form as:

$$2.30\ CuFeS_{1.83} + 0.574 Fe_2(SO_4)_3 = 0.47\ CuSO_4 + 1.252 FeSO_4 + 1.83 CuFe_{1.2}S_{2.3}$$

Once the composition $CuFe_{1.2}S_{2.3}$ is reached, the dissolution of the solid leads directly to the formation of elemental sulphur, and the following reaction can be assumed:

$$CuFe_{1.2}S_{2.3} + 2.2 Fe_2(SO_4)_3 = CuSO_4 + 5.6 FeSO_4 + 2.3S.$$

3.1.2 Particle Size and Sample Weight

Fig. 24 , Tables B-11.5, B-11.6, B-11.7 in Appendix B, shows the rate dependence on particle size and Fig. 25 , Tables B-11.4, B-11.5 shows the effect of sample weight.

It can be seen that, for the first and second stage of β-chalcopyrite dissolution, the rate of copper removed was increased by a reduction in the size of the particles. This fact agrees with the findings for the effect of temperature on the dissolution of β (Section 3.1.1), where a mechanism mainly controlled by diffusion of copper atoms from their positions in the crystal lattice to the solid-liquid interface was suggested.

These diffusion distances are reduced by the reduction in grain size, accounting for an increase in the leaching rate.

Also the amount of copper dissolved in the first and second parts of the reaction, was proportional to the initial weight of β-chalcopyrite, leading therefore to the same percentage, as shown in Fig. 25 . This confirms that the homogeneous reaction occuring simultaneously with the diffusion process was not a significant rate controlling reaction.

The third stage of the dissolution, above 30-35% of the copper removed, apparently was not affected by reduction in particle size. The end shape of the leaching curves is reasonably explained as the result of the transport of both reactants and products through the sulphur layer that builds up on the solid, and therefore is affected by the size of the particles.

The decrease in the size of the particles should increase the surface area, but in fact the α-chalcopyrite type structure being dissolved during this stage was so porous that subh decrease in size led to no significant increase in the solid liquid interface.

The independence of particle size found for the third part of the leaching reaction confirms the existence of a chemically controlled reaction.

On the other hand, the effect of sample weight, Fig. 25 , seems difficult to interpret due to the intense iron hydrolysis occurring when the amount of sample was doubled. However, the detection of small amounts of copper entrained by the iron

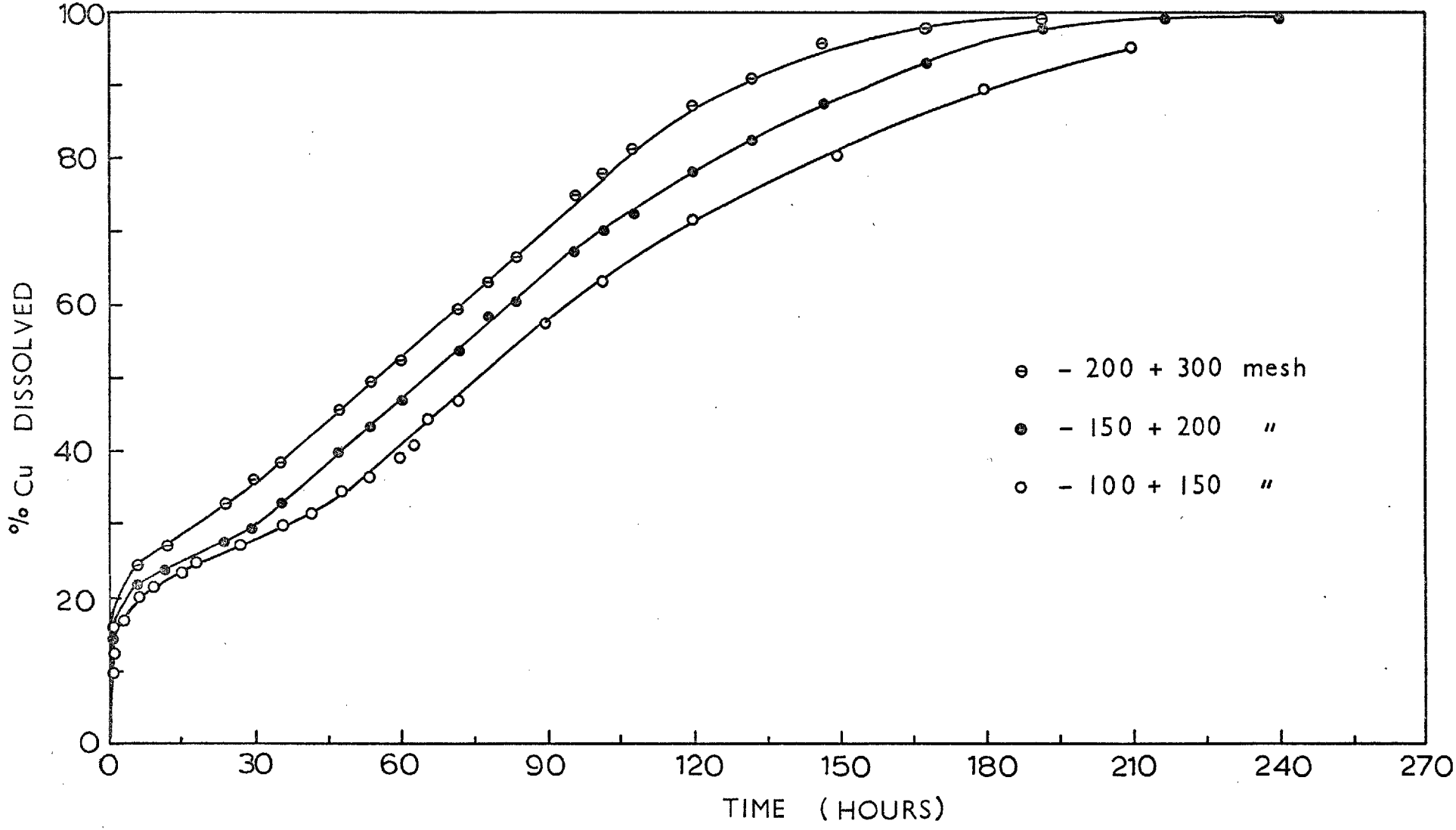

Fig. 24. Effect of particle size on the rate of leaching of β-chalcopyrite.

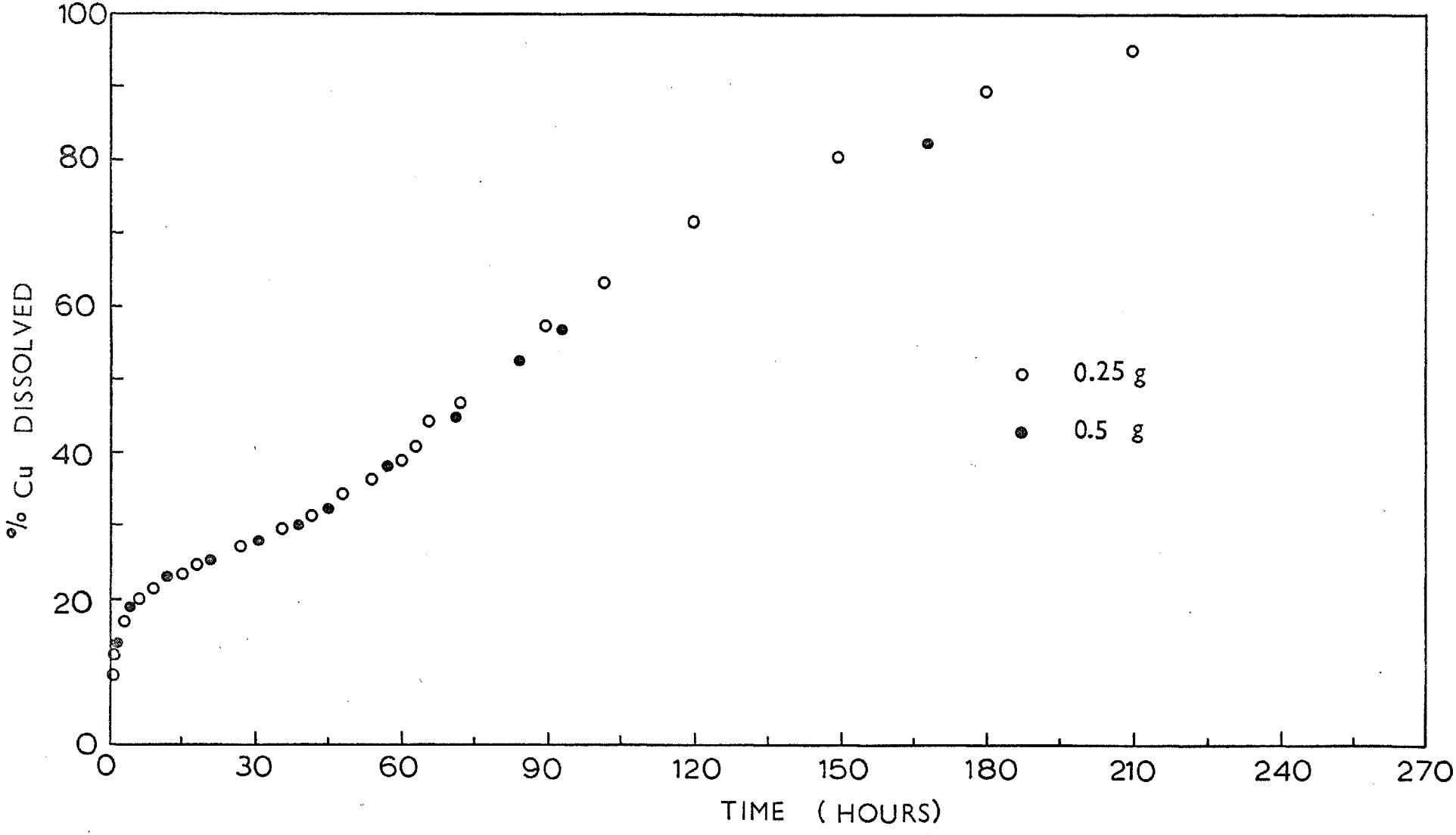

Fig. 25. Effect of sample weight on the rate of leaching of β-chalcopyrite

precipitate formed, will probably justify the displacement of the values obtained for the 0.5g sample to positions slightly above the corresponding values for the 0.25g sample.

It is worth noting, that it seems possible that preferential attack takes place in the pores and cracks, which will also result in this third stage not being affected by particle size. This type of attack is in good agreement with the small amount of sulphur detected in those faults.

3.1.3 Ferric Iron Concentration

Fig. 26 Shows the effect of ferric iron concentration on the first stage of leaching of β-chalcopyrite and the set of values obtained by the use of 0.01M and 0.03M Fe^{III} solutions at pH≈1 and T = 80°C are presented in Tables B-11.3, B-11.8, Appendix B.

From the plotted values it is evident that in the range 0 to about 20% of copper removal, the change in concentration of ferric ion has no effect on the leaching rate.

This behaviour shows that the rate-controlling step for the first part of the reaction is not a chemical process. Together with the relatively low apparent activation energy and dependence on the particle size this gives enough evidence to prove that the rate-controlling process is copper diffusion in the lattice.

Above 20% of copper removed, it is difficult to make a direct comparison between the results from the two ferric ion concentrations considered, since extensive hydrolysis occurred. This reduced the ferric ion activity and lowered the apparent percentage of copper removed, by entrainment of this element in the precipitate formed. X-ray analysis results (Section 3.2) seem to indicate the presence of two iron hydrolysed compounds; a jarosite-type produced in solution, and goethite on the walls of the reaction vessel, above the liquid level. This is in agreement with the reported studies by Brown[83-84], Section 1.7, on the equilibrium relationship between jarosite and goethite, the first being dominant at $pH_{25°C}$ values less than 3 and goethite stable at $pH_{25°C}$ greater than 3.

As during the leaching reaction the pH of the solution remained near to 1, goethite formation is believed to be due to the liquor splashes contacting water running down the walls from the condenser, and leading to a pH greater than 3.

Also iron hydrolysis is responsible for the slight lowering of pH during the dissolution of copper. This is shown by the values found for the final leach liquor and listed below

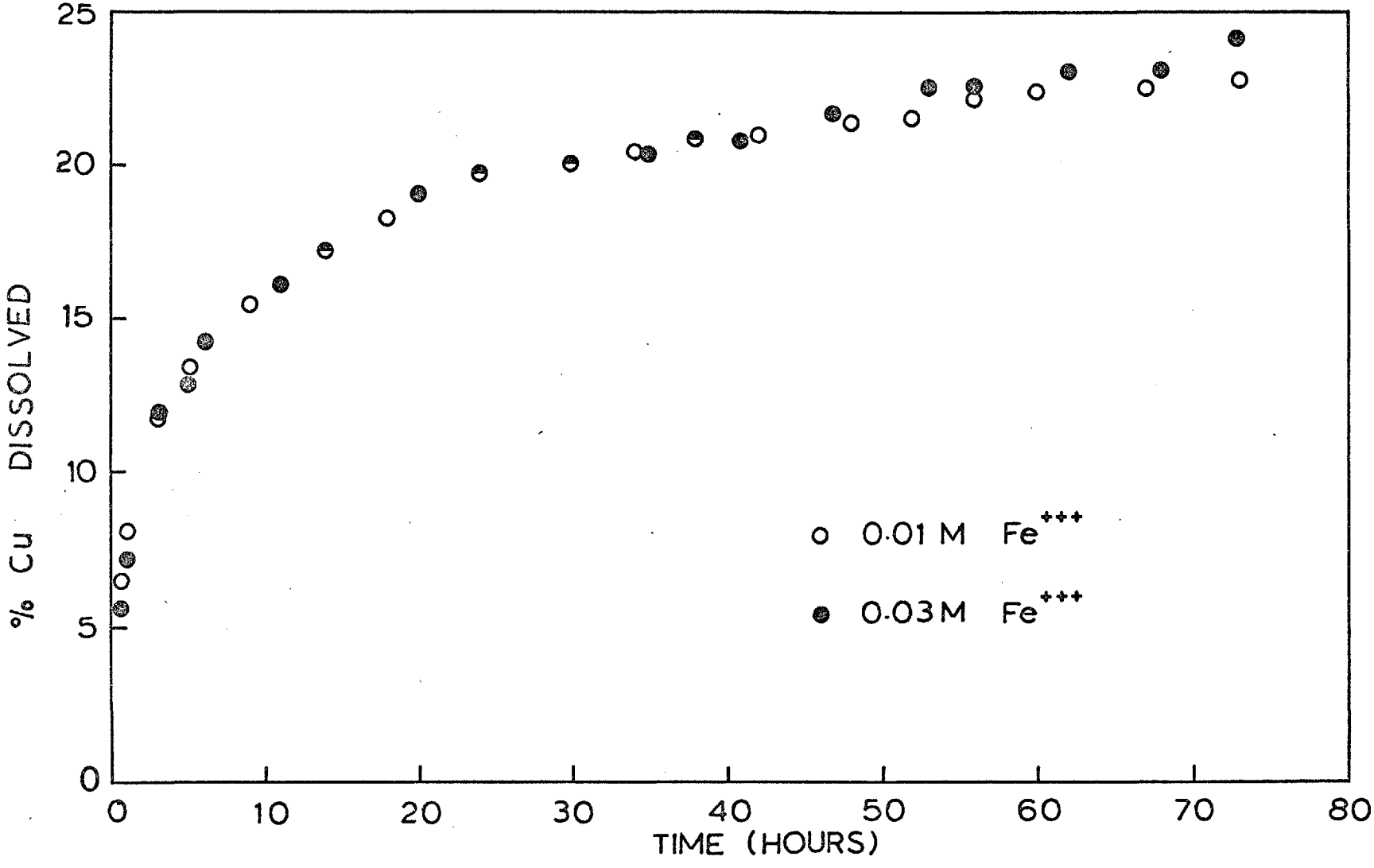

Fig. 26. Effect of ferric ion concentration on the rate of leaching of β-chalcopyrite (1st stage)

Initial pH = 1.00

Sample weight (g)	Particle size (mesh)	Temperature (°C)	Fe^{+++} (M)	Cu removed %	Final pH
0.5	-100 + 150	80	0.01	22.7	0.93
0.5	-100 + 150	80	0.03	60.2	0.96
0.5	-100 + 150	95	0.03	∿82.3	0.96
0.5	-100 + 150	65	0.03	25.9	0.98
0.5	-100 + 150	50	0.03	26.4	1.00
0.25	-100 + 150	95	0.03	95.0	0.96
0.25	-150 + 200	95	0.03	98.7	0.98
0.25	-200 + 300	95	0.03	98.9	0.98

It is also worth noting that these experiments to determine the effect of ferric ion concentration on the rate of leaching should have been carried out in a N_2 atmosphere since, in presence of air, the Cu^{++} acts as a catalyst for the oxidation Fe^{++} to Fe^{+++}.

3.2 X-ray Powder Diffraction Study of the Leach Residues

The method used for X-ray powder diffraction analysis was described in Section 2.3.4.

X-ray powder photographs of the leach residues obtained from the attack of β-chalcopyrite with acidic ferric sulphate solutions under different conditions, and for the range 0 to 98.74% of copper removed, are shown in Fig.B-1 to B-4, Appendix B. Data obtained from measurements on these photographs of both d-spacings and relative intensities are tabulated in Appendix B, Table B-22.3.

Attempts to calculate the integrated intensities of two very close lines, by the method described in Section 2.3.4.3, were unsuccessful in most cases, exception being made of the initial unleached samples, due to the poor resolution of the densitometer used. Therefore, in order to avoid misinterpretation whenever two or more lines were near to each other, the overall integrated intensity was calculated.

As already mentioned, the pattern obtained for the unleached β-chalcopyrite is in excellent agreement with those of Cabri[47] and Hiller and Probsthain[34], (see Section 2.1.1 and Table B-22.2 in Appendix B).

The variation of the d-spacings for the more important reflections is shown graphically in Fig. 27 to 29, and the data is presented in Appendix B, Table B-22.4, as a function of the percentage of copper removed for the range considered (0 to 98.74%).

The analysis of the results obtained, indicated that after 6.5% of copper removal there was a relatively smooth displacement in the d-spacings for the residues up to about 17.5% of copper removed, corresponding to a range of non-stoichiometry within the β-chalcopyrite phase and a contraction in the unit cell.

Intensity measurements, Table B-22.5, Appendix B, showed a disordered variation, this fact being possibly associated with the appearance of broadening in some of the lines while the others remained sharp. It is known that this broadening corresponds to a deviation from Bragg's law, when the reflection appears over a range of the angle.

The source of diffraction broadening of X-ray reflection in

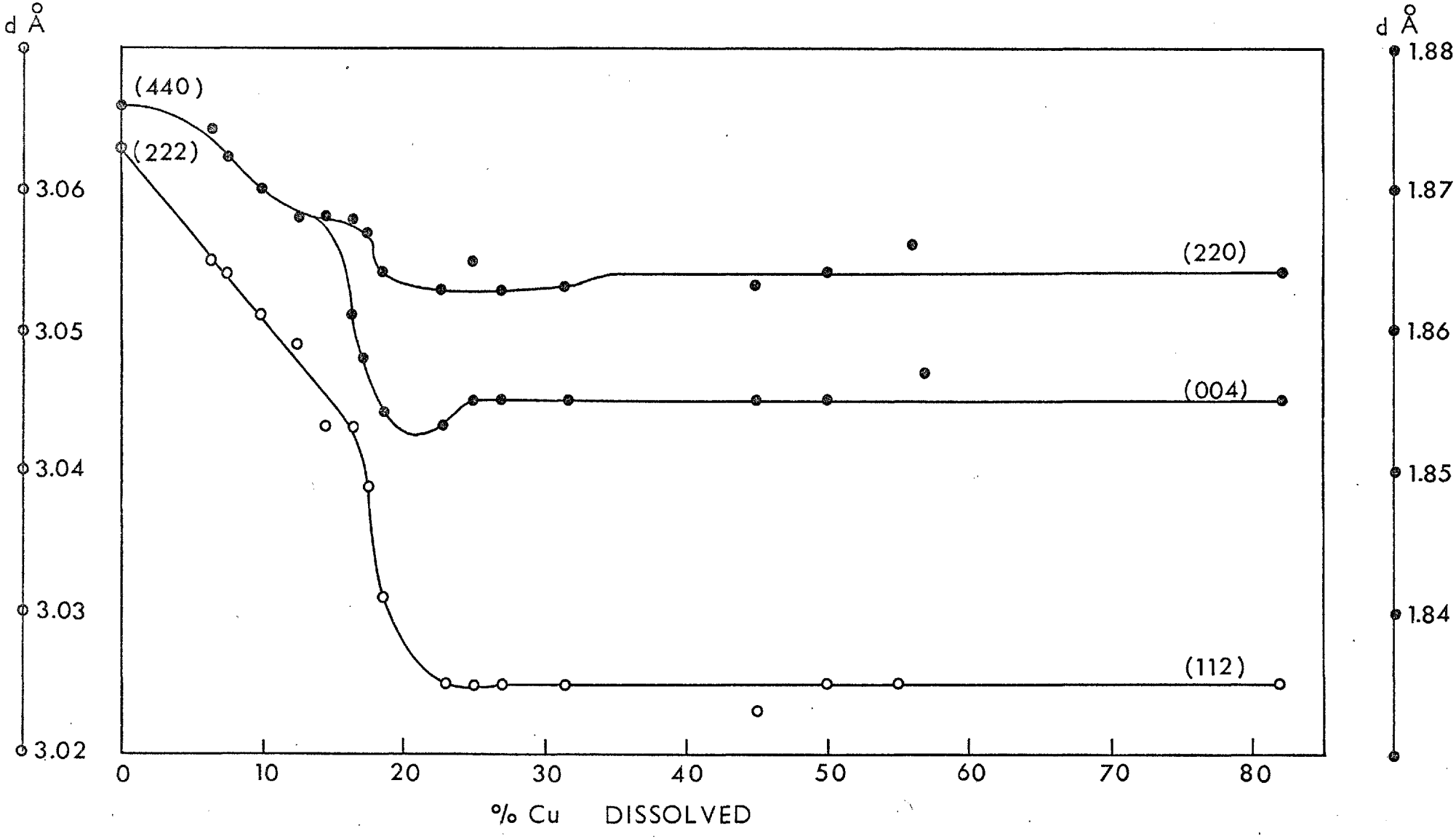

Fig. 27. Variation of the d-spacings with percentage of copper removed from β-chalcopyrite

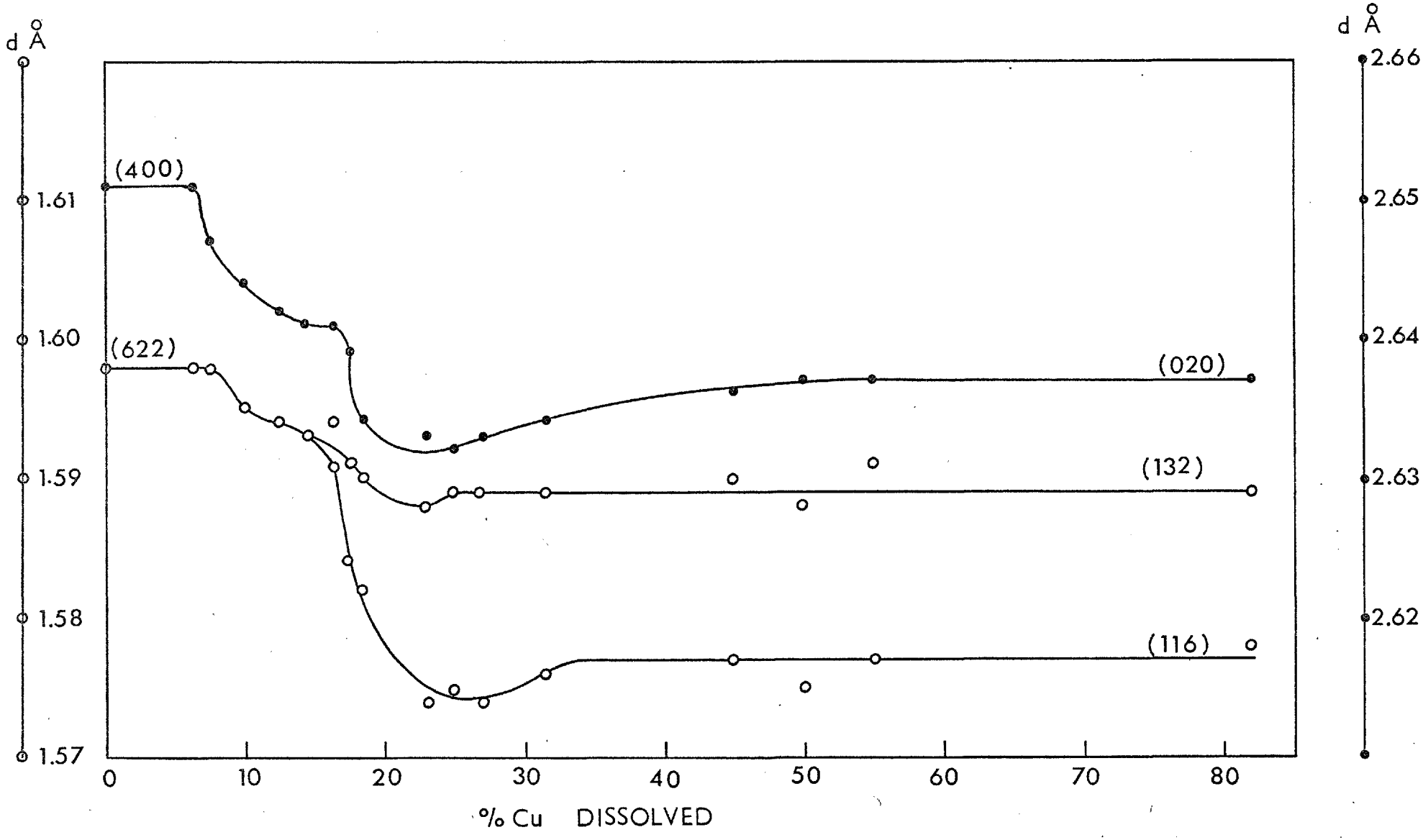

Fig. 28. Variation of the d-spacings with percentage of copper removed from β-chalcopyrite

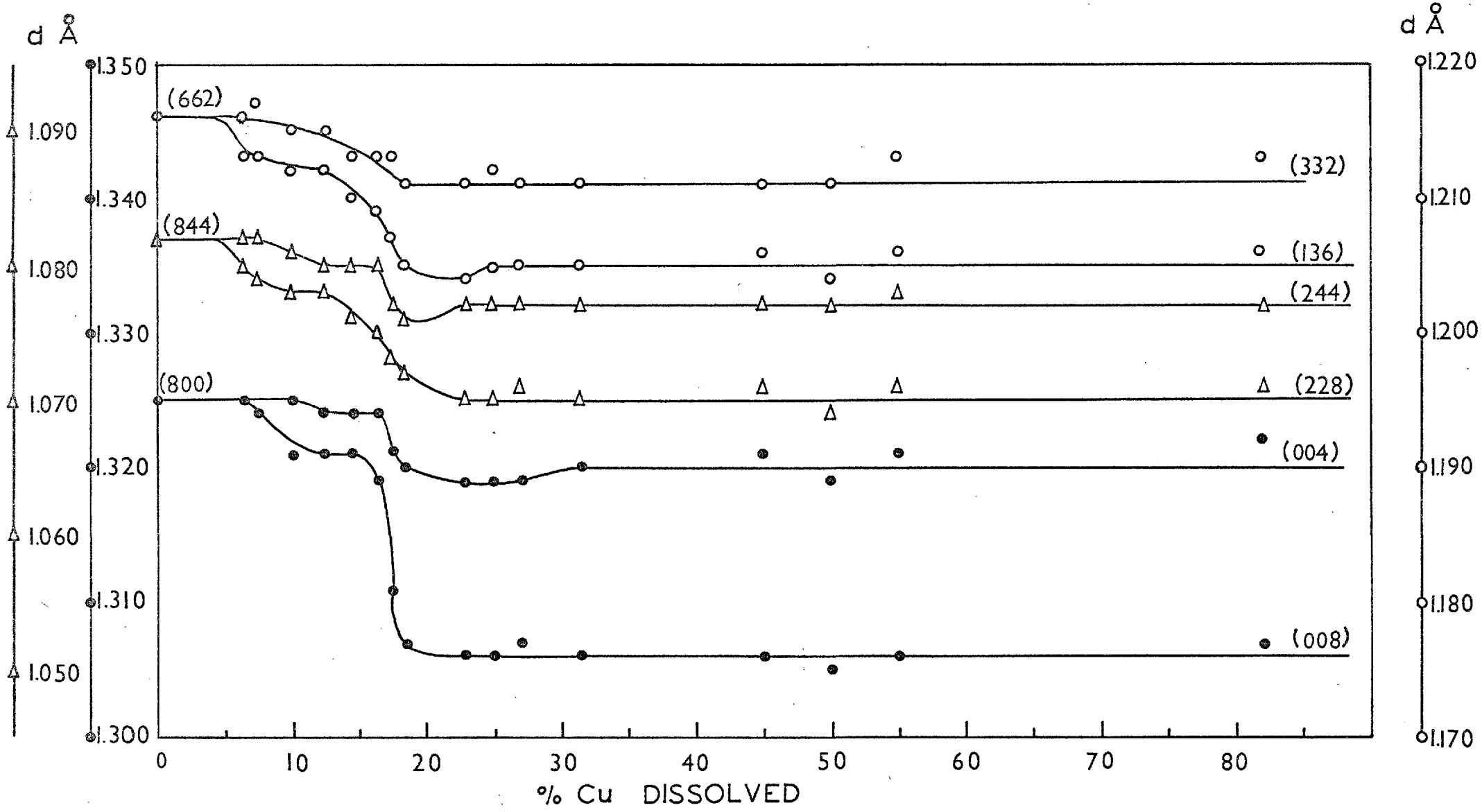

Fig. 29. Variation of the d-spacings with percentage of copper removed from β-chalcopyrite

the present case seems to be structural faults, since this broadening occurred in some of the lines but not in others, while for lattice distortion or small crystallite size all reflections are broadened. A typical case is when the faults simulate a certain structure, sharpening those reflections that are common to the simulated and basic structure and broadening those that are not common (Lipson and Steeple[108]).

This also suggestes that preferential attack will occur in those faults leading to the formation of cracks and pores. Fig. 27 and 28, show that the variation of d-spacings associated with the (440), (222), (400) and (622) reflections seems to suggest curves with an inflexion point, before they split into two lines, and this is caused by the difficulty of detecting the true point of separation. However a comparison with the values for (662), (844) and (800) where more accurate measurements were possible, showed that splitting starting at about 6.5% of copper removed. Fig29. Also during the first stage of leaching most of the very weak superstructure lines disappeared.

An abrupt collapse of the structure occurred at about 17.5% removal, when the limit of non-stoichiometry is reached, leading to d-values below the final stable interplanar spacings of α-chalcopyrite. The structure only "recovers" from this collapse after about 31.5% of the copper was removed. In this region, corresponding to the second stage of the leaching reaction, there is a range of non-stoichiometry that seems to be of non-equilibrium nature, similar to that found by King[81] for the leaching of chalcocite, which he suggested to be produced artificially by copper diffusion.

Also, the relative intensities for the reflections are reasonably constant, Table B-22.5, Appendix B, and near to ASTM values for tetragonal chalcopyrite, Table B-22.1, Appendix B.

During this stage it was possible to detect, apart from the reflections corresponding to α-chalcopyrite, several very weak lines, most of them persisting to the completion of the leaching. In fact, they seem to correspond to jarosite-type compounds but due to the extremely weak character of the reflection it was not possible to make a precise identification.

It is worth noting that in this stage, although small amounts of sulphur in the pores and cracks were observed by microscope examination (Section 3.6), no corresponding reflections were detected in the X-ray powder diffraction photographs.

The residues from the third stage of the leaching reaction, above 30-35% of copper removed, showed no appreciable variation of the d-spacing values. However, the start of this third stage corresponded to an abrupt increase in the relative intensities of all reflections (or a decrease in the (112) reference reflection) that remained, with random variations, to the end of the leaching.

Appart from the jarosite-type lines already mentioned, no sulphur reflections were detected, up to ∿99% of copper removed, although its presence was obvious, in edges pores and cracks, and floating in the solution.

It is worth mentioning that, if the almost linear curve for the variation of the d-spacing (222) d≃3.06 to (112) d≃3.03 in the range 0 to 15% of copper removed is prolonged, Fig. 27 it will join the line (112) d≃3.03 at about 35% of copper removed. This extrapolation will correspond to a case where the abrupt collapse of the structure does not occur, and to the assumption of a regular displacement in the residue lines. Table B-22.3, for the final leach residues of β and Table B-22.11, for the unleached α-chalcopyrite, show the similarities of the d-spacings obtained for both solids.

During the course of the experiments, when it was found that the composition of the residue after 30-35% of the copper had been removed was approximately $CuFe_{1.2}S_{2.3}$, there seemed to be a possibility of the existence in the residue of non-stoichiometric iron sulphides. For this reason a small sample of Pyrite (Premier) was heated in a sealed long quartz tube of small diameter, previously evacuated and filled with argon. This tube was placed in the furnace described in Appendix C, the sample being in the hot zone and the other extreme of the tube in a cooler part to allow the sulphur to condense. Thus, X-ray patterns of sulphur deficient iron sulphides were determined from a sample taken first to 650°C and later to 726°C (Table B-22.7, Appendix B, Fig. B-5 , Appendix B). None of the very strong sulphur reflections (Table B-22.6) was present in the X-ray powder photographs of the solid taken to these temperatures and the d-spacings seemed to indicate a transition from pyrite to pyrrhotite.

The obtained values, together with the ASTM data for pyrite and sulphur deficient iron sulphides (Table B.22-6, Appendix B) showed that none of these products seem to exist in the leach residues and none is responsible for the extra lines later attributed to jarosite-type compounds.

A second experiment involved the reaction of both β and α-chalcopyrites with a solution of sulphuric acid, pH∿0.5, at 95°C.

After removing 24% of copper from both synthetic products, each of them was divided into two fractions, one being washed just with water and the other also with carbon tetrachloride. The resulting X-ray patterns for the two fractions of both β and α-chalcopyrite residues are shown in Tables B-22.9 and B-22.10 Appendix B.

From the results obtained, it is apparent that the water-washed residues produced very intense sulphur lines (Fig. B-6 , Appendix B), which disappeared on washing with CCl_4.

They also show that the remaining reflections of the β-residues from the sulphuric leach are similar to those obtained in ferric sulphate solutions, for the same amount of copper removal. As for α , they approach the values determined on the residues of the third stage of the ferric sulphate leaching.

This, together with the attempts at sulphur dissolution mentioned in Section 3.1.1, seems to indicate that, during the ferric sulphate leaching, the elemental sulphur formed either floats away from the solid surface, or has an amorphous structure, therefore giving no X-ray reflections.

Drops of CCl_4, placed on a polished section of the β-residues, dissolved a small amount of the sulphur present in the pores and cracks, but it was impossible to decide whether the remaining sulphur was insoluble or just protected from the solvent by the mounting resin.

Finally, the red-brown flakes, found covering the walls of the reaction vessel above the liquid level (Section 3.1.1) were analysed by X-ray powder diffraction and the pattern obtained identified them as goethite (Table B-22.8, Appendix B, and Fig.B-5 Appendix B), in agreement with Brown's[84] findings (see Section 1.7).

3.3 Electron Probe Microanalysis

Electron Probe Microanalysis was performed on polished samples of both unleached β-chalcopyrite and residues from the acidic ferric sulphate leachings.

As already reported this method confirmed the homogeneity of the synthetic material prepared and showed no variation of composition on the lamellae type structure, visible under the microscope.

Attempts were made to obtain an electron probe scan for copper, iron and sulphur across the grains of leach residues. However, this method proved to be unsuccessful due to the peculiar behaviour of the samples under the probe. Thus by the simple action of the beam sweeping across the leached particles, cracks were immediately formed, and normally in a second passage they broke apart and apparently shrank. The corresponding scan was rough and non-reproducible, this effect increasing with the percentage of copper removed.

This method was abandoned in favour of point counting in fixed positions using very low current in order to avoid damage on the particles.

Special care was taken to reduce possible sources of errors, and for this a block of resin was cast and small holes drilled, where the powder-residues were placed, then refilled with resin and finally polished. It was possible, in a suitable size block for the probe, to hold 20 samples including a copper standard from spectrographically pure rod, and an iron standard from "Remko" rod (see Section 2.4 for specifications). For sulphur, pyrite was used as standard.

In the conditions mentioned above, consistent results were only obtained for the initial untreated β-chalcopyrite and residue from 6.5% of copper removal, Table B-21.2, Appendix B.

Above this value it can be seen that even two different sets of counts, each consisting of the average counting on a series of fixed positions across the same grain, gave different values. Appreciable variations during the actual counting in a fixed position were obtained.

The reason for this behaviour seems to be the very porous nature of the leach residues that are unable to dissipate the energy of the incident beam, leading to the crumbling of the structure and are not, therefore, due to heterogeneities.

3.4 Change of Colour

There was a progressive change in the colour of the residues during leaching of β-chalcopyrite with acidic ferric sulphate solution. This change was a function of the amount of copper removed and, therefore, of the stage of the leaching reaction.

Below are listed the colours observed during the dissolution of the solid:

Copper removed %	Colour
0	Brass yellow
6.5	-
7.5	Copper colour dark
10.0	Copper colour light
12.5	"
14.5	"
16,5	"
17.5	Copper cclour metallic
18.5	Copper colour light
23.0	Metallic yellow
25.0	Yellow grey
27.0	"
31.5	"
45.0	-
50.0	Dark yellow grey
55.0	-
82.0	Very dark yellow grey

3.5 Leaching with Hydrogen Peroxide

In view of the results described so far, it seemed useful to carry out an oxidizing leach of β-chalcopyrite without introducing iron or sulphate ions, apart from those derived from the dissolution of the solid under attack.

With this method it was expected that it would be possible to follow in more detail the variation of composition of the solid residue as copper was removed, by analysis of the solution.

The oxidant chosen was a solution containing 1 part of 20-volume hydrogen peroxide to 3 parts of hydrochloric acid solution adjusted to pH ~1. A 0.2g of -200 + 300 mesh β-chalcopyrite was leached with 200 ml of this solution at 65°C. The initial pH of 1.00 was found to have varied to pH 1.03 after removal of about 80% of the copper.

Thus, using atomic absorption spectrophotometry for the iron and copper in solution and nephelometry for the sulphate it was possible to determine by difference the ratios Cu:Fe and Metal:S in the solid residue as a function of the copper removed. The results obtained in this experiment are presented in Table B-11.9, Appendix B, and Fig. 30 to 32 .

The analysis of the curve relating the percentage of copper to that of iron removed, Fig. 30 , indicates that there was an initial removal of 6-7% of the former without any apparent dissolution of iron. This corresponds to the range where no noticeable variation was found for the cell parameters, as can be seen in Fig. 27 to 29 , and seems to be explained by the great mobility of some copper atoms in interstitial positions, as assumed by Hiller and Probsthain (34) - Section 1.2.

At about 17.5% of copper removed a change of slope occurred coinciding with the collapse of the structure. At the same time the Me:S ratio in the residue reached a value of 2:2 from its initial 2:1.83 ratio (Table B-11.9, Fig. 31). This seems in fact to be the limiting composition where the β-phase is no longer stable.

After this stage of leaching, a second change of slope occured in the curve % copper removed versus % iron removed, when 34% of the former was dissolved and the solid reached a composition between $CuFe_{1.2}S_{2.3}$ and $CuFe_{1.2}S_{2.4}$.

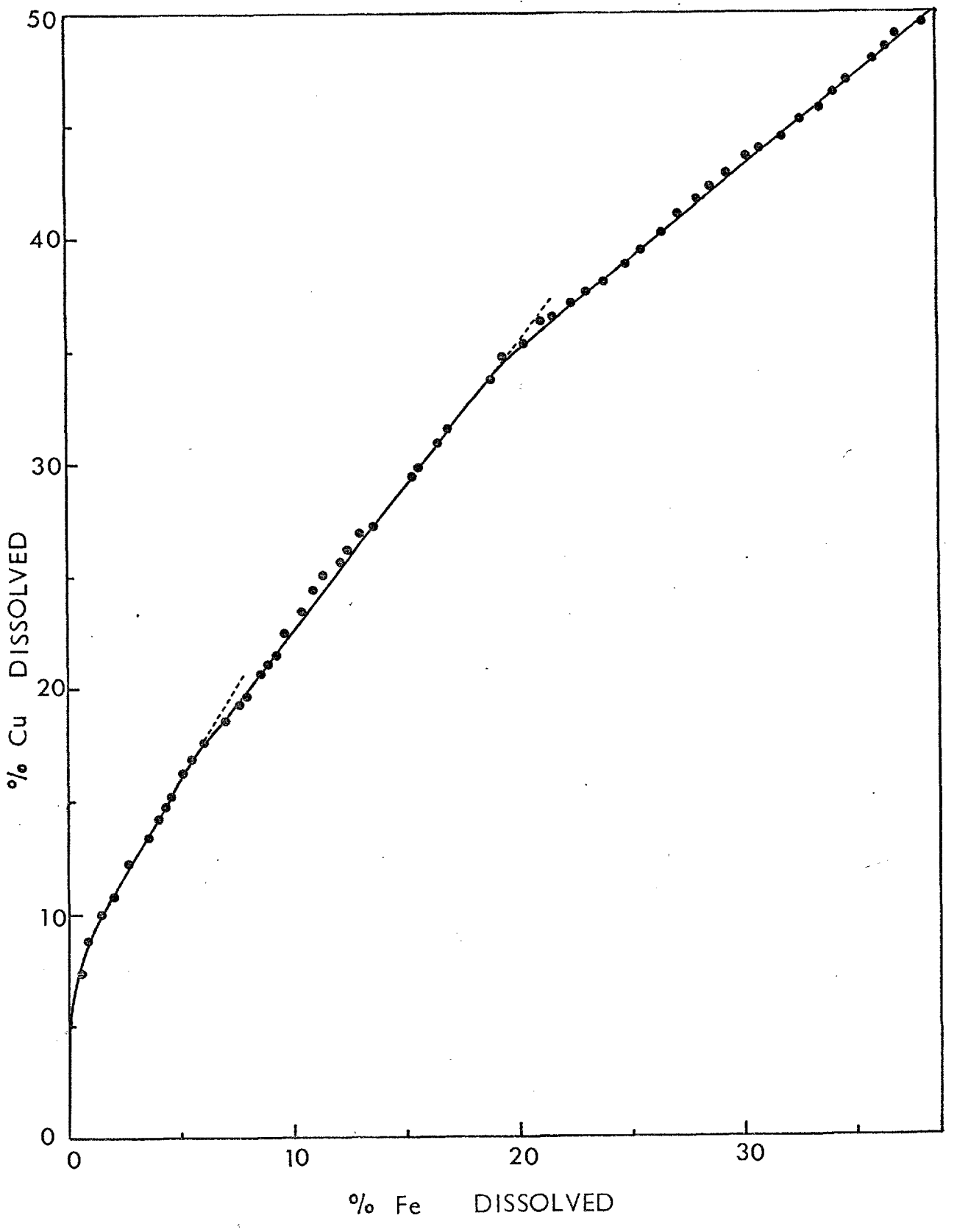

Fig. 30. Curve relating the percentage of copper to that of iron removed during leaching of β-chalcopyrite with hydrogen peroxide

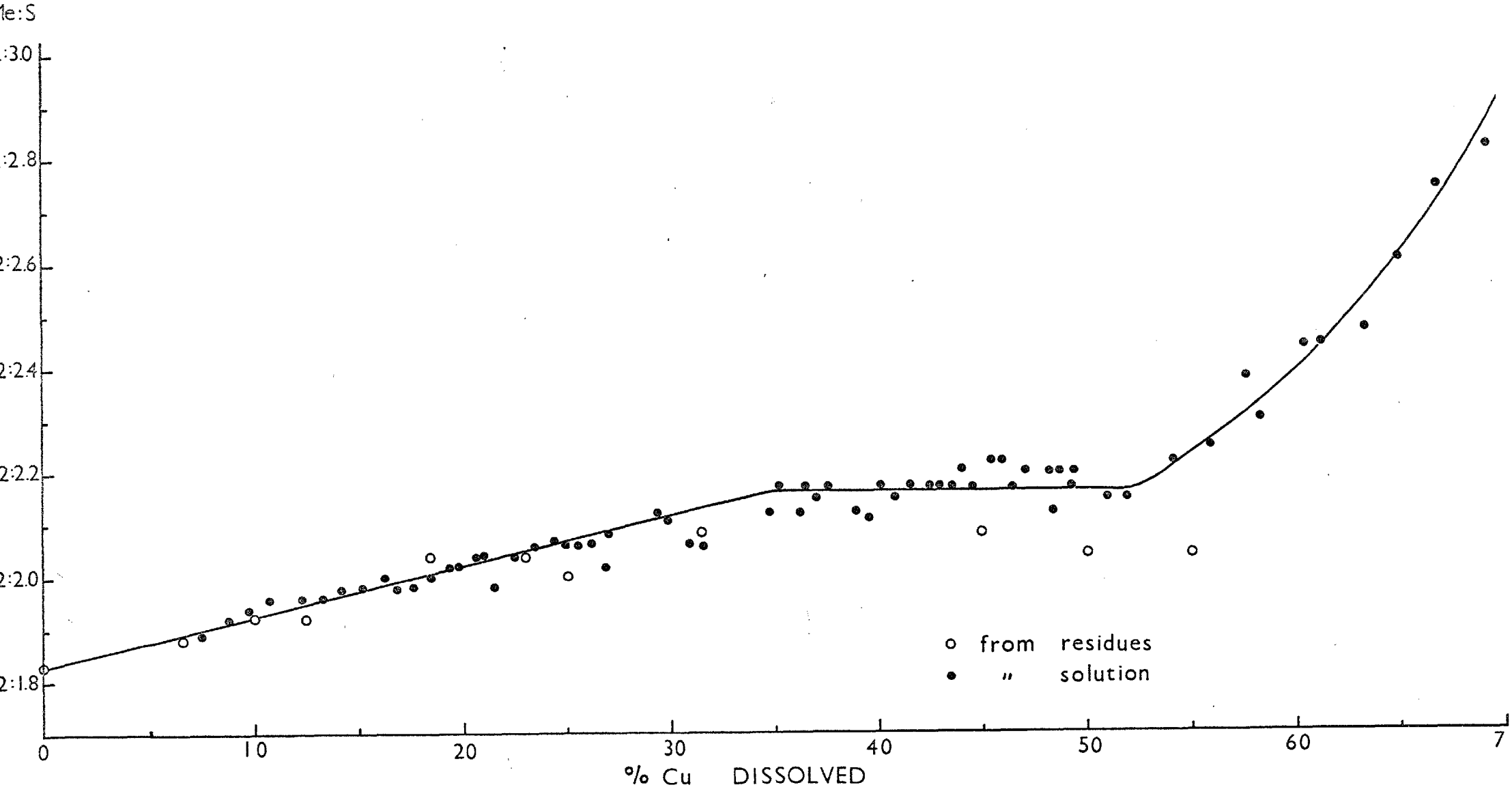

Fig. 31. Variation of the Metal to Sulphur ratio in the leach residues of β-chalcopyrite

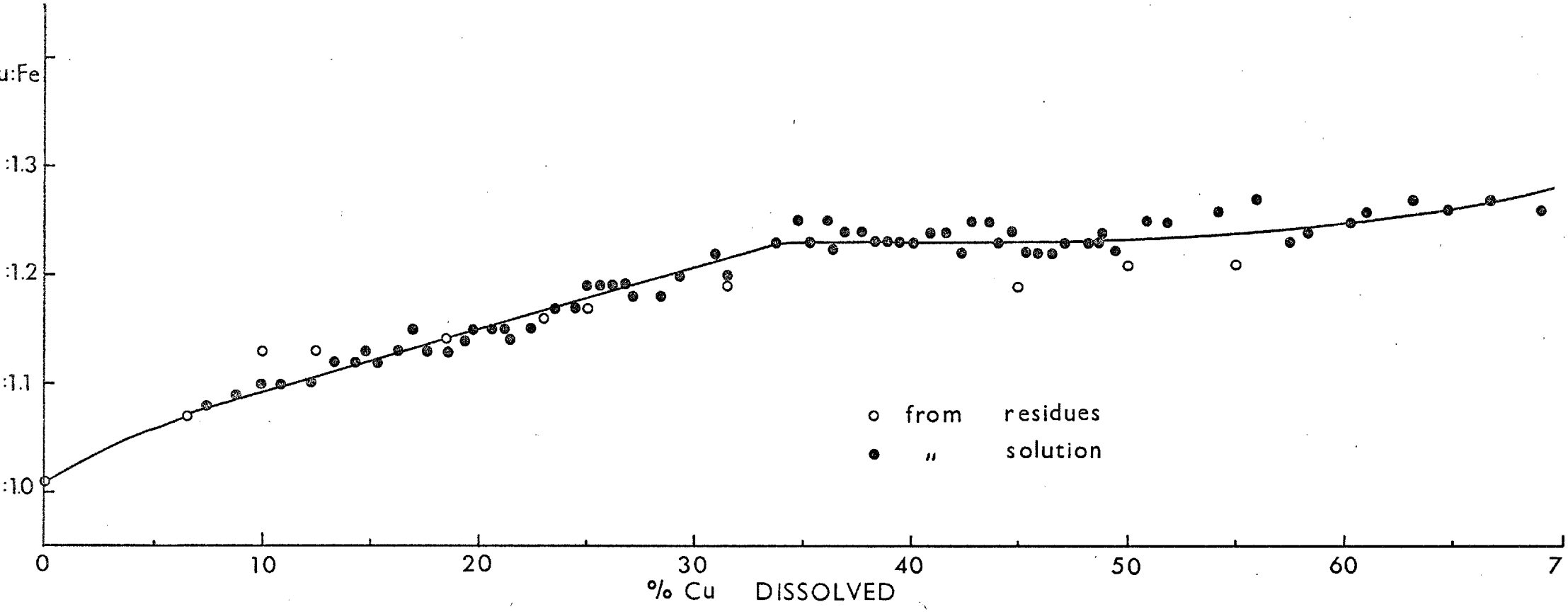

Fig. 32. Variation of the Copper to Iron ratio in the leach residues of β-chalcopyrite

Above this value of copper removal the composition remained approximately constant until about 50% had gone into solution. At this stage small amounts of sulphur and a fine white precipitate were noticeable, both increasing rapidly as the reaction proceeded.

Analysis of the precipitate showed it to contain appreciable amounts of iron, and this is reflected in the diagram of the Cu:Fe ratio, by an apparent increase of iron content in the residue. A similar effect occurs for sulphur since the Me:S ratio was calculated in the basis of sulphate concentration in solution. This also explains the deviation between the values of the curves and the values determined by direct analysis of the residues.

Although quantitatively inaccurate, these diagrams produced useful information to confirm the results found previously.

3.6 Microscope Examination

In order to observe microscopically the changes occurring in the solid residues, the leached samples having different amounts of copper removed were mounted in "Araldite" resin and polished. The corresponding photomicrographs of the polished sections are presented in Appendix B, Fig. B-9 to B-17 .

Fig. B-10 shows that particulate unleached β-chalcopyrite (-100 + 150 mesh) has very few pores, and this remains the case while the first 6.5% of copper is removed (Fig. B-11). During this part of the leaching reaction the measured d-spacings remained practically constant, Fig. 27 to 29, and as was shown by the leaching reaction with hydrogen peroxide, 6 to 7% of the copper is removed without dissolution of any iron. It has been suggested above that the mechanism of this initial part of the reaction is diffusion of copper in interstitial positions, without significant change of the lattice parameters.

Residues in a slightly more advanced stage of leaching (12.5% Cu removed) showed an uneven surface and irregular edges, Fig. B-12 , due to the number of pores and cracks formed, but the particles retained, more or less, their initial size. This remained the case until the end of the first stage of leaching, when 17.5% of the copper had been removed, and the structure collapsed with the formation of many much smaller particles, as shown in Fig. B-13 .

From this point onward the pores and cracks increased slightly in size but few new ones were formed, Fig. B-14 , suggesting preferential attack, and corresponding to the second stage of the reaction where the structure "recovered" from the abrupt change, until the α-chalcopyrite lattice type was reached. Except for the small amounts of sulphur found in the pores and cracks, no other phase was found to be present in the residues. Fig. B-14 , also indicates that the lamellae type structure found in the unleached sample of β-chalcopyrite (Fig. B-9) was still present after 23% of the copper had been dissolved, and shows no preferential attack along the lamellae.

The third stage of leaching, above 30-35% of copper removal,

corresponding to direct formation of elemental sulphur from the compound with the α-chalcopyrite type structure, presented problems of polishing, due to the very porous and fragile residues obtained.

The particles show, Fig. B-15 , an increasing attack of the surface, especially along the pores and cracks, and the grains simply broke into smaller particles until almost complete disappearance of the solid Fig. B-15 , to B-17.

It is possible that the lamellae structure remained to the end of the leaching since it is still visible on the photomicrographs for 45 and 55% of copper dissolution. Also no other phase was detected until the last sample of residue apart from small amounts of sulphur.

This element was found in all residues with more than about 12.5% of copper dissolved. Drops of CCl_4 on the polished section showed that part of sulphur was extracted but it was impossible to say if the rest was insoluble or if it was protected by a layer of the mounting resin.

SECTION 4

α-CHALCOPYRITE: RESULTS AND DISCUSSION

4.1 Ferric Sulphate Leaching. Kinetic Rate-Curves

Experiments involving the leaching of α-chalcopyrite with acidic ferric sulphate solutions showed that the rate of copper removal was slower than the rate obtained under identical conditions with β-chalcopyrite.

The results obtained with the α-form and the experimental conditions considered are summarized in Table B-12.1 to B-12.4, Appendix B, and discussed in the following sections.

4.1.1 Effect of Storage Time

The first example of peculiar behaviour of the synthetic α-chalcopyrite was found from the kinetic curves, when leaching samples of this material under identical conditions, but after different storage times. In Fig. 33 are shown curves obtained using 1g samples, ground to -100 + 150 mesh, and treated at 80°C with 0.1M Fe^{+++} solution (pH1). The times between the synthesis of the solid and the start of the leaching runs were 6, 40 and 78 days.

It is apparent that the initial rate increased from one experiment to the next and that the rate of the second part of the reaction decreased. This variation was found to be complete after 14 months had passed since the α-form material was prepared.

Examination under the microscope (Section 4.5) after 9 months of storage, showed that the unleached solid was fractured, and that segregation had occurredat some of the external edges. A small number of pores had also formed. This, together with the results from the electron probe microanalysis, where a higher copper content was found at the edge and around the pores of the stored sample, (Section 4.2) suggested that a copper segregation occurred by diffusion of this element to the edges and this caused fracture of the material, making easier removal of some copper by the leaching solution.

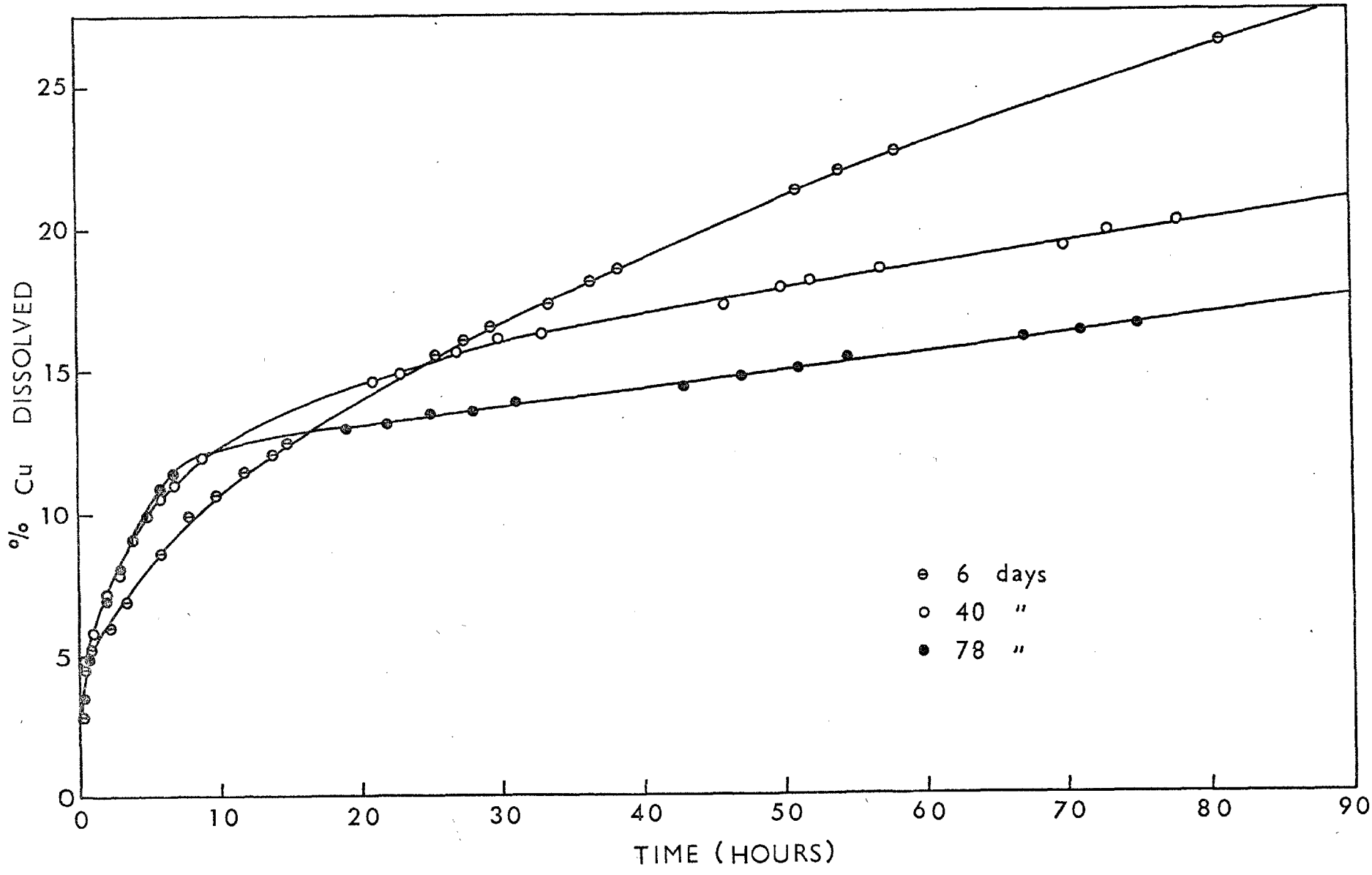

Fig. 33. Effect of storage time on the rate of leaching of α-chalcopyrite

This seems to indicate that the form prepared, $Cu_{1.12}Fe_{1.09}S_2$, was metastable tending to change to the more stable $CuFeS_2$ form.

A leaching experiment conducted after 14 months of storage showed, Fig. 34 , Tables B-12.6 and B-11.5, Appendix B, that about 11-12% of copper were easily removed and from then on the behaviour was very similar to natural chalcopyrite. This initial copper removal corresponded approximately to the excess existing (10.7%) over the stoichiometric.

Also the atomic absorption analysis of the leach residues, presented below,

% Cu removed		Residue Cu Atoms	Fe Atoms	S Atoms	Me:S
0	($Cu_{1.12}Fe_{1.09}S_2$)	1.00	0.97	1.79	2:1.81
16.0		1.00	1.11	1.97	2:1.87
17.9		1.00	1.09	2.01	2:1.92
27.1		1.00	1.09	1.97	2:1.89
32.1		1.00	1.09	1.99	2:1.90

seem to indicate that the dissolution of the excess copper was not accompanied by removal of the excess iron (8.3%) over the stoichiometric $CuFeS_2$. It was later confirmed, Section 4.3, that the removal of 13.2% of copper corresponded to an iron removal of about 2.6%.

The tabulated atomic absorption results also show that for the range of copper removal considered, the composition of the final residue, $\simeq Cu_{1.0}Fe_{1.1}S_{2.0}$, remained constant and within the region of existence of the α-chalcopyrite form found by Yund and Kullerud[38].

It is worth comparing the leaching experiment mentioned above using solid which has been stored for 14 months, with the experiment carried out under similar conditions using a sample of β-chalcopyrite. The results for both are shown in Fig. 34 , which shows clearly the difference in reaction rates.

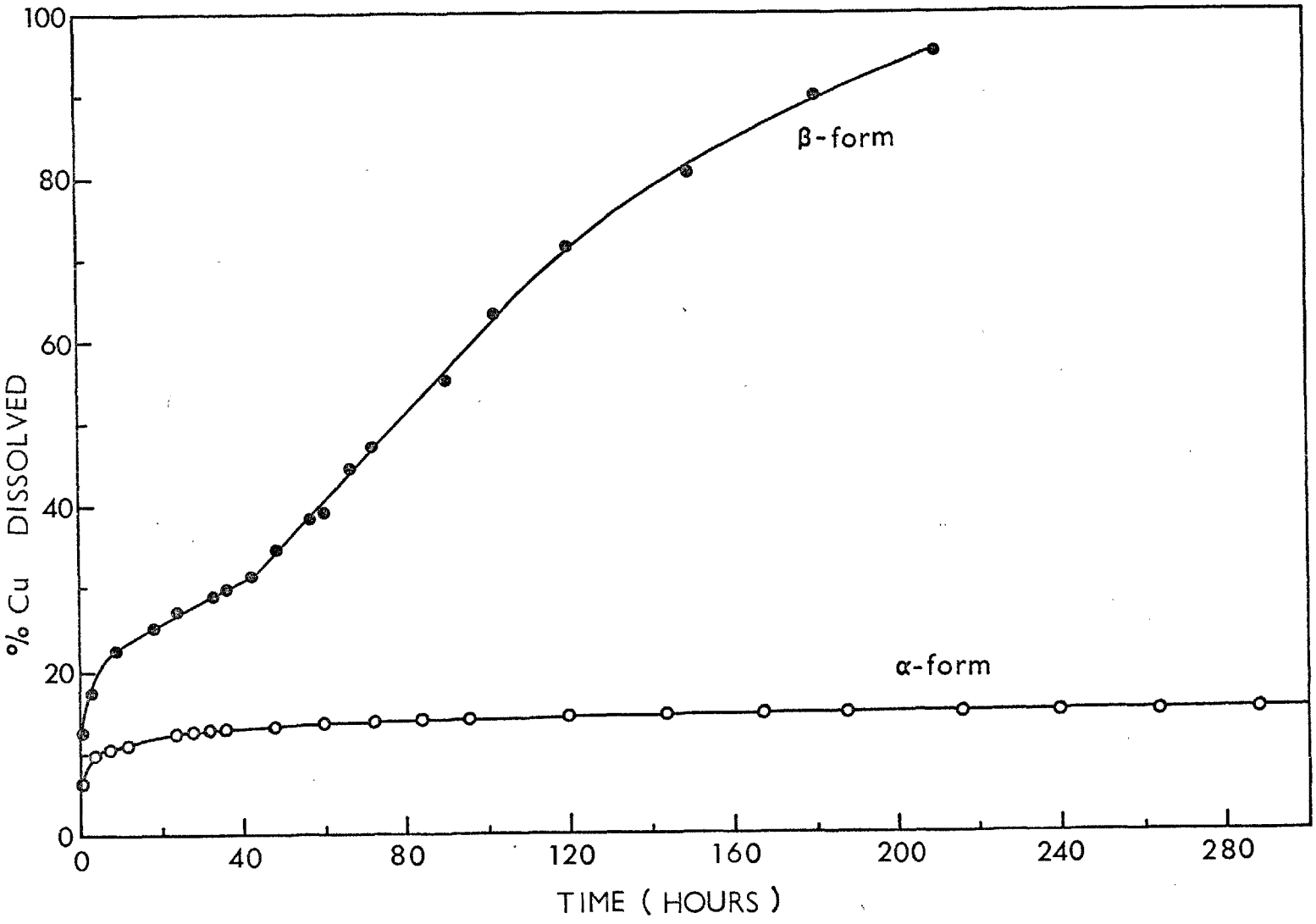

Fig. 34. Comparison of a leaching experiment conducted on a stable sample of α-chalcopyrite, with a leaching experiment conducted on a sample of β-chalcopyrite under identical conditions.

Summarising, the dissolution of synthetic α-chalcopyrite appears to proceed in two stages, the first corresponding to the removal of excess copper over the stoichiometric $CuFeS_2$ composition, and the second the straight forward dissolution of the near-stoichiometric form to give elemental sulphur:

$$CuFeS_2 + 2Fe_2(SO_4)_3 = CuSO_4 + 5FeSO_4 + 2S^{\circ}.$$

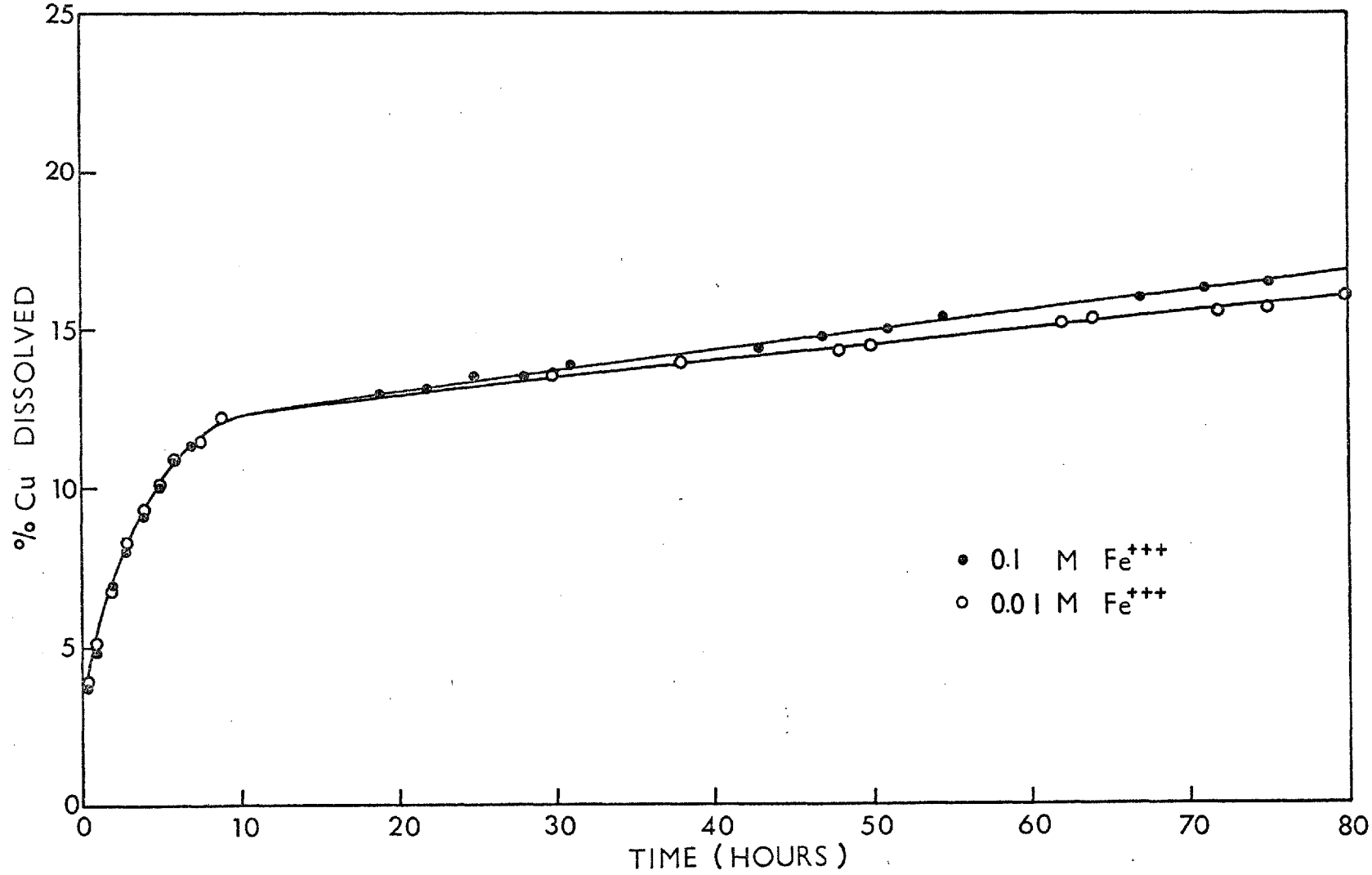

Fig. 35. Effect of ferric ion concentration on the rate of leaching of α-chalcopyrite.

4.1.2 Effect of Ferric Ion Concentration

In view of the slow kinetics for the dissolution of α-chalcopyrite under atmospheric pressure, even at temperatures as high as 95°C(*), the only factor considered was the effect of ferric ion concentration on the leaching rate. Fig. 35 , Tables, B-12.3, B-12.4, shows two rate curves under the same experimental conditions, but where the ferric ion concentrations are different by a factor of 10. It shows that the initial removal of excess copper over the stoichiometric $CuFeS_2$ (∿ 11%) was not affected by an increase in ferric ion concentration, in agreement with a diffusion mechanism.

For the subsequent reaction it is difficult to draw firm conclusions. Hydrolysis of the iron, and corresponding lowering of the Fe^{+++} ion activity, is greater in the more concentrated solution, but it seems that the rate of leaching was increased by the increase in the concentration of iron. This suggests that the reaction is straightforward, with $CuFeS_2$ giving elemental sulphur directly. On the other hand, the experiments were carried out when the α-chalcopyrite was 78 and 85 days old, the first being with the more concentrated (0.1M) ferric solution. The difference in rate might, therefore, be due to the age of the solid.

(*) At the rate shown in Fig. 34 it would take about 270 days at 95°C for 100% copper removal from a 14 months old α-chalcopyrite.

4.2 Electron Probe Microanalysis

Copper, iron and sulphur scans across two pieces of α-chalcopyrite are shown in Fig. 36-37. The first scan corresponding to a sample stored for 35 days after synthesis, shows reasonable homogeneity and it also indicates no apparent variation due to the lamellae structure, as already mentioned in Section 2.1.2.

The second scan corresponds to a storage time of 95 days and shows a relative increase of copper concentration in the pores, cracks and edge. This is in agreement with diffusion and final segregation of the copper in excess of the stoichiometric composition $CuFeS_2$, which facilitates its removal on leaching.

As for β-chalcopyrite (see Section 3.3), it was found that the α-leach residues were too porous and cracked for any reproducible values to be obtained, either by scanning the sample across or by fixed positions point counts.

Finally there was an apparent increase in the content of sulphur near the edge of the sample stored for 95 days, in the trace shown in Fig. 37 . This was due to topographic effects, since it can be seen that, when the beam was moved in the opposite direction, there was no such increase.

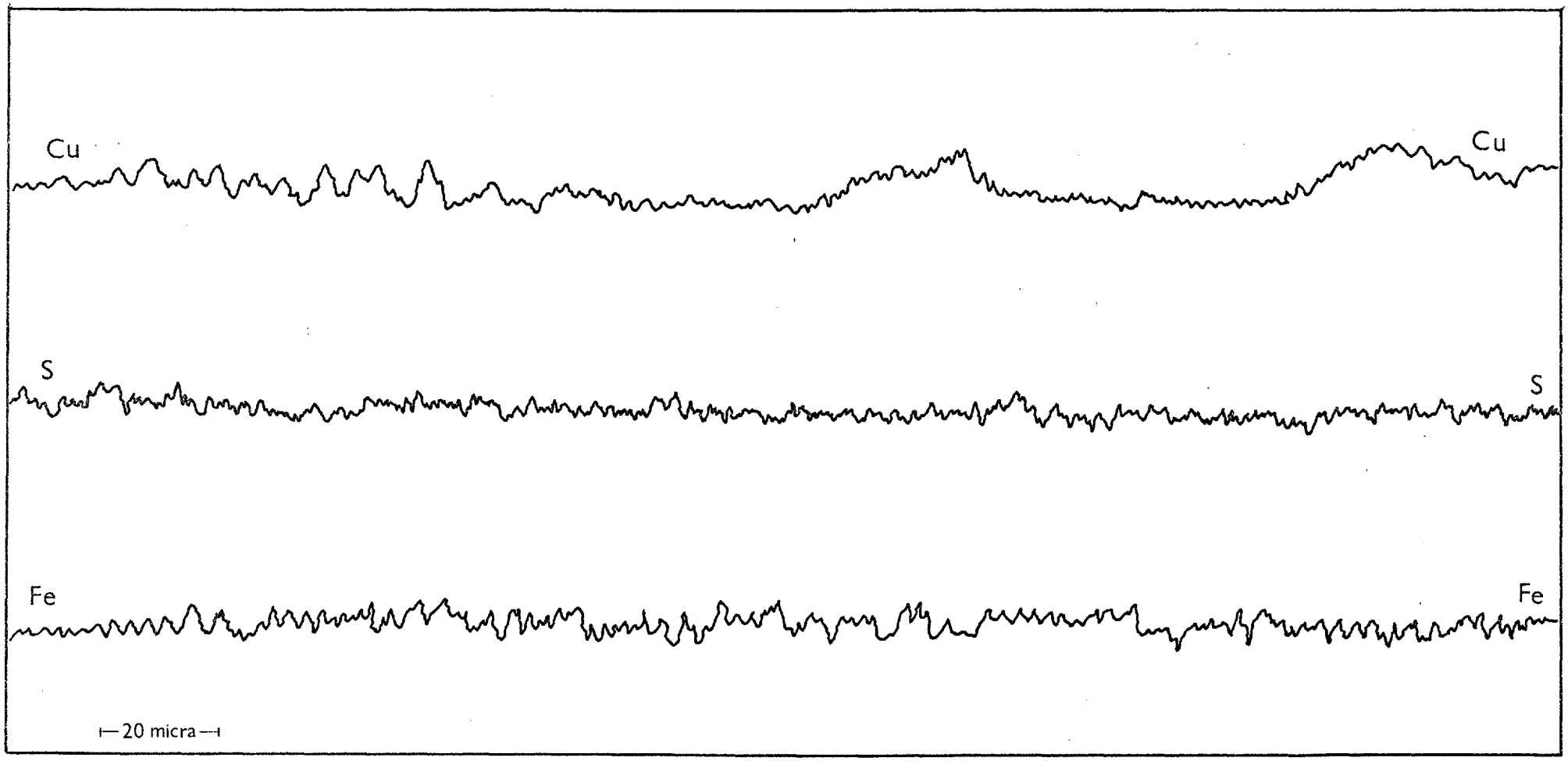

Fig. 36. Electron probe scan across a piece of α-chalcopyrite stored for 35 days after synthesis

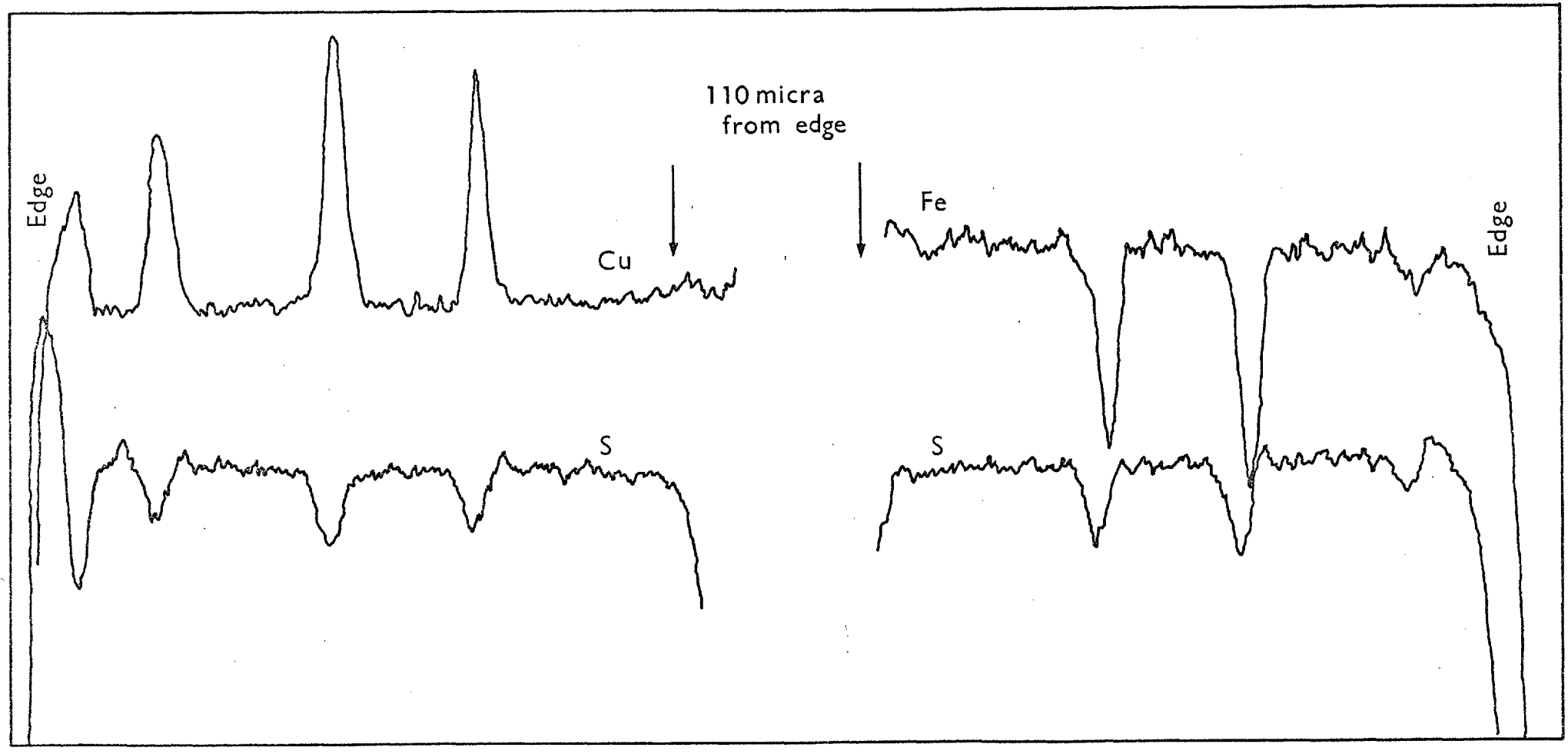

Fig. 37. Electron probe scan across a piece of α-chalcopyrite stored for 95 days after synthesis

4.3 Leaching with Hydrochloric Acid. Effect of Chloride Ion on the Leaching Rate.

On leaching α-chalcopyrite, $Cu_{1.12}Fe_{1.09}S_2$, with hydrochloric acid at 80°C, it was found that the rate of copper dissolution was much faster than when using, at 95°C, ferric sulphate solutions acidified to pH 1 with sulphuric acid, as is shown in Fig. 38 , and Tables B-12.5 and B-12.6, Appendix B.

In both experiments 0.2g of α-chalcopyrite, which had been stored for one year and 75 days were used. Ferric sulphate leaching (0.03M in Fe^{+++}) was conducted using a -100 + 150 mesh particle size fraction, while in the HCl leaching (10^{-1}N) a -200 + 300 mesh fraction was used.

Both copper and iron in this last experiment were determined in the leach liquor using atomic absorption spectrophotometry, and sulphate by nephelometry. However, no traces of sulphate were detected during the run, but elemental sulphur was found in substantial proportions in the reaction vessel. Also no odour of H_2S was apparent while the leaching reaction proceeded.

Analysis of the leach liquor showed that during the period that the 11% excess copper over the stoichiometric $CuFeS_2$ was removed, only a small percentage of iron went into solution. After this initial period both elements were dissolved at the same rate, and the ratio Cu:Fe was kept constant and near to 1, Fig. 39 .

A test with ammonium thiocyanate showed that almost all iron in the solution was Fe^{++}, with a very small amount in the Fe^{+++} form.

To check for the effect of Cl^- on the dissolution rate of α-chalcopyrite, 0.1 mole of NaCl was added to the ferric sulphate leaching run mentioned above, after 15% of the copper had been removed. Fig. 38 and Table B-12.6 show the immediate change of rate that occured due to this additon. The rate obtained with HCl alone was not reached, however.

Referring to the E-pH diagram drawn by Urgarte-Alvarez (109) for the system Cu - Cl - H_2O at 100°C Fig. 40 , it is evident that, under the conditions of the reaction with dilute hydrochloric acid, the stable specie in solution is $CuCl_2^-$.

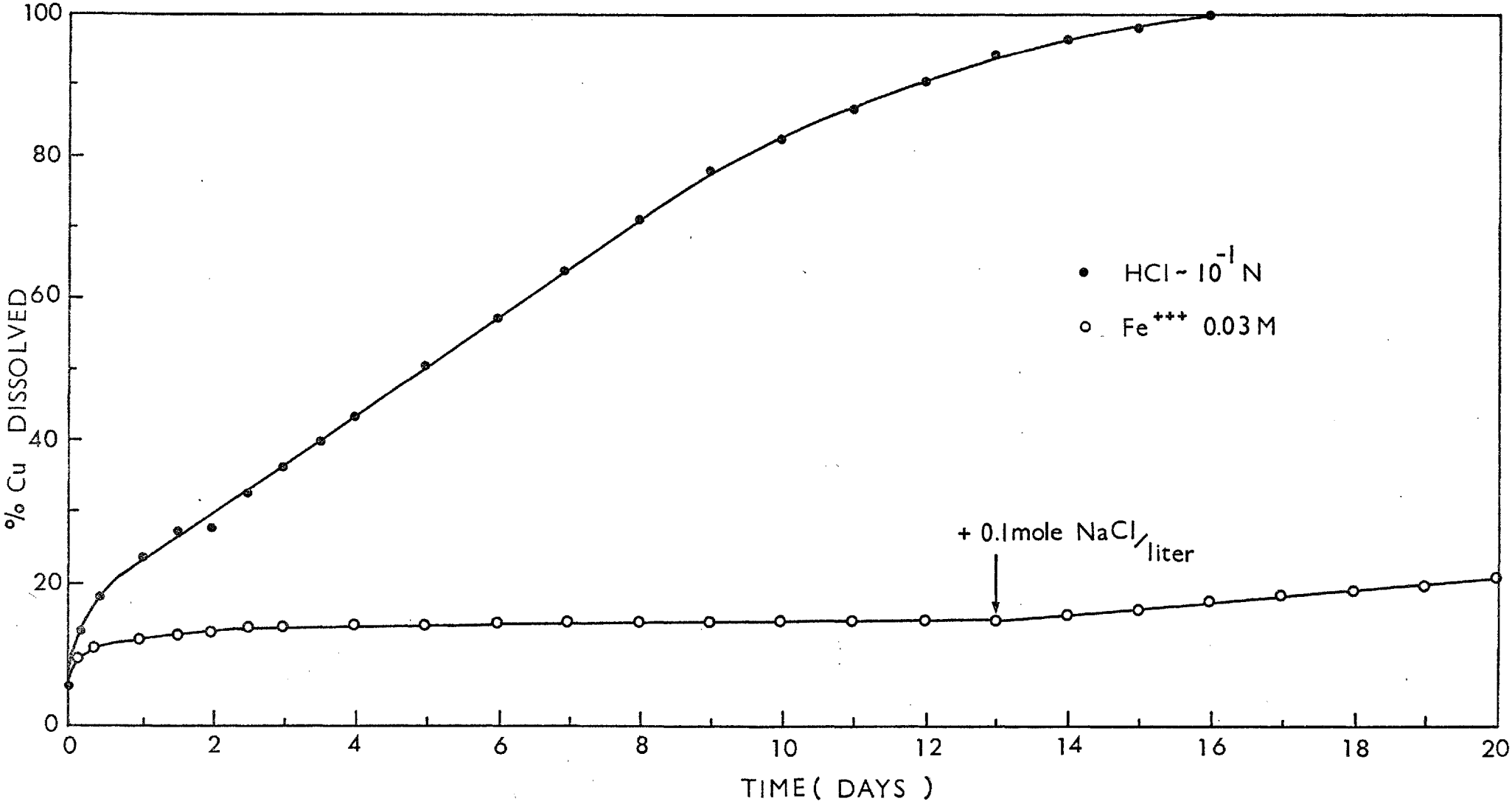

Fig. 38. Effect of chloride ion on the rate of leaching of α-chalcopyrite

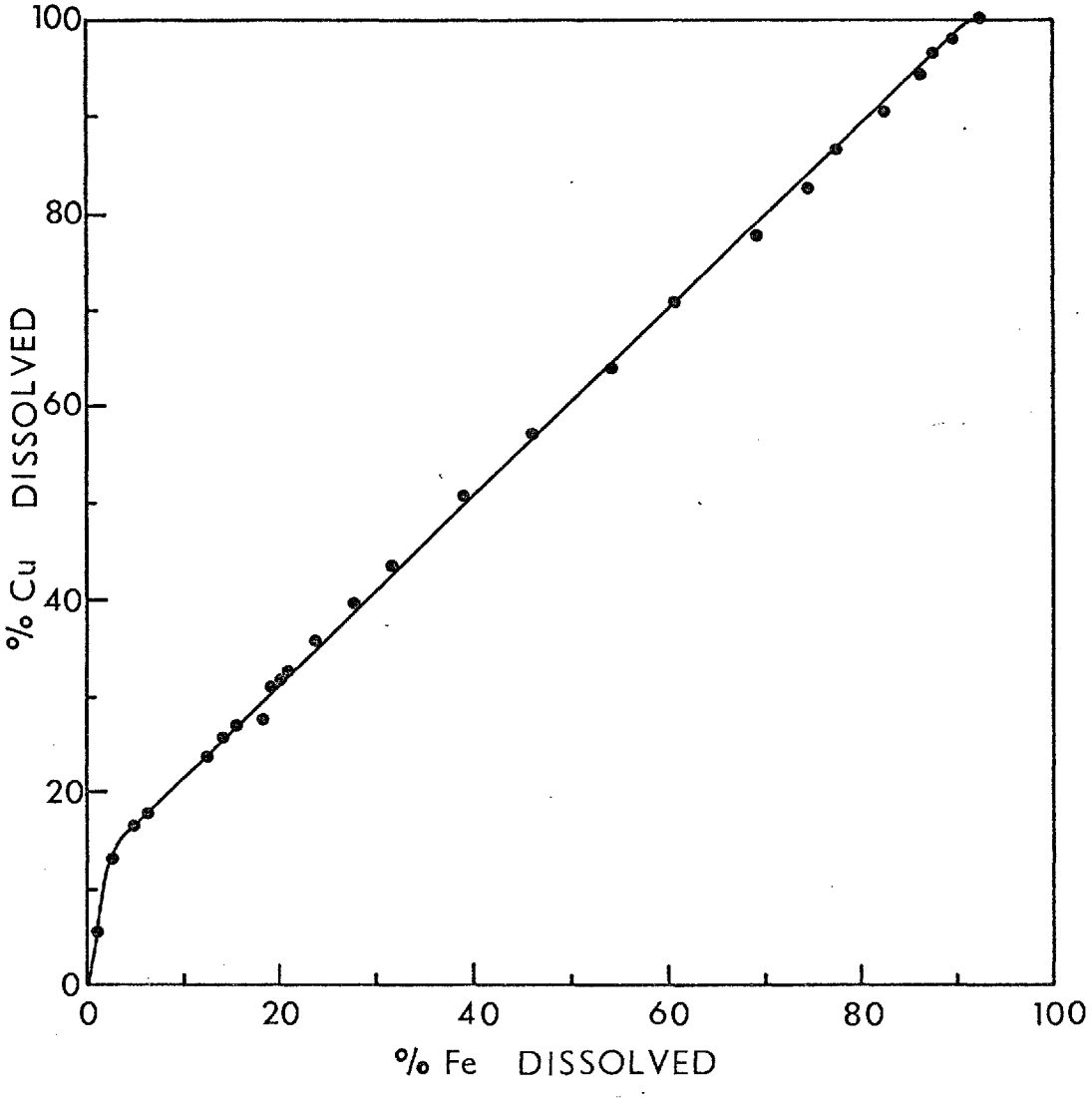

Fig. 39. Curve relating the percentage of copper to that of iron removed during leaching of α-chalcopyrite with hydrochloric acid solution

Also according to the findings of Kametani[110] the reduction of cupric ion in chloride solutions to metallic copper by ferrous ions, proceeds in two steps, based on the theoretical E-pH diagram reproduced in Fig. 41 . The first takes place in the range pH 1.5-4 and leads to the formation of a cuprous complex

$$Cu^{++} + Fe^{++} + 3H_2O + 2Cl^- = CuCl_2^- + Fe(OH)_3 + 3H^+$$

The second step, reduction of this complex to metallic copper, takes place above pH 5-6.

$$CuCl_2^- + Fe^{++} + 3H_2O = Cu^o + Fe(OH)_3 + 3H^+ + 2Cl^-$$

The mechanism suggested indicates that if any Cu^{++} is formed during the dissolution of α-chalcopyrite it will be reduced by the Fe^{++} present. This reaction, together with the presence of the air during the leaching experiment will account for the formation of the small amount of Fe^{+++} detected.

The only mechanism whereby the reaction with HCl can be explained readily is to assume that copper, which is in the Cu^+ state in the solid, dissolves forming the $CuCl_2^-$ complex. The higher the temperature the more stable are the cuprous species, (See Appendix A).

At the same time the Fe^{+++} oxidizes S^{--} ions to elemental sulphur by electron transfer in the solid, since no odour of H_2S was detected, and is itself reduced to Fe^{++}.

In the case of ferric sulphate leaching where NaCl was added, the oxidation potential was outside the region of stability of the Cu^+ ion in solution, and dissolution due to oxidation to Cu^{++} will prevail over the formation of the $CuCl_2^-$ complex species.

Finally, it is worth noting that the rate of dissolution of α-chalcopyrite, using dilute HCl, dropped after about 70% of the copper had been removed. This again can be explained, as for the β-form, by the formation of anelemental sulphur coating on the surface of the residue, slowing down the reaction. This sulphur was detected under the microscope, in the pores, cracks and edges of the grains. Drops of CCl_4 dissolved part of this sulphur.

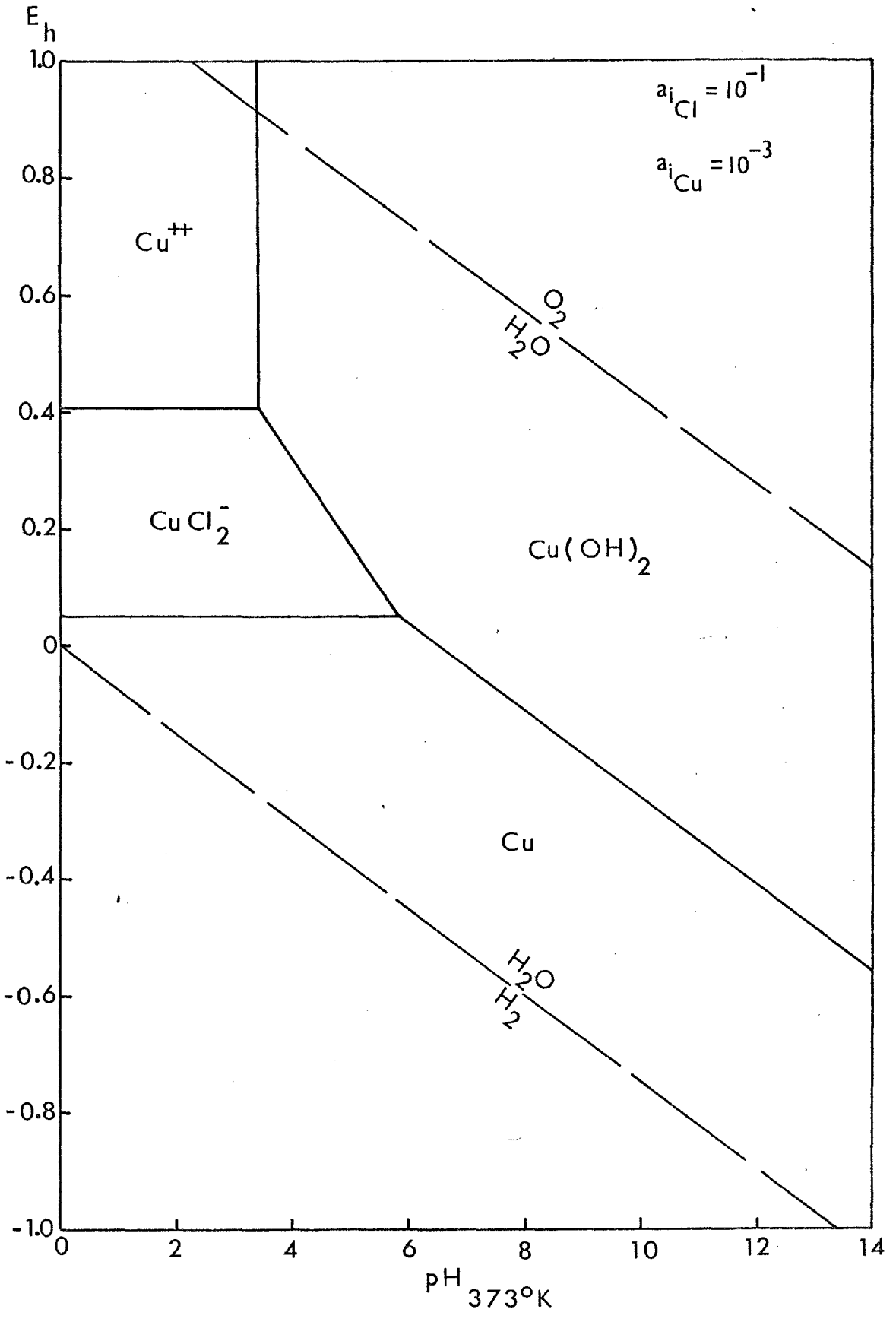

Fig. 40. Equilibrium diagram for the copper-chlorine-water system at 100°C and 1 atm pressure - Ugarte-Alvarez (109)

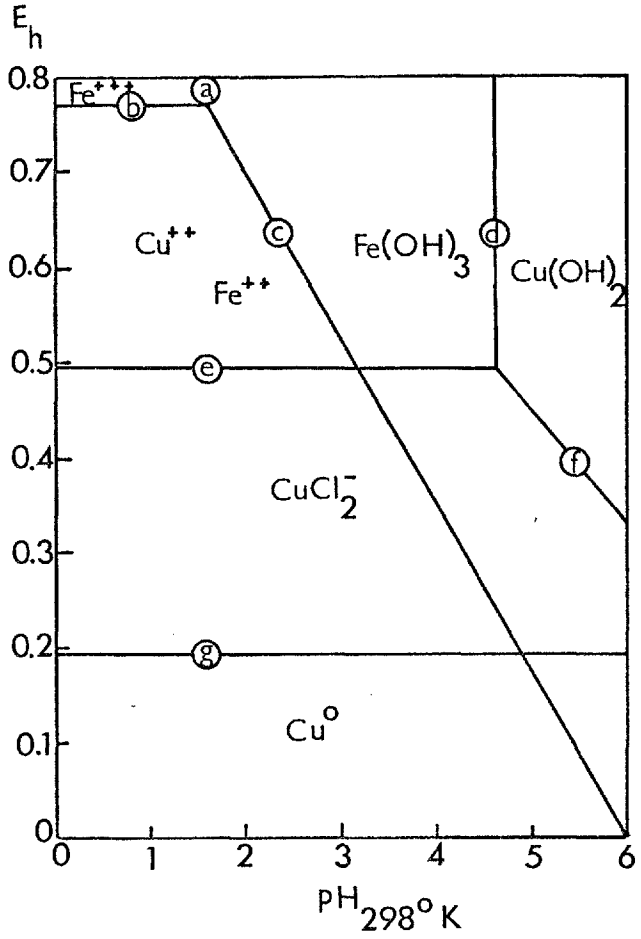

Fig. 41. Potential-pH diagram for the chloride system at 25°C (for 1.0M concentration) - Kametani (110).

(a) $Fe^{+++} + 3H_2O = Fe(OH)_3 + 3H^+$
(b) $Fe^{++} = Fe^{+++} + e$
(c) $Fe^{++} + 3H_2O = Fe(OH)_3 + 3H^+ + e$
(d) $Cu^{++} + 2H_2O = Cu(OH)_2 + 2H^+$
(e) $CuCl_2^- = Cu^{++} + 2Cl^- + e$
(f) $CuCl_2^- + 2H_2O = Cu(OH)_2 + 2H^+ + 2Cl^- + e$
(g) $Cu^o + 2Cl^- = CuCl_2^- + e$

4.4 X-ray Powder Diffraction Study of the Leach Residues

X-ray powder photographs of α-chalcopyrite leach residues are shown in Fig. B-7 and B-8 , Appendix B. The X-ray diffraction data calculated from measurements of these photographs are presented in Table B-22.12.

Due to the lengthy process of dissolution of α-chalcopyrite it was not possible to cover the complete range of residues from 0 to 100% of copper removed. The few results obtained showed, however, that some of the lines present in the original unleached material, disappeared during the leaching reaction, and this probably corresponds to the removal of the excess copper over the stoichiometric $CuFeS_2$.

Leach residues obtained under different conditions, and for different proportions of copper dissolution, showed reasonably constant values of the d-spacings and approximate relative intensities.

An important point found on these photographs was the reversal of the relative intensities of reflections corresponding to the d-spacings sets 1.869-1.854Å and 1.214-1.205Å when compared with the observed densities for the unleached sample. As already reported in Section 2.1.2, the synthetic α-chalcopyrite showed a "strong" reflection for d=1.869Å and "medium" for d = 1.854Å; also d = 1.214Å was "medium" while d = 1.205Å was "weak". The corresponding intensities found for these reflections on the photographs of the leach residues were respectively:

d ≈ 1.869Å, medium; d ≈ 1.854Å, strong; d ≈ 1.214Å, weak;
d ≈ 1.205Å, medium,

in agreement with the A.S.T.M.(94) data.

Again the excess copper seems to be responsible for this reversal in the densities of the lines.

The X-ray photographs of leach residues from experiments involving Cl^- ions have more reflections than those obtained from ferric sulphate leaching, and the main reflections are very similar, with the exception of the intensities mentioned above, to the unleached α-chalcopyrite pattern.

The relatively small number of lines detected for the ferric sulphate leaching residues was most probably due to the poor quality of the X-ray powder photographs obtained with the equipment initially used.

It is worth comparing the data determined in this present report for α-chalcopyrite residues with the values found for the leach residues obtained from a Temagami chalcopyrite[95], and note the similarity of most reflections (See Table B-22.13, Appendix B).

As far as the storage effect is concerned, it was not possible to follow any changes by the use of X-ray diffraction, since CuK_α was the only radiation available for more than one year after the synthesis of the α-chalcopyrite.

4.5 Microscope Examination

Polished sections of the unleached α-chalcopyrite revealed the lamellae type structure shown in Fig. B-18 , Appendix B. This structure was observed even after long periods of storage without any apparent change. Extensive cracks were found after storage for 9 months, Fig. B-19 .

A block of the synthetic material was sectioned to give two pieces and the central portion edge, freshly cut, was compared with the corresponding external edge of the same piece.

Photomicrographs reproduced in Fig. B-20 and B-21 , correspond to these two edges and as can be seen, the external one shows segregation. By the use of electron probe micro-analysis it was shown to contain a higher copper content (Section 4.2).

The other half of the piece was enclosed in a platinum wire cage and suspended in a stirred acidic ferric sulphate solution (0.01M Fe^{+++}, pH~1) at 80°C for 60 hours. A polished section of this leached piece is shown in Fig. B-22 and the porous nature of the residue obtained can be seen as well as some kind of tunneling effect. The same type of structure was observed in a particulate residue of α-chalcopyrite, Fig. B-23 obtained under the conditions described in Table B-12.6 , Appendix B . Apart from elemental sulphur in the pores and cracks, no other phase was found in these residues.

SECTION 5

CONCLUSIONS

5.1 Summary of Results

Two forms of chalcopyrite were synthesized. The first, a β-form, cubic, of composition $CuFeS_{1.83}$, was similar to Hiller and Probsthain's[34] synthetic material. The X-ray powder pattern obtained was identical with that of Cabri's[47] new copper-iron sulphide. It was homogeneous, isotropic and showed a lamellae type structure in polished sections, with no apparent variation of composition under the electron probe. The second, an α-chalcopyrite, tetragonal material, with composition $Cu_{1.12}Fe_{1.09}S_2$, contained 10.7% excess copper and 8.3% excess iron over the stoichiometric composition $CuFeS_2$. Its X-ray pattern was similar to those found for natural chalcopyrite ores, but with some superstructure reflections probably due to the excess metal present. The solid showed reasonable homogeneity and weak anisotropy, and had lamellae type structure, slightly different from that reported for β, showing no variation in composition.

β-chalcopyrite was found to be stable when stored over periods of three years.(*) The α-chalcopyrite changed slowly, reaching a stable state after 14 months in storage, with formation of cracks and segregation of a copper rich phase.

The leaching of β-chalcopyrite with acidic ferric sulphate solutions, proceeded in three stages, the first characterised by the dissolution of ∿17.5% of copper, the rate being controlled mainly by the diffusion of the copper atoms to the solid-liquid interface. At the same time there was a contraction of the lattice structure which accounted for the reduction in the rate of reaction.

The second stage occurred with the collapse of the β-lattice structure and appearance of a metastable α-form. Transformation of this form was complete when about 30 to 35% of copper was removed, and a final composition $CuFe_{1.2}S_{2.3}$, having the α-chalcopyrite structure, was reached. This stage was characterised by two competing reactions, one homogeneous the other heterogeneous, with different apparent activations energies, the homogeneous being favoured at higher temperatures.

(*) Yund and Kullerud[38] did not observe any change in an isometric form (β) over a period of 5 years.

The third stage was the straightforward reaction of $CuFe_{1.2}S_{2.3}$ to form elemental sulphur, which coated the residue. Since transport of reactants and products through it is necessary, this coating reduced the rate of reaction.

In both the first and second stages of the leaching reaction it can be assumed that in addition to the copper diffusion to the surface, an electron transfer occurs within the solid in order to keep charge neutrality. This corresponds to the hypothetical Fe^{++} in the solid being oxidized to Fe^{+++}, the effect being more pronounced in the second part of the reaction.

Theoretically 34% of the copper should be removed in order to achieve this oxidation, but in practice it was found that the change from the previous stages to the last occurred at about 32% removal. Thus, some iron still remains in the Fe^{++} form but this is apparently tolerated by the lattice structure.

The two initial stages can be represented by the idealised reaction:

$$2.30CuFeS_{1.83}+0.574Fe_2(SO_4)_3=0.47\ CuSO_4+1.252FeSO_4+1.83CuFe_{1.2}S_{2.3}$$

and the third stage by

$$CuFe_{1.2}S_{2.3} + 2.2Fe_2(SO_4)_3 = CuSO_4 + 5.6FeSO_4 + 2.3S.$$

For the synthetic α-chalcopyrite, $Cu_{1.12}Fe_{1.09}S_2$, the storage time affected the leaching rate. Using acidic ferric sulphate solutions as oxidizing agent, there was found to be an increase in the initial rate of dissolution with increasing storage time, while for the second half of the reaction the rate decreased significantly on storing, until no further variation occurred after 14 months. Microscopic observations showed that during this period, cracks spread over the whole synthetic material, and electron probe microanalysis detected a higher content of copper at the edges, as well as in the pores and cracks. To explain this it seems reasonable to assume the diffusion of the excess copper atoms to the surface of the synthetic material, which is in agreement with the rapid removal of about 11% of this metal at the beginning of the leaching reaction.

It was also shown that during this initial dissolution very little iron, if any, went into solution and this is believed to be due to the higher mobility of copper compared with iron in the solid.

After this stage the reaction proceeded with direct reaction of the solid obtained in the first half, $CuFe_{1.1}S_2$, to form elemental sulphur, with a ratio of copper to iron removed equal to 1.

The leaching of this near-to-stoichiometric solid can be represented by the reaction

$$CuFeS_2 + 2Fe_2(SO_4)_3 = CuSO_4 + 5FeSO_4 + 2S^o.$$

Leaching of α-chalcopyrite with dilute HCl (pH 1) proved to take place much faster than when acidic ferric sulphate solutions were used. About 100% of the copper was recovered in 16 days using HCl, and a recovery of 100% may be possible in 270 days using ferric sulphate. This is due to the formation of the $CuCl_2^-$ complex, which is stable under these conditions of leaching.

Although residues of the α-form after any amount of leaching and residues from β-chalcopyrite after 32% of copper dissolution were very similar, the rates found for such materials were quite different. The relative proportion of the elements in the lattice structure seems, therefore, to play a more important role than the structure itself.

Finally, it can be seen that both a roast around 750°C, in the absence of air, or an activation with metallic copper, will increase the rate of the leaching reaction.

Also, with the sulphur-deficient material, reduction in the particle size will reduce the time of dissolution.

Apparently the addition of Cl^- makes the reaction proceed faster, but this would create important problems of corrosion of the equipment.

The behaviour of the metastable synthetic α-chalcopyrite seems to illustrate what probably happened in nature during the formation of chalcopyrite ores at high temperatures. Segregations similar to those found occurring for α, as described in the present work, and high pressures required to get the amount of sulphur for the composition $CuFeS_2$ into the structure, are possibly responsible for the impurities always associated with natural chalcopyrite ores.

5.2 Comparison of the Present Investigation with Previous Work

No direct comparison is possible between the leaching curves of the present work and those obtained by Dutrizac et al.[15], since their results were obtained from the amount of copper dissolved from a polished face of a disc of synthetic chalcopyrite, while in the present work, known weights of sample were used.

Also, the true surface area of the synthetic material prepared by Dutrizac et al. was not known due to the porosity of the sample used, but they estimated it on the basis that the density found was about 80% of the theoretical value.

However, knowing the dimensions of this synthetic disc of chalcopyrite and taking into account the porosity of the material an approximate calculation showed that the leaching rate curves obtained by Dutrizac et al. were similar to those found in the present work with β-chalcopyrite, Fig. 42 Furthermore, the difference found by those authors in the leaching rate curves for their synthetic material and for a natural chalcopyrite from Temagami, are of the same order of magnitude as the differences found here between β-chalcopyrite and stable α-chalcopyrite, after removal of the 11% excess copper in the last case.

Related to this there is also the similarity between the X-ray pattern of this α-chalcopyrite, and the values obtained from a Temagami chalcopyrite[95] as mentioned in Section 4.4.

Dutrizac et al. suggested that the difference in rates for the two types of chalcopyrite used, synthetic and natural, was due either to the porosity of the synthetic material or to the existence of impurities in the natural material, (FeS, ZnS, $MgCO_3.CaCO_3$, $FeCO_3$) reducing the rate of the diffusion process which they assumed for the dissolution.

These authors found for the ''activation enthalpy'' a value of 17±3Kcal, similar to the value obtained in the present work for the second and third stage of leaching of β-chalcopyrite.

In this thesis, the leaching process is considered to involve both a homogeneous and a heterogeneous reaction.

Dutrizac et al., however, considered that the value found , 17Kcal $mole^{-1}$, "was consistent with rate control by a diffusion process". However, in reactions which are entirely

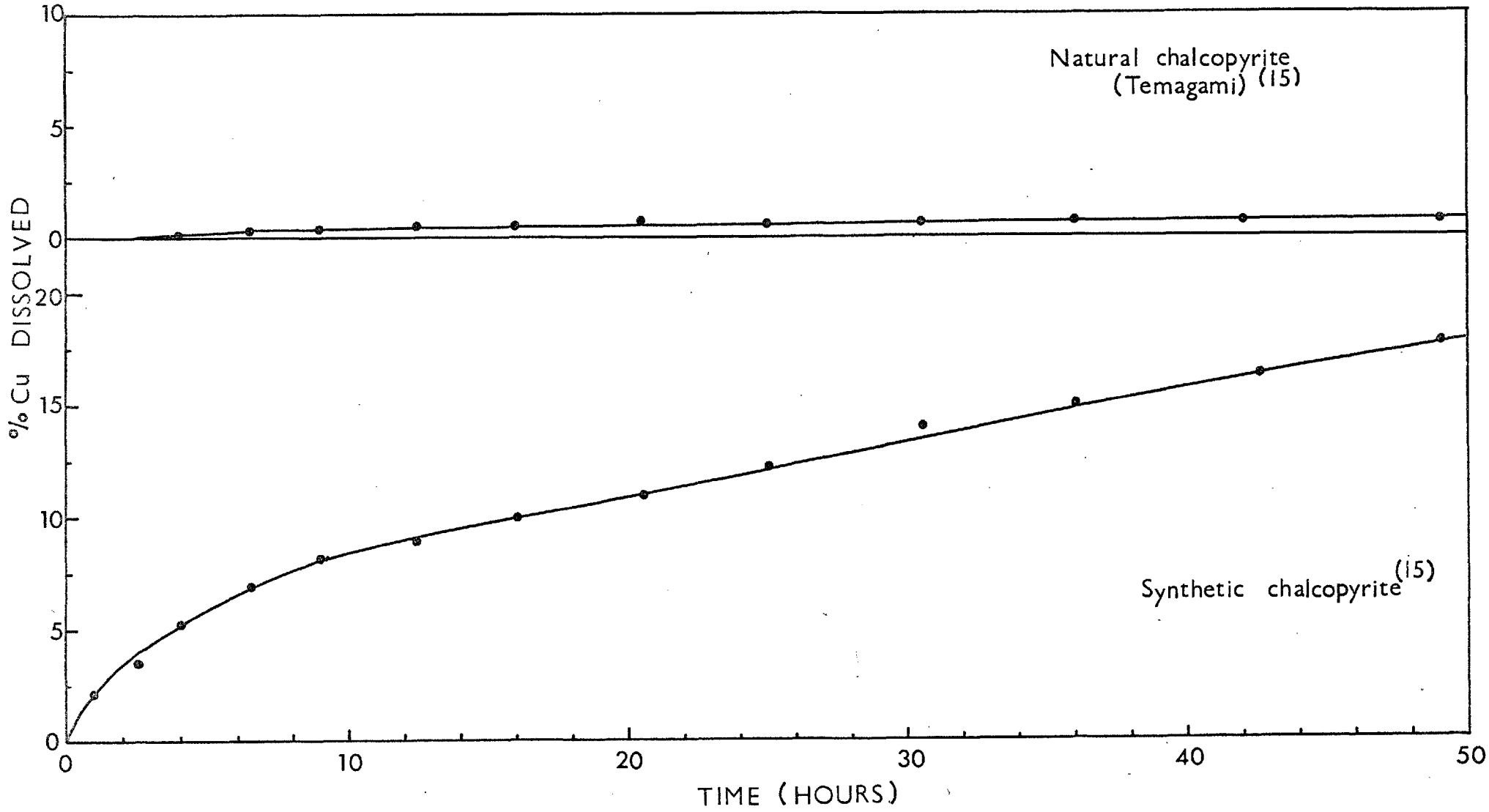

Fig. 42. Dissolution of synthetic and natural chalcopyrite according to Dutrizac et al.(15) (as shown in Fig. 4), after an approximate conversion to percentage of copper removed

transport controlled, the critical increment of energy is considered to be of the order of the energy of activation for diffusion, approximately 4Kcal $mole^{-1}$(106).

Dutrizac et al. found that the sulphur coating the residue during the leaching process was removed quantitatively by the use of carbon disulphide. However, in the present work only minute amounts of elemental sulphur were extracted from the residues by the use of that solvent.

The pressure leaching experiments of Warren et al.(14), at 90°C, 4.8 atm oxygen pressure and with sulphuric acid solutions, on a calcined sample of chalcopyrite concentrate, seem in fact to have been conducted on a material very similar to the β-chalcopyrite synthesized and described in this report.

Apparently the calcination was conducted in the absence of air at 825°C, corresponding to a total loss of sulphur of about 6%(*). Warren et al. assumed that this loss could be from pyrite, since the concentrate contained about 2% of this, but the suggestion does not seem feasible. Also the X-ray diffraction data presented by these authors is similar to the pattern described for β-chalcopyrite with the merging of the 1.57-1.59Å and 1.85-1.86Å reflections.

Their results obtained with the calcined sample are in agreement with the present work, for example the increased leaching rate obtained when compared with the original chalcopyrit concentrate.

Another interesting detail was the finding by Warren et al. that the dissolution of iron from the calcined concentrate was slower than that of copper, as found here for β-chalcopyrite, while the original chalcopyrite had a ratio of copper to iron dissolution of 1, as observed in the present work for α-chalcopyrite.

Leaching experiments conducted by Warren et al. using both calcined and original concentrate, showed that intense iron hydrolysis occurred when between 40 and 60% of the copper had dissolved, and both produced elemental sulphur. They also found a high molar ratio of copper leached to elemental sulphur, during the

(*) A total loss of 9% is necessary to obtain the β-form with composition $CuFeS_{1.82}$ as reported by Hiller and Probsthain(34).

early stages of reaction, identical with the behaviour found here for β-chalcopyrite.

Björling and Kolta[7] found that chalcopyrite $CuFeS_2$ could be activated by partial roasting in a small rotating furnace at 550°C in the absence of air, giving higher recoveries in less time, in both open vessel and autoclave leaching experiments.

To explain the results observed they supposed that the final product obtained by heating chalcopyrite had the composition $Cu_2S.2FeS$, but most probably they had present a sulphur-deficient form of chalcopyrite.

Björling and Lesidrenski[16] observed that very good results were obtained by leaching chalcopyrite activated with metallic copper in presence of sulphuric acid and at low oxygen pressure.

They said that the activation carried out at about 450°C led to the formation of Cu_2S and FeS, but no mention was made as to the identification of these two products.

The work of Sullivan[111] on a natural chalcopyrite with composition 31.34% Cu, 31.00% Fe, 34.06%S and 2.32% of insolubles, leached with acidified ferric sulphate solutions, showed that the behaviour of this ore approximated to that of the synthetic α-chalcopyrite.

He found that more copper was extracted than free sulphur formed, and assumed, unlike Dutrizac, that some was oxidized. However, it should be noted that Sullivan determined the sulphur, as he pointed out, "in a form soluble in CS_2".

Dutrizac et al.[112] found that the rate of dissolution of cubanite ($CuFe_2S_3$) was increased by the presence of the Cl^- ion, but unlike the case of α-chalcopyrite in the present work, sodium chloride seemed to be more effective than hydrochloric acid.

This effect of Cl^- on the dissolution rate of chalcopyrite was also found by Haver and Wong[20], and they explained it by the possible formation of complexes.

Most of the works mentioned in the literature survey Section 1.1, cannot be compared with the present report, since the experiments were carried out with samples of natural chalcopyrite containing an important percentage of impurities, as for example, those used by Warren[1], ~20% of pyrite; Dobrokhotov and Maiorova[4], 2-25% pyrite and 5-20% bornite; Vizsolyi et al.[12], 4.5% pyrrhotite.

In fact, Majima[113] found that the oxidation of complex sulphides was enhanced by the presence of pyrite, due to galvanic action between pyrite and the complex sulphide.

It is worth noting that Dobrokhotov and Maiorova[4] found, when using solutions of low acidity and impure natural chalcopyrite that "an intensive deposition of ferric hydroxide occurred on the internal wall of the autoclave".

Vizsolyi et al.[12], during the pressure leaching of natural chalcopyrite, also found in the leach residue a mixture of ferric hydroxide and basic ferric sulphate, $Fe(SO_4)OH$, and they explained this by saying that one half of the sulphate sulphur formed stays in solution while the other half hydrolyses with iron. This is in good agreement with what was observed during the experiments described in the present work.

APPENDIX A

HIGH TEMPERATURE POTENTIAL-pH DIAGRAMS FOR THE SULPHUR-WATER, COPPER OXIDES AND SULPHIDES-WATER AND IRON OXIDES AND SULPHIDES-WATER SYSTEMS

ABSTRACT

Potential-pH equilibria diagrams for the systems sulphur-water, copper oxides and sulphides-water, iron oxides and sulphides-water, are presented for 25°C, 100°C and 150°C. Thermodynamic calculations and methods are described. Some features of the diagrams and comparisons with results of other authors are also presented.

A-1. Introduction

In order to predict what species should form under certain conditions of oxidation potential and pH at several temperatures, for the systems mentioned above, the most suitable approach is to draw the potential-pH diagrams.

The main interest in this report was concerned with the leaching of copper and iron sulphides ores, and the range of temperature (25 to 150°C) was limited by the possibility of liquid sulphur coating the surface of the ore at temperatures above 112.8°C. The upper temperature, already above the maximum permissible, was included in these calculations in order to show how the stability regions of the species in solution, and solid phases, change with rising temperature.

The E-pH diagrams presented were based on calculations involving activities rather than concentrations. In order to apply these diagrams it will be necessary to use an extended form of the Debye-Hückel equation (as for example the relation presented elsewhere in this report) to obtain the activity coefficients at high temperatures.

The range of activities chosen was such as to include the values used during the leaching experiments.

Criss and Cobble's "Correspondence Principle" made possible the computation of high temperature heat capacity data of ions in solution.

A-2 Relations Used

For the calculations of equilibria relations the following equations have been used.

A-2.1 Non Redox Reactions

The relation between standard free energy change and equilibrium constant can be written

$$\ln K_T = - \frac{\Delta G^\circ_T}{RT}$$

A-2.2 Redox Reactions

In a general way the reaction can be written for the full-cell(*)

$$aA + bB - zH^+ = cC + dD - \frac{z}{2} H_2$$

and half-cell

$$aA + bB + ze = cC + dD.$$

The half-cell reduction potential E_T is given by the Nernst equation:

$$E_T = E^\circ_T - \frac{RT}{zF} \ln \frac{a_C^c \cdot a_D^d}{a_A^a \cdot a_B^b}$$

with $$E^\circ_T = - \frac{\Delta G^\circ_T}{zF}$$

A-2.3 Calculation of ΔG°_T

ΔG°_T was calculated using the relations

$$\Delta G^\circ_{T_2} = \Delta H^\circ_{T_2} - T_2 \Delta S^\circ_{T_2}$$

$$\Delta H^\circ_{T_2} = \Delta H^\circ_{T_1} + \int_{T_1}^{T_2} \Delta C^\circ_p \, dT$$

$$\Delta S^\circ_{T_2} = \Delta S^\circ_{T_1} + \int_{T_1}^{T_2} \frac{\Delta C^\circ_p}{T} \, dT .$$

(*) See section A-2.4 for details

By taking $\overline{\Delta C_p^o}]_{T_1}^{T_2}$ as the average value of ΔC_p^o between the two temperatures considered these relations lead to

$$\Delta G^o_{T_2} = \Delta G^o_{T_1} - \Delta S^o_{T_1} (T_2-T_1) + \overline{\Delta C_p^o}]_{T_1}^{T_2} (T_2-T_1) - T_2\overline{\Delta C_p^o}]_{T_1}^{T_2} \ln \frac{T_2}{T_1},$$

T_1, being the standard state, is conventionally taken as 298°K.

The average heat capacities for non ionic species were evaluated using existing data. Calculations using Criss and Cobble Correspondence Principle[114] were employed for the ionic species. This Principle shows that if a standard state is chosen properly by fixing the entropy of $H^+_{(aq)}$ at each temperature, then the partial molal ionic entropies at that temperature are linearly related to their corresponding entropies at same reference temperature. Their choice of standard state at 298°K corresponded to an entropy for the hydrogen ion of -5.0 cal $mole^{-1}$ $°K^{-1}$ in agreement with the values for the 'absolute' ionic entropy of $H^+_{(aq)}$ suggested by other authors.

The Correspondence Principle can be described by the general relationship

$$\overline{S}^o_{T_2} (abs) = a_{T_2} + b_{T_2} \cdot \overline{S}^o_{298} (abs) \qquad (A_1)$$

where a_{T_2} and b_{T_2} are constants dependent on the class of ions (cations, anions, oxyanions and acidoxyanions) and on the temperature considered.

$\overline{S}^o_{298}$ (abs) refers to the ionic partial molal entropies on an "absolute" scale(*) considering the above mentioned standard state at 298°K.

$$\overline{S}^o_{298} (abs) = \overline{S}^o_{298} (conventional) - 5.0z$$

where z is the ionic charge.

Applying these considerations to the average value of the partial molal heat capacity between 298°K and temperature T_2 considered, it follows that

(*) This scale is not, in fact, absolute.

$$\overline{C}^{o}_{p}\Big]_{298}^{T_2} = \frac{\overline{S}^{o}_{T_2}\ (abs) - \overline{S}^{o}_{298}\ (abs)}{\ln \frac{T_2}{298}}$$

and from (A_1)

$$\overline{C}^{o}_{p}\Big]_{298}^{T_2} = \alpha_{T_2} + \beta_{T_2}\ \overline{S}^{o}_{298}\ (abs)$$

where α_{T_2} and β_{T_2} are constants dependent on the class of ions and temperature considered, and are related to the constants a_{T_2} and b_{T_2} mentioned above.

A-2.4 Use of Half-Cell Reactions - Thermodynamic Properties of the Electron

It is normal procedure when determining E-pH diagrams at 298°K to consider only the half cell redox reaction

$$aA + bB + ze = cC + dD, \qquad (A_2)$$

if the normal conventions are taken into account for the reference hydrogen half-cell reaction (SHE).

In fact, the universal usage is to define for the reference hydrogen half-cell reaction

$$H^{+}(aq) + e^{-} = \tfrac{1}{2}\ H_2(g) \qquad (A_3)$$

values of

$$\Delta G^{o}_{298} = 0 \quad (E^{o}_{298} = 0)\ (a_{H^+} = 1,\ P_{H_2} = 1)$$

the fugacity coefficient of hydrogen gas equals 1 for all relevant conditions, and $\Delta H^{o}_{298} = 0$.

The emf of the complete cell is defined as

$$E_{298}(cell) = E_{298}(\text{half cell}) - E_{298}(SHE),$$

becoming

$$E_{298}(cell) = E_{298}(\text{half-cell})$$

by assuming the above mentioned conventions.

Problems arise when extrapolating E-pH diagrams to higher temperatures using relations such as

$$\Delta G^{\circ}_{T} = \Delta G^{\circ}_{298} - (T-298)\,\Delta S^{\circ}_{298} + (T-298)\,\overline{\Delta C^{\circ}_{p}}\Big]_{298}^{T} - T\,\overline{\Delta C^{\circ}_{p}}\Big]_{298}^{T} \ln \frac{T}{298} \qquad (A_4)$$

When calculating ΔS°_{298} values it can be seen that the relation

$$\Delta G = \Delta H - T\Delta S \qquad (A_5)$$

does not apply to any half-cell reaction, if thermodynamic values for the electron are ignored. So far no study has been found involving half-cell potentials where the values for the electron were considered.

The thermodynamic properties of the electron, at any temperature, are easily determined considering the SHE half-cell reaction and the normal conventions.

As the variation of E° for the SHE with temperature is not known, it is usual to assign for the hydrogen half cell the following values at all temperatures:

(i) ΔG°_{T} (SHE) = 0, $E^{\circ}_{T} = 0$, $a_{H^+} = 1$, $P_{H_2} = 1$ atm.

Using the Gibbs-Helmholtz equation

$$\Delta H^{\circ}_{T} = nF\left[T\,\frac{dE^{\circ}}{dT} - E^{\circ}\right]$$

and

$$\Delta S^{\circ}_{T} = nF\,\frac{dE^{\circ}}{dT}$$

and

$$\Delta C^{\circ}_{p_T} = \left(\frac{\partial \Delta H^{\circ}}{\partial T}\right)_{p}$$

we have at all temperatures

(ii) ΔH°_{T} (SHE) = 0

(iii) ΔS°_{T} (SHE) = 0

(iv) $\Delta C^{\circ}_{p_T}$(SHE) = 0

From i, ii, iii and iv thermodynamic values for the electron at all temperatures are obtained

$$\overline{\Delta G^{\circ}_{T}}\ [e^-] = 0$$

$$\overline{\Delta H^{\circ}_{T}}\ [e^-] = 0$$

$$\overline{S}^{\circ}_{T}\ [e^-] = \tfrac{1}{2}\ \overline{S}^{\circ}_{T}\ [H_2(g)] - \overline{S}^{\circ}_{T}\ [H^+(aq)]$$

$$\overline{C}^{\circ}_{p_T}\ [e^-] = \tfrac{1}{2}\ \overline{C}^{\circ}_{p_T}[H_2(g)] - \overline{C}^{\circ}_{p_T}[H^+(aq)]$$

It can be seen that different values are obtained for ΔS^{o}_{298} and $\Delta C^{o}_{p_{298}}$ (or at any other temperature) if we consider a half cell reaction with or without taking into account the $\overline{S}^{o}$ and $\overline{C}^{o}_{p}$ values for the electron.

Even if "absolute" entropies (as defined by Criss and Cobble) are used instead of the conventional ones, it is still necessary to take into account the entropy of the electron.

In conventional entropies it is normal practice to set $\overline{S}^{o}_{T}\ [H^{+}] = 0$ at all temperatures. At 298°K using for hydrogen gas the value $\overline{S}^{o}_{298}\ [H_2] = 31.211$ cal mole^{-1} °K^{-1} we obtain $\overline{S}^{o}_{298}\ [e^{-}] = 15.606$ cal mole^{-1}°K^{-1}, in agreement with the value presented by Eggers et al.[115].

On the absolute scale $\overline{S}^{o}_{T}\ [H^{+}]$ varies with the temperature; by taking Criss and Cobble's value $\overline{S}^{o}_{298}\ [H^{+}] = -5.0$ cal mole^{-1}°K^{-1} a different entropy for the electron is obtained

$$\overline{S}^{o}_{298}\ [e^{-}]_{\text{absolute}} = 20.606 \text{ cal mole}^{-1}\ {}^{o}K^{-1}.$$

The problem of involving the properties of the electron in calculations can be easily overcome if the complete cell reaction is written

$$aA + bB - zH^{+} = cC + dD - \frac{z}{2} H_2 \qquad (A_6)$$

because the electrons are eliminated between the half-cell reaction previously considered (A_2) and the hydrogen half-cell (A_3)(*)

Calculations of free energies, enthalpies, entropies, or heat capacities can therefore be made at any temperature (providing that a suitable method of extrapolation is used) in a straight forward fashion as for example using relation (A_4).

Feeding the ΔG^{o}_{T} values obtained by this method into the Nernst equation applied to (A_6)

$$E_T = -\frac{\Delta G^{o}_{T}}{zF} - \frac{RT}{zF} \ln \frac{a_C^{c} \cdot a_D^{d} \cdot a_{H^+}^{z}}{a_A^{a} \cdot a_B^{b} \cdot \gamma_{H_2}^{Z/2}}$$

and considering that

$$\Delta G^{o}_{T} = c\overline{\Delta G}^{o}_{T}(C) + d\overline{\Delta G}^{o}_{T}(D) - a\overline{\Delta G}^{o}_{T}(A) - b\overline{\Delta G}^{o}_{T}(B) + \text{(complete cell)}$$

$$+ z(\overline{\Delta G}^{o}_{T}(H^{+}) - \tfrac{1}{2}\,\overline{\Delta G}^{o}_{T}(H_2)) = \Delta G^{o}_{T} \text{ (half cell)}$$

(*) In fact the two half cell reactions cannot go independently because of charge generation.

with the normal conventions

ΔG_T^o (SHE) = 0 and a_{H^+}, P_{H_2} = 1 at all temperatures, the half cell (A_2) is regenerated and the Nernst equation becomes

$$\underset{\text{(complete-cell)}}{E_T} = \underset{\text{(half-cell)}}{E_T} = E_T^o - RT \ln \frac{a_C^c \cdot a_D^d}{a_A^a \cdot a_B^b} \qquad (A_7)$$

Another feature that makes full-cell reactions so attractive is that they lead to the same result for ΔS^o_{298}, using either conventional or absolute values.

A-2.5 Variation of Activity Coefficients and pH with Temperature(*)

Cobble[116] suggested the use of the equation

$$\log \gamma_{\pm} = - A_\gamma |z_+ z_-| \frac{I^{\frac{1}{2}}}{1+I^{\frac{1}{2}}} + \frac{2\nu^+ \nu^-}{\nu} B_{(m)} m$$

to describe the variation of the activity coefficient with the temperature.

In this relation, I is the ionic strength and $B_{(m)}$ is a concentration-dependent parameter, ν^+ and ν^- are the number of cations and anions and z^+ and z^- the respective charges.

A compilation of A_γ values up to 250°C is given by Cobble[116] and $B_{(m)}$ values at 25°C by Lewis and Randall[117], as a function of molality.

The variation of the pH of a solution with temperature is not easy to measure and is difficult to compute once it involves a change in activity of the ions, including H^+ and OH^-, and hydrolysis of the species in solution.

Cobble[116], using experimental data obtained by others, predicted from the Correspondence Principle values for the dissociation constant of water up to 350°C. From these values were calculated the corresponding pH for the neutral point for each temperature, summarized in the following table.

(*) Thanks are due to Mr. T. Mason, Dr. F. Ugarte-Alvarez and Mr. H. Saricimen for useful discussions on this topic.

t, °C	pK_w^o	pH_t (neutrality)
25	13.997	7.00
60	13.0_5	6.53
100	12.2_1	6.11
150	11.6_5	5.83
200	11.3_0	5.65
250	11.1_8	5.59
300	11.1_9	5.60
350	11.3_3	5.67

However, these values fix only one corresponding point on the pH scales at different temperatures.

To solve this problem, and assuming that the pH change which occurs on heating the solution is due to hydrolysis and changes in activity of all ions, including H^+ and OH^- ions involved in the hydrolysis of water, Robins[118] suggested the individual application of Criss and Cobble Principle to the hydrolysis of each ion in solution, and the use of an extended Debye-Hückel equation to determine the activity coefficients of the ions at high temperatures. With this method he was able to represent the effect of temperature on the pH. Although interesting, this method must be looked upon with reserve since Robins does not seem to have followed the normal conventions for the reference hydrogen half cell reaction, for temperatures other than 298°K, and assumed variation of ΔG^o with temperature for that reaction.

Another system was proposed by Ashworth and Boden[119], based on the fact that when the temperature is raised, equivalent amounts of additional H^+ and OH^- are produced and therefore the ionic product of the water at that temperature will become

$$Kw_t = (a_{H^+\,24^oC} + x)\,(a_{OH^-\,24^oC} + x),$$

x being the increase in ion activity. At 24°C a pH = n corresponds to $a_{H^+24^oC} = 10^{-n}$ and $a_{OH^-\,24^oC} = 10^{-(14-n)}$, therefore

$$K_{W_t} = (10^{-n} + x)\,(10^{-(14-n)} + x)$$

and the new pH^t becomes $-\log_{10}(10^{-n} + x)$.

However, this method did not take into account the hydrolysis of the other ions in solution.

In the present work only the pH scale at the temperature of the calculations was considered, leaving the possibility of using any type of extrapolation to room temperature.

A-3 Simplified Relations for Each Temperature

A-3.1. $t = 25^{\circ}C$ $T = 298^{\circ}K$

$$\log K_{298} = - \frac{\Delta G^{\circ}_{298} \text{ (cal mole}^{-1})}{1.364 \times 10^{3}}$$

$$E^{\circ}_{298} = - \frac{\Delta G^{\circ}_{298} \text{ (cal mole}^{-1})}{z \times 23.06 \times 10^{3}} \text{ volt}$$

$$E_{298} = E^{\circ}_{298} - \frac{0.0591}{z} \log \frac{a_C^c \cdot a_D^d}{a_A^a \cdot a_B^b} \text{ volt}$$

A-3.2 $t = 100^{\circ}C$ $T = 373^{\circ}K$

$$\Delta G^{\circ}_{373} = \Delta G^{\circ}_{298} - 75\Delta S^{\circ}_{298} - 8.73 \left[\overline{\Delta C}^{\circ}_{p}\right]_{298}^{373}$$

$$\log K_{373} = - \frac{\Delta G^{\circ}_{373} \text{ (cal mole}^{-1})}{1.707 \times 10^{3}}$$

$$E^{\circ}_{373} = - \frac{\Delta G^{\circ}_{373} \text{ (cal mole}^{-1})}{z \times 23.06 \times 10^{3}} \text{ volt}$$

$$E_{373} = E^{\circ}_{373} - \frac{0.0740}{z} \log \frac{a_C^c \cdot a_D^d}{a_A^a \cdot a_B^b} \text{ volt}$$

A-3.3 $t = 150^{\circ}C$ $T = 423^{\circ}K$

$$\Delta G^{\circ}_{423} = \Delta G^{\circ}_{298} - 125\Delta S^{\circ}_{298} - 23.16 \left[\overline{\Delta C}^{\circ}_{p}\right]_{298}^{423}$$

$$\log K_{423} = - \frac{\Delta G^{\circ}_{423} \text{ (cal mole}^{-1})}{1.936 \times 10^{3}}$$

$$E^{\circ}_{423} = - \frac{\Delta G^{\circ}_{423} \text{ (cal mole}^{-1})}{z \times 23.06 \times 10^{3}} \text{ volt}$$

cont.....

A-3.3 cont.

$$E_{423} = E^{o}_{423} - \frac{0.0839}{z} \log \frac{a_C^c \cdot a_D^d}{a_a \cdot a_b} \text{ volt}$$

A-4 Sulphur-Water System

A-4.1 - Reactions

1) $HSO_4^- = H^+ + SO_4^=$

2) $H_2S_{(aq)} = H^+ + HS^-$

3) $HS^- = H^+ + S^=$

4) $HSO_4^- + H^+ + 3H_2 = 4H_2O + S$
$(HSO_4^- + 7H^+ + 6e = 4H_2O + S)$

5) $SO_4^= + 2H^+ + 3H_2 = 4H_2O + S$
$(SO_4^= + 8H^+ + 6e = 4H_2O + S)$

6) $S + H_2 = H_2S_{(aq)}$
$(S + 2H^+ + 2e = H_2S)$

7) $S + H_2 = HS^- + H^+$
$(S + H^+ + 2e = HS^-)$

8) $SO_4^= + H^+ + 4H_2 = HS^- + 4H_2O$
$(SO_4^= + 9H^+ + 8e = HS^- + 4H_2O)$

9) $SO_4^= + 4H_2 = S^= + 4H_2O$
$(SO_4^= + 8H^+ + 8e = S^= + 4H_2O)$

10) $SO_4^= + 2H^+ + 4H_2 = H_2S_{(aq)} + 4H_2O$
$(SO_4^= + 10H^+ + 8e = H_2S_{(aq)} + 4H_2O)$

11) $O_2 + 2H_2 = 2H_2O$
$(O_2 + 4H^+ + 4e = 2H_2O)$

continued

12) $2H^+ + 2e = H_2$

$2H^+ + H_2 = H_2 + 2H^+$

The following equilibrium relation was also considered

6-A) $HSO_4^- + 4H_2 + H^+ = H_2S_{(aq)} + 4H_2O$

$(HSO_4^- + 9H^+ + 8e = H_2S_{(aq)} + 4H_2O)$

A-4.2 - Potential-pH Relationships

A-4.2.1 - t = 25°C T = 298°K

1) $-pH + \log \{SO_4^{=}\} - \log \{HSO_4^{-}\} = -1.91$

2) $-pH + \log \{HS^{-}\} - \log \{H_2S_{(aq)}\} = -7$

3) $-pH + \log \{S^{=}\} - \log \{HS^{-}\} = -14$

4) $E_{298} = +0.338 - 0.0693\ pH + 0.0099 \log \{HSO_4^{-}\}$

5) $E_{298} = +0.357 - 0.0792\ pH + 0.0099 \log \{SO_4^{=}\}$

6) $E_{298} = +0.142 - 0.0591\ pH - 0.0295 \log \{H_2S_{(aq)}\}$

7) $E_{298} = -0.065 - 0.0295\ pH - 0.0295 \log \{HS^{-}\}$

8) $E_{298} = +0.252 - 0.0665\ pH - 0.0074 \log \dfrac{\{HS^{-}\}}{\{SO_4^{=}\}}$

9) $E_{298} = +0.148 - 0.0591\ pH - 0.0074 \log \dfrac{\{S^{=}\}}{\{SO_4\}}$

10) $E_{298} = +0.303 - 0.0738\ pH - 0.0074 \log \dfrac{\{H_2S_{(aq)}\}}{\{SO_4^{=}\}}$

11) $E_{298} = +1.229 - 0.0591\ pH + 0.0148 \log P_{O_2}$

From now on we will consider $P_{O_2} = 1$ (unit fugacity of oxygen)

$$E_{298} = +1.229 - 0.0591\ pH$$

12) $E_{298} = -0.0591\ pH - 0.0295 \log P_{H_2}$

For the same reasons presented in (11) we consider $P_{H_2} = 1$

$$E_{298} = -0.0591\ pH.$$

A-4.2.2 $\underline{t = 100^{o}C}$ $\underline{T = 373^{o}K}$

1. $-pH + \log \frac{\{SO_4^{=}\}}{\{HSO_4^{-}\}} = -3.02$

2. $-pH + \log \frac{\{HS^{-}\}}{\{H_2S_{(aq)}\}} = -6.70$

3. $-pH + \log \frac{\{S^{=}\}}{\{HS^{-}\}} = -11.95$

4. $E_{373} = +0.314 - 0.0861\ pH + 0.0123 \log \{HSO_4^{-}\}$

5. $E_{373} = +0.351 - 0.0987\ pH + 0.0123 \log \{SO_4^{=}\}$

6. $E_{373} = +0.136 - 0.0740\ pH - 0.0370 \log \{H_2S_{(aq)}\}$

7. $E_{373} = -0.112 - 0.0370\ pH - 0.0370 \log \{HS^{-}\}$

8. $E_{373} = +0.235 - 0.0833\ pH - 0.0093 \log \frac{\{HS^{-}\}}{\{SO_4^{=}\}}$

9. $E_{373} = +0.125 - 0.0740\ pH - 0.0093 \log \frac{\{S^{=}\}}{\{SO_4^{=}\}}$

10. $E_{373} = +0.297 - 0.0925\ pH - 0.0093 \log \frac{\{H_2S_{(aq)}\}}{\{SO_4^{=}\}}$

11. $E_{373} = +1.167 - 0.0740\ pH + 0.0185 \log P_{O_2}$

($E_{373} = +1.167 - 0.0740\ pH$ for $P_{O_2} = 1$)

12. $E_{373} = -0.0740\ pH - 0.0370 \log P_{H_2}$

($E_{373} = -0.0740\ pH$ for $P_{H_2} = 1$)

and also considered

6-A) $E_{373} = +0.269 - 0.0833\ pH - 0.0093 \log \frac{\{H_2S_{(aq)}\}}{\{HSO_4^{-}\}}$

A-4.2.3. $\underline{t = 150^{o}C}$ $\underline{T = 423^{o}K}$

1. $-pH + \log \frac{\{SO_4^{=}\}}{\{HSO_4^{-}\}} = -3.68$

2. $-pH + \log \frac{\{HS^{-}\}}{\{H_2S_{(aq)}\}} = -6.95$

3. $-pH + \log \frac{\{S^{=}\}}{\{HS^{-}\}} = -10.81$

4. $E_{423} = +0.301 - 0.0979\ pH + 0.0140 \log \{HSO_4^{-}\}$

5. $E_{423} = +0.352 - 0.1119\ pH + 0.0140 \log \{SO_4^{=}\}$

6. $E_{423} = +0.140 - 0.0839\ pH - 0.0420 \log \{H_2S_{(aq)}\}$

7. $E_{423} = -0.152 - 0.0420\ pH - 0.0420 \log \{HS^{-}\}$

8. $E_{423} = +0.226 - 0.0944\ pH - 0.0105 \log \frac{\{HS^{-}\}}{\{SO_4^{=}\}}$

9. $E_{423} = +0.113 - 0.0839\ pH - 0.0105 \log \frac{\{S^{=}\}}{\{SO_4^{=}\}}$

10. $E_{423} = +0.299 - 0.1049\ pH - 0.0105 \log \frac{\{H_2S_{(aq)}\}}{\{SO_4^{=}\}}$

11. $E_{423} = +1.127 - 0.0839\ pH + 0.0210 \log P_{O_2}$

$(E_{423} = +1.127 - 0.0839\ pH$ for $P_{O_2} = 1)$

12. $E_{423} = -0.0839\ pH - 0.0420 \log P_{H_2}$

$(E_{423} = -0.0839\ pH$ for P_{H_2} for $P_{H_2} = 1)$

and also considered

6-A) $E_{423} = +0.260 - 0.0944\ pH - 0.0105 \log \frac{\{H_2S_{(aq)}\}}{\{HSO_4^{-}\}}$

A-4.3 Discussion on the Sulphur-Water System

The diagrams are presented (Fig.A-1,2,3) for the cases when the activity of sulphur ions in solution are 10^{-1} and 10^{-4}M at 1 atm pressure.

According to the diagrams and for the presented conditions, all substances considered are stable in aqueous solution once their domain, or at least part of it, lies within the stability region of water. However, there are other ions not represented, because they do not seem to be relevant in this study. In fact, determinations by D'yachkova and Khodakovskiy[120] for the equilibrium constants of disproportionation reactions for thiosulphate and sulphite forms gave

		25°C	50°C	100 °C	150°
$S_2O_3^= + H_2O \rightleftharpoons SO_4^= + S^= + 2H^+$	pK	16.13	15.40	14.61	14.47
$4SO_3^= \rightleftharpoons 3\ SO_4^= + S^=$	pK	-35.23	-33.12	-29.55	-26.6

Their calculations using these constants showed that equilibrium concentrations of thiosulphate and sulphite forms of sulphur (taking into account the hydrolysis of $SO_3^=$ and $S_2O_3^=$) were substantially lower than the concentrations of its sulphide and sulphate forms, in the range of pH,E and temperatures considered.

They also mentioned the experimental work of Pryor[121] which showed that at high temperature even the Kinetic effect did not introduce any important correction into the theoretical calculations. Pryor's experiments showed that a solution of 0.83M $Na_2S_2O_3$ (pH 6.00) when heated for 8 hours to 270°C produced 0.62M sulphide, 0.76M sulphate, 0.00M sulphite, 0.01M polysulphide-sulphur and 0.07M thiosulphate.

According to the equilibria relations given and the diagrams presented, the following details can be pointed out.

For the non-redox homogeneous reaction -1-

$$HSO_4^- = H^+ + SO_4^=$$

$$pH_{298} = 1.91$$
$$pH_{373} = 3.02$$
$$pH_{423} = 3.68$$

The equilibrium line shifts to the right with increase in temperature, extending the stability area of HSO_4^- to a higher pH.

For the relation -2- also a non-redox homogeneous reaction

$$H_2S_{(aq)} = H^+ + HS^-$$
$$pH_{298} = 7.00$$
$$pH_{373} = 6.70$$
$$pH_{423} = 6.95$$

This equilibrium line H_2S/HS^- moves towards lower pH by increasing the temperature up to 373°K. Above this value it shifts to higher pH due to the appearance of the equilibrium $SO_4^=/H_2S$.

For the same type of reaction, relation -3-

$$HS^- = H^+ + S^=$$
$$pH_{298} = 14.00$$
$$pH_{373} = 11.95$$
$$pH_{423} = 10.81$$

This shows that for the range of pH values from zero to 14, this equilibrium need not be considered at temperatures below 298°K. Above this value the ions $S^=$ must be considered.

Assuming that all the species in solution have the same activity, these three equilibria are independent of ionic activity once they are represented by the equilibrium relation

$$-pH + \log \frac{\{A\}}{\{\overline{B}\}} = \log K$$

For the remaining equilibria some are homogeneous reactions, others heterogeneous, but all of them are pH and potential dependent.

Special reference should be made to equilibrium relation -7- for activities of sulphur species equal to 10^{-1}M

$$S + H^+ + 2e = HS^-$$

This equilibrium disappears at about 373°K and above this temperature there is no possibility of sulphur being reduced to HS^-, because the upper limit of stability of sulphur remains below the lower limit of stability of HS^-. Related to this, is the case of $SO_4^=$ reduction in acidic

solutions below 373°K, (equilibrium relation -5-) which produces sulphur, which in turn should give H_2S. But at higher temperatures, besides these equilibria a new one can occur (equilibrium relation -10-) due to the shrinking of sulphur zone, allowing direct reduction of $SO_4^=$ to H_2S.

This occurence is similar to what happens at 298°K when concentrations are lowered, which causes the eventual disappearance of the sulphur zone and formation of a boundary $H_2S/SO_4^=$ as seen for 10^{-4}M solutions.

In brief the following conclusions can be drawn:

Within the range of temperatures considered (298, 373 and 423°K), H_2S, HS^- and $S^=$ ionic species are stable in water and aqueous solutions free from oxidizing agents, H_2S in acid solutions, HS^- mainly in the alkaline zone (lowest pH being 6.7 at 373°C) and $S^=$ at very high pH values. The stability of HSO_4^- is predominant at very low pH values. In 10^{-1} solutions it leads to sulphur upon reduction, and similarly $SO_4^=$, below 373°K, leads to sulphur in the acid zone, but to HS^- in an alkaline medium, and to sulphur, H_2S or HS^-, according to the pH value, for temperatures above 373°K.

Sulphur lies completely within the stability domain of water and is stable in solutions free from oxidizing agents, the upper pH limit of stability being affected by an increase in temperature.

This increase in temperature makes the potential for equilibria relations -4- and -5- fall to less positive values, the potential for equilibrium -6- remaining quite unchanged. Thus, the area of sulphur shrinks and probably disappears at higher temperatures. This is similar to what happens for 10^{-4}M solutions where the sulphur zone is quite small even at 298°K, disappearing between this temperature and 373°K.

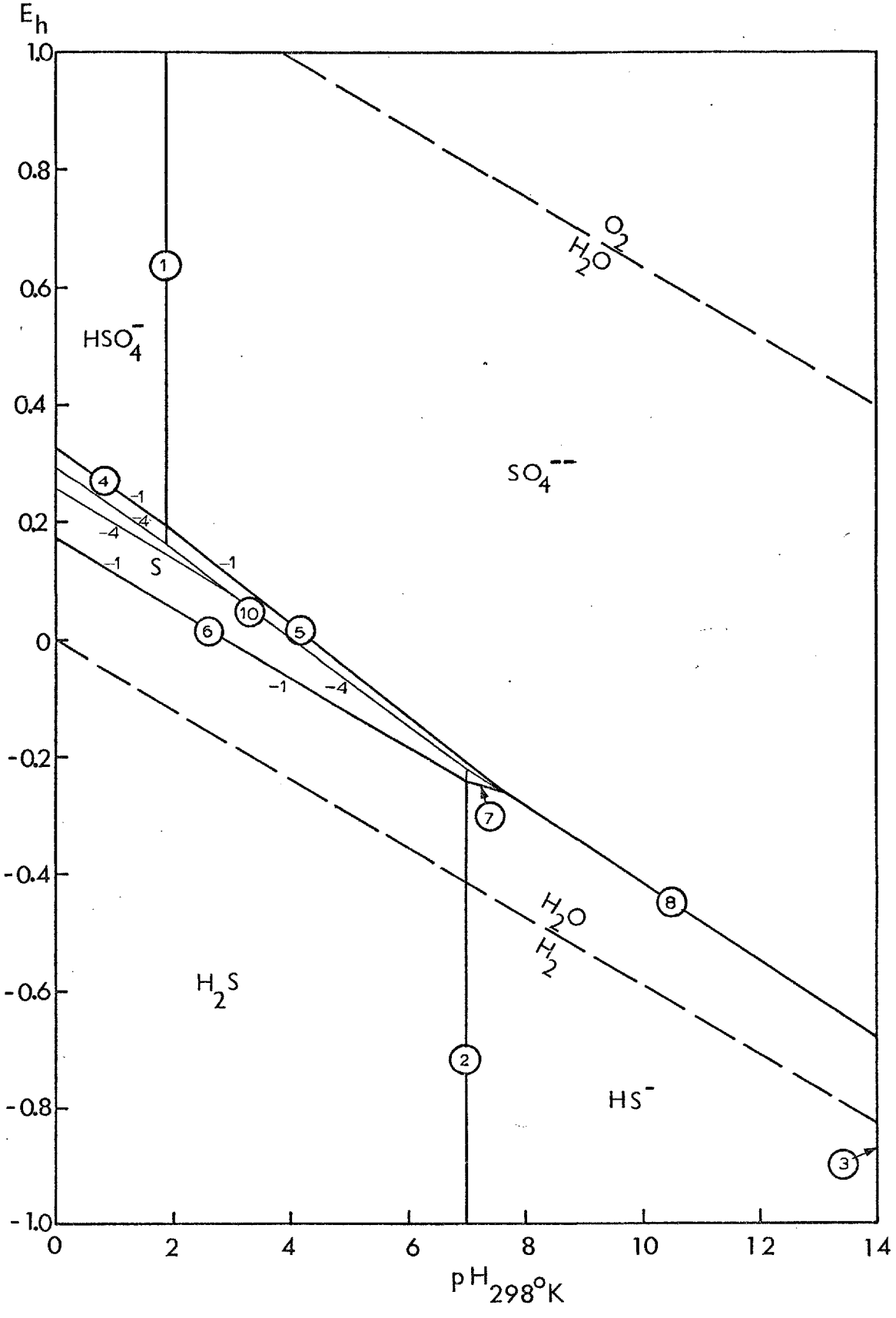

Fig. A-1 Equilibrium diagram for sulphur at 298°K and 1 atm pressure. Activities of sulphur containing ions: 10^{-1} and 10^{-4}M

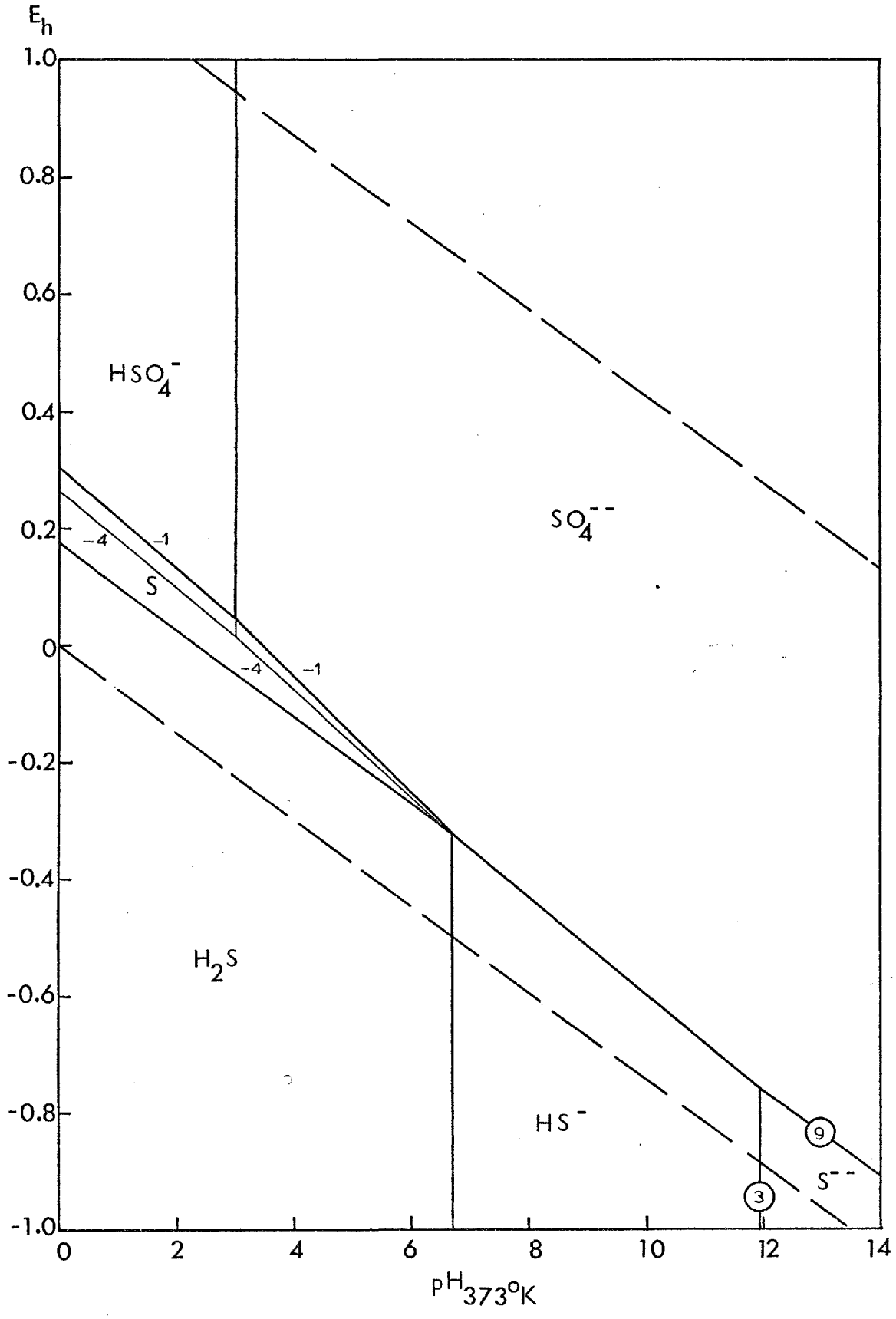

Fig. A-2 Equilibrium diagram for sulphur at 373°K and 1 atm pressure. Activities of sulphur containing ions: 10^{-1} and 10^{-4}M

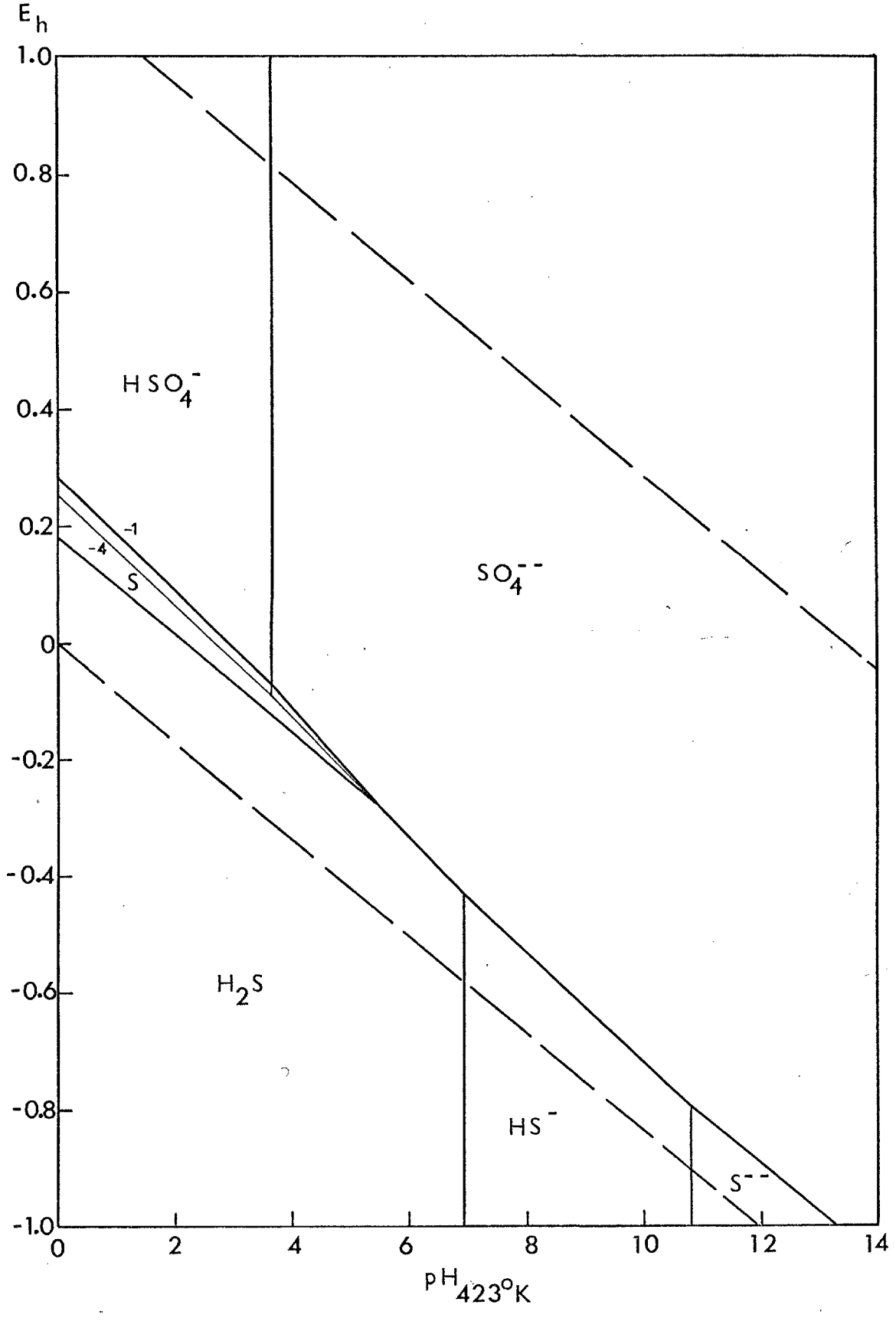

Fig. A-3. Equilibrium diagram for sulphur at 423°K and 1 atm pressure. Activities of sulphur containing ions: 10^{-1} and 10^{-4}M

A-5. Copper Oxides and Sulphides - Water System

A-5.1. Reactions

1. $Cu^{++} + H_2O = CuO + 2H^+$

2. $CuO + H_2O = CuO_2^= + 2H^+$

3. $CuO_2^= + H^+ = HCuO_2^-$

4. $CuO + H_2O = H^+ + HCuO_2^-$

5. $2CuO + H_2 = Cu_2O + H_2O$

   $(2CuO + 2H^+ + 2e = Cu_2O + H_2O)$

6. $Cu_2O + H_2 = 2Cu + H_2O$

   $(Cu_2O + 2H^+ + 2e = 2Cu + H_2O)$

7. $Cu^{++} + H_2 = Cu + 2H^+$

   $(Cu^{++} + 2e = Cu)$

8. $Cu^+ + \frac{1}{2} H_2 = Cu + H^+$

   $(Cu^+ + e = Cu)$

9. $= Cu^{++} + \frac{1}{2} H_2 = Cu^+ + H^+$

   $(Cu^{++} + e = Cu^+)$

10. $2Cu^{++} + H_2O + H_2 = Cu_2O + 4H^+$

    $(2Cu^{++} + H_2O + 2e = Cu_2O + 2H^+)$

11. $2Cu^{++} + HSO_4^- + 5H_2 = Cu_2S + 4H_2O + 3H^+$

    $(2Cu^{++} + HSO_4^- + 7H^+ + 10e = Cu_2S + 4H_2O)$

12. $2Cu^{++} + SO_4^= + 5H_2 = Cu_2S + 4H_2O + 2H^+$

    $(2Cu^{++} + SO_4^= + 8H^+ + 10e = Cu_2S + 4H_2O)$

13. $2Cu^{++} + H_2S_{(aq)} + H_2 = Cu_2S + 4H^+$

    $(2Cu^{++} + H_2S_{(aq)} + 2e = Cu_2S + 2H^+)$

14. $2Cu^{++} + HS^- + H_2 = Cu_2S + 3H^+$

    $(2Cu^{++} + HS^- + 2e = Cu_2S + H^+$

15. $2CuS + H_2 = Cu_2S + H_2S_{(aq)}$

$(2CuS + 2H^+ + 2e = Cu_2S + H_2S_{(aq)})$

16. $2CuS + H_2 = Cu_2S + HS^- + H^+$

$(2CuS + H^+ + 2e = Cu_2S + HS^-)$

17. $Cu_2S + SO_4^{=} + 2H^+ + 3H_2 = 2CuS + 4H_2O$

$(Cu_2S + SO_4^{=} + 8H^+ + 6e = 2CuS + 4H_2O)$

18. $Cu_2S + HSO_4^- + H^+ + 3H_2 = 2CuS + 4H_2O$

$(Cu_2S + HSO_4^- + 7H^+ + 6e = 2CuS + 4H_2O)$

19. $2Cu + HSO_4^- + H^+ + 3H_2 = Cu_2S + 4H_2O$

$(2Cu + HSO_4^- + 7H^+ + 6e = Cu_2S + 4H_2O)$

20. $2Cu + SO_4^{=} + 2H^+ + 3H_2 = Cu_2S + 4H_2O$

$(2Cu + SO_4^{=} + 8H^+ + 6e = Cu_2S + 4H_2O)$

21. $Cu_2S + H_2 = H_2S_{(aq)} + 2Cu$

$(Cu_2S + 2H^+ + 2e = H_2S_{(aq)} + 2Cu)$

22. $2HCuO_2^- + 2H^+ + H_2 = Cu_2O + 3H_2O$

$(2HCuO_2^- + 4H^+ + 2e = Cu_2O + 3H_2O)$

23. $2CuO_2^{=} + 4H^+ + H_2 = Cu_2O + 3H_2O$

$(2CuO_2^{=} + 6H^+ + 2e = Cu_2O + 3H_2O)$

24. $CuO_2^{=} + 2H^+ + H_2 = Cu + 2H_2O$

$(CuO_2^{=} + 4H^+ + 2e = Cu + 2H_2O$

A-5.2 Potential-pH Relationships

A-5.2.1. $t = 25^{o}C$ $T = 298^{o}K$

1. $-2pH - \log \{Cu^{++}\} = -7.889$
2. $\log \{CuO_2^{=}\} - 2pH = -31.94$
3. $\log \{HCuO_2^{-}\} - \log \{CuO_2^{=}\} + pH = +13.135$
4. $-pH + \log \{HCuO_2^{-}\} = -18.8$
5. $E_{298} = +0.670 - 0.0591\ pH$
6. $E_{298} = +0.471 - 0.0591\ pH$
7. $E_{298} = +0.337 + 0.0295 \log \{Cu^{++}\}$
8. $E_{298} = +0.521 + 0.0591 \log \{Cu^{+}\}$
9. $E_{298} = +0.153 - 0.0591 \log \{Cu^{+}\} + 0.0591 \log \{Cu^{++}\}$
10. $E_{298} = +0.203 + 0.0591\ pH + 0.0591 \log \{Cu^{++}\}$
11. $E_{298} = +0.427 + 0.0118 \log \{Cu^{++}\} + 0.00591 \log \{HSO_4^{-}\} - 0.0414\ pH$
12. $E_{298} = +0.438 + 0.0118 \log \{Cu^{++}\} + 0.00591 \log \{SO_4^{=}\} - 0.0473\ pH$
13. $E_{298} = +0.978 + 0.0591 \log \{Cu^{++}\} + 0.0295 \log \{H_2S_{(aq)}\} + 0.0591 pH$
14. $E_{298} = +1.187 + 0.0591 \log \{Cu^{++}\} + 0.0295 \{HS^{-}\} + 0.0295\ pH.$
15. $E_{298} = +0.081 - 0.0295 \log \{H_2S_{(aq)}\} - 0.0591\ pH$
16. $E_{298} = -0.127 - 0.0295 \log \{HS^{-}\} - 0.0295\ pH$
17. $E_{298} = +0.377 + 0.00985 \log \{SO_4^{=}\} - 0.0788\ pH$
18. $E_{298} = +0.358 + 0.00985 \log \{HSO_4^{-}\} - 0.0689\ pH$
19. $E_{298} = +0.488 + 0.00985 \log \{HSO_4^{-}\} - 0.0689\ pH$
20. $E_{298} = +0.506 + 0.00985 \log \{SO_4^{=}\} - 0.0788\ pH$
21. $E_{298} = -0.303 - 0.0295 \log \{H_2S_{(aq)}\} - 0.0591\ pH$
22. $E_{298} = +1.78 + 0.0591 \log \{HCuO_2^{-}\} - 0.1182\ pH$
23. $E_{298} = +2.56 + 0.0591 \log \{CuO_2^{=}\} - 0.1773\ pH$
24. $E_{298} = +1.515 + 0.02955 \log \{CuO_2^{=}\} - 0.1182\ pH.$

A-5.2.2. $\underline{t = 100^{o}C}$ $\underline{T = 373^{o}K}$

1. $-2pH - \log \{Cu^{++}\} = - 5.589$
2. $\log \{CuO_2^{=}\} - 2pH = - 28.42$
3. $\log \{HCuO_2^{-}\} - \log \{CuO_2^{=}\} + pH = + 12.00$
4. $-pH + \log \{HCuO_2^{-}\} = - 16.46$
5. $E_{373} = 0.654 - 0.0740\ pH$
6. $E_{373} = + 0.434 - 0.0740\ pH$
7. $E_{373} = + 0.337 + 0.0370 \log \{Cu^{++}\}$
8. $E_{373} = + 0.509 + 0.0740 \log \{Cu^{+}\}$
9. $E_{373} = + 0.165 - 0.0740 \log \{Cu^{+}\} + 0.0740 \log \{Cu^{++}\}$
10. $E_{373} = + 0.241 + 0.0740\ pH + 0.0740 \log \{Cu^{++}\}$
11. $E_{373} = + 0.414 + 0.0148 \log \{Cu^{++}\} + 0.0074 \log \{HSO_4^{-}\} - 0.0518\ pH$
12. $E_{373} = + 0.437 + 0.0148 \log \{Cu^{++}\} + 0.0074 \log \{SO_4^{=}\} - 0.0592\ pH$
13. $E_{373} = + 0.993 + 0.0740 \log \{Cu^{++}\} + 0.0370 \log \{H_2S_{(aq)}\} + 0.0740\ pH$
14. $E_{373} = + 1.241 + 0.0740 \log \{Cu^{++}\} + 0.0370 \log \{HS^{-}\} + 0.0370\ pH$
15. $E_{373} = + 0.083 - 0.0370 \log \{H_2S_{(aq)}\} - 0.0740\ pH$
16. $E_{373} = - 0.165 - 0.0370 \log \{HS^{-}\} - 0.0370\ pH$
17. $E_{373} = + 0.369 + 0.0123 \log \{SO_4^{=}\} - 0.0987\ pH$
18. $E_{373} = + 0.331 + 0.0123 \log \{HSO_4^{-}\} - 0.0863\ pH$
19. $E_{373} = + 0.466 + 0.0123 \log \{HSO_4^{-}\} - 0.0863\ pH$
20. $E_{373} = + 0.503 + 0.0123 \log \{SO_4^{=}\} - 0.0987\ pH$
21. $E_{373} = - 0.318 - 0.0370 \log \{H_2S_{(aq)}\} - 0.0740\ pH$
22. $E_{373} = + 1.868 + 0.0740 \log \{HCuO_2^{-}\} - 0.1480\ pH$
23. $E_{373} = + 2.756 + 0.0740 \log \{CuO_2^{=}\} - 0.2220\ pH$
24. $E_{373} = + 1.596 + 0.0370 \log \{CuO_2^{=}\} - 0.1480\ pH$

A-5.2.3. $\underline{t = 150^{\circ}C}$ $\underline{T = 423^{\circ}K}$

1. $-2pH - \log \{Cu^{++}\} = -4.530$
2. $\log \{CuO_2^{=}\} - 2pH = -27.26$
3. $\log \{HCuO_2^{-}\} - \log \{CuO_2^{=}\} + pH = +11.48$
4. $-pH + \log \{HCuO_2^{-}\} = -15.81$
5. $E_{423} = +0.644 - 0.0839\ pH$
6. $E_{423} = +0.411 - 0.0839\ pH$
7. $E_{423} = +0.337 + 0.0420 \log \{Cu^{++}\}$
8. $E_{423} = +0.495 + 0.0839 \log\{Cu^{+}\}$
9. $E_{423} = +0.179 - 0.0839 \log \{Cu^{+}\} + 0.0839 \log \{Cu^{++}\}$
10. $E_{423} = +0.266 + 0.0839\ pH + 0.0839 \log \{Cu^{++}\}$
11. $E_{423} = +0.408 + 0.0168 \log \{Cu^{++}\} + 0.00839 \log\{HSO_4^{-}\} - 0.0587\ pH$
12. $E_{423} = +0.439 + 0.0168 \log \{Cu^{++}\} + 0.00839 \log\{SO_4^{=}\} - 0.0671\ pH$
13. $E_{423} = +0.998 + 0.0839 \log \{Cu^{++}\} + 0.0420 \log \{H_2S_{(aq)}\} + 0.0839\ pH$
14. $E_{423} = +1.289 + 0.0839 \log\{Cu^{++}\} + 0.0420 \log \{HS^{-}\} + 0.0420\ pH$
15. $E_{423} = +0.094 - 0.0420 \log \{H_2S_{(aq)}\} - 0.0839\ pH$
16. $E_{423} = -0.199 - 0.0420 \log \{HS^{-}\} - 0.0420\ pH$
17. $E_{423} = +0.368 + 0.01398 \log \{SO_4^{=}\} - 0.1119\ pH$
18. $E_{423} = +0.315 + 0.01398 \log \{HSO_4^{-}\} - 0.0979\ pH$
19. $E_{423} = +0.455 + 0.01398 \log \{HSO_4^{-}\} - 0.0979\ pH$
20. $E_{423} = +0.507 + 0.01398 \log \{SO_4^{=}\} - 0.1119\ pH$
21. $E_{423} = -0.321 - 0.0420 \log \{H_2S_{(aq)}\} - 0.0839\ pH$
22. $E_{423} = +1.966 + 0.0839 \log \{HCuO_2^{-}\} - 0.1678\ pH$
23. $E_{423} = +2.930 + 0.0839 \log \{CuO_2^{=}\} - 0.2517\ pH$
24. $E_{423} = +1.671 + 0.04195 \log \{CuO_2^{=}\} - 0.1678\ pH$

A-5.3 Conclusions on Copper Oxides and Sulphides-Water System

Diagrams are presented (Fig.A-4,5,6) for the cases where the activities of copper ions in solution are 10^{-6} and 10^{-3}M, and the activity of each sulphur-containing species in solution is 10^{-1}M, at 1 atm pressure.

Reaction -2-

$$CuO + H_2O = CuO_2^{=} + 2H^+$$

is a non redox reaction and the boundary $CuO/CuO_2^{=}$ is represented by a vertical line. Comparing the pH values for this boundary with those of reactions -3- and -4- when the activities of copper-containing ions in solution are 10^{-6} we have

-2-	-3-	-4-
$CuO/CuO_2^{=}$	$CuO_2^{=}/HCuO_2^{-}$	$CuO/HCuO_2^{-}$
$pH_{298} = 12.97$	$pH_{298} = 13.14$	$pH_{298} = 12.8$

This data can be represented schematically

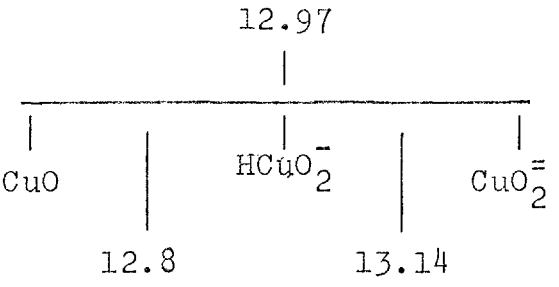

This means that there is no equilibrium between CuO and $CuO_2^{=}$, or more accurately, the concentration of $CuO_2^{=}$ at pH values below 13.14 is very small and therefore the equilibrium $CuO/CuO_2^{=}$ (relation -2-) can be neglected. Similar considerations apply at temperatures of 373° and 423°K.

In solutions where the activities of the copper-containing ions are of the order of 10^{-3}M, the equilibria at 298°K for the relations -2-3- and -4- are established at the following pH values:

-2-	-3-	-4-
$CuO/CuO_2^=$	$CuO_2^=/HCuO_2^-$	$CuO/HCuO_2^-$
$pH_{298} = 14.47$	$pH_{298} = 13.14$	$pH_{298} = 15.80$

and thus equilibria -2- and -3- can be neglected for the reasons mentioned above. In addition, equilibrium -4- is out of the pH range under consideration.

At higher temperatures, equilibrium -4- shifts to lower pH values while -2- and -3- can still be neglected.

It is also interesting to compare the equilibria relations -7-8- and -9- at different temperatures. These relations are independent of the pH and therefore the boundaries are represented by lines at constant potential values. In solutions where the activities of copper-containing ions are of the order 10^{-6} the equilibrium values obtained are:

-7-	-8-	-9-
Cu^{++}/Cu	Cu^{+}/Cu	Cu^{++}/Cu^{+}
E_{298}=+0.160 volt	E_{298}=+0.166 volt	E_{298}=+0.153 volt
E_{373}=+0.115 volt	E_{373}=+0.065 volt	E_{373}=+0.165 volt
E_{423}=+0.085 volt	E_{423}=-0.008 volt	E_{423}=+0.179 volt

At 298°K these equilibria can be represented as follows:

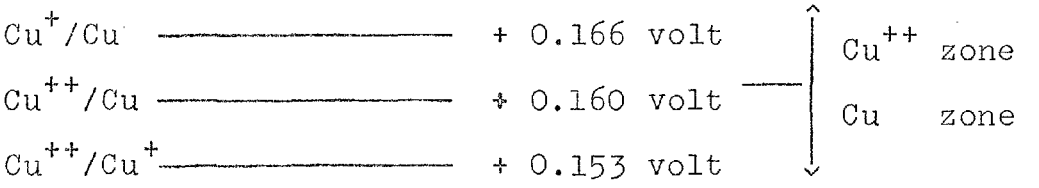

At potentials below +0.160 volt, copper metal is the stable phase and the equilibrium Cu^{++}/Cu^{+} is of no significance, because the activity of Cu^{+} ions is negligibly small.

Similar considerations apply at potentials above +0.160 volt, the Cu^{++} zone, and therefore the equilibria -8- Cu^{+}/Cu and -9- Cu^{++}/Cu^{+} can be neglected.

However, at higher temperatures the results obtained are different:

	373°K	423°K
Cu^{++}/Cu^{+} ———	+ 0.165 volt	+ 0.179 volt
Cu^{++}/Cu ———	+ 0.115 volt	+ 0.085 volt
Cu^{+}/Cu ———	+ 0.065 volt	- 0.008 volt

At 373°K and a potential of + 0.065 volt the Cu metal is oxidized to Cu^{+}. The Cu metal zone lies below this value and oxidation of Cu metal to Cu^{++} ion is very unlikely to occur directly. On the other hand, it is possible to achieve the oxidation of Cu^{+} to Cu^{++} ion at higher potential values (above + 0.165 volt). As a result the equilibrium -7- Cu^{++}/Cu can be neglected at 373°K, but not equilibria -8- and -9-, the same considerations applying at 423°K. In brief, it can be said that at 298°K the Cu^{+} ion can be neglected but at 373°K and 423°K there is already a significant region within which Cu^{+} ions are stable. For these temperatures it is also necessary to include the equilibria Cu^{+}/Cu_2S and Cu^{+}/Cu_2O.

At 298°K, the stability region of Cu^{+} ions does become significant if the activities of copper ions in solution is taken as 10^{-8}M.

When considering solutions where copper ion species have higher activities (10^{-3}M) the existence of Cu^{+} can be neglected together with equilibria -8- and -9-, at temperatures up to 423°K.

It should be noted that relations -1- to -10- are independent of the activities of the sulphur-containing ions and the same equilibrium relations apply to the Cu-water system.

Another interesting feature is found with the equilibrium Cu^{++}/CuS, which occurs at negative pH values for 298°K and positive but almost zero values at 373°K and 423°K in solutions with low copper ion activities.

Relation -16- tends to disappear with increasing temperature because the CuS zone shifts to the left, out of the HS^{-} stability region.

Relation -19- is only relevant in solutions where activities are about 10^{-3}M and at temperatures above 298°K. Summarising, we can say that the equilibrium diagram for copper lies within the stability domain of water for any temperature within the range considered. Covellite (CuS) and sulphur can both exist

together in equilibrium, between 298°K and 423°K. Cu^+ ions, unstable at 298°K, have a significant zone of stability at 373°K and 423°K, in solutions where activities of copper-containing species are about 10^{-6}M.

The hydroxide $Cu(OH)_2$ was not considered here because it is less stable than the oxide CuO.

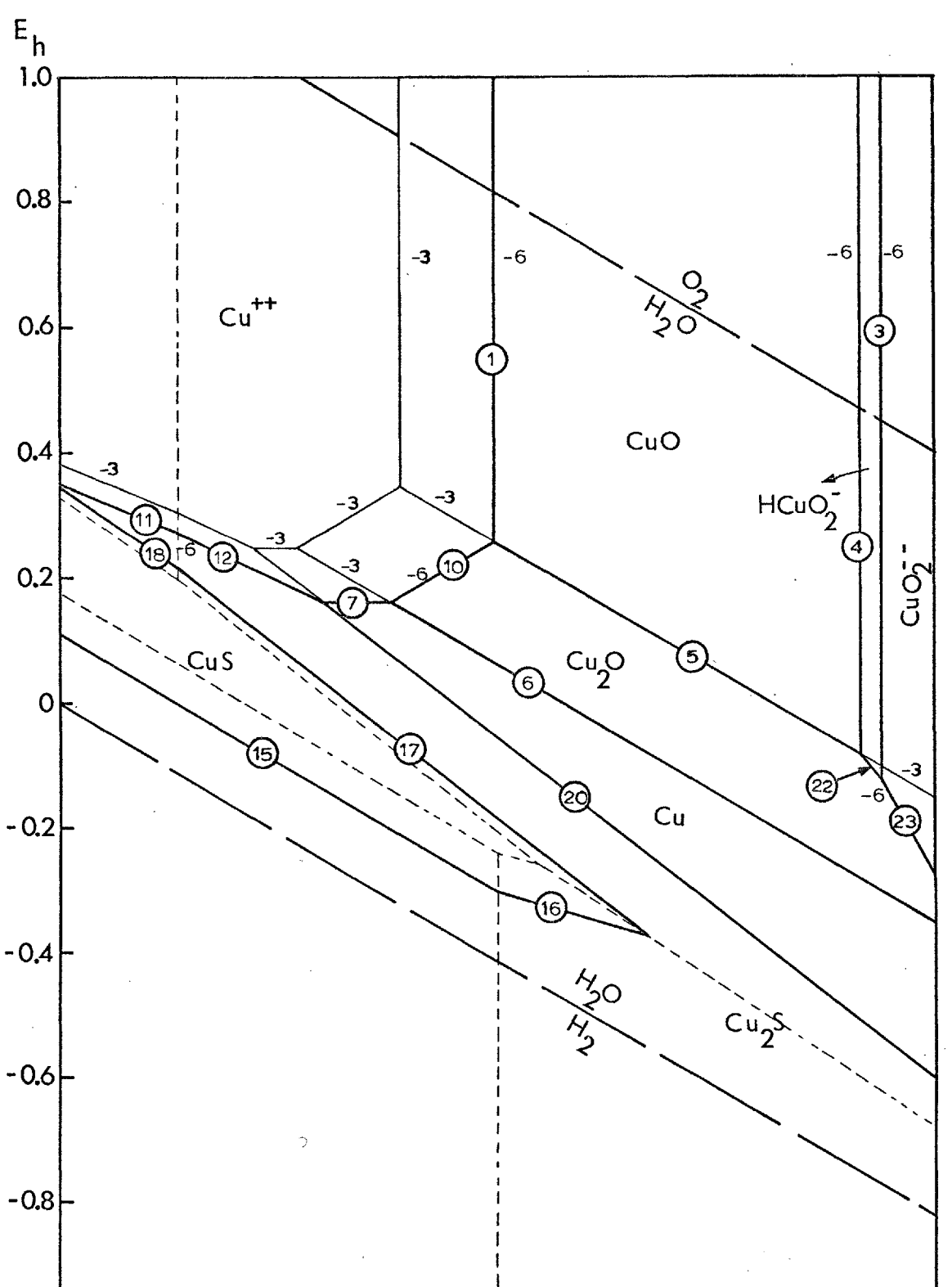

Fig. A-4. Equilibrium diagram for copper oxides and sulphides in water at 298°K and 1 atm pressure. Activities of copper containing ions: 10^{-3} and 10^{-6}M; of sulphur containing ions: 10^{-1}M

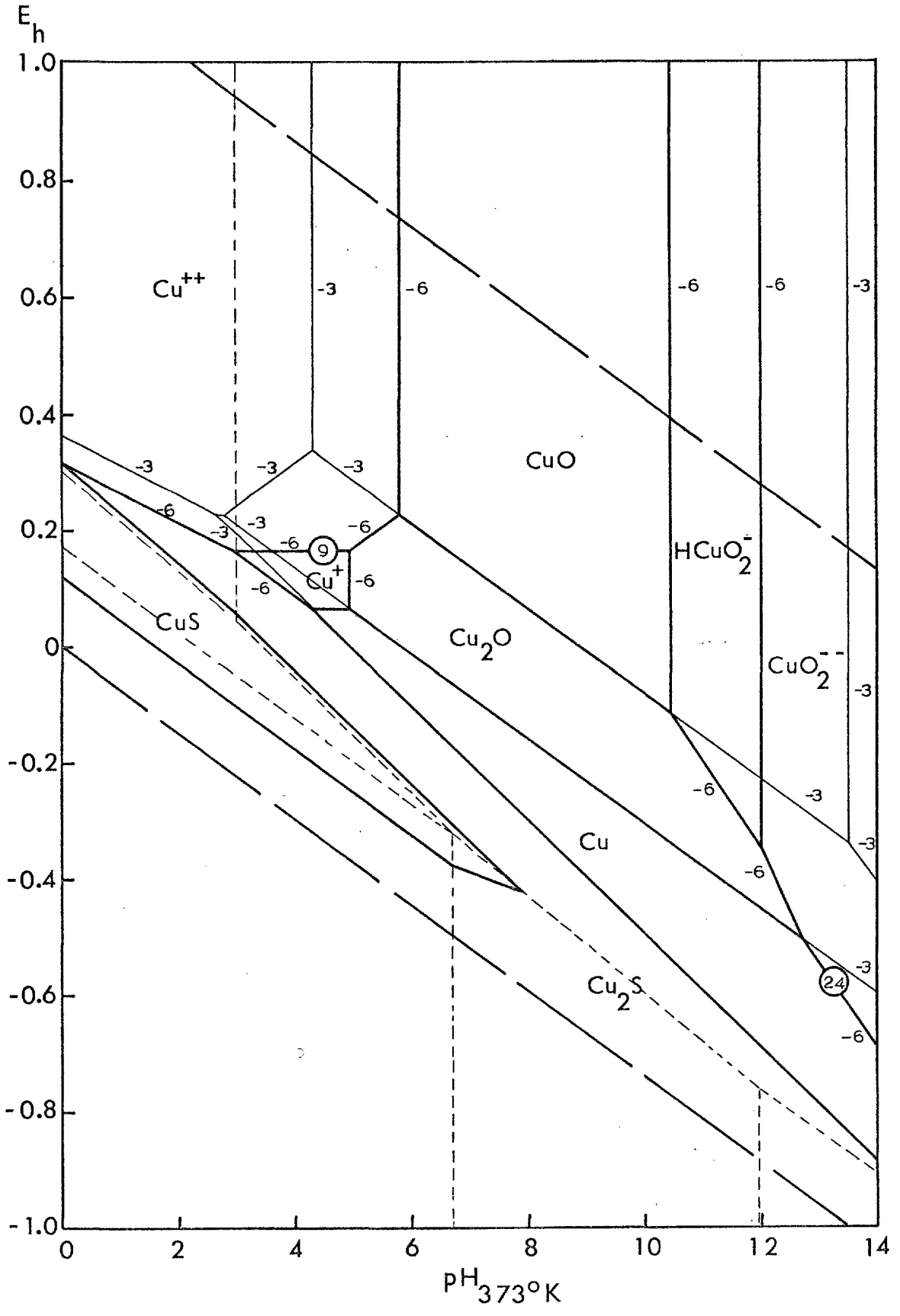

Fig. A-5. Equilibrium diagram for copper oxides and sulphides in water at 373°K and 1 atm pressure. Activities of copper containing ions: 10^{-3} and 10^{-6} M; of sulphur containing ions: 10^{-1}M

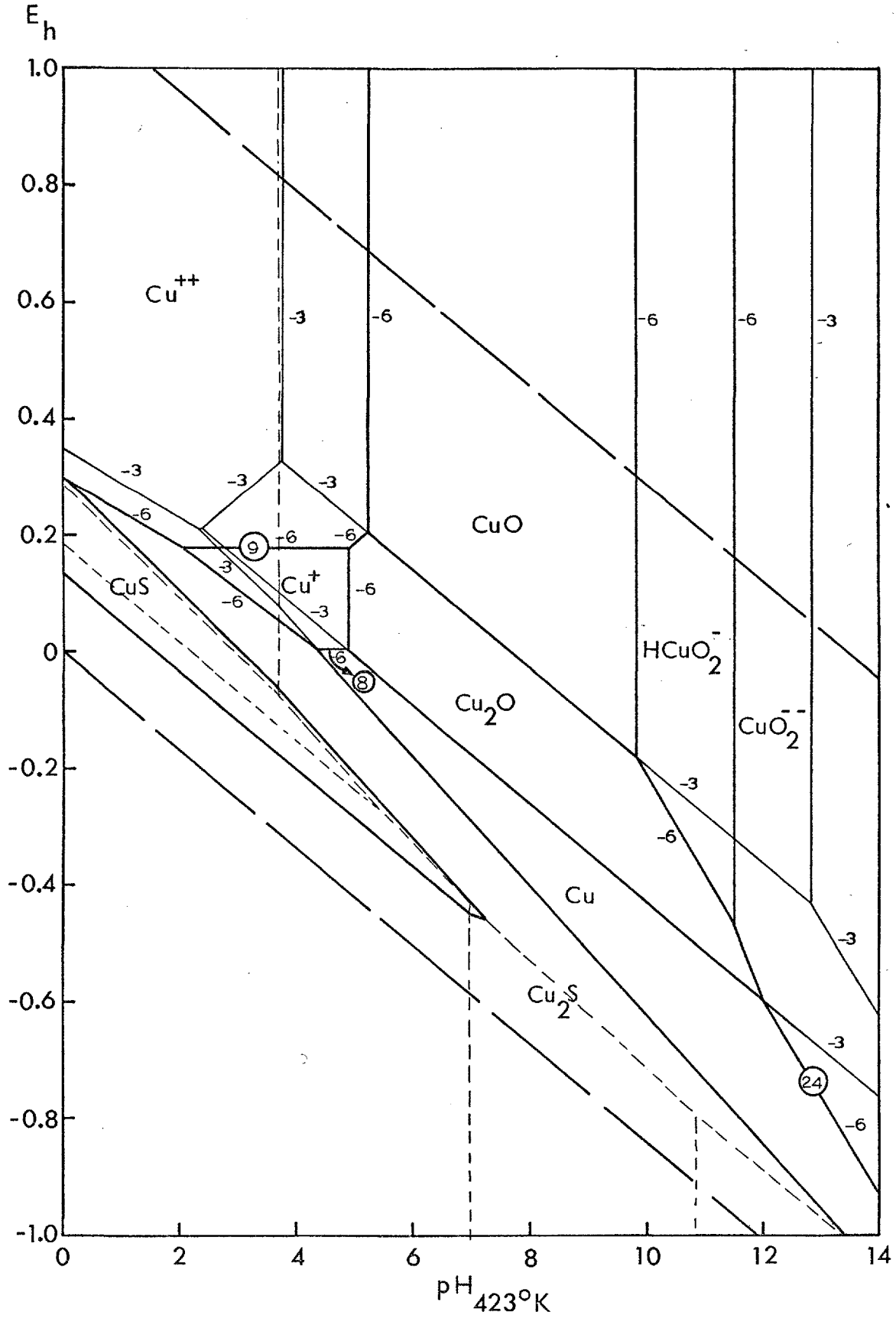

Fig. A-6. Equilibrium diagram for copper oxides and sulphides in water at 423°K and 1 atm pressure. Activities of copper containing ions: 10^{-3} and 10^{-6}M; of sulphur containing ions: 10-1M

A-6 Iron Oxides and Sulphides-Water System

A-6.1 Reactions

1. $Fe^{++} + 2HSO_4^- + 7H_2 = FeS_2 + 8H_2O$

   $(Fe^{++} + 2HSO_4^- + 14H^+ + 14e = FeS_2 + 8H_2O)$

2. $Fe^{++} + 2SO_4^{=} + 2H^+ + 7H_2 = FeS_2 + 8H_2O$

   $(Fe^{++} + 2SO_4^{=} + 16H^+ + 14e = FeS_2 + 8H_2O)$

3. $FeS_2 + 2H^+ + H_2 = Fe^{++} + 2H_2S_{(aq)}$

   $(FeS_2 + 4H^+ + 2e = Fe^{++} + 2H_2S_{(aq)})$

4. $Fe_2O_3 + 4SO_4^{=} + 8H^+ + 15H_2 = 2FeS_2 + 19H_2O$

   $(Fe_2O_3 + 4SO_4^{=} + 38H^+ + 30e = 2FeS_2 + 19H_2O)$

5. $Fe_3O_4 + 6SO_4^{=} + 12H^+ + 22H_2 = 3FeS_2 + 28H_2O$

   $(Fe_3O_4 + 6SO_4^{=} + 56H^+ + 44e = 3FeS_2 + 28\ H_2O)$

6. $3FeS_2 + 4H_2O + 2H_2 = Fe_3O_4 + 6HS^- + 6H^+$

   $(3FeS_2 + 4H_2O + 4e = Fe_3O_4 + 6HS^- + 2H^+)$

7. $FeS + 2H^+ = Fe^{++} + H_2S_{(aq)}$

8. $Fe_3O_4 + 3HS^- + 3H^+ + H_2 = 3FeS + 4H_2O$

   $(Fe_3O_4 + 3HS^- + 5H^+ + 2e = 3FeS + 4H_2O)$

9. $FeS_2 + H_2 = FeS + HS^- + H^+$

   $(FeS_2 + H^+ + 2e = FeS + HS^-)$

10. $Fe^{++} + 2S + H_2 = FeS_2 + 2H^+$

    $(Fe^{++} + 2S + 2e = FeS_2)$

11. $3Fe_2O_3 + H_2 = 2Fe_3O_4 + H_2O$

    $(3Fe_2O_3 + 2H^+ + 2e = 2Fe_3O_4 + H_2O)$

12. $Fe_2O_3 + 4H^+ + H_2 = 2Fe^{++} + 3H_2O$

    $(Fe_2O_3 + 6H^+ + 2e = 2Fe^{++} + 3H_2O)$

13. $Fe_2O_3 + 6H^+ = 2Fe^{+++} + 3H_2O$

14. $Fe^{+++} + \frac{1}{2}H_2 = Fe^{++} + H^+$

    $(Fe^{+++} + e = Fe^{++})$

The following equilibrium relations were also considered

4-A. $Fe_2O_3 + 4HSO_4^- + 4H^+ + 17H_2 = 2FeS_2 + 19H_2O$

$(Fe_2O_3 + 4HSO_4^- + 34H^+ + 30e = 2FeS_2 + 19H_2O)$

6-A. $3FeS_2 + 4H_2O + 2H_2 = Fe_3O_4 + 6S^= + 12H^+$

$(3FeS_2 + 4H_2O + 4e = Fe_3O_4 + 6S^= + 8H^+)$

8-A. $Fe_3O_4 + 3S^= + 6H^+ + H_2 = 3FeS + 4H_2O$

$(Fe_3O_4 + 3S^= + 8H^+ + 2e = 3FeS + 4H_2O)$

9-A. $FeS_2 + H_2 = FeS + H_2S_{(aq)}$

$(FeS_2 + 2H^+ + 2e = FeS + H_2S_{(aq)})$

A-6.2 Potential-pH Relationships

A-6.2.1 $t = 25^{o}C$ $T = 298^{o}K$

1. $E_{298} = 0.351 - 0.0591pH + 0.0084 \log\{HSO_4^-\} + 0.0042 \log\{Fe^{++}\}$
2. $E_{298} = 0.367 - 0.0675pH + 0.0084 \log\{SO_4^{=}\} + 0.0042 \log\{Fe^{++}\}$
3. $E_{298} = -0.140 - 0.118pH - 0.0591 \log\{H_2S_{(aq)}\} - 0.0295 \log\{Fe^{++}\}$
4. $E_{298} = 0.391 - 0.075pH + 0.0079 \log\{SO_4^{=}\}$
5. $E_{298} = 0.395 - 0.075\ pH + 0.0080 \log\{SO_4^{=}\}$
6. $E_{298} = -1.322 - 0.089 \log\{HS^-\} + 0.0295\ pH$
7. $\log\{Fe^{++}\} + \log\{H_2S_{(aq)}\} = 2.58 - 2pH$
8. $E_{298} = 1.373 + 0.089 \log\{HS^-\} - 0.148\ pH$
9. $E_{298} = -0.423 - 0.0295pH - 0.0295 \log\{HS^-\}$
10. $E_{298} = +0.424 + 0.0295 \log\{Fe^{++}\}$
11. $E_{298} = 0.221 - 0.059\ pH$
12. $E_{298} = 0.728 - 0.059 \log\{Fe^{++}\} - 0.177\ pH$
13. $\log\{Fe^{+++}\} = -0.72 - 3pH$
14. $E^{o}_{298} = 0.771$

Also considered the relations

6-A. $E_{298} = -2.564 - 0.0887 \log\{S^{=}\} + 0.1182\ pH$

8-A. $E_{298} = +2.615 + 0.0887 \log\{S^{=}\} - 0.2364\ pH$

9-A. $E_{298} = -0.216 - 0.0295 \log\{H_2S_{(aq)}\} - 0.0591\ pH$

A-6.2.2 $\underline{t = 100^{o}C}$ $\underline{T = 373^{o}K}$

1. $E_{373} = 0.328-0.0740pH + 0.0106 \log\{HSO_4^-\} + 0.0052 \log \{Fe^{++}\}$
2. $E_{373} = 0.360-0.0846pH + 0.0106 \log \{SO_4^=\} + 0.0052 \log \{Fe^{++}\}$
3. $E_{373} = - 0.140-0.1480p_H - 0.0740 \log\{H_2S_{(aq)}\} - 0.0370 \log\{Fe^{++}\}$
4. $E_{373} = 0.378 - 0.0937 \text{ pH} + 0.0099 \log \{SO_4^=\}$
5. $E_{373} = 0.382 - 0.0942 \text{ pH} + 0.0101 \log \{SO_4^=\}$
6. $E_{373} = -1383 - 0.1110 \log \{HS^-\} + 0.0370 \text{ pH}$
7. $\log \{Fe^{++}\} + \log \{H_2S_{(aq)}\} = 1.716 - 2pH$
8. $E_{373} = 1.411 + 0.1110 \log\{HS^-\} - 0.1850 \text{ pH}$
9. $E_{373} = - 0.452 - 0.0370 \text{ pH} - 0.0370 \log \{HS^-\}$
10. $E_{373} = 0.411 + 0.0370 \log \{Fe^{++}\}$
11. $E_{373} = 0.208 - 0.0740 \text{ pH}$
12. $E_{373} = 0.641 - 0.0740 \log \{Fe^{++}\} - 0.222pH$
13. $\log \{Fe^{+++}\} = - 2.96 - 3pH$
14. $E^{o}_{373} = 0.860$

Also considered the relations

6-A. $E_{373} = - 2.709 - 0.1110 \log \{S^=\} + 0.148 \text{ pH}$

8-A. $E_{373} = + 2.737 + 0.1110 \log \{S^=\} - 0.296 \text{ pH}$

9-A. $E_{373} = - 0.203 - 0.0370 \log \{H_2S_{(aq)}\} - 0.0740 \text{ pH}$

A-6.2.3 $\underline{t = 150^{\circ}C}$ $\underline{T = 423^{\circ}K}$

1. $E_{423} = 0.315-0.0839pH+0.0120 \log\{HSO_4^-\} + 0.0060 \times \log\{Fe^{++}\}$
2. $E_{423} = 0.360-0.0959pH+0.0120 \log \{SO_4^=\} + 0.0060 \log\{Fe^{++}\}$
3. $E_{423} = - 0.123 - 0.1678\ pH - 0.0839 \log \{H_2S_{(aq)}\} - 0.0420 \log\{Fe^{++}\}$
4. $E_{423} = 0.375 - 0.1063\ pH + 0.0112 \log \{SO_4^=\}$
5. $E_{423} = 0.379 - 0.1068\ pH + 0.0114 \log \{SO_4^=\}$
6. $E_{423} = - 1.450 - 0.1259 \log \{HS^-\} + 0.0420\ pH$
7. $\log \{Fe^{++}\} + \log \{H_2S_{(aq)}\} = 1.482 - 2pH$
8. $E_{423} = 1.468 + 0.1259 \log \{HS^-\} - 0.2098\ pH$
9. $E_{423} = - 0.477 - 0.0420\ pH - 0.0420 \log \{HS^-\}$
10. $E_{423} = 0.403 + 0.0420 \log \{Fe^{++}\}$
11. $E_{423} = 0.201 - 0.0839\ pH$
12. $E_{423} = 0.586 - 0.0839 \log \{Fe^{++}\} - 0.2517\ pH$
13. $\log\{Fe^{+++}\} = - 3.983 - 3pH$
14. $E^{\circ}_{423} = 0.921.$

Also considered the relations

6-A. $E_{423} = - 2.811 - 0.1259 \log \{S^=\} + 0.1678\ pH$

8-A. $E_{423} = + 2.829 + 0.1259 \log \{S^=\} - 0.3356\ pH$

9-A. $E_{423} = - 0.186 - 0.0420 \log \{H_2S\} - 0.0839\ pH$

A-6.3 Conclusions on Iron Oxides and Sulphides-Water System

Diagrams are presented (Fig.A-7,8,9) for the case when the activities of iron ions in solution are 10^{-6} and 10^{-1}M, and the activity of each sulphur-containing species in solution is 10^{-1}M at 1 atm pressure.

The results and diagrams at 298°K and 10^{-6}M iron ion activities have already been presented and fully discussed by Burkin[106], and therefore they will only be compared to the results at 373°K and 423°K.

It can be seen that there is no great change in the shape of the diagram due to increase in temperature. However, at 298°K there are important changes when the activity of sulphur-containing ions is altered. This can be seen by comparison with Burkin's diagram for solutions where the activity of iron ions is 10^{-6}M but the activity of sulphur-containing species in solution is 10^{-6}M. He showed that, in this case, a shrinkage in the iron sulphide region occurs with appearance of pyrrhotite (FeS), stable under strongly reducing conditions in the pH range between 7 and 9.5 approximately.

Only a few points need be noted for the stability zones at 373 and 423°K. At these temperatures it is still possible for sulphur and Fe^{++} to exist together. This coexistence can be neglected for more concentrated solutions in the range of pH and temperature considered, as shown by the equilibria lines when the iron ionic species activities are 10^{-1}M.

The pyrite region is, up to 423°K, partially overlapped by the sulphur stability zone, allowing these substances to exist together. This coexistence is also negligible for more concentrated solutions in the range of pH and temperature considered. The pyrrhotite stability zone, quite small at 298°K, tends to disappear with increasing temperature and is practically non-existent at 423°K.

The stability zone of Fe^{++} is reduced either by an increase in temperature or by an increase in iron ion activities. Also for both activities considered, at 298°K Fe_3O_4 is stable in strong reducing conditions at very high pH values; but at higher temperatures its stability domain is extended to lower

pH values.

The stability zone of Fe^{+++} ions is reduced by an increase in temperature, in solutions where iron species are 10^{-6}M and sulphur-containing species 10^{-1}M. In more concentrated solutions (10^{-1}M sulphur and iron) this zone can be altogether neglected.

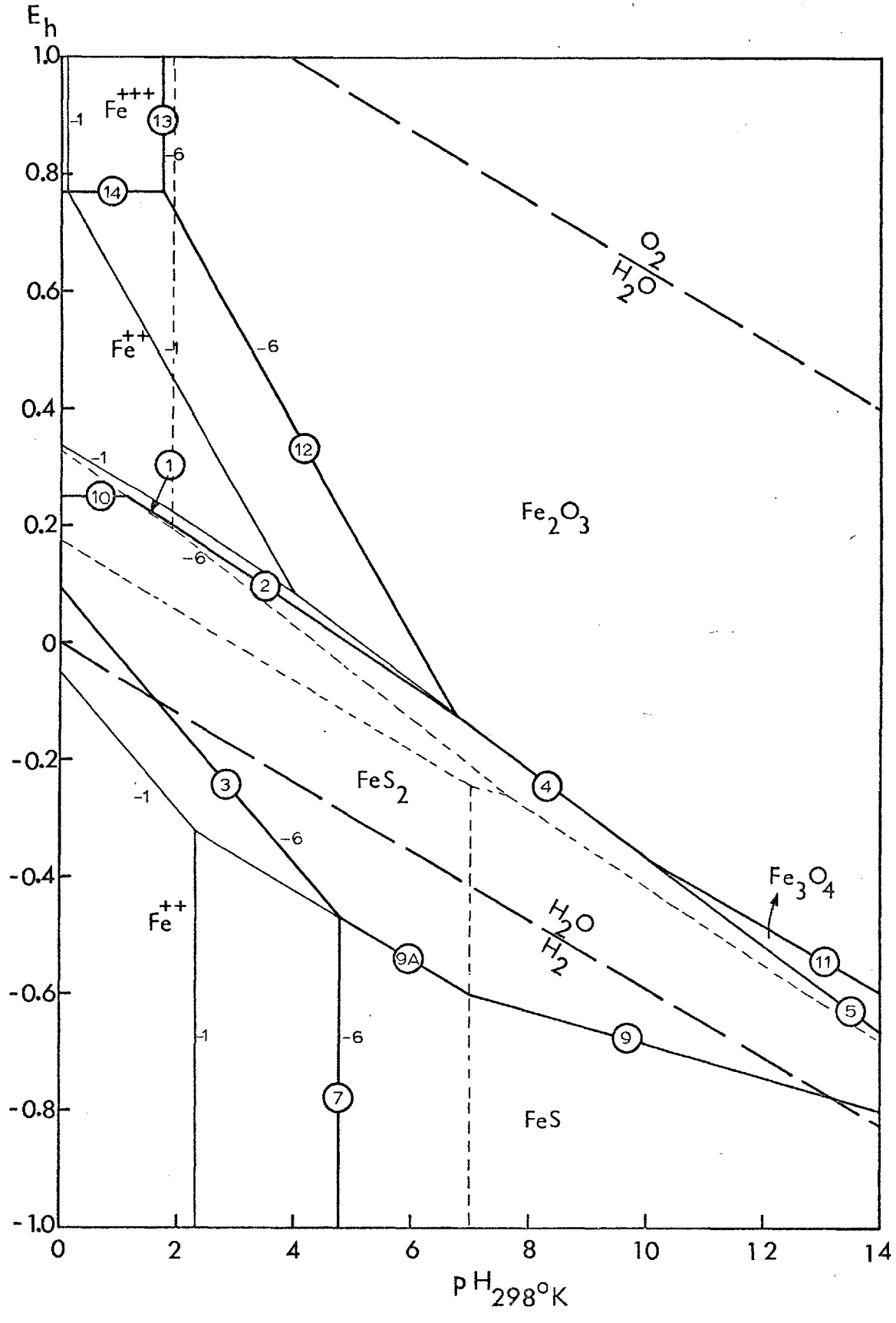

Fig. A-7. Equilibrium diagram for iron oxides and sulphides in water at 298°K and 1 atm pressure. Activities of iron ions: 10^{-1} and 10^{-6}; of sulphur containing ions: 10^{-1}M

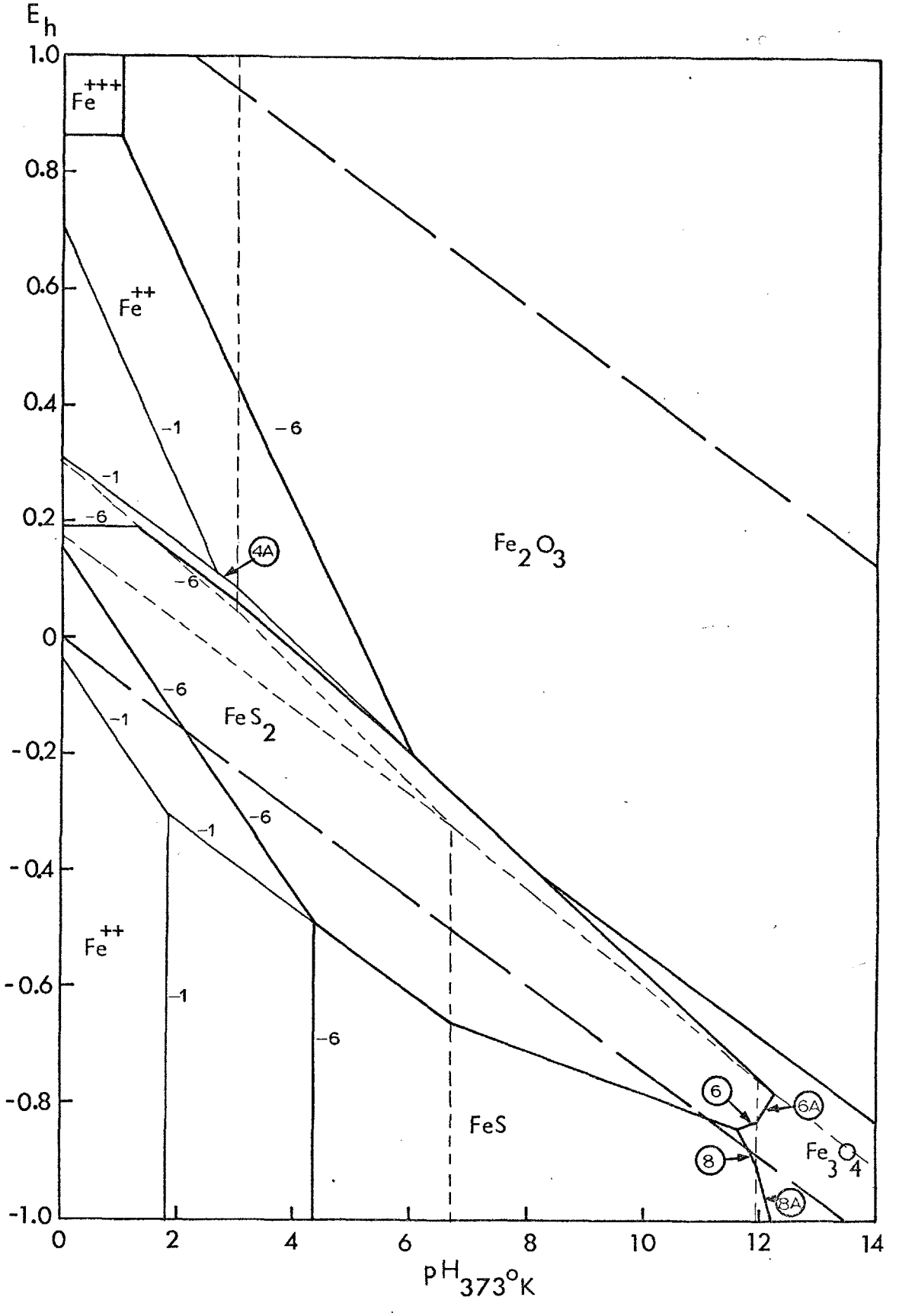

Fig. A-8. Equilibrium diagram for iron oxides and sulphides in water at 373°K and 1 atm pressure. Activities of iron ions: 10^{-1} and 10^{-6}M; of sulphur containing ions: 10^{-1}M

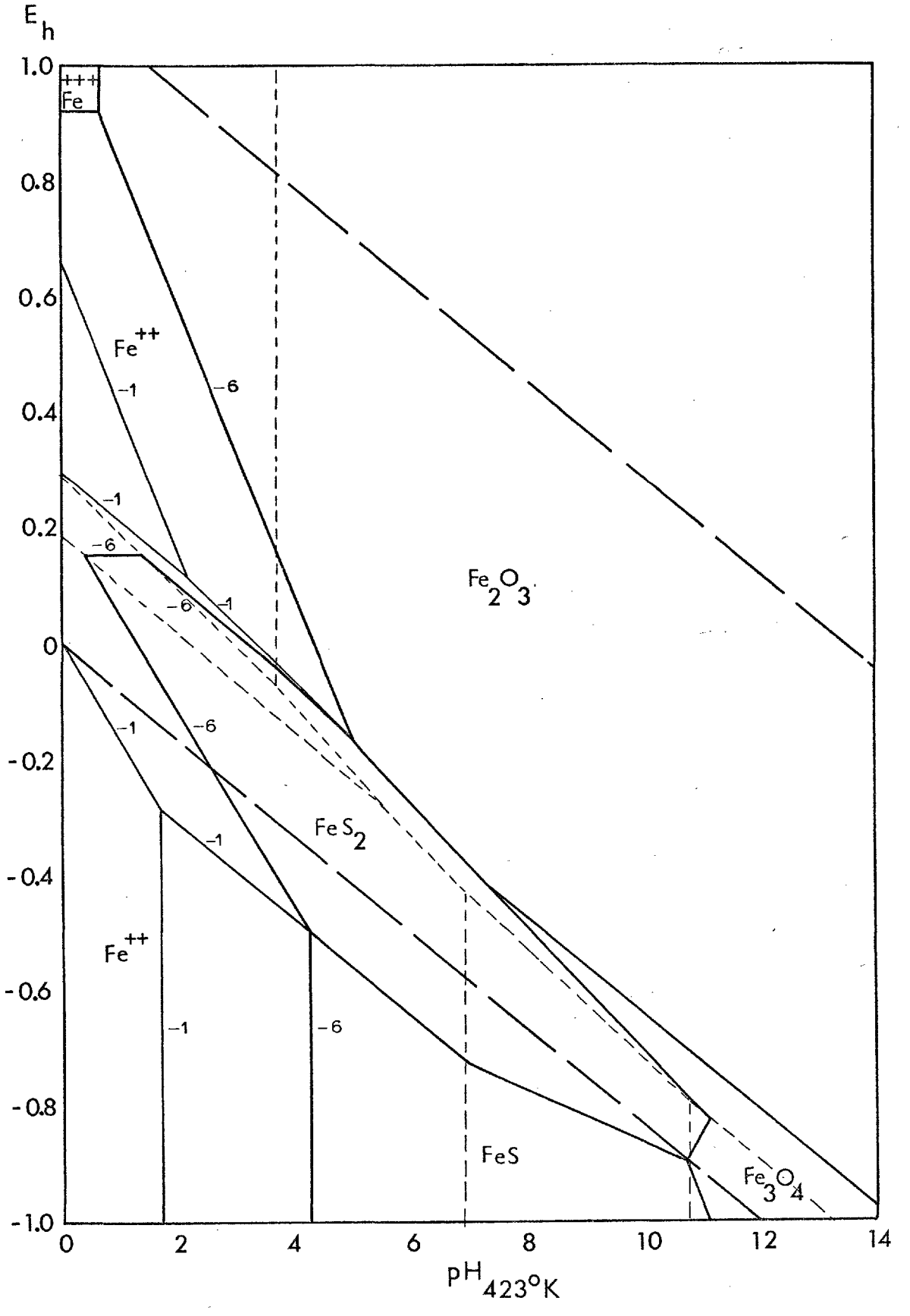

Fig. A-9. Equilibrium diagram for iron oxides and sulphides in water at 423°K and 1 atm pressure. Activities of iron ions: 10^{-1} and 10^{-6} M; of sulphur containing ions: 10^{-1}M.

A-7 Some Comparisons with Results of Other Authors

Diagrams for the system sulphur-water at 25°C were constructed by Valensi[122], Pourbaix[123] and Garrels and Naeser[124]. A study at temperatures other than 25°C was accomplished by Barnes[125], later reviewed by Barnes and Kullerud[126], for the system Fe-S-O. Calculations by these authors involved the use of the Van't Hoff relationship, assuming a constant value for the entalpy ΔH, in the range of temperatures considered. This method allowed the extrapolation of thermodynamic data up to 250°C.

Their own experimental work showed considerable deviations from the calculated values based on the vant'Hoff extrapolation for ionic species. Using an excellent compilation of equilibrium constants and respective uncertainties, they constructed interesting, although inaccurate, P_{O_2}-pH diagrams.

D'yachkova and Khodakovskiy[120] based their study for the system sulphur-water, in the range 25°-300°C, on an extrapolation relation for ΔG° obtained by Khodakovskiy et al.[127] The relation was applicable to dissociations of weak electrolytes, redox reactions, solutions of gases and sparingly soluble compounds.

This relation

$$\Delta G^\circ_{reaction} = A' - D'T + C'T^2$$

was deduced assuming a linear variation of ΔC°_p with temperature

$$\Delta C^\circ_p = - 2C'T$$

and from

$$\Delta G^\circ_T = - RT \ln K^\circ$$

a final expression was obtained

$$\log K^\circ_{reaction} = - \frac{A^*}{T} + D^* - C^* T,$$

and

$$\Delta H^{\circ}_{reaction} = A' - C'T^2$$

$$\Delta S^{\circ}_{reaction} = D' - 2C'T.$$

Experimental data were used by Khodakovsky et al. to derive the coefficients of these expressions and evaluate the dissociation constants up to 300°C.

Applying this method D'yachkova and Khodakovsky constructed diagrams where $\Sigma S=10^{-1}$, for 25°C and 1 atm pressure, 150° and 300°C at 5 and 85 atm pressures respectively, (water vapour pressures at these temperatures).

Since the conventions used in the present report were also followed by these authors, the two diagrams at 25°C (both for the same conditions) are comparable.

It can be seen that at 25°C they are similar, except for the stability region of $S^{=}$. This disagreement is due to the use in this report of thermodynamic data compiled by Latimer[86]. If values from the recent NBS tables[128] are used, different results are derived for the equilibrium relation

$$HS^{-} = H^{+} + S^{=}$$

as presented below:

Latimer[86]			NBS[128]	
$\overline{\Delta G}^{\circ}_{298}$	$\overline{\Delta S}^{\circ}_{298}$		$\overline{\Delta G}^{\circ}_{298}$	$\overline{\Delta S}^{\circ}_{298}$
+ 3.01	+ 14.6	HS^{-}	+ 2.88	+ 15.0
+ 22.1	- 6.4	$S^{=}$	+20.50	- 3.5

Calculations employing the two sets of values lead to

		pH_{298}	pH_{373}	pH_{423}
Latimer	$HS^{-}/S^{=}$	14.00	11.95	10.81
NBS	$HS^{-}/S^{=}$	12.92	10.98	9.89

The value pH_{298} 12.92 for the equilibrium $HS^{-}/S^{=}$ agrees with the diagram constructed by D'yachkova and Khodakovsky.

This system (sulphur-water) was also studied by Biernat and Robins[129] applying the same type of relations as used in the present report. They considered a range of temperatures from 25° up to 300°C and constructed diagrams for solutions of unit activity of dissolved sulphur.

From the results obtained by these authors for the equilibrium relations, it seems that extrapolations to temperatures above 25°C were made using half-cell reactions, and values of ΔS°_{298} (reaction) and ΔC°_{p298} (reaction) which had been calculated without taking into account the thermodynamic values for the electron. On the other hand, Biernat and Robins apparently considered variation of the potential E° with temperatures for the standard hydrogen half-cell reaction. This does not agree with the universal conventions used in the present work.

A very interesting work by Michard and Allègre[130] proposed the substitution of E-pH diagrams by diagrams log S-pH, where S was the total concentration of sulphur in the oxidation state -2. To justify their idea, they considered the sulphate-sulphide reaction (first step on the formation of metal sulphides) where the reaction proceeds very slowly, far from the equilibrium. They point out that equations like

$$E_{298} = + 0.148 - 0.0591 pH - 0.0074 \log \frac{\{S^{=}\}}{\{SO_4^{=}\}}$$

were derived assuming that the equilibrium $SO_4^{=} \rightleftarrows S^{=}$ had been reached, while real potential measurements in sulphide solutions are in fact due to the pair sulphide-polysulphide which reaches equilibrium fairly quickly. These measured potentials, do not represent the ratio sulphide-sulphate as would be suggested by the relation above. They also mentioned that since the equilibrium of the redox reactions was not reached the notion of E had no meaning and measured potentials were in fact mixed potentials for which the Nernst equation was not applicable.

To solve this problem, they decided to introduce the amount of sulphide on the diagrams, since it is a well defined and measurable quantity, using Ag/Ag_2S electrodes, even at very low concentrations. There was, therefore, no need to assume that the equilibrium sulphate-sulphide had been reached, since

the amount of sulphide measured gives accurately the degree of progress of the reaction.

Michard and Allègre gave the basic principles to establish their own type of diagram, and presented various examples and applications.

Although extremely useful and practical it seems rather difficult to extrapolate to temperatures above 25°C.

A-8 Auxiliary Thermodynamic Data

Formula	$\overline{\Delta G}^{o}_{298}$ Kcal mole^{-1}	$\overline{S}^{o}_{298}$ cal mole^{-1} $^{o}K^{-1}$	$\overline{C^{o}_{p}}]^{373}_{298}$ cal mole^{-1} $^{o}K^{-1}$	$\overline{C^{o}_{p}}]^{423}_{298}$ cal mole^{-1} $^{o}K^{-1}$
$H^{+}_{(aq)}$	0	0	+ 31	+ 33
$H_2O_{(\ell)}$	- 56.69	+ 16.716	+ 18.03[a]	+ 18.14[a]
H_2	0	+ 31.211	+ 6.9[a]	+ 6.9[a]
O_2	0	+ 49.003	+ 8.3[a]	+ 8.3[a]
HSO_4^{-}	- 179.94	+ 30.32	- 10	- 18
$SO_4^{=}$	- 177.34	+ 4.1	- 108	- 105
$H_2S_{(aq)}$	- 6.54	+ 29.2	+ 64[b]	+ 61[b]
HS^{-}	+ 3.01	+ 14.6	- 58	- 62
$S^{=}$	+ 22.1	- 6.4	- 58[c]	- 61[c]
$S_{(rh)}$	0	+ 7.62	}+ 5.9[a]	}+ 6.4[a]
$S_{(mon)}$	+ 0.023	+ 7.78		
Cu	0	+ 7.96	+ 5.91	+ 5.94
Cu^{+}	+12	- 6.3?	+52	+53
Cu^{++}	+ 15.53	- 23.6	+64	+66
CuO	- 30.4	+ 10.4	+10.87	+11.00
Cu_2O	- 34.98	+ 24.1	+16.81	+16.95
$CuO_2^{=}$	- 43.5	- 23.0[d]	- 167.12[d]	- 162.51[d]
$HCuO_2^{-}$	- 61.42	+ 10.0[d]	- 126.80[d]	- 121.65[d]
$CuS_{(\alpha)}$	- 20.6	+ 28.9	+19.50	+21.5
CuS	- 11.7	+ 15.9	+11.49	+11.55
Fe^{++}	- 20.30	- 27.1	+66	+68
Fe^{+++}	- 2.53	- 70.1	+93	+96
FeS_2	- 39.84	+ 12.7	+15.2	+15.6
FeS	- 23.32	+ 16.1	+15.2	+15.5
Fe_2O_3	- 177.1	+ 21.5	+26.5	+27.2
Fe_3O_4	- 242.4	+ 35.0	+38.1	+39.3

Remarks:

(i) $\overline{\Delta G}^{\circ}_{298}$ and $\overline{\Delta S}^{\circ}_{298}$ values, unless specified, are from Latimer[86].

(ii) The ionic heat capacities, unless specified, are from Criss and Cobble[131].

(iii) Heat capacities for non-ionic species, unless specified, are from Kubaschewski and Evans[88].

(iv) Heat capacities (a) are from Perry[132].

(v) Heat capacities (b), for $H_2S_{(aq)}$ were calculated using pK_1 values from Cobble. However, more recent values were found in the literature, but they do not alter significantly the results obtained:

Source	pK_1		pK_2	
	100°C	150°C	100°C	150°C
Cobble[116]	6.71	6.96	11.80	10.50
D'yachkova et al.[120]	6.50	6.70	11.45	11.15
Ellis & Giggenbach[133]	6.60	6.80	≃16.00	≃13.00

Applying Cobble values to $\Delta G^{\circ}_T = -RT \ln K_T$ the following values were obtained for the reaction $H_2S_{(aq)} = H^+ + HS^-$

$$\Delta G^{\circ}_{373} = + 11.44 \times 10^3 \text{ cal mole}^{-1}$$
$$\Delta G^{\circ}_{423} = + 13.47 \times 10^3 \text{ cal mole}^{-1}$$

and using the relations

$$\Delta G^{\circ}_{373} = \Delta G^{\circ}_{298} - 75\ \Delta S^{\circ}_{298} - 8.73\ \overline{\Delta C^{\circ}_p}\Big]^{373}_{298}$$

and

$$\Delta G^{\circ}_{423} = \Delta G^{\circ}_{298} - -25\ \ \Delta S^{\circ}_{298} = 23.16\ \overline{\Delta C^{\circ}_p}\Big]^{423}_{298}$$

the average heat capacities change were determined:

$$\overline{C^{\circ}_p}\Big]^{373}_{298}\ (H_2S) = + 64 \text{ cal mole}^{-1}\ {}^{\circ}K^{-1}$$

$$\overline{C^{\circ}_p}\Big]^{423}_{298}\ (H_2S) = + 61 \text{ cal mole}^{-1}\ {}^{\circ}K^{-1}$$

(vi) Heat capacities (c), for $S^{=}$, Cu^{+} and Fe^{++}, were calculated by using Criss and Cobble[114] relationship

$$\overline{C_p^o}]_{298}^{T} = \alpha_{(T)} + \beta_{(T)} \overline{S_{298}^o} \text{ (absolute)}$$

where

$$\overline{S_{298}^o} \text{ (absolute)} = \overline{S_{298}^o} \text{ (conventional)} - 5.0Z,$$

Z is the ionic charge and the constants $\alpha_{(T)}$ and $\beta_{(T)}$ are

T,K°	Cations		Anions	
	$\alpha_{(T)}$	$\beta_{(T)}$	$\alpha_{(T)}$	$\beta_{(T)}$
373	46	-0.55	-58	0.000
423	46	-0.59	-61	-0.03

(vii) The entropy value for the Cu^{+} ion, $\overline{S_{298}^o}$ = - 6.3, was taken from Latimer's compilation. However in the recent NBS Technical Note[128] the value is tabulated as $\overline{S_{298}^o}$ = + 9.7 cal $mole^{-1}$ $^oK^{-1}$.

Entropy values (d) for $CuO_2^{=}$ and $HCuO_2^{-}$ were estimated using the relation for oxy-anions of Connick and Powell[134].

$$\overline{S_{298}^o}_{(conv)} = 43.5 - 46.5\,(Z-0.28n)$$

where Z is the number of unit charges carried by the ion and n is the number of oxygen atoms exclusive of those included in hydroxyl groups.

The values obtained using this relation were

$$S_{298}^o\ (conv)\ [CuO_2^{=}] = -23 \text{ cal } mole^{-1}\ ^oK^{-1}$$

$$S_{298}^o\ (conv)\ [HCuO_2^{-}] = +10 \text{ cal } mole^{-1}\ ^oK^{-1}$$

Using Criss and Cobble[131] relation

$$\overline{C_p^o}]_{298}^{T} = \alpha_{(T)} + \beta_{(T)} \overline{S}_{298}^o \quad \text{(abs)}$$

and $\overline{S}^{o}_{298\ (abs)} = \overline{S}^{o}_{298\ (conv)} - 5.0Z$

together with the values for $\alpha_{(T)}$ and $\beta_{(T)}$ given by these authors for the oxy anions

T (^{o}K)	$\alpha_{(T)}$	$\beta_{(T)}$
373	-138	2.24
423	-133	2.27

the corresponding average value heat capacities were

$$[CuO_2^{=}] \rightarrow \overline{C}^{o}_{p}]_{298}^{373} = -167.12, \quad \overline{C}^{o}_{p}]_{298}^{423} = -162.51$$

$$[HCuO_2^{-}] \rightarrow \overline{C}^{o}_{p}]_{298}^{373} = -126.80, \quad \overline{C}^{o}_{p}]_{298}^{423} = -121.65$$

APPENDIX B

EXPERIMENTAL RESULTS FROM THE LEACHING RUNS

			Page
B-1	Leach Liquor		232
	B-1.1	β-chalcopyrite	232
	B-1.2	α-chalcopyrite	248
B-2	Solid Residues		256
	B-2.1	Atomic Absorption and Electron Probe Analyses	256
	B-2.2	X-ray Powder Diffraction Analyses	258
	B-2.3	X-ray Powder Photographs	293
	B-2.4	Photomicrographs of the Residues	302

B-1 Leach liquor

B-1.1 β-chalcopyrite

TABLE B-11.1

Sample weight: 0.500g β-chalcopyrite
Particle size: -100 + 150 mesh
Temperature : 50°C
pH : 1
Fe^{+++} : 0.03M

Sample Time	% Cu dissolved
30 min	3.2
1 hr	3.9
2	4.7
3	5.6
4	5.9
5	6.4
6	6.9
7	7.2
8	7.3
11	8.1
14	9.0
17	9.0
20	9.8
23	10.0
24	10.0
26	10.4
28	10.5
29	10.6
32	11.2
35	11.2
38	11.6
41	11.7
44	11.8
47	12.4
49	12.4
50	12.4
53	12.3
56	12.9
59	13.0
62	13.0
65	13.1
68	13.2
71	13.1
71	13.3
73	13.3
74	13.8
77	13.7
80	13.4
83	14.2
86	13.9

continued .....

Sample Time	% Cu dissolved
89	13.9
92	14.0
95	14.4
96	14.4
98	14.4
101	14.8
123	15.4
144	16.5
168	17.1
192	17.5
216	17.7
240	18.0
264	18.3
288	18.7
315	18.8
420	22.0
600	26.4

TABLE B-112

Sample weight: 0.500g β-chalcopyrite
Particle size: -100 + 150 mesh
Temperature : 65°C
pH : 1
Fe^{+++}: 0.03M

Sample time	% Cu dissolved
30 mins	3.8
1 hr	4.8
2	6.2
3	7.3
4	8.1
5	8.7
6	9.4
8	10.1
9	9.7
12	10.4
15	11.7
18	12.0
21	12.8
24	13.5
25	13.7
26	14.0
27	13.7
29	14.3
30	14.5
31	14.7
33	14.8
36	15.1
39	15.4
42	15.6
45	15.7
48	15.9
50	16.5
51	16.8
52	16.8
54	16.8
56	17.1
57	16.9
60	17.9
63	17.9
66	17.9
69	18.2
72	18.2
75	18.3
78	18.7
81	18.7
84	18.7
87	18.9
90	19.0

continued .....

Sample Time	% Cu dissolved
93	19.0
96	19.3
102	20.0
126	20.8
152	21.3
171	21.7
194	22.1
218	22.4
243	22.7
265	22.9
289	25.2
330	25.9

TABLE B-11.3

Sample weight: 0.500g β-chalcopyrite
Particle size: -100 + 150 mesh
Temperature : 80°C
pH : 1
Fe^{+++}: 0.03M

Sample Time	% Cu dissolved
30 mins	5.6
1 hr	7.0
2	9.4
3	10.4
4	11.6
5	12.5
6	13.3
8	15.1
11	16.2
14	17.3
17	18.2
20	19.0
22	19.3
23	19.6
24	19.6
26	19.6
27	19.8
28	19.8
30	19.8
32	20.1
35	20.3
38	20.8
41	20.7
47	21.6
49	22.1
51	22.4
53	22.5
56	22.5
62	23.0
65	23.0
68	23.0
71	23.8
73	24.0
74	24.4
77	24.4
83	24.4
86	24.4
89	25.4
94	25.5
95	25.9
98	25.9
122	28.0
174	31.4
204	38.0
240	45.4
270	50.4
332	60.2

TABLE B-11.4

Sample weight: 0.500 g β-chalcopyrite
Particle size: -100 + 150 mesh
Temperature : 95°C
pH : 1
Fe^{+++}: 0.03M

Sample Time	% Cu dissolved
15 mins	7.8
30	9.9
1 hr	12.6
90 mins	14.0
2 hr	15.2
3	17.2
4	19.0
6	19.3
7	21.2
8	21.8
9	22.0
10	22.0
11	22.2
12	23.0
13	23.3
14	23.5
15	23.8
16	24.0
17	24.2
18	24.7
19	24.9
20	25.1
21	24.9
22	25.4
23	25.9
24	25.9
25	25.1
26	26.2
27	26.6
29	26.9
31	27.9
33	28.5
35	29.0
37	29.5
39	29.8
41	30.8
42	31.6
43	32.4
44	32.1
45	32.3
46	33.6
47	33.6

continued .....

Sample Time	% Cu dissolved
48	34.1
49	34.4
50	35.2
51	35.2
53	36.3
55	38.3
57	38.3
59	39.4
61	40.4
63	41.4
65	42.0
66	43.4
67	43.2
68	45.1
69	44.0
71	44.8
74	45.5
75	46.1
77	48.9
78	50.2
81	51.3
83	51.8
85	52.3
87	52.6
89	54.9
90	55.0
91	53.6
92	56.4
93	56.5
96	59.8
(164	(79.9 (*)
168)	82.3)

(*) Not very reliable - strong Fe precipitation.

TABLE B-11.5

Sample weight: 0.250g β-chalcopyrite
Particle size: -100 + 150 mesh
Temperature : 95°C
pH : 1
Fe^{+++} : 0.03M

Sample time	% Cu dissolved
30 mins	9.7
1 hr	12.5
3	17.0
6	20.0
9	21.9
15	23.5
18	24.9
24	27.1
27	27.2
30	28.1
36	29.9
39	31.1
42	31.2
45	33.1
48	34.4
51	35.1
54	36.1
57	38.3
60	39.0
63	40.5
66	44.2
72	47.1
90	57.2
102	63.2
120	71.2
150	80.1
180	89.5
210	95.0

TABLE B-11.6

Sample weight: 0.250g β-chalcopyrite
Particle size: -150 + 200 mesh
Temperature : 95°C
pH : 1
Fe^{+++}: 0.03M

Sample Time	% Cu dissolved
1 hr	14.6
6	21.7
12	23.6
24	27.1
30	28.9
35	32.4
47	39.7
54	43.3
60	47.0
72	53.6
78	58.5
84	60.1
96	67.0
102	69.7
108	72.1
120	78.1
132	82.5
147	87.6
168	93.1
193	97.9
217	98.7
240	98.7

TABLE B-11.7

Sample weight: 0.250g β-chalcopyrite
Particle size: -200 + 300 mesh
Temperature : 95°C
pH : 1
Fe^{+++}: 0.03M

Sample Time	% Cu dissolved
1 hr	16.0
6	24.5
12	26.9
24	32.8
30	36.1
35	38.4
47	45.9
54	49.5
60	52.2
72	59.4
78	63.2
84	66.3
96	74.7
102	78.0
108	81.3
120	87.4
132	90.8
147	96.0
168	98.0
193	98.9

TABLE B-11.8

Sample weight: 0.500g β-chalcopyrite
Particle size: -100 + 150 mesh
Temperature : 80°C
pH : 1
Fe^{+++}: 0.01M

Sample Time	% Cu dissolved
30 mins	6.4
1 hr	8.1
2	10.4
3	11.8
4	12.6
5	13.4
6	14.0
7	14.2
8	14.6
9	15.4
10	16.3
12	16.7
14	17.2
15	17.6
16	18.0
18	18.2
23	19.6
24	19.6
25	19.6
26	19.6
27	19.6
28	19.6
29	19.8
30	19.8
31	20.0
34	20.3
35	20.4
36	20.6
37	20.7
38	20.8
39	20.8
42	20.9
43	21.1
44	21.1
48	21.3
49	21.3
50	21.3
51	21.4
52	21.5
53	21.5
54	21.5
55	22.1
56	22.1

continued.....

Sample Time	% Cu dissolved
57	22.1
58	22.1
60	22.4
62	22.4
65	22.4
66	22.4
67	22.4
68	22.4
71	22.4
72	22.5
73	22.7

TABLE B-11.9

Leaching with Hydrogen Peroxide

Sample weight: 0.200g β-chalcopyrite
Particle size: -200 + 300 mesh
Temperature : 65°C
pH: 1.00
H_2O_2 : 20 volume (1 part)
HCl_{dil} pH∿1 (3 parts)

	Copper		Iron		Sulphur		Residue			
	% removed	% left	% removed	% left	% removed	% left	Cu Atoms	Fe Atoms	S Atoms	Me:S
0	0	100	0	100	0	100	1.00	1.01	1.83	2:1.83
1	7.30	92.70	0.48	99.52	0.18	99.82	1.00	1.08	1.97	2:1.89
2	8.75	91.25	0.82	99.18	0.21	99.79	1.00	1.09	2.01	2:1.92
3	9.94	90.06	1.31	98.69	0.09	99.91	1.00	1.10	2.03	2:1.93
4	10.74	89.26	1.98	98.02	0.28	99.72	1.00	1.10	2.06	2:1.96
5	12.26	87.74	2.67	97.33	1.68	98.32	1.00	1.10	2.05	2:1.96
6	13.38	86.72	3.53	96.47	1.13	98.87	1.00	1.12	2.08	2:1.96
7	14.25	85.75	3.93	96.07	1.79	98.21	1.00	1.12	2.09	2:1.98
8	14.71	85.29	4.19	95.81	2.31	97.69	1.00	1.13	2.11	2:1.98
9	15.18	84.82	4.60	95.40	2.08	97.92	1.00	1.12	2.11	2:1.98
10	16.20	83.80	5.03	94.97	2.46	97.54	1.00	1.13	2.13	2:2.00

11	16.83	83.17	5.46	94.54	3.61	96.39	1.00	1.15	2.13	2:1.98
12	17.61	82.39	6.07	93.93	3.72	96.28	1.00	1.13	2.12	2:1.98
13	18.53	81.47	7.00	93.00	4.28	95.72	1.00	1.13	2.13	2:2.00
14	19.33	80.67	7.64	93.26	4.40	95.60	1.00	1.14	2.16	2:2.02
15	19.73	80.27	7.96	92.04	4.83	95.17	1.00	1.15	2.18	2:2.02
16	20.68	79.32	8.61	91.39	5.11	94.89	1.00	1.15	2.20	2:2.04
17	21.09	78.91	8.95	91.05	5.23	94.77	1.00	1.15	2.19	2:2.04
18	21.49	79.51	9.30	90.70	7.64	92.36	1.00	1.14	2.11	2:1.98
19	22.46	77.54	9.65	90.35	6.60	93.40	1.00	1.15	2.19	2:2.04
20	23.45	76.55	10.48	89.52	7.40	92.60	1.00	1.17	2.23	2:2.06
21	24.44	75.56	10.85	89.15	7.40	92.60	1.00	1.17	2.25	2:2.07
22	25.03	74.97	11.37	88.63	7.90	92.10	1.00	1.19	2.25	2:2.06
23	25.62	74.38	12.08	87.92	8.23	91.77	1.00	1.19	2.27	2:2.06
24	26.21	73.79	12.48	87.52	8.85	91.15	1.00	1.19	2.26	2:2.06
25	26.82	73.18	13.04	86.96	11.63	88.37	1.00	1.19	2.22	2:2.02
26	27.14	72.86	13.61	86.39	9.59	90.41	1.00	1.18	2.27	2:2.08
27	29.43	70.57	15.30	84.70	10.24	89.76	1.00	1.18	2.31	2:2.12
28	29.79	70.21	15.59	84.41	11.51	88.49	1.00	1.20	2.31	2:2.11
29	30.86	69.14	16.52	83.48	13.58	86.42	1.00	1.22	2.29	2:2.06
30	31.52	68.48	16.98	83.02	13.24	86.76	1.00	1.20	2.30	2:2.06
31	33.72	66.28	18.88	81.12	14.57	85.43	1.00	1.23	2.36	2:2.11

32	34.70	65.30	19.39	80.61	14.55	85.45	1.00	1.25	2.40	2:2.12
33	35.28	64.72	20.38	79.62	14.37	85.63	1.00	1.23	2.42	2:2.17
34	36.28	63.72	21.07	79.93	16.48	83.52	1.00	1.25	2.39	2:2.12
35	36.43	63.57	21.61	78.39	16.02	83.98	1.00	1.22	2.41	2:2.17
36	37.01	62.99	22.48	77.52	17.38	82.62	1.00	1.24	2.40	2:2.15
37	37.58	62.42	23.20	76.80	17.40	82.60	1.00	1.24	2.44	2:2.17
38	38.30	61.70	24.07	75.93	25.81	74.19	1.00	1.23	2.19	2:1.96
39	39.01	60.99	24.81	75.19	20.98	79.02	1.00	1.23	2.38	2:2.12
40	39.45	60.55	25.54	74.46	22.12	77.88	1.00	1.23	2.34	2:2.11
41	40.17	59.83	26.45	73.55	20.99	79.01	1.00	1.23	2.42	2:2.17
42	40.88	59.12	22.22	72.78	25.49	74.51	1.00	1.24	2.31	2:2.15
43	41.60	58.40	28.15	71.85	23.21	76.79	1.00	1.24	2.43	2:2.17
44	42.47	57.53	28.77	71.23	23.60	76.40	1.00	1.22	2.41	2:2.17
45	42.78	57.22	29.39	70.61	24.16	75.84	1.00	1.25	2.44	2:2.17
46	43.65	56.35	30.34	69.66	24.40	75.60	1.00	1.25	2.46	2:2.17
47	44.10	55.90	30.82	69.18	24.89	75.11	1.00	1.23	2.46	2:2.20
48	44.69	55.31	31.93	68.07	26.75	73.25	1.00	1.24	2.44	2:2.17
49	45.42	54.58	32.75	67.25	26.11	73.89	1.00	1.22	2.46	2:2.22
50	46.01	53.99	33.58	66.42	26.98	73.02	1.00	1.22	2.48	2:2.22
51	46.46	53.54	34.25	65.75	28.94	71.06	1.00	1.22	2.41	2:2.17
52	47.04	52.96	34.60	65.40	28.94	71.06	1.00	1.23	2.45	2:2.20
53	48.34	51.66	35.75	64.25	32.90	67.10	1.00	1.23	2.37	2:2.12

54	48.24	51.76	35.80	64.20	30.68	69.32	1.00	1.23	2.44	2:2.20
55	48.55	51.45	35.59	64.41	30.70	69.30	1.00	1.23	2.44	2:2.20
56	48.70	51.30	36.98	63.02	31.92	68.08	1.00	1.24	2.45	2:2.20
57	49.42	50.58	37.67	62.33	32.09	67.91	1.00	1.22	2.43	2:2.20
58	49.29	50.71	37.88	62.12	32.56	67.44	1.00	1.22	2.41	2:2.17
59	50.98	49.02	39.03	60.97	34.87	65.13	1.00	1.25	2.43	2:2.15
60	51.85	48.15	40.03	59.97	36.60	63.40	1.00	1.25	2.42	2:2.15
61	54.12	45.88	42.49	57.51	36.39	63.61	1.00	1.26	2.52	2:2.22
62	55.88	44.12	44.52	55.48	38.74	61.26	1.00	1.27	2.55	2:2.25
63	57.52	42.48	47.06	52.94	37.78	62.22	1.00	1.23	2.65	2:2.38
64	58.21	41.79	48.21	51.79	41.06	58.94	1.00	1.24	2.57	2:2.30
65	60.30	39.70	49.86	50.14	40.13	59.87	1.00	1.25	2.75	2:2.44
66	61.01	38.99	51.05	48.95	41.16	58.84	1.00	1.26	2.77	2:2.44
67	63.13	36.87	53.53	46.47	43.11	56.89	1.00	1.27	2.81	2:2.47
68	64.87	35.13	55.89	44.11	43.88	56.12	1.00	1.26	2.94	2:2.60
69	66.64	33.36	57.81	42.19	43.57	56.42	1.00	1.27	3.12	2:2.74
70	68.99	31.01	60.88	39.12	45.68	54.32	1.00	1.26	3.19	2:2.82
71	72.64	27.36	65.13	34.87	46.31	53.69	1.00	1.30	3.63	2:3.18
72	(79.87)	(20.13)	(71.53)	(28.47)	(47.70)	(52.30)	(1.00)	(1.45)	(4.80)	(2:3.93)
73	(82.76)	(17.24)	(73.29)	(26.71)	(48.49)	(51.51)	(1.00)			
74	(87.81)	(12.19)	(72.51)	(27.49)						

B-1.2 α-chalcopyrite

TABLE B-12.1

Sample weight : 1.00g α-chalcopyrite
Particle size: -100 + 150 mesh
Temperature : 80°C
pH : 1
Fe^{+++} : 0.1M
Storage time : 6 days

Sample time	% Cu dissolved
15 mins	2.8
30	4.6
1 hr	5.2
1½	5.5
2½	5.9
3½	6.9
6	8.6
8	9.8
10	10.6
11	10.9
12	11.4
13	11.4
14	12.0
15	12.4
25½	15.4
26½	15.9
27½	16.0
28½	16.1
29½	16.3
31½	16.7
33½	17.2
36½	18.1
37½	18.3
38½	18.5
51	21.2
52	21.5
54	21.9
56	22.2
58	22.6
81	26.5
120	32.1

TABLE B-12.2

Sample weight :	1.00g α-chalcopyrite
Particle size :	-100 + 150 mesh
Temperature :	80°C
pH :	1
Fe^{+++} :	0.1M
Storage time :	40 days

Sample time	% Cu dissolved
30 mins	4.8
1 hr	5.8
2	7.2
3	7.8
4	9.1
5	9.9
6	10.5
7	11.0
9	11.9
21	14.6
22	14.9
23	14.8
24	15.1
25	15.6
26	15.4
27	15.6
28	15.6
29	15.9
30	16.1
33	16.2
46	17.2
47	17.5
50	17.8
52	18.0
54	18.0
57	18.4
70	19.2
71	19.5
73	19.8
78	20.1

TABLE B-12.2 (continued)

Sample time	% Cu dissolved
141	24.8
146	25.6
148½	25.9
165½	27.1

TABLE B-12.3

Sample weight : 1.00g α-chalcopyrite
Particle size : -100 + 150 mesh
Temperature : 80°C
pH : 1
Fe^{+++} : 0.1M
Storage time : 78 days

Sample time	% Cu dissolved
20 mins	3.6
1 hr	4.7
2	6.8
3	8.0
4	9.1
5	9.9
6	10.8
7	11.3
19	12.9
20	13.1
21	13.1
22	13.1
23	13.1
25	13.4
27	13.4
29	13.4
31	13.8
43	14.3
45	14.7
47	14.7
49	15.0
51	15.0
53	15.2
54½	15.3
67	16.0
71	16.2
75	16.4
77½	16.5
91	17.6
96	17.9

TABLE B-12.4

Sample weight : 1.00g α-chalcopyrite
Particle size : -100 + 150 mesh
Temperature : 80°C
pH : 1
Fe^{+++} : 0.01M
Storage time : 85 days

Sample time	% Cu dissolved
30 mins	3.7
1 hr	5.0
2	6.6
3	8.3
4	9.2
5	10.1
6	10.8
7½	11.4
9	11.7
30	13.6
38	13.9
48	14.3
50	14.5
62	15.2
64	15.3
72	15.6
75	15.7
80	16.0

TABLE B-12.5

Sample weight : 0.200g α-chalcopyrite
Particle size : -200 + 300 mesh
Temperature : 80°C
pH : 1
HCl : $\sim 10^{-1}$N
Storage time : 1 year and 75 days

(No Sulphate detected in solution)

Sample time	% Cu dissolved	% Fe dissolved
1 hr	5.8	1.0
4½	13.2	2.6
8	16.2	4.8
11½	17.9	6.3
24	23.8	12.4
29	25.6	13.9
32	26.2	14.5
35½	26.8	15.6
48	27.4	18.6
52	30.8	19.3
56	31.7	19.9
59½	32.6	21.0
72	35.9	23.9
83½	39.6	27.7
96	43.1	31.6
120	50.5	39.2
144	56.9	46.0
167	63.7	54.2
192	70.7	60.6
216	77.8	69.3
240	82.3	74.6
264	86.4	77.5
288	90.5	82.5
312	94.1	86.1
336	96.4	87.5
360	98.0	89.6
384	100.1	92.5

TABLE B-12.6

Sample weight : 0.200g α-chalcopyrite
Particle size : -100 + 150 mesh
Temperature : 95°C
pH : 1

Leaching conditions { 0.03M Fe^{+++} up to 14.9% Cu removed
0.1M NaCl added above this value

Storage time : 1 year and 75 days

Sample time	% Cu dissolved
1 hr	6.5
4½	9.9
8	10.4
11½	10.8
24	12.3
29	12.4
32	12.5
35	12.7
48	13.1
52	13.2
56	13.4
59½	13.5
72	13.6
83½	13.8
96	13.9
120	14.0
144	14.1
167	14.2
192	14.3
216	14.4
240	14.6
264	14.7
288	14.8
312	14.9

TABLE B-12.6 (continued)

Added 0.1M of NaCl

Sample time	% Cu dissolved
336	15.7
360 (15 days)	16.6
16 days	17.4
17	18.2
18	19.0
19	19.8
20	20.7
21	21.5
22	21.7
23	22.8

B-2 Solid Residues

B-2.1 Atomic Absorption and Electron Probe Analyses

TABLE B-21.1

Atomic Absorption Spectrophotometer Analyses of the Residues from Leaching β-chalcopyrite with Acidic Ferric Sulphate Solutions

% Cu removed	Residue			
	Cu Atoms	Fe Atoms	S Atoms	Me:S
0	1.00	1.00	1.83	2:1.83
6.5	1.00	1.07	1.95	2:1.88
7.5	-	-	-	-
10.0 } 12.5 }	1.00	1.13	2.04	2:1.92
14.5	-	-	-	-
16.5	-	-	-	-
17.5	-	-	-	-
18.5	1.00	1.14	2.18	2:2.04
23.0	1.00	1.14	2.18	2:2.04
25.0	1.00	1.17	2.17	2:2.00
27.0	-	-	-	-
31.5 } 45.0 }	1.00	1.19	2.28	2:2.08
50.0	1.00	1.21	2.25	2:2.04
55.0	1.00	1.21	2.25	2:2.04
82.0	1.00	1.20	2.24	2:2.04

TABLE B-21.2

Electron Probe Microanalyses of the β-Solid Residues

% Cu removed	Cu (wt.%)	Fe (wt.%)	S (wt.%)	Total %	Cu Atoms	Fe Atoms	S Atoms	Me:S Ratio
0	35.3	31.4	32.5	99.2	1	1.01	1.83	2:1.82
6.5	34.1	32.1	33.4	99.6	1.00	1.07	1.94	2:1.87
7.5	-	-	-	-	-	-	-	-
10.0	33.3	34.2	34.1	101.6	1.00	1.17	2.03	2:1.87
12.5	-	-	-	-	-	-	-	-
14.5	32.3	31.1	32.9	96.3	1.00	1.10	2.02	2:1.92
16.5	{29.6 31.8	{31.1 33.2	{34.1 31.8	{94.8 96.8	{1.00 1.00	{1.20 1.19	{2.28 1.92	{2:2.07 2:1.75
17.5	31.5	35.3	31.8	98.6	1.00	1.28	2.00	2:1.75
18.5	30.6	32.9	34.7	98.2	1.00	1.22	2.25	2:2.03
23.0	{30.5 30.2	{36.1 34.8	{32.2 34.0	{98.8 99.0	{1.00 1.00	{1.35 1.31	{2.09 2.23	{2:1.78 2:1.93
25.0	{30.9 30.5	{34.5 35.2	{35.5 34.0	{100.9 99.7	{1.00 1.00	{1.27 1.31	{2.28 2.21	{2:2.01 2:1.91
27.0	31.0	32.8	32.5	96.3	1.00	1.20	2.08	2:1.89
31.5	30.9	33.1	33.8	97.8	1.00	1.22	2.17	2:1.96
45.0	30.0	37.9	36.8	104.7	1.00	1.44	2.43	2:1.99
50.0	30.2	33.9	34.0	98.1	1.00	1.28	2.23	2:1.96
55.0	30.2	35.7	34.5	100.4	1.00	1.35	2.26	2:1.92
82.0	31.2	35.0	34.5	100.7	1.00	1.28	2.19	2:1.92

B-2.2 X-ray Powder Diffraction Analyses

ABBREVIATIONS USED

[ ]	-	Shadows of doubtful existence
A	-	Average value
M	-	Maximum value
m	-	Minimum value
T	-	Almost two lines
R	-	Perfectly resolved lines
SB	-	Line starts broadening
B	-	Broad line (average value)
Sh	-	Shadow (average value)
ND	-	Not detected by the Densitometer
ew	-	Extremely weak line
vw	-	Very weak line
w	-	Weak line
med	-	Medium line
s	-	Strong line
vs	-	Very strong line
α-cp	-	α-chalcopyrite
S	-	Sulphur
•	-	Reference for line undergoing transformation or transformed
←	-	Shadow on the right of line
→	-	Shadow on the left of line
<	-	Less than

TABLE B-22.1

Line No.	Synthetic Sample Kept at 700°C.	α-chalcopyrite (135-a) A.S.T.M.	Bornite (135-b) A.S.T.M.	Pyrite (135- A.S.T.M.
1	[shadows]	-	(3 lines)	-
2	3.30 w	-	3.31^{40}	-
3	3.14 w	-	$3.18\text{-}3.15^{60}$	3.128^{36}
4	3.04vs	3.03^{100}	-	-
5	2.710 w	-	2.74^{40}	2.709^{84}
6	2.648 w	2.63^{5}	2.63^{5}	-
7	2.504 w	-	2.50^{40}	-
8	2.423 w	-	-	2.423^{66}
9	2.210 w	-	-	2.2118^{52}
10	1.935 s	-	1.937^{100}	-
11	1.912 w	-	-	1.9155^{40}
12	1.871 med	1.865^{40}	-	-
13	1.853 s	1.854^{80}	1.850^{10}	-
14	1.633 w	-	-	1.6332^{100}
15	1.591 s	1.591^{60}	-	-
16	1.574 w	1.573^{20}	-	1.564^{14}
17	1.518 w	1.518^{5}	-	-
18	1.504 w	-	-	1.5025^{20}
19	1.446 w	-	1.42^{20}	1.4448^{24}
20	-	-	1.37^{20}	-
21	1.322 w	1.323^{10}	-	-
22	1.304 w	1.303^{5}	-	-
23	(line)	-	1.258^{50}	1.247^{12}
24	1.211 w	1.214^{10}	-	1.2113^{14}
25	1.204 med	1.205^{30}	1.198^{10}	-
26	1.182 vw	-	-	1.1823^{7}
27	1.116 vw	-	1.119^{50}	1.1548^{6}
28	1.108 vw	-	-	1.1057^{6}
29	1.078 med	1.077^{60}	-	-
30	1.069 w	1.069^{30}	-	-
31	1.043 vw	-	-	1.0427^{27}
32	1.019 vw	1.018^{20}	-	-
33	1.014 vw	1.014^{10}	-	-
34	1.006 vw	1.005^{5}	-	10060^{8}

TABLE B-22.2 β-CHALCOPYRITE

hkl	CABRI[47] (new Copper-iron osulphide d(Å)	I/I_1	HILLER&PROBSTHAIN[34] d(Å)	I/I_{1calc}	I/I_{1obs}	THIS WORK d(Å)	I/I_{obs}
110	7.52	30	-	5	-	7.54	N.D.
200	5.33	2.5	-	<1	-	5.25	N.D.
211	4.32	5	-	3	-	-	-
220	3.75	40	-	2	-	3.77	8
310	3.36	20	-	1	-	3.35	< 2
-	-	-	-	-	-	≈[3.07]	N.D.
222	3.043	100	3.06	100	100	3.063	100
321	2.831	10	-	2	-	2.844	< 2
400	2.656	50	2.652	18	45-50	2.651	20
411, 330	2.507	20	-	-	-	≈2.499	N.D.
420	2.371	2.5	-	-	-	≈2.372	N.D.
-	-	-	-	-	-	≈[2.264]	N.D.
332	2.254	10	-	<1	-	≈2.254	N.D.
422	2.168	10	-	<1	-	2.164	< 2
510, 431	2.071	20	-	<1	-	≈2.073	N.D.
521	-	-	-	<1	-	-	-
440	1.879	90	1.874	96	89-100	1.876	94
530,433	-	-	-	<1	-	-	-
600, 442	-	-	-	<1	-	-	-
611, 532	-	-	-	<1	-	-	-

/cont....

620	1.680	5	-	<1	-	-		
541	-	-	-	<1	-	≈[1.612]	N.D.	
622	1.598	70	1.600	35	67-75	1.589	68	
631	-	-	-	<1	-	-	-	
444	1.532	2	1.516	4	11-13	1.533	3	
710,550,543	1.501	5	-	<1	-	-	-	
640	-	-	-	<1	-	-	-	
421,633,552	1.443	2.5	-	<1	-	-	-	
642	1.415	2.5	-	<1	-	≈1.415	N.D.	
730	1.390	2.5	-	<1	-	-	-	
732,651	-	-	-	<1	-	≈1.340	N.D.	
800	1.327	40	1.326	18	45-50	1.325	29	
662	1.210	50	1.216	20	56-63	1.216	45	
752	1.202	5	-	<1	-	-	-	
840	1.180	20	1.186	7	11-25	1.186	5	
844	1.079	60	1.082	78	67-88	≈1.089	N.D.	
						1.082	81	
10.2.2,666	1.0193	50	1.020	46	56-63	1.020	59	
880	0.9360	50	-	-	-	[shadows]		

TABLE B-22.3

X-ray Patterns of Leach Residues of β-chalcopyrite
Ferric Sulphate Leaching

Line No.	% of COPPER DISSOLVED									
	0		6.5		7.34		10.21		12.44	
	d(Å)	I/I_1	d(Å)	I/I_1	d(Å)	I/I_1	d(Å)	I/I_1	d(Å)	I/I_1
1	~7.54	ND	~7.50	ND	~7.48	ND	-		-	
2	-		-		-		-		-	
3	~5.25	ND	-		-		-		-	
4	-		-		-		-		-	
5	3.77	8	3.75	4	3.74	4	3.74	3	3.73	<2
6	3.35	<2	3.35	<2	3.35	<2	-		-	
7	~[3.07]	100	~[3.07]	100	~[3.07]	100	~[3.06]	100	~[3.06]	100
8	3.063)		3.055)		3.054)		3.051)		3.048)	
9	-		-		-		-		-	
10	-		-		-		-		-	
11	2.844	<2	2.826	<2	-		-		-	
12	-		-		-		-		-	
13	2.651	20	2.651	15	2.647	6	2.644	25	2.642	13
14	-		-		-		-		-	
15	~2.499	ND	~2.496	ND	~2.499	ND	-		-	
16	~2.372	ND	~2.366	ND	-		-		-	

17	-		-		-		-		-			
18	~[2.26]	ND	-		-		-		-			
19	~ 2.254	ND	~2.257	ND	-		-		-			
20	2.165	<2	2.164	<2	2.163	<2	2.159	<2	2.163	<2		
21	-		-		-		-		-			
22	~ 2.073	ND	~2.080	ND	-		-		-			
23	-		~[2.04]	ND	-		-		-			
24	-		-		-		-		-			
25	1.876	94	1.874	107	1.872 (A)	116	1.880 (A)	129	1.868 (A)	121		
26	-		-		-		-		-			
27	~1.612)	68	-		-		-		-			
28	1.598)		1.598	72	1.598 (A)	89	1.595 (A)	92	1.594 (A)	94		
29	-		-		-		-		-			
30	1.533	3	1.531	<2	1.531	3	1.527	8	1.527	~2		
31	-		-		-		-		-			
32	~1.415	ND	-		-		-		-			
33	~1.340	ND	-		-		-		-			
34	1.325	29	1.325	21	1.324 (A)	29	1.325-M) 1.321-m) (SB)	35	1.324-M) 1.321-m)	29		
35	-		-		-							
36	1.216	45	1.216-M)	53	1.217-M)	42	1.215-M)	50	1.215-M)	42		
37	-		~1.214-m)		1.214-m)		1.212-m (T)		1.212-m)			
38	1.186	5	1.185	2	1.185	3	1.183	5	1.184	2		
39	~1.089	ND	-		-		-		-			
40	1.082	81	1.082)	76	1.082)	93	1.081-M)	115	1.080-M)	94		
41	-		1.080 (R)		1.079 (R)		1.078-m)		1.078-m)			
42	1.020	59	1.019	69	1.020-M)	62	1.019-M)	79	1.019-M)	66		
43	-		-		1.018-m)		1.017-m)		1.016-m)			
44	-		-		-		-		-			
?	Shadows		Shadows		Shadows		Shadows		Shadows			

Line No.	% of COPPER DISSOLVED									
	13.28		14.40		15.38		16.50		17.06	
	d(Å)	I/I_1	d(Å)	I/I_1	d(Å)	I/I_1	d(Å)	I/I_1	d(Å)	I/I_1
1	-		-		-		-		-	
2	-		-		-		-		-	
3	-		-		-		-		-	
4	-		-		-		-		-	
5	3.74	<2	3.73	<2	3.73	<2	3.73	<2	3.73	ND
6	-		-		-		-		-	
7	~[3.06]	100	[shadow]	100	[shadow]	100	[shadow]	100	[shadow]	100
8	3.044		3.043		3.043		3.043		3.043	
9	-		-		-		-		-	
10	-		-		-		-		-	
11	-		-		-		-		-	
12	-		-		-		-		-	
13	2.642	10	2.640	13	2.641	12	2.642	8	2.641	10
14	-		-		-		-		-	
15	-		-		-		-		-	
16	-		-		-		-		-	
17	-		-		-		-		-	
18	-		-		-		-		-	
19	-		-		-		-		-	
20	2.155	<2	[shadow]	ND	[shadow]	ND	-		-	
21	-		-		-		-		-	
22	-		-		-		-		-	
23	-		-		-		-		-	
24	-		-		-		-		-	

25	1.868 (A)	108	1.868 (A)	113	1.867 (A)	107	1.868-M 1.861-m	97	1.868-M 1.859-m	118
26	-		-		-		-		-	
27	-		-		-		-		-	
28 29	1.594 shadow	82	1.594 shadow	78	1.592 shadow	81	1.594 1.579 Sh	65	1.594 1.584 (Sh)	87
30	1.528	2	1.527	<2	1.525	<2	1.525	<2	1.523	2
31	-		-		-		-		-	
32	-		-		-		-		-	
33	-		-		-		-		-	
34 35	1.324-M 1.321-m	27	1.325-M 1.321-m	23	1.323-M 1.320-m	30	1.324-M 1.319-m	21	1.321 1.314 (Sh)	26
36 37	1.214-M 1.211-m	42	1.213-M 1.209-m	34	1.213-M 1.209-m	64	1.213-M 1.209-m	37	1.213-M 1.208-m	43
38	1.184	<2	shadow	ND	shadow	ND	shadow	ND	shadow	ND
39	-		-		-		-		-	
40 41	1.080-M 1.077-m	85	1.079-M 1.076-m	66	1.080-M 1.076-m	98	1.080-M 1.075-m	58	1.077 (B) 1.073 (Sh)	70
42 43	1.018-M 1.015-m	41	1.018-M 1.014-m	43	1.018-M 1.015-m	59	1.018-M 1.014-m	39	(Diffuse)	51
44	-		-		-		-		-	
?	Shadows		Shadows		Shadows		Shadows		Shadows	

Line No.	% of COPPER DISSOLVED									
	17.69		18.04		18.32		18.66		19.01	
	d(Å)	I/I_1	d(Å)	I/I_1	d(Å)	I/I_1	d(Å)	I/I_1	d(Å)	I/I_1
1	-		-		-		-		-	
2	-		-		-		-		-	
3	-		-		-		-		-	
4	-		-		-		~ [4.70]	ND	-	
5	shadow	ND	shadow	ND	shadow	ND	3.73	ND	-	
6	-		-		-		-		-	
7	[shadow]	100	[shadow]	100	[shadow]	100	-		[shadow]	100
8	3.038		3.036		3.034		3.034	100	3.025	
9	-		-		-		-		-	
10	-		-		-		-		-	
11	-		-		-		-		-	
12	-		-		-		-		-	
13	2.639	10	2.636	10	2.636	3	2.634	14	2.632	3
14	-		-		-		-		-	
15	-		-		-		-		-	
16	-		-		-		-		-	
17	-		-		-		~[2.294]	ND	-	
18	-		-		-		-		-	
19	-		-		-		-		-	
20	-		-		-		-		-	
21	-		-		-		-		-	
22	-		-		-		-		-	
23	-		-		-		-		-	
24	-		-		-		-		-	

25	1.867-M)	128	1.865-M)	141	1.864-M)	130	1.864-M)	123	1.864-M)	100
26	1.858-m)		1.856-m)		1.855-m)		1.855-m)		1.853-m)	
27	-		-		-		-		-	
28	1.591)	92	1.591)	118	1.591)	91	1.590)	107	1.589)	85
29	1.584(Sh)		1.583(R)		1.584)		1.581)		1.580)	
30	1.522	<2	1.521	<2	1.521	<2	1.519	2	1.517	<2
31	-		-		-		-		-	
32	-		-		-		-		-	
33	-		-		-		-		-	
34	1.322)	26	1.321)	29	1.320)	30	1.320)	28	1.320)	26
35	1.310(Sh)		1.310(R)		1.309)		1.307)		1.306)	
36	1.213-M)	51	1.212-M)	69	1.212-M)	47	1.211-M)	49	1.210-M)	58
37	1.207-m)		1.207-m)		1.206-m)		1.206-m)		1.203-m)	
38	shadow	ND	shadow	ND	shadow	ND	-		-	
39	-		-		-		-		-	
40	1.078(B))	79	1.076(B))	132	1.076(B))	89	1.077(B))	75	1.076(B))	90
41	1.073(Sh)		1.073(Sh)		1.072(Sh)		1.073(Sh)		1.071(Sh)	
42	1.018-M)	34	1.017-M)	92	1.017-M)	66	1.017-M)	58	~1.016-M)	66
43	1.014-m)		1.013-m)		1.013-m)		1.014-m)		~1.011-m)	
44	-		[shadows]		~[1.006])		[shadow]		~[1.004])	
?	shadows		shadows		shadows		shadows		shadows	

Line No.	% of COPPER DISSOLVED									
	22.66		22.81		22.92		24.50		25.35	
	d(Å)	I/I_1	d(Å)	I/I_1	d(Å)	I/I_1	d(Å)	I/I_1	d(Å)	I
1	-		-		-		-		-	
2	[shadow]	ND	[shadow]	ND	-		-		-	
3	[shadow]	ND	~4.72	<2	~4.69	ND	~4.74	<2	[shadow]	ew
4	[shadow]	ND	~3.98	<2	-		4.03	ND	[shadow]	ew
5	[shadow]	ND	~3.67	<2	[shadow]	ND	[shadow]	ND	[shadow]	ew
6	[shadow]	ND	~3.35	~5?	~3.34	ND	~3.34	ND	~3.34	vw
7	[shadow]	100	[shadow]	100	[shadow]	100	[shadow]	100	[shadow]	ew
8	3.025		3.025		3.025		3.025		3.025	vs
9	~2.905	ND	~[2.934]	ND	-		-		-	
10	-		~[2.895]	ND	[shadow]	ND	-		-	
11	-		-		-		-		-	
12	-		~[2.084]	ND	-		-		-	
13	2.632	17	2.635	16	2.631	15	2.630	12	2.634	w
14	-		~[2.603]		~[2.603]		~[2.615]		~[2.615]	ew
15	-		-		-		-		-	
16	-		-		-		-		-	
17	~2.300	2	~2.299	<2	~[2.298]	ND	~[2.296]	ND	~2.300	ew
18	-		-		-		-		-	
19	-		-		-		-		-	
20	-		-		-		-		-	
21	-		-		-		-		-	
22	-		-		-		-		-	
23	-		~2.045	<2	-		-		-	
24	-		~1.948	<2	-		-		-	
25	1.864-M	119	1.863-M	118	1.863-M	117	1.864-M	111	1.865-M	w
26	1.853-m		1.854-m		1.853-m		1.855-m		1.854-m	med
27	-		-		-		-		-	
28	1.589	94	1.588	94	1.588	80	1.589	72	1.589	med
29	1.576		1.574		1.574		1.575		1.574	w
30	1.517	2	1.517	5	~1.517	<2	1.519	<2	1.519	vw

31	-		-		-		-		-			
32	-		-		-		-		-			
33	-		-		-		-		-			
34	1.319	20	1.319	25	1.318	17	1.319	20	1.319		w	
35	1.307		1.306		1.305		1.305		1.306		vw	
36	1.210	30	1.211	36	1.211	44	1.211	40	1.212		vw	
37	1.206(T)		1.205(T)		1.204(T)		1.204(T)		1.205(T)		w	
38	-		-		-		-		-			
39	-		-		-		-		-			
40	1.077	?	1.077	68	1.076	73	1.077	79	1.077		med	
41	1.070(T)		1.070(T)		1.070(R)		1.070		1.070		w	
42	~1.017				~1.017		~1.018		~1.018		w	
43	~1.013	?	Diffuse		~1.012	47	~1.013	39	~1.013		w	
44	~[1.007]				~[1.005]		~[1.007]		~[1.007]		vw	
45	shadows		shadows		shadows		shadows		shadows			

Line No.	% of COPPER DISSOLVED											
	27.00		31.58		45.00		50.35		54.98		82.32	
	d(Å)	I/I_1	d(Å)	I/I_1	d(Å)	I/I_1	d(Å)	I/I_1	d(Å)	I/I_1	d(Å)	I/I_1
1	-		-		-		-		-		-	
2	-		-		-		-		-		-	
3	~4.71	<2	~4.68	<2	4.69	ND	4.70	ND	4.71	ND	4.70	ND
4	-		-		-		-		-		-	
5	-		[shadow]	ND	-		-		-		-	
6	-		-		~3.32	ND	~3.35	ND	-		~3.35	ND
7	~[3.04] 3.025 (B)	100	~[3.04] 3.025 (B)	100	~[3.04] 3.023 (B)	100	~[3.04] 3.025 (B)	100	~[3.05] 3.025 (B)	100	[3.05] 3.025 (B)	100
8												
9	-		-		~2.901	ND	~2.905	ND	~2.906	ND	~2.906	ND
10	-		-		-		-		-		-	
11	-		-		-		-		-		-	
12	-		~2.794	ND	~2.803	ND	-		~2.801	ND	~2.794	ND
13	2.633	11	2.634	27	2.636	23	2.636	13	2.637	29	2.637	25
14	~2.615		~2.609		2.604		2.609		2.606		2.612	
15	-		-		-		-		-		-	
16	-		-		-		-		-		-	
17	~2.298	ND	~2.296	ND	~2.300	<2	~2.299	<2	~2.299	<2	~2.301	<2
18	-		-		-		-		-		-	
19	-		-		-		-		-		-	
20	-		-		-		-		-		-	

21	-		~[2.115]	ND	-		-		-		-	
22	-		-		-		-		-		-	
23	-		-		-		-		-		-	
24	~1.947	ND	~1.952	ND	~1.948	ND	~1.951	ND	-		~1.950	ND
25	1.863-M	117	1.863-M	180	1.863	191	1.864	130	1.866	143	1.863	154
26	1.855-m		1.855-m		1.855 (T)		1.855 (R)		1.857		1.855	
27	-		-		-		-		-		-	
28	1.589	86	1.589	154	1.590	184	1.588	112	1.591	132	1.589	140
29	1.574		1.576		1.577		1.575		1.577		1.578	
30	1.518	<2	1.518	<2	1.519	11	1.518	2	1.519	2	1.520	5
31	-		-		-		-		-		-	
32	-		-		-		-		-		-	
33	-		-		-		-		-		~[1.351]	ND
34	1.319	24	1.320	61	1.321	63	1.319	40	1.321	39	1.322	42
35	1.307		1.306		1.306		1.305		1.306		1.307	
36	1.211	37	1.211	80	1.211	89	1.211	61	1.213	67	1.213	85
37	1.205 (T)		1.205 (R)		1.206		1.204		1.206		1.207	
38	~[1.180]	ND	~[1.179]	ND	~1.179	ND	-		-		~1.181	ND
39	-		-		~[1.170]	ND	-		-		-	
40	1.077	74	1.077	157	1.077	146	1.077	96	1.078	112	1.077	139
41	1.071		1.070		1.071		1.069		1.071		1.071	
42	~1.018		~1.018		~1.018		~1.017		~1.018		~1.018	
43	~1.013	43	~1.014	117	~1.013	114	~1.012	72	~1.014	98	~1.014	102
44	~1.008		~1.006		~1.007		~1.006		~1.006		~1.006	
?	shadows		shadows		shadows		shadows		shadows		shadows	

Line No.	% of COPPER DISSOLVED 98.74 d(Å)	I		Line No.	98.74 d(Å)	I	
1	–			23			
2	–			24	~1.957	ew	α-cp?
3	4.72	w	α-cp	25	1.866-M	vs	α-cp
4	4.25	vw		26	1.854-m		α-cp
5	~[4.16]	ew		27	~1.697	ew	
6	3.35	w	α-cp	28	1.592	s	α-cp
7	~[3.06]	ew	α-cp	29	1.578	med	α-cp
8	3.023(B)	vs	α-cp	30	1.521	w	α-cp
9	2.914	vw		31	1.445	vw	
10	~[shadow]	ew		32	~1.373	ew	
11	~[shadow]	ew		33	~1.351	ew	
12	2.703	vw		34	1.323	med	α-cp
13	2.646	med	α-cp	35	1.308	w	α-cp
14	2.615	vw	α-cp?	36	1.213	vw	α-cp
15	~2.516	ew		37	1.206	w	α-cp
16	~2.449	ew		38	~1.181	ew	α-cp
17	2.304	w	α-cp	39	–		
18	~[2.204]	ew		40	1.078	med	α-cp
19	–			41	1.071	w	α-cp
20	–			42	1.018-M	w	α-cp
21	[shadow]	ew		43	1.014-m	w	α-cp
22	–			44	~1.007	vw	α-cp
	(cont. next column)			?	shadows		

TABLE B-22.4

Variation of the d-spacings as a Function of Copper Removed During the Leaching of β-chalcopyrite

% of Cu removed	Reflections						
	222(vs)	400(w)	440(s)	622(s)	800(w)	622(med)	844(s)
0	3.063	2.651	1.876	1.598	1.325	1.216	1.082
6.5	3.055	2.651	1.874	1.598	1.325	1.216-1.214	1.082-1.080
7.5	3.054	2.647	1.872	1.598	1.324	1.217-1.214	1.082-1.079
10.0	3.051	2.644	1.870	1.595	1.325 1.321	1.215-1.212	1.081-1.078
12.5	3.048	2.642	1.868	1.594	1.324 1.321	1.215-1.212	1.080-1.078
14.5	3.043	2.641	1.868	1.593	1.324 1.321	1.213-1.210	1.080-1.076
16.5	3.043	2.642	1.868-1.861	1.594	1.324 1.319	1.213-1.209	1.080-1.075
17.5	3.039	2.639	1.867-1.858	1.591-1.584	1.321 1.311	1.213-1.207	1.077-1.073
18.5	3.031	2.634	1.864-1.854	1.590-1.582	1.320 1.307	1.211-1.205	1.076-1.072
23.0	3.025	2.633	1.863-1.853	1.588-1.574	1.319 1.306	1.211-1.204	1.077-1.070
25.0	3.025	2.632	1.865-1.855	1.589-1.575	1.319 1.306	1.212-1.205	1.077-1.070
27.0	3.025	2.633	1.863-1.855	1.589-1.574	1.319 1.307	1.211-1.205	1.077-1.071
31.5	3.025	2.634	1.863-1.855	1.589-1.576	1.320 1.306	1.211-1.205	1.077-1.070
45.0	3.023	2.636	1.863-1.855	1.590-1.577	1.321 1.306	1.211-1.206	1.077-1.071
50.0	3.025	2.636	1.864-1.855	1.588-1.575	1.319 1.305	1.211-1.204	1.077-1.069
55.0	3.025	2.637	1.866-1.857	1.591-1.577	1.321 1.306	1.213-1.206	1.078-1.071
82.0	3.025	2.637	1.863-1.855	1.589-1.578	1.322 1.307	1.213-1.207	1.077-1.071
	112(vs)	020,004(w)	220(s)-024(s)	132(s)-116,033(med)	040(med)-008(w)	332(w)-136,143(med)	244(s)-228(w)

Reflections

TABLE B-22.5

Variation of the Reflection Intensities (I/I_1) as a Function of Copper Removed During the Leaching of β-chalcopyrite

% of Cu removed	Reflections						
	222	400	440	622	800	662	844
0	100	20	94	68	29	45	81
6.5	100	15	107	72	21	53	76
7.5	100	6	116	89	29	42	93
10.0	100	(25)	129	92	35	50	115
12.5	100	13	121	94	29	42	94
14.5	100	12	109	80	27	47	83
16.5	100	8	97	65	21	37	58
17.5	100	10	129	99	27	54	93
18.5	100	7	118	94	28	51	85
23.0	100	16	118	89	21	37	71
25.0	100	12	111	72	20	40	79
27.0	100	11	117	86	24	37	74
31.5	100	27	180	154	61	80	157
45.0	100	23	191	184	63	89	146
50.0	100	(13)	(130)	(112)	(40)	(61)	(96)
55.0	100	29	143	132	39	67	112
82.0	100	25	154	140	42	85	139
	112	020,004	220-024	132-116,033	040-008	332-136,143	244-228
	Reflections						

( ) Not very reliable

TABLE B-22.6

FeS_2

IRON SULPHIDE-PYRITE(135-c)

d(Å)	I/I_1	d(Å)	I/I_1
3.128	36	0.8565	7
2.079	84	.8261	4
2.423	66	.8166	4
2.2118	52	.7981	5
1.9155	40		
1.6332	100		
1.5640	14		
1.5025	20		
1.4448	24		
1.2427	12		
1.2113	14		
1.1823	7		
1.1548	6		
1.1057	6		
1.0427	27		
1.0060	8		
0.9882	6		
.9577	12		
.9030	15		
.8788	8		

$Fe_{1-x}S$ (x=0.12)

IRON SULPHIDE-PYRRHOTITE(135-d)

d(A)	I/I_1	d(Å)	I/I_1
5.75	20	2.701	5
5.67	20	2.671	5
5.27	5	2.647	30
5.24	10	2.635	90
4.68	10	2.621	80
3.65	5	2.540	10
3.59	10	2.435	5
3.42	10	2.415	10
3.38	5	2.411	5
3.32	5	2.368	10
3.28	5	2.348	5
3.21	10	2.232	5
3.18	5	2.202	5
3.13	5	2.198	10
3.11	5	2.158	10
2.966	90	2.149	5
2.847	5	2.091	5
2.840	10	2.064	40
2.745	5	2.057	100
2.726	5	2.047	90

/cont....

cont.

IRON SULPHIDE-PYRRHOTITE(135-d)

d(Å)	I/I_1	d(Å)	I/I_1
2.042	30	1.442	10
2.014	5	1.438	10
2.005	5	1.434	20
1.977	5	1.421	30
1.967	10	1.351	5
1.919	5	1.343	5
1.780	5	1.322	10
1.757	5	1.318	20
1.756	5	1.312	30
1.714	80		
1.685	5		
1.674	5		
1.629	10		
1.605	10		
1.601	10		
1.594	20		
1.591	5		
1.571	5		
1.553	5		
1.484	20		

$Fe_{1-x}S$ (x=.094)

IRON SULPHIDE-PYRRHOTITE(135-e)

d(Å)	I/I_1
5.83	5
2.98	70
2.64	90
2.067	100
1.720	80
1.610	20
1.490	?
1.444	10
1.323	50
1.293	10
1.250	5
1.177	10
1.109	10
1.103	70
1.071	10
0.995	20

TABLE B-22.6 (cont)

ORTHORHOMBIC SULPHUR(135-f)

d(Å)	I/I_1
7.69	6
5.76	14
5.68	5
4.80	2
4.19	2
4.06	11
3.91	12
3.85	100
3.57	8
3.44	40
3.38	3
3.33	25
3.21	60
3.11	25
3.08	17
3.06	+
2.842	18
2.688	2
2.673	1
2.621	13
2.614	4
2.569	8
2.501	7
2.424	13
2.404	2
2.375	4
2.366	4
2.288	6
2.215	2
2.146	4
2.112	10B
2.098	2
2.057	1
2.041	1
2.003	2
1.988	4
1.957	2
1.926	1
1.900	7B
1.856	1
1.838	1
1.823	4
1.781	11
1.754	7
1.725	8
1.698	7
1.665	2
1.658	2
1.647	5
1.622	6
1.607	6
1.601	2
1.595	3
1.563	2
1.542	1
1.531	1
1.515	1

d(Å)	I/I_1
1.504	1
1.490	1
1.475	2
1.461	1
1.439	3
1.424	3
1.419	1
1.391	1
1.362	1
1.354	3

TABLE B-22.7

"Premier" Pyrite → Pyrrhotite

X-ray Pattern

Line No.	Before Heating		After Heating to 650°C		After Heating to 726°C	
	d(Å)	I	d(Å)	I	d(Å)	I
1	-		-		5.62	w
2	-		-		~[5.30]	ew
3	-		-		4.85	vw
4	-		-		3.46	vw
5	-		-		3.37	ew
6	-		-		~[3.18]	ew
7	3.126	w	3.126	w	3.131	ew
8	-		3.038	ew	-	
9	2.991	ew	2.983	ew	2.970	s
10	2.708	s	2.708	s	2.704	w
11	2.677	ew	2.674	ew	2.632	s
12	2.423	s	2.420	s	2.423	w
13	-		-		~[2.263]	ew
14	2.211	s	2.211	s	2.211	vw
15	-		-		2.172	vw
16	-		2.114	ew	-	vw
17	-		~[2.060]	ew	2.049	vs
18	-		-		1.984	ew
19	1.916	med	1.916	med	1.916	ew
20	1.804	vw	1.803	vw	-	
21	-		-		~[1.797]	ew
22	-		~[1.721]	ew	1.716	s

/cont...

23	1.634		vs	1.633		vs	1.633	w
24	1.564		w	1.565		w	1.593	w
25	1.503		w	1.503		w	[shadow]	ew
26	1.448		w	1.448		w	1.448	ew
27		-			-		1.437	vw
28		-			-		~[1.424]	ew
29		-			-		~[1.414]	ew
30	~[1.356]		ew		-			-
31	~[1.339]		ew		-			-
32	~[1.306]		ew		-		1.315	med
33	~[1.278]		ew		-		~[1.278]	ew
34	1.243		w	1.243		vw	~[1.242]	ew
35	1.212		w	1.211		vw	~[1.210]	ew
36	1.183		w	1.183		vw	~[1.182]	ew
37	1.155		w	1.155		vw	1.166	vw
38	1.106		w	1.105		vw	1.101	med
39		-		~[1.062]		ew	1.092	med
40		-		~[1.057]		ew		-
41	1.043		s	1.042		s	1.043	s
42	1.006		med	1.006		med	1.006	vw
43	0.989		med	0.989		med	0.991	w
44		-		~[0.970]		ew	0.965	w
45	0.958		med	0.958		s	0.958	w
46	~[0.915]		ew	lines	{?}	ew		-
47	~[0.912]		ew					-
48	0.903		med	0.903		med	~[0.903]	ew

TABLE B-22.8

Line No.	Flakes on the wall of the reaction vessel		Goethite (135-g)	
	d(Å)	I	d(Å)	I/I_1
1	4.99	vw	4.98	10
2	4.19(B)	vs	4.18	100
3	3.85	vw	-	-
4	[3.70]	vw	-	-
5	3.39(B)	vw	3.38	10
6	3.22	vw	-	-
7	3.05	s	-	-
8	2.71(B)	med	2.69	30
9	2.585	w	2.58	8
10	2.523	vw	2.520	4
11	Continuous shadow between lines		2.490	16
12	2.453	w	2.452	10
13	2.256	w	2.252	10
14	~2.201(B)	w	2.192	20
15	~2.015	ew	2.009	2
16	1.924	ew	1.920	6
17	1.864		-	-
18	~1.804	ew	1.799	8
19	-		1.770	2
20	1.720	w	1.721	20

/cont....

21	1.698	w	1.694	10
22	Continuous shadow between lines		1.661	4
23	1.592	w	1.606	6
24	1.566	w	1.564	16
25	1.511	w	1.509	10
26	-	-	1.467	4
27	1.455	w	1.453	10
28	1.423	vw	1.418	2
29	[Shadow]	ew	1.392	8
30	~[1.361]	ew	1.357	8
31	1.320	w	1.317	8
32	?)		1.264	2
33	?) Diffuse lines		1.241	2
34	?)		1.198	2
35	~ 1.207	ew	-	-
36	~[1.127]	ew	-	-
37	~ 1.077	ew	-	-

TABLE B-22.9

X-ray Pattern of Residues from Leaching of β-Chalcopyrite with Sulphuric Acid (pH∿0.5 T=95°C)

(24% of Cu Removed)

Line No.	Without Washing		Washed with CCl_4	
	d(Å)	I	d(Å)	I
1	7.69 (S)	w	-	
2	6.35	vw	-	
3	5.74 (S)	w	-	
4	line	ew	4.72 (α-cp)	ew
5	4.49	vw	-	
6	4.24 (S)	med	-	
7	4.05 (S)	med	-	
8	3.90 (S)	w	-	
9	3.84 (S)	st	-	
10	3.67	vw	-	
11	3.55 (S)	w	-	
12	line	ew	3.46 (?)	w
13	3.43 (S)	med	-	
14	3.33 (S)	med	-	
15	3.21 (S)	s	-	
16	3.11 (S)	med	-	
17	3.03	vs	3.03 (α-cp)	vs
18	line	ew	2.914(α-cp)	ew
19	2.85 (S)	med	-	
20	line	ew	-	
21	2.68 (S)	w	-	
22	line	ew	2.634(α-cp)	w
23	2.62	med	-	
24	2.566(S)	vw	-	
25	2.495(S)	w	-	
26	2.419(S)	w	-	
27	2.372(S)	w	-	
28	2.335(?)	vw	-	
29	line	ew	2.299(α-cp)	ew
30	2.287(S)	w	-	
31	line	ew	-	
32	2.146(S)	vw	-	
33	2.114(S)	w	-	
34	2.057(S)	w	2.053(α-cp)	w
35	1.986	vw	-	
36	1.961	vw	-	
37	1.903	med	-	
38	1.865-M	s	1.865-M	s
39	1.854-m (B)		1.854-m (B) (α-cp)	
40	line	ew		

Table B-22.9 cont

41		1.782	w		-
42		1.755	w	1.756 (?)	vw
43		1.725	w		-
44		1.698	w		-
45		1.646	w		-
46		1.623	w		-
47		1.609	vw		-
48		1.588-M)	med	1.589-M)	(α-cp) (med)
49		1.574-m)		1.574-m)	
50		line	ew	1.520 (α-cp)	vw
51		1.475	vw		-
52		1.437	vw		-
53		1.419	vw		-
54		1.391	vw		-
55		1.355	vw		-
56		line	ew	1.332 (α-cp)	ew
57		1.322	vw	1.320 (α-cp)	w
58		$1.207_{(A)}$ {?}	med	1.211-M)	(α-cp) s
59				1.205-m)	
60		-		1.189	(α-cp) ew
61		$1.076_{(A)}$ {?}	med	1.078-M)	(α-cp) s
62				1.072-m)	
63		$1.014_{(A)}$ {?}	med	$1.015_{(A)}$ {?}	(α-cp) s
64					
65		shadows		shadows	

TABLE B-22.10

X-ray Pattern of the Residue from Leaching of α-chalcopyrite with Sulphuric Acid (pH∿0.5 T=95°C)

(24% Cu removed)

Line No.	Without Washing		Washed with CCl_4	
	d(Å)	I	d(Å)	I
1	7.70	w	-	
2	line	ew	-	
3	6.33	vw	-	
4	5.75	w	-	
5	line	ew	4.71 (α-cp)	vw
6	4.47	vw	-	
7	4.24	w	-	
8	4.05	w	-	
9	3.91	w	-	
10	3.84	s	-	
11	3.66	ew	-	
12	3.55	w	-	
13	3.44	med	-	
14	3.33	med	3.35 (α-cp)	w
15	3.21	med	-	
16	3.10	w	-	
17	line	ew	-	
18	3.04	vs	3.036 (α-cp)	vs
19	line	ew	2.905 (α-cp)	ew
20	2.84	w	-	
21	line	ew	-	
22	2.684	ew	-	
23	2.633	w	2.638 (α-cp)	w
24	2.567	w	2.605 (α-cp)	vw
25	2.500	w	-	
26	2.428	w	-	
27	2.376	w	-	
28	line	ew	2.300 (α-cp)	vw
29	2.289	w	-	
30	line	ew	-	
31	2.146	vw	-	
32	2.114	w	∿[2.083] (?)	ew
33	2.054	w	∿[2.060] (?)	ew
34	1.987	vw	∿[2.050] (α-cp)	ew
35	1.963	vw	-	
36	1.903	med	-	
37	1.864	s	1.865 (α-cp)	med
38	1.853	s	1.853 (α-cp)	s
39	1.823	vw	-	
40	1.783	w	-	

/cont....

41	1.756	w	1.755	(?)	vw
42	1.725	w	∿[1.738]	(?)	ew
43	1.698	w	-		
44	1.667	vw	-		
45	1.648	w	-		
46	1.620	w	-		
47	1.605	vw	-		
48	1.591	s	1.590	(α-cp)	s
49	1.575	med	1.574	(α-cp)	med
50	lines {?}	ew	1.516	(α-cp)	vw
51			-		
52	1.354	w	-		
53	1.320	w	1.321	(α-cp)	w
54	1.304	w	1.303	(α-cp)	vw
55	1.212	w	1.211	(α-cp)	w
56	1.205	med	1.205	(α-cp)	med
57	1.077	med	1.077	(α-cp)	med
58	1.070	w	1.069	(α-cp)	w
59	1.017	w	1.017	(α-cp)	w
60	1.013	w	1.013	(α-cp)	w
61	other lines -		∿[1.005]	(α-cp)	vw
62	shadows		shadows		

TABLE B-22.11

Line No.	α-Synthetic Sample CuK_α radiation (This work)		α-Synthetic Sample CoK_α radiation (This work)		Chalcopyrite Frueh($_{32}$)(*) CoK_α radiation		Chalcopyrite(ASTM) Berry & Thompson(94) FeK_α radiation		Tilt Cove chalcopyrite (95)		Temagami chalcopyrite (95)	
	d(Å)	I	d(Å)	I	d(Å)	I	d(Å)	I/I_1	d(Å)	I/I_1	d(Å)	I/I_1
1	-		7.47	vw	-		-		-		-	
2	-		4.71	vw	4.67	vw	-		-		-	
3	-		3.74	vw	-		-		-		-	
4	-		3.35	vw	-		-		-		-	
5	-		≈[3.06]	ew	-		-		-		-	
6	3.03	vs	3.02	vs	3.01	vs	3.03	100	3.0317	100	3.0317	100
7	-		≈2.899	ew	2.87	vw	-		-		2.8926	2?
8	-		≈2.815	ew	-		-		-		(2.78)	
9	-		≈2.723	ew	-		-		-		-	
10	2.637	w	2.641	w	2.62	med	2.63	5	2.6492	5	2.6360	15
11	2.598	vw	2.603	ew	2.57	med	-		-		2.5999	5
12	-		-		-		-		2.5288	10	-	
13	-		2.490	ew	-		-		-		-	
14	-		2.301	ew	2.28	vw	-		2.2804	5	(2.3)	
15	-		2.255	ew	-		-		-		-	
16	-		2.155	ew	-		-		-		-	
17	-		2.068	ew	-		-		2.0867	5	-	
18	-		1.931	ew	-		-		-		-	
19	1.868	s	1.869	s	-		1.865	40	1.8664	60	1.8652	70
20	1.852	med	1.854	med	1.853	s	1.854	80	1.8538	75	1.8528	85

(*) Only the forms yielding intense reflections were considered by this author.

/cont...

21	-		-		1.836	s	-		-		-	
22	1.598	s	1.592	med	-		1.591	60	1.5907	45	1.5905	60
23	1.573	w	1.574	w	-		1.573	20	1.5735	25	1.5737	35
24	-		~1.527	ew	-		-		-		-	
25	1.520	vw	~1.517	ew	-		1.518	5	-		(1.515)	
26	-		-		-		-		1.4827	5	-	
27	-		-		-		-		1.3522	2	-	
28	1.320	w	1.322	w	-		1.323	10	1.3212	10	1.3209	20
29	1.302	vw	1.304	vw	-		1.303	5	1.3031	5?	1.3020	10
30	1.211	w	1.214	med	-		1.214	10	1.2108	20	1.2112	20
31	1.204	w	1.205	w	-		1.205	30	1.2044	20	1.2043	25
32	-		~[1.182]	ew	-		-		-		-	
33	1.077	med	1.082	w	-		-		-		-	
34	-		1.077	med	-		1.077	60	1.0762	25	1.0768	35
35	1.069	med	1.070	w	-		1.069	30	1.0688	15	1.0693	20
36	1.017	med	1.018	w	-		1.018	20	1.0168	10?	1.0176	15
37	-		1.013	vw	-		1.014	10			1.0136	5?
38	-		1.004	vw	-		1.005	5	1.0059	15	1.0047	5?

Remarks for this Table Only:

i) [ ] - values in brackets for synthetic samples indicate either a faint line or shadow, and the estimated readings are not reliable.

ii) ( ) - values in parenthesis for Temagami chalcopyrite were for lines which could be seen visually but not read; ? indicate diffuse band or not readable. For this sample reflections were also found for the following values:

$$0.98926 - 0.957712 - 0.903015 - 0.87888$$

TABLE B-22.12

X-ray Pattern of Leach Residues of α-Chalcopyrite

Line No.	% of COPPER DISSOLVED											
	unleached		Acidic Ferric Sulphate Leach								HCl leach	$Fe_2(SO_4)_3$+NaCl leach
	0		16.0		17.9		27.1		32.1		28.8	22.8
	d(Å)	I	d(Å)	I	d(Å)	I	d(Å)	I	d(Å)	I	d(Å) I	d(Å) I
1	7.47	vw	-		-		-		-		-	-
2	4.71	vw	~[4.74]	ew	~[4.50]	ew	~[4.72]	ew	~[4.74]	ew	4.71 w	4.72 vw
3	-		~[4.20]	ew	-		-		-		-	-
4	3.74	vw	-		-		-		~[3.86]	ew	3.85 w	-
5	3.35	vw	~[3.34]	ew	-		~[3.35]	ew	~ 3.36	vw	3.36 w	3.35 w
6	~[3.06]	ew	-		-		-		-		3.22-3.1 vw	-
7	3.02	vs	3.03	vs	3.03	vs	3.03	vs	3.03	vs	3.04 vs	3.04 vs
8	~2.899	ew	~[2.908]	ew	-		-		-		2.910 vw	~2.906 ew
9	~2.815	ew	-		-		-		-		~[2.849-2.804] ew	-
10	~2.723	ew	-		-		-		-		-	-
11	2.641	w	~[2.638]	ew	2.637	w	2.638	w	2.641	vw	2.641 med	2.639 w
12	2.603	ew	2.601	vw	2.604	vw	~[2.606]	ew	~2.609	ew	2.615 w	2.608 vw
13	2.490	ew	-		-		-		-		-	-
14	2.301	ew	~[2.298]	ew	~[2.300]	ew	~[2.303]	ew	~[2.301]	ew	2.303 vw	~2.303 ew
15	2.255	ew	-		-		-		-		-	-
16	2.155	ew	-		-		-		-		-	-
17	2.068	ew	~[2.057]	ew	-		-		~[2.066]	ew	2.059 vw	2.062 vw
18	-		-		-		-		-		2.050 w	2.048 vw
19	1.931	ew	-		-		-		-		-	[shadow]

/cont....

20	1.869	s	1.865	med	1.867	med	1.866	med	1.869	med	1.866	med	1.869	med
21	1.854	med	1.853	s	1.855	s	1.855	s	1.854	s	1.857	s	1.854	s
22	-		-		-		-		-		1.756	vw	1.757	vw
23	-		-		-		-		-		1.739	ew	1.739	ew
24	1.592	med	1.593	med	1.590	med	1.588	med	1.591	med	1.590	s	1.590	med
25	1.574	w	1.575	w	1.576	w	1.573	w	1.575	w	1.577	med	1.575	w
26	~[1.527-1.517]	ew	1.517	vw	1.520	vw	~[1.518]	ew	1.519	vw	1.518	vw	1.518	vw
27	-		-		-		-		-		~[1.456]	ew	~[1.459]	ew
28	1.322	w	1.321	w	1.322	w	1.319	w	1.321	w	1.321	med	1.322	w
29	1.304	vw	1.307	vw	1.305	vw	1.304	vw	1.304	vw	1.304	w	1.304	vw
30	1.214	med	1.211	w	1.213	w	1.211	w	1.212	w	1.212	w	1.213	w
31	1.205	w	1.204	med	1.205	med	1.204	w	1.205	med	1.204	med	1.205	med
32	-		-		-		-		-		~[1.188]	ew	~[1.188]	ew
33	~[1.182]	ew	-		-		-		-		~[1.179]	ew	~[1.180]	ew
34	1.082	w	-		-		-		-		-		-	
35	1.077	med	1.076	med	1.077	med	1.076	med	1.076	med	1.077	s	1.077	s
36	1.070	w	1.069	w	1.069	w	1.068	w	1.070	w	1.069	med	1.069	med
37	1.018	w	~1.017-M	w	~1.018-M	w	~1.018-M	vw	1.018	w	1.017	med	~1.018-M	w
38	1.013	vw	~1.012-m	w	~1.012-m	w	~1.012-m	vw	1.013	w	1.012	med	~1.013-m	w
39	1.004	vw	~1.004	vw	~1.005	vw	~1.005	ew	1.004	vw	1.005	w	~1.005	vw
?	shadows		shadows		shadows		shadows		shadows		shadows		shadows	

TABLE B-22.13

X-ray Patterns of Leach Residues of TEMAGAMI Chalcopyrite(95)

Line No.	Acid Washed Leach Residue		H_2O- Washed Leach Residue	
	d(Å)	I/I_1	d(Å)	I/I_1
1	-		5.9269	5?
2	-		5.7929	2?
3	-		5.1204	30
4	-		4.7180	5
5	3.8491	5	-	
6	-		3.6572	5
7	3.4378	2?	-	
8	-		3.3390	5
9	3.3260	5	-	
10	3.2113	5	-	
11	-		3.1018	65
12	$3.0335_{(B)}$	100	3.0358	100
13	-		2.9067	5
14	-		-	
15	2.6374	10	2.6427	15
16	2.6003	5	2.6030	5
17	-		2.5612	5
18	-		2.3117	5
19	-		1.9833	15
20	1.8660	70	1.8670	60

/cont....

21	1.8535		80	1.8551	75
22		-		1.8308	20
23	1.5908		60	1.5912	50
24	1.5742		35	1.5746	30
25		-		1.5493	2
26	1.5181		2		-
27		-		1.3439	5
28	1.3219		15	1.3212	15
29	1.3020		10	1.3015	10
30		-		1.2550	2?
31	1.2122		15	1.2125	15
32	1.2048		30	1.2045	25
33	1.0767		35	1.0763	30
34	1.0688		20	1.0684	20
35	1.0173		30	1.0171	20
36	1.0129		5?	1.0123	15?
37	1.0037		5	1.0035	10
38	0.9346		5?	0.9348	10
39		-			-
40	0.9280		15	0.9278	10

TABLE B-22.14

Debye-Scherrer camera calibration
using NaCl as standard

NaCl This work	NaCl A.S.T.M.(135-h)
d(Å)	d(Å)
3.250	3.258
∿[3.117]	-
2.814	2.821
1.990	1.994
1.697	1.701
1.625	1.628
1.408	1.410
-	1.294
1.260	1.261
1.1507	1.1515
-	1.0855
0.9967	0.9969
0.9531	0.9533
0.9397	0.9401
-	0.8917
-	0.8601
-	0.8503
-	0.8141

B-2.3 X-ray Powder Photographs

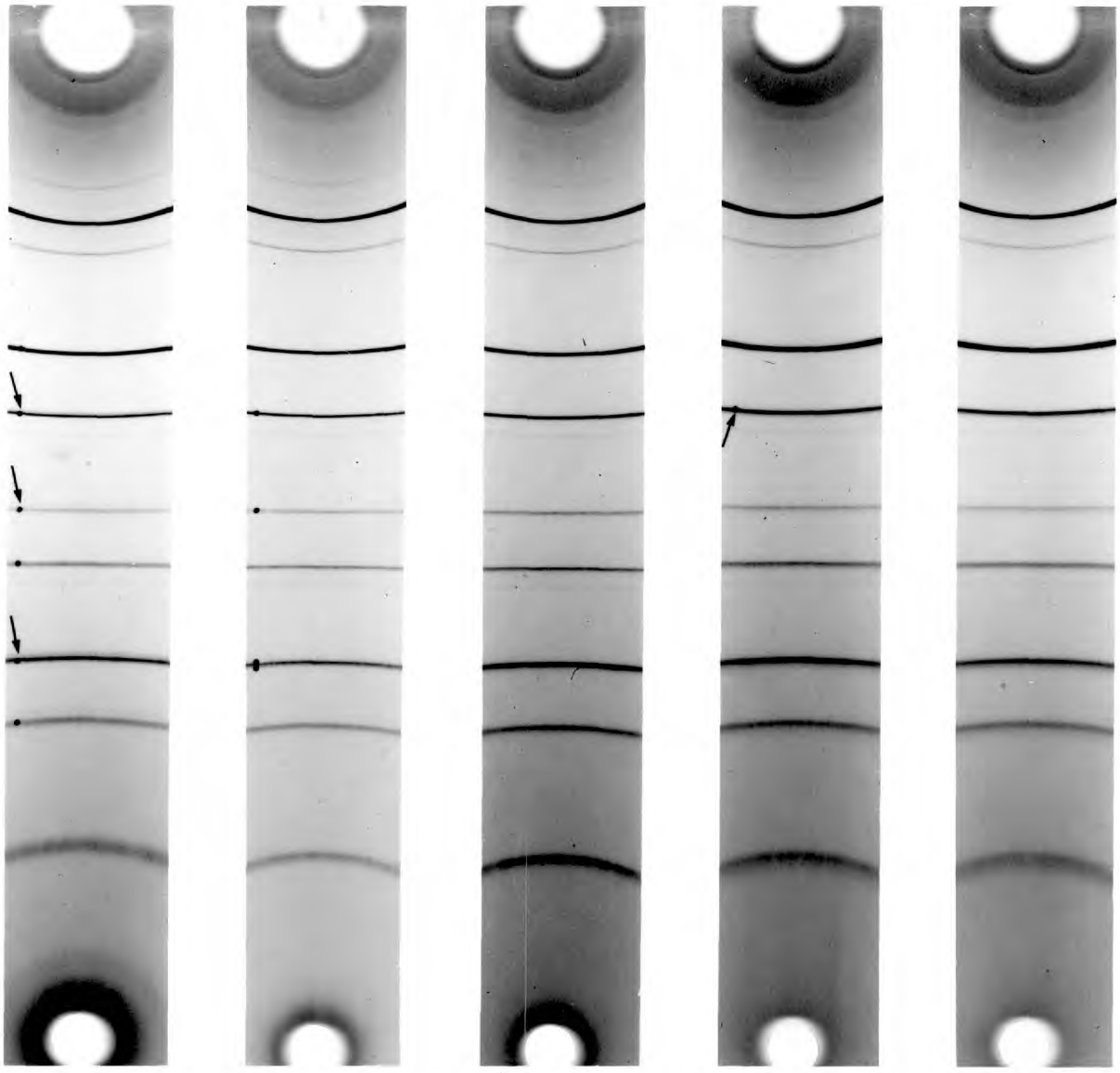

Fig. B - 1 X-ray Powder Photographs of leach residues of β-chalcopyrite
a) β-chalcopyrite ($CuFeS_{1.83}$)
b) 6.50% Cu removed
c) 10.21%
d) 16.50%
e) 17.69%

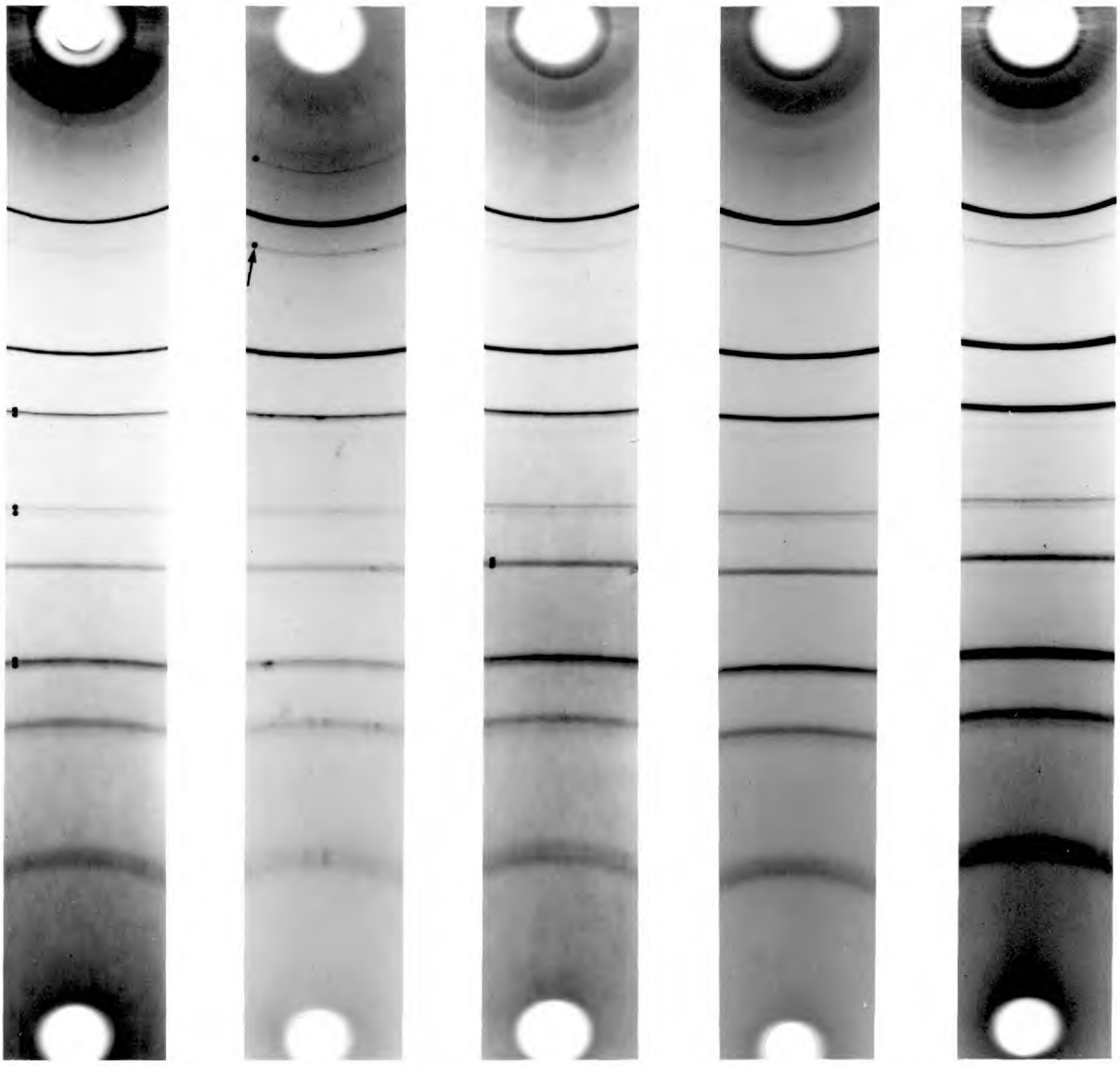

Fig. B-2 X-ray Powder Photographs of β-residues (continued)
f) 19.01% Cu removed
g) 22.81%
h) 24.50%
i) 27.00%
j) 31.58%

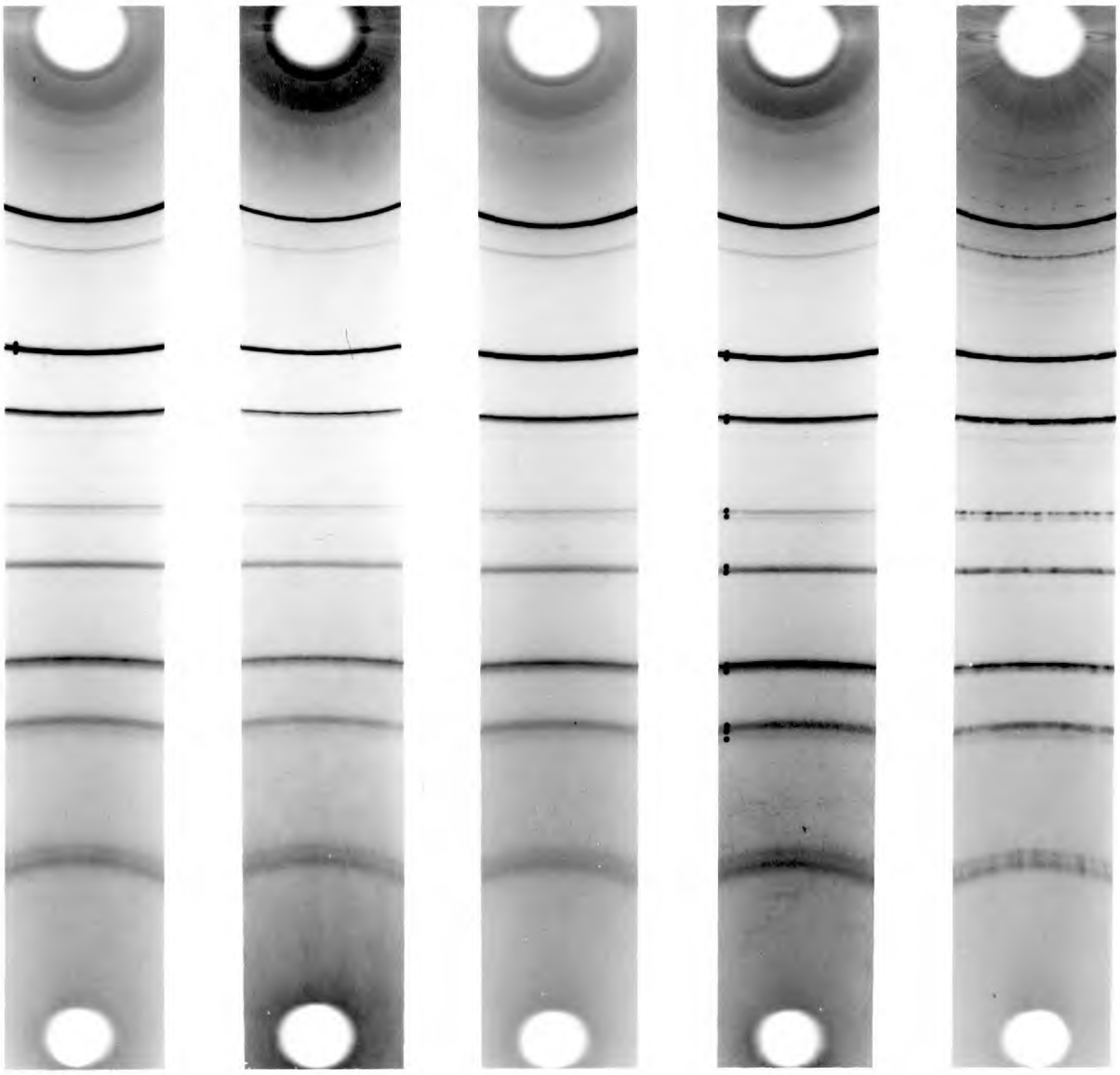

k l m n o

Fig. B-3 X-ray Powder Photographs of β-residues (continued)
k) 45.00%
l) 50.35%
m) 54.98%
n) 82.32%
o) 98.74%

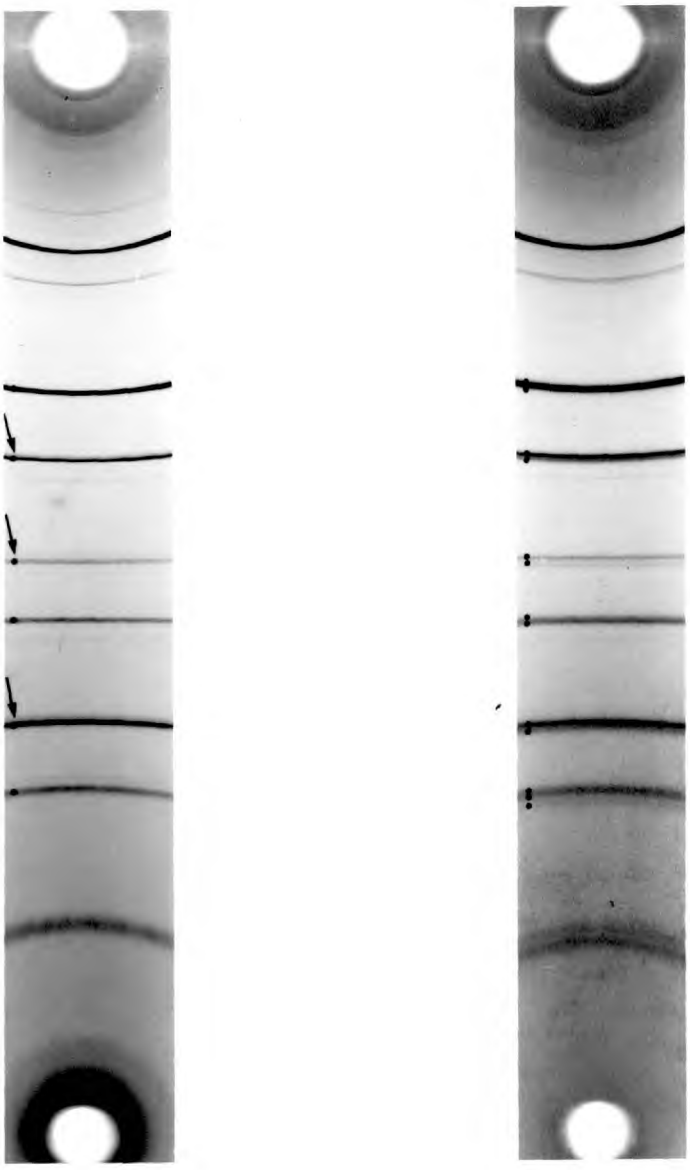

a b

Fig.B-4 Comparison between X-ray Powder Photographs of unleached β-chalcopyrite (a) and residue corresponding to 82.32% Cu removed (b).

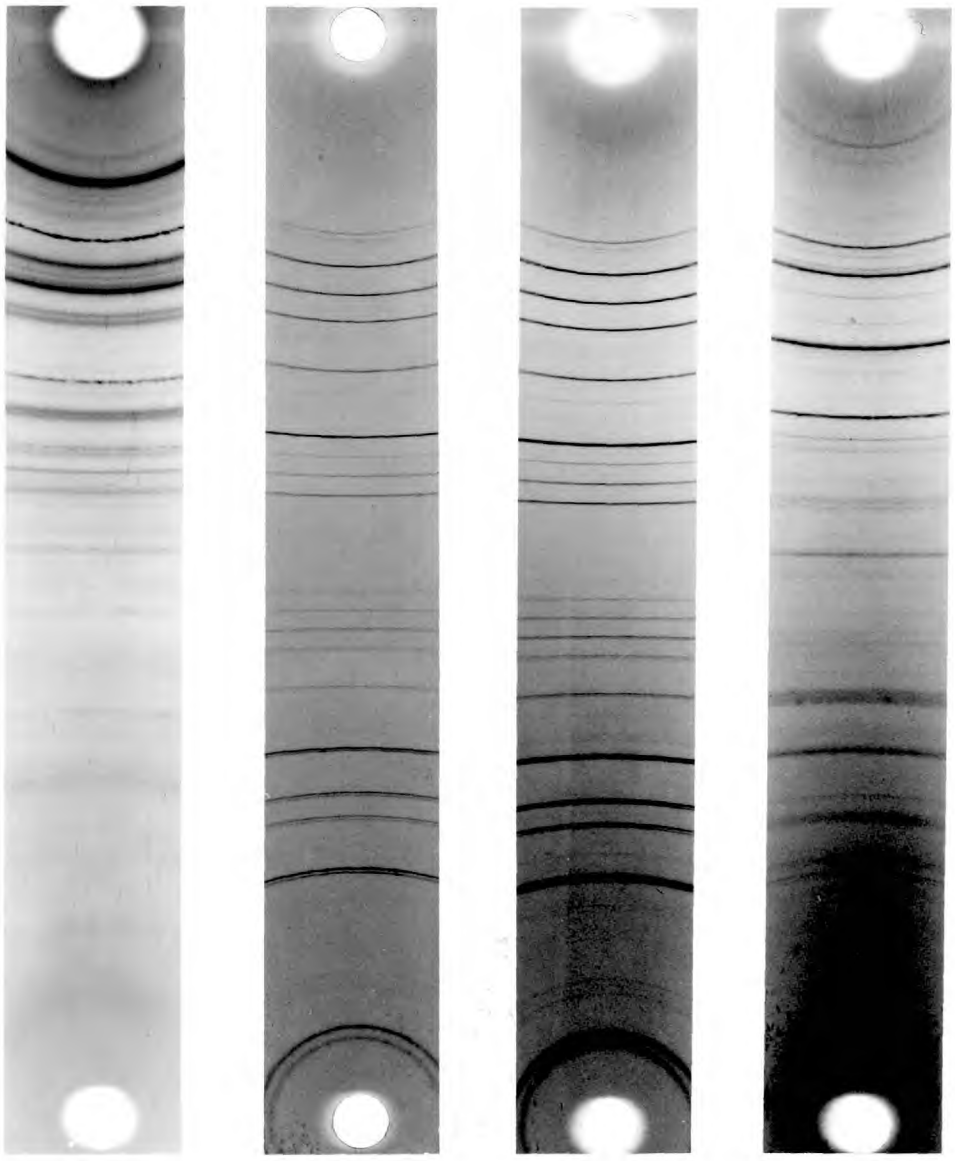

i ii iii iv

Fig. B-5 X-ray Powder Photographs of
i) goethite flakes
ii) "Premier" pyrite untreated
iii) " " heated to 650°C
iv) " " heated to 726°C

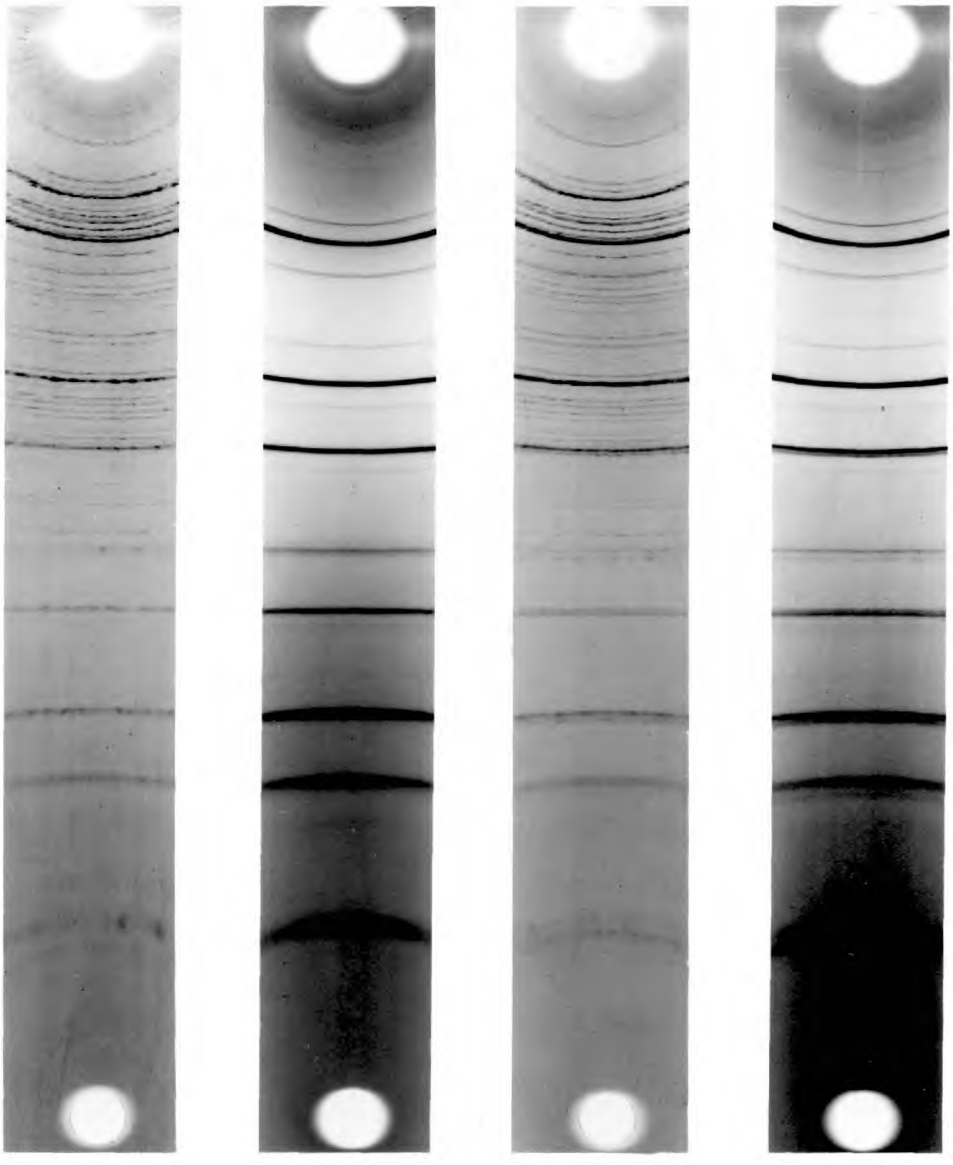

i ii iii iv

Fig. B-6 X-ray Powder Photographs of the residues from

i) β-chalcopyrite leached with H_2SO_4 (pH∿0.5)
ii) as i) but sample washed with CCl_4
iii) α-chalcopyrite leached with H_2SO_4 (pH∿0.5)
iv) as iii) but sample washed with CCl_4

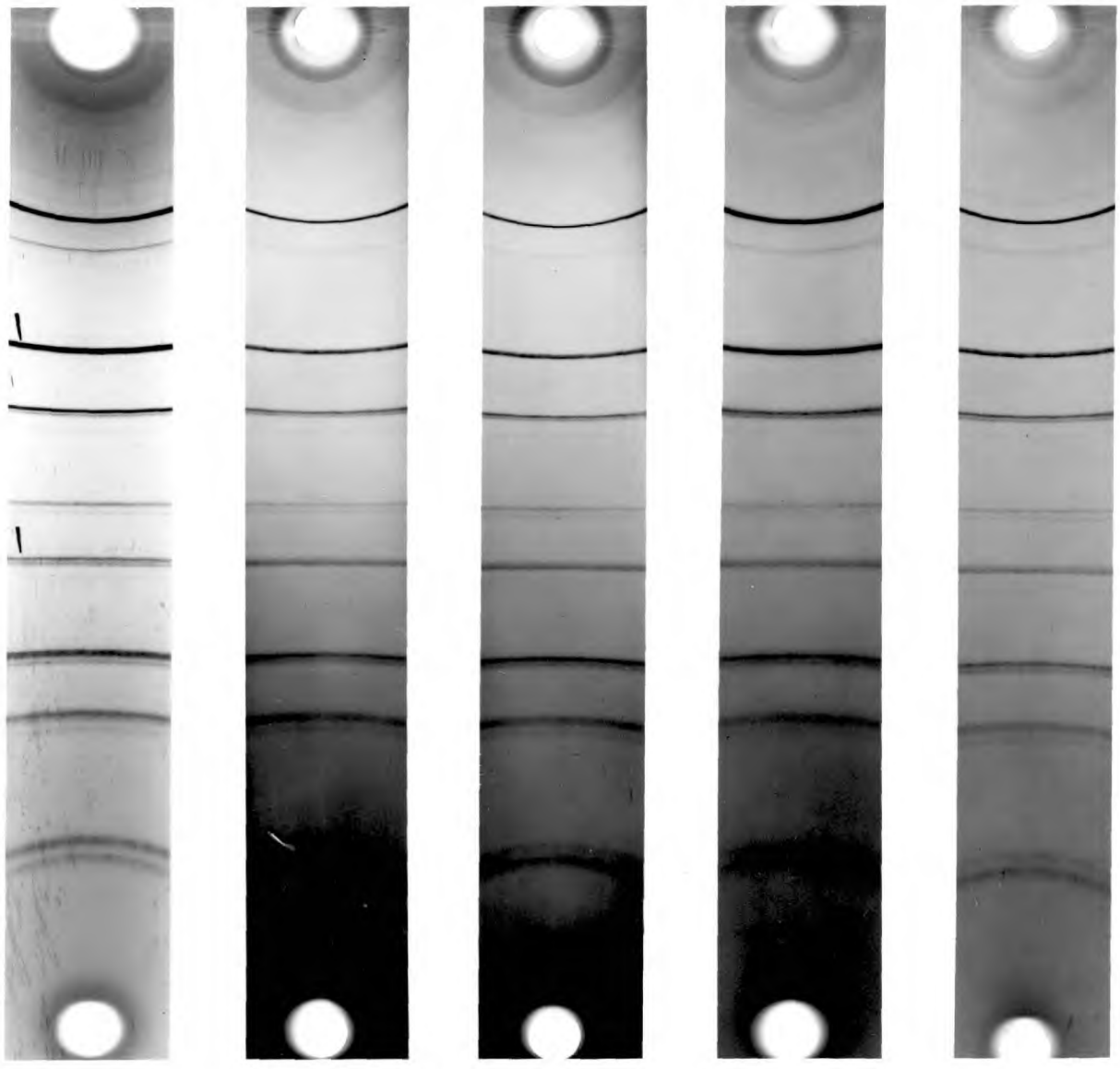

Fig. B-7 X-ray Powder Photographs of α-residues (ferric sulphate leach).
a) α-chalcopyrite ($Cu_{1.12}Fe_{1.09}S_2$)
b) 16.0% Cu removed
c) 17.9%
d) 27.1%
e) 32.1%

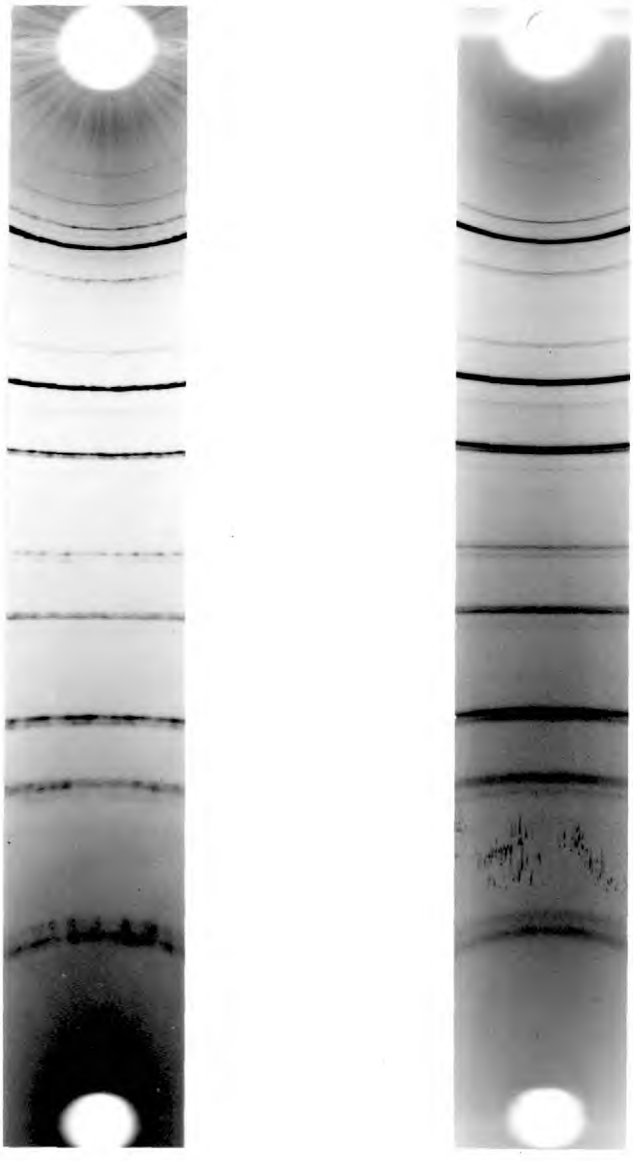

i ii

Fig. B-8 X-ray Powder Photographs of α-residues.
i) HCl leach
ii) $Fe_2(SO_4)_3$ + NaCl leach

B-2.4 Photomicrographs of the Residues

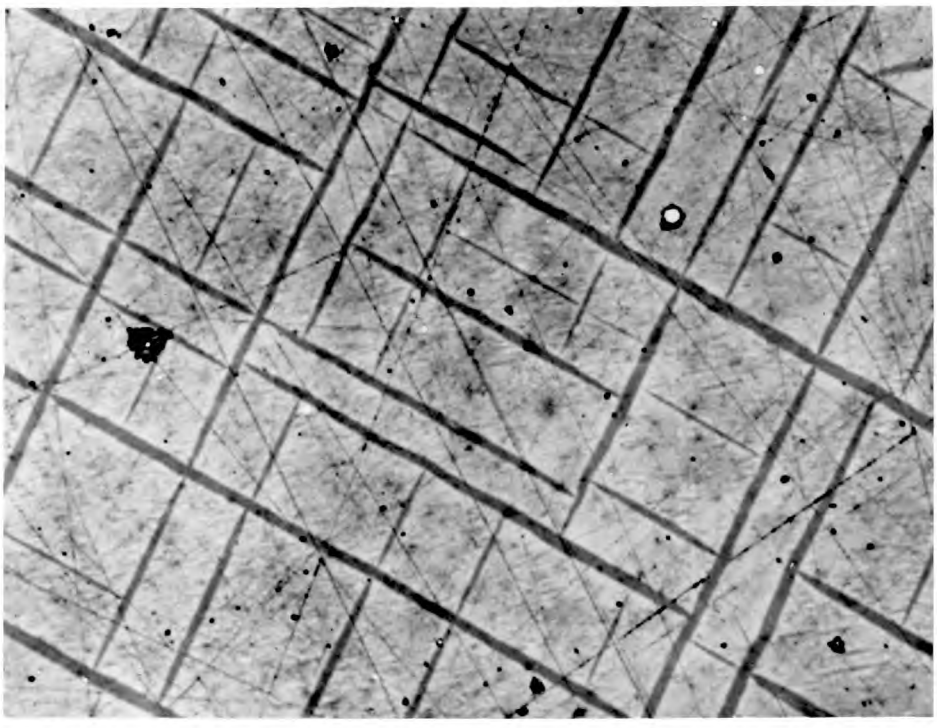

Fig.B-9 Synthetic β-chalcopyrite showing the lamellae type structure (x150)

a) x 180



b) x 600

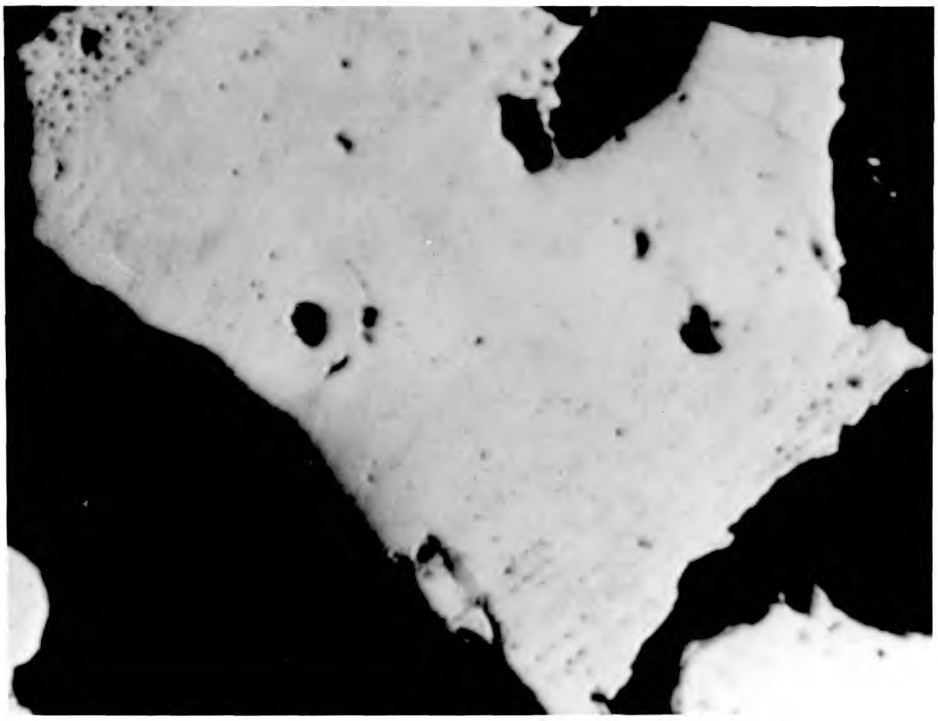

Fig. B-10 Sample of unleached β-chalcopyrite (-100+150 mesh)



Fig.B-11 β-leach residue (6.5% Cu dissolved) showing no alteration at the polished surface (x 200)

a) x 180

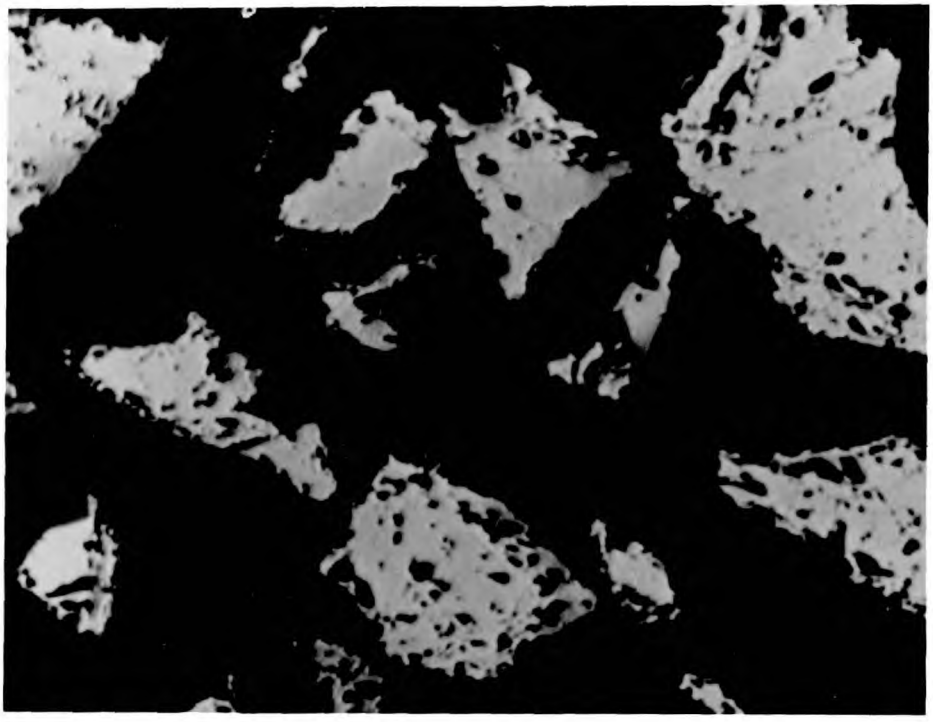

b) x 600

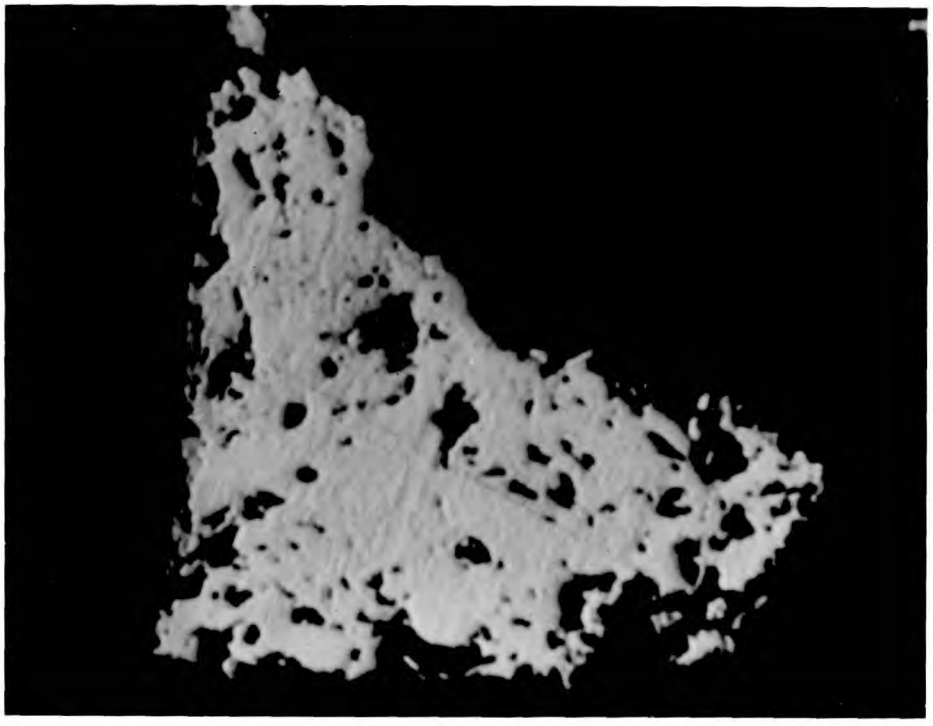

Fig. B-12 β-leach residue (12.5% Cu dissolved) showing the attack leading to pore formation.

a) x 180

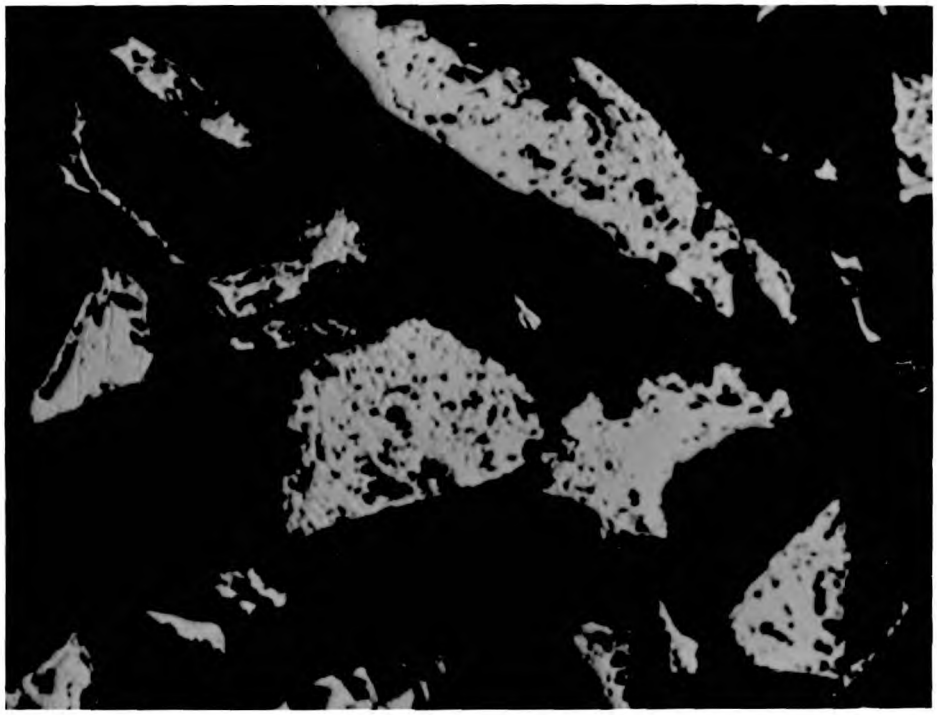

b) x 600

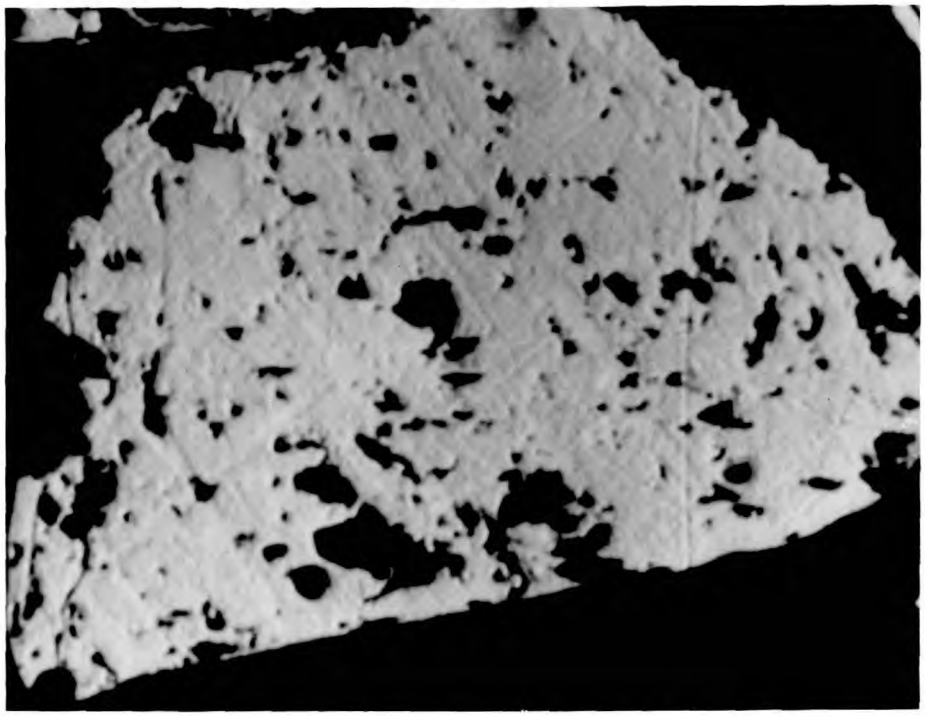

Fig.B-13β-leach residue (23.0% Cu dissolved).

a) x 180



b) x 750

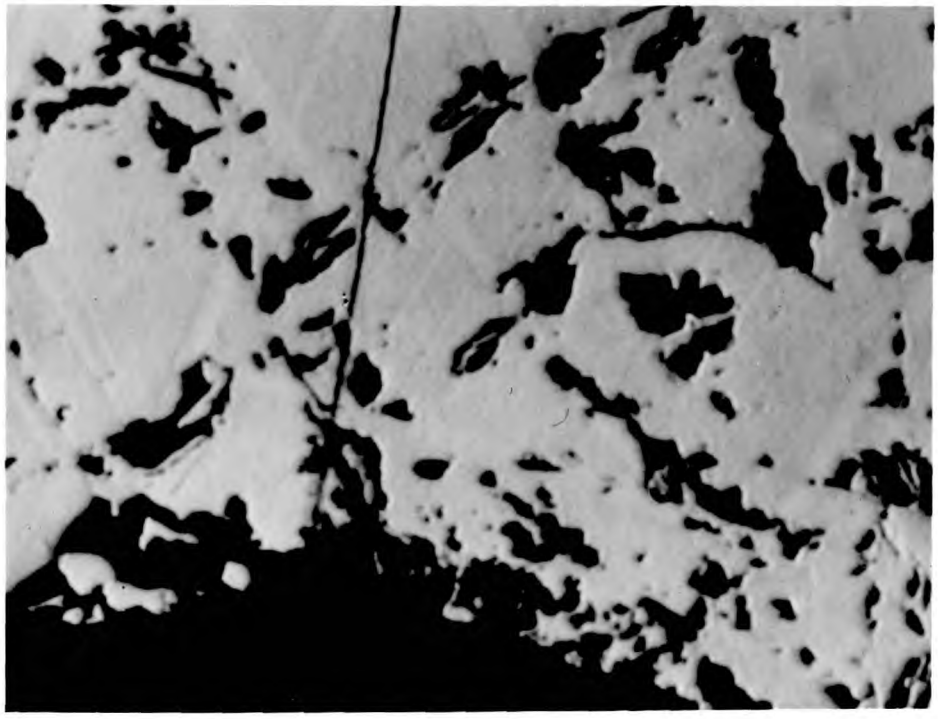

Fig.B-14 β-leach residue (31.5% Cu dissolved).
The higher magnification shows that the lamellae type structure is not preferentially attacked.

a) x 180

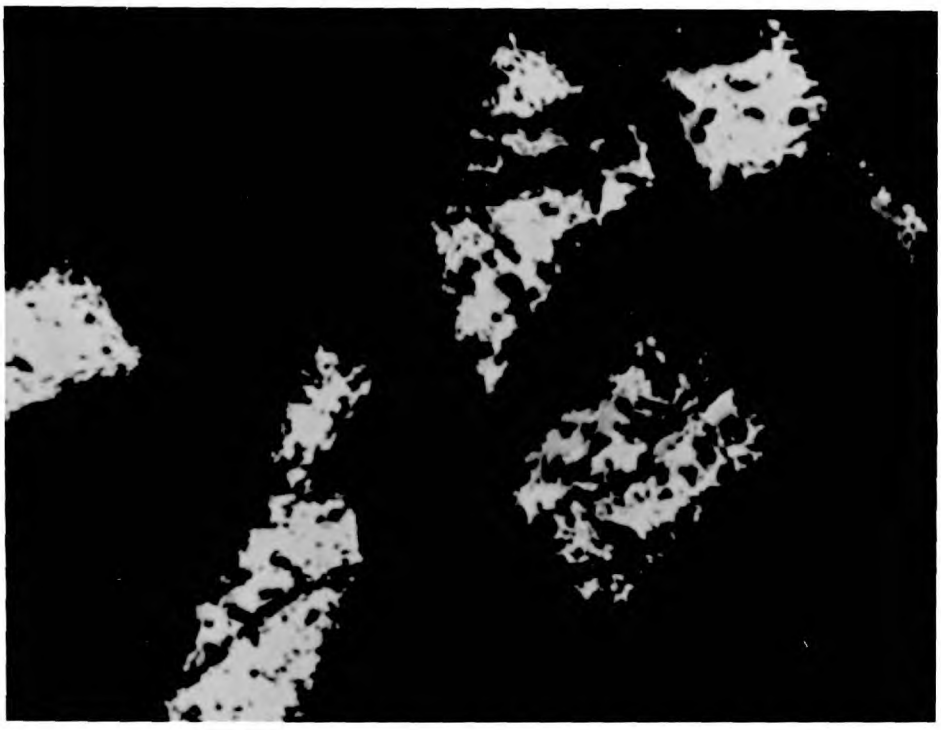

b) x 600

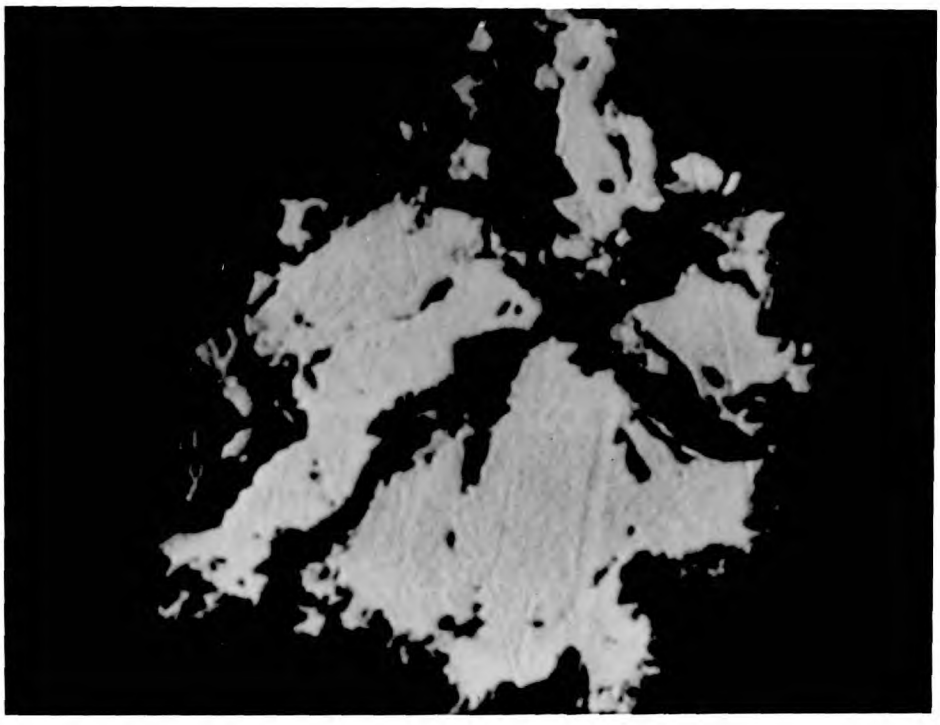

Fig.B-15 β-leach residue (45% Cu dissolved).
Lamellae structure still visible.

a) x 180

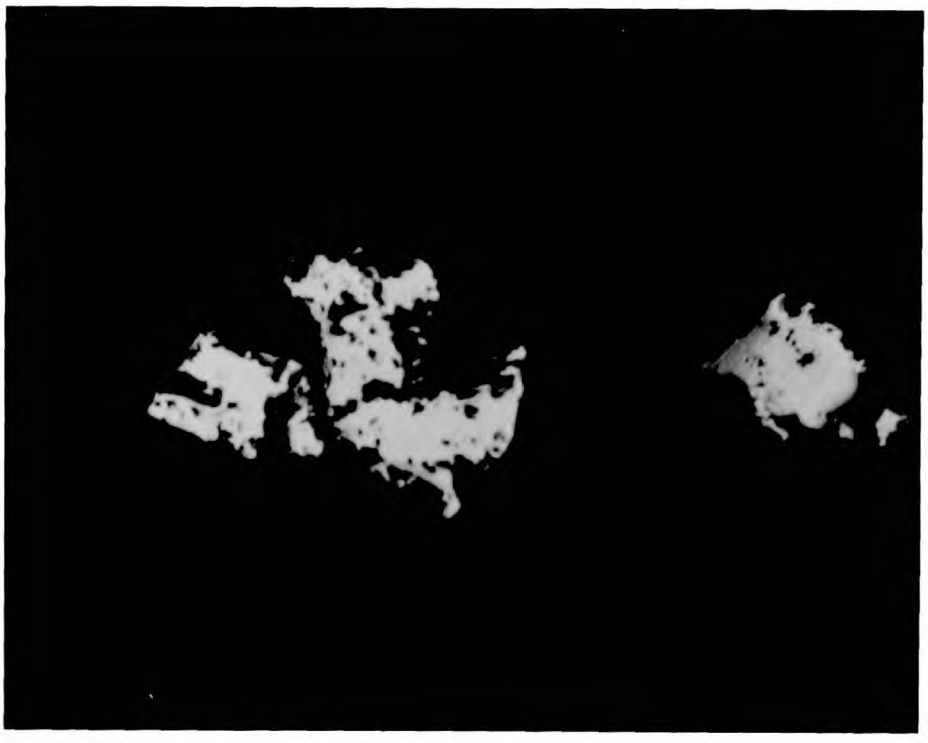

b) x 600

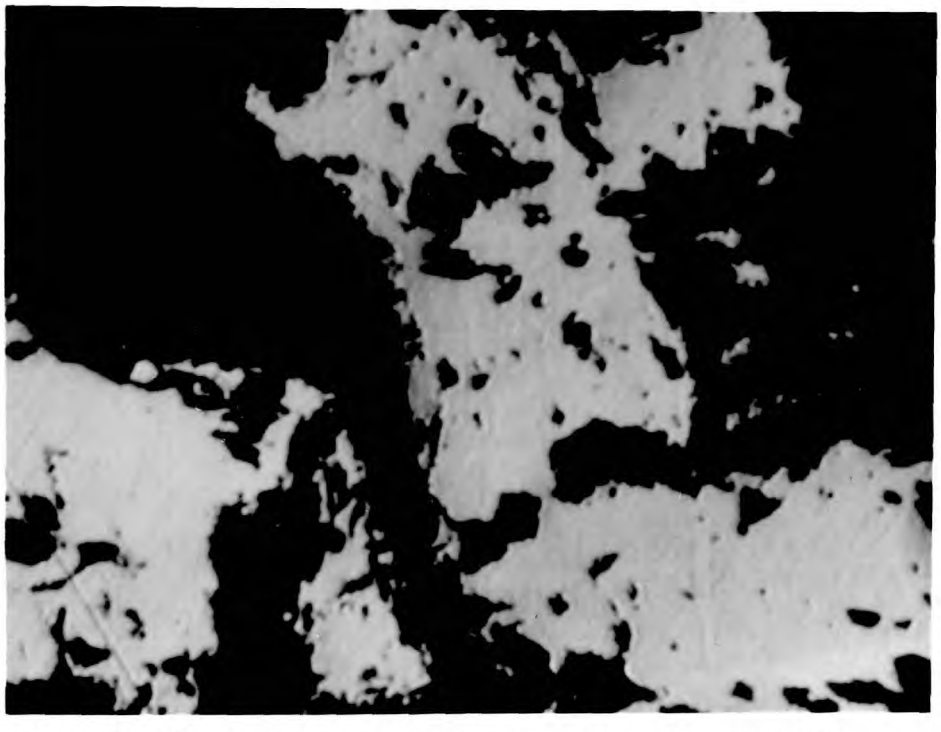

Fig. B-16β-leach residue (55% Cu dissolved).

a) x 180

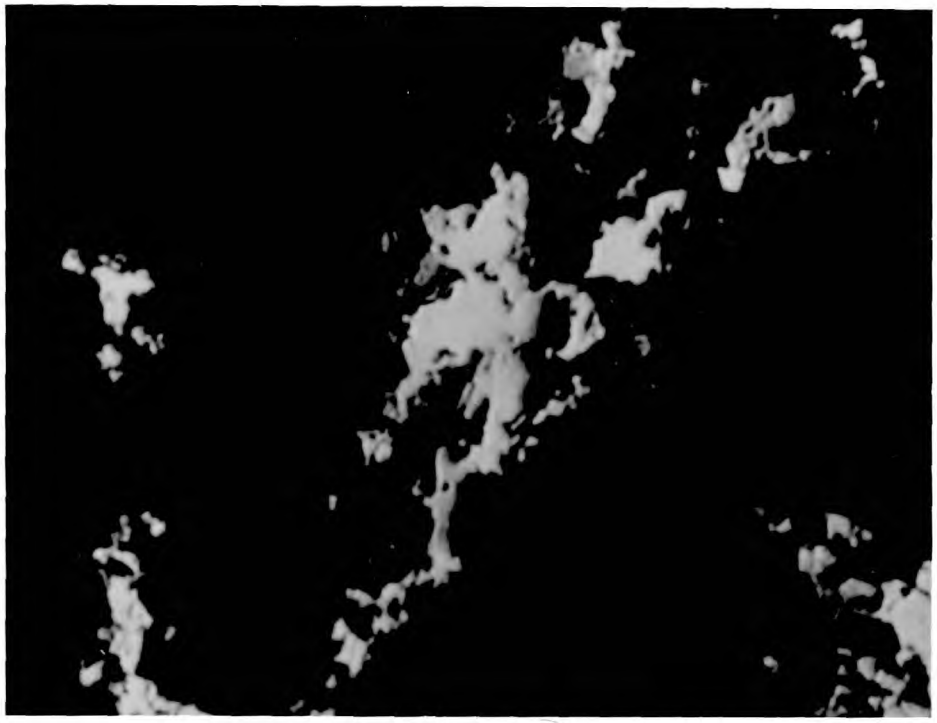

b) x 600

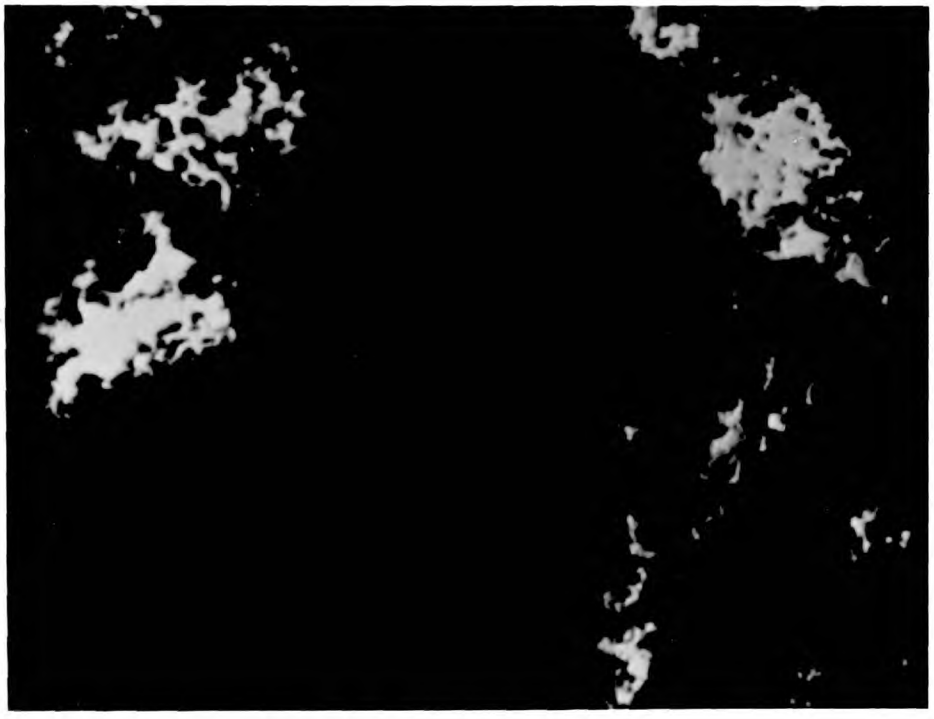

Fig.B-17 β-leach residue (82% Cu dissolved).

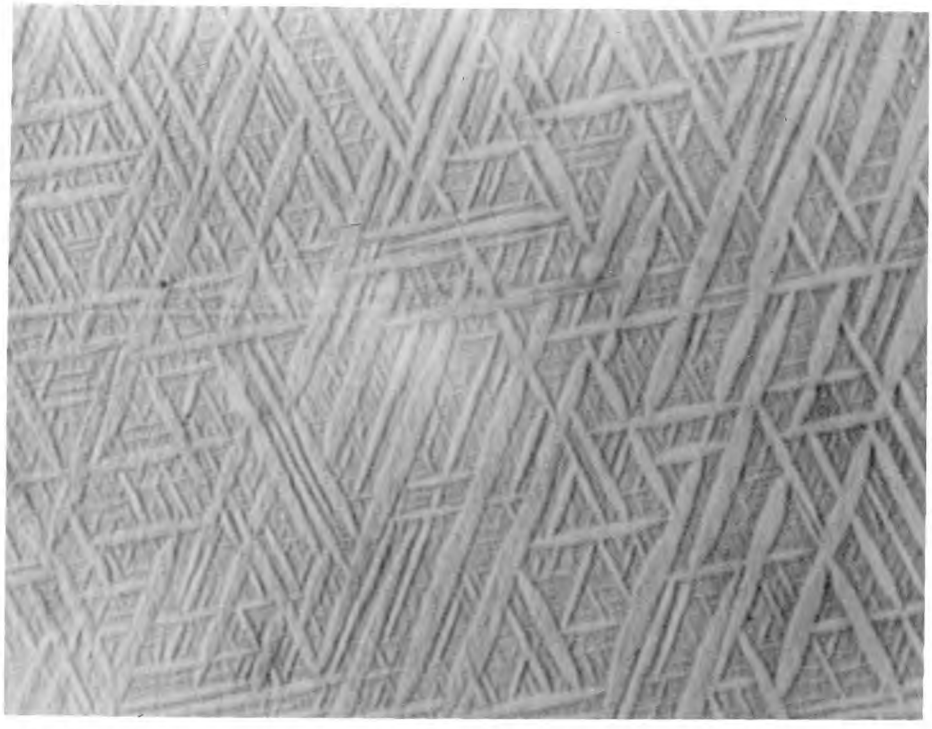

Fig. B-18Synthetic α-chalcopyrite showing the lamellae type structure (x 300)



Fig.B-19 Sample of synthetic α-chalcopyrite (-100+150 mesh) before leaching, showing the formation of fractures after 9 months of storage. (x 180)

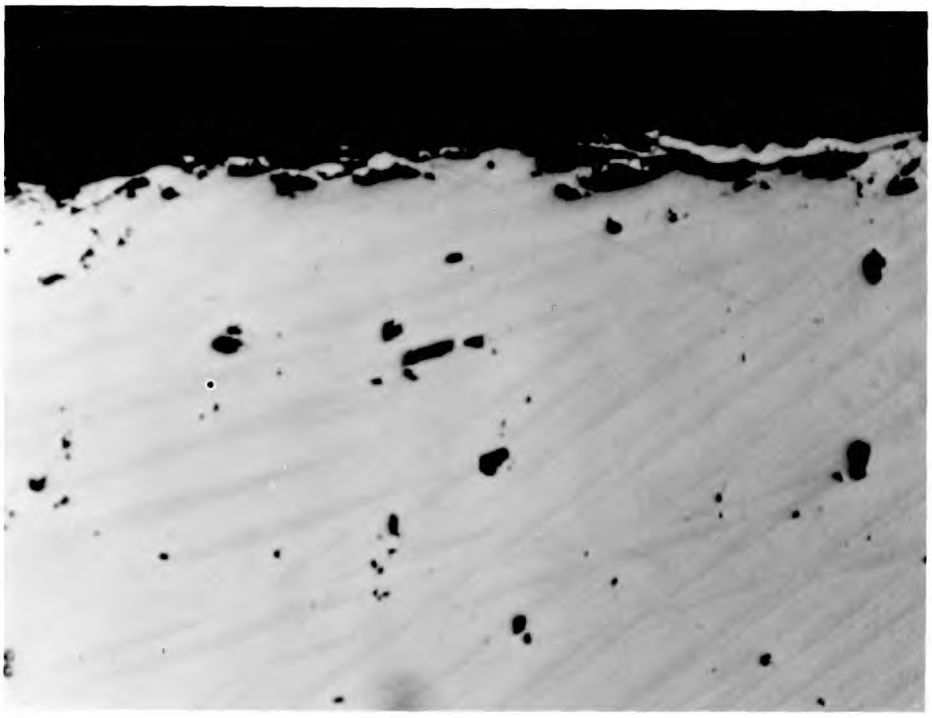

Fig B-20 Central portion of a piece of synthetic α-chalcopyrite before leaching, freshly cut edge. (x 300)

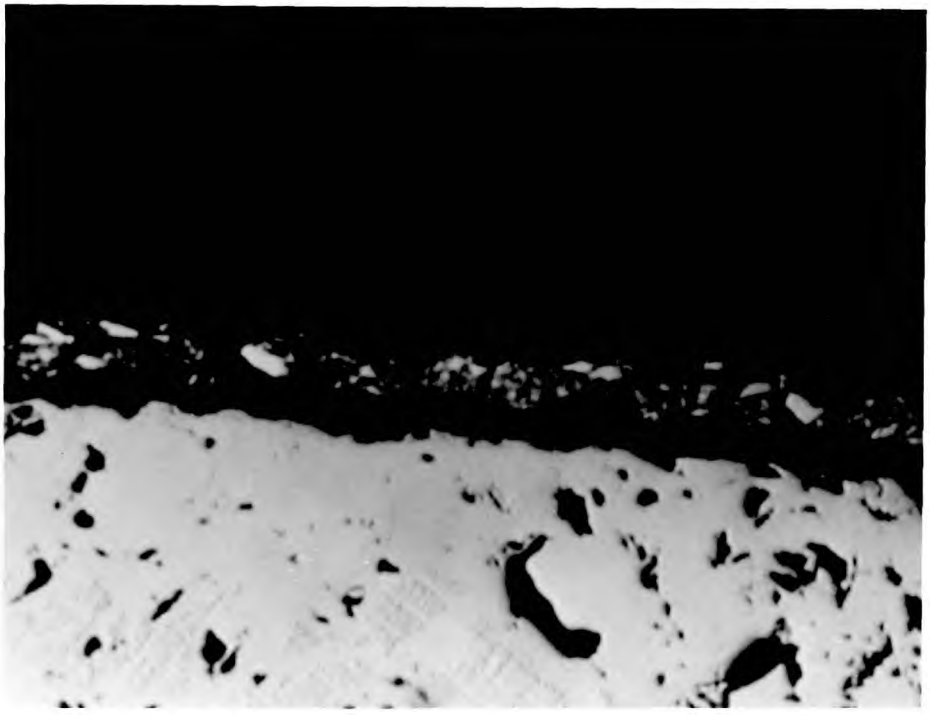

Fig. B-21 Edge of the synthetic α-chalcopyrite before leaching, after storage for 9 months, showing segregation at the outside of the piece. (x 300)

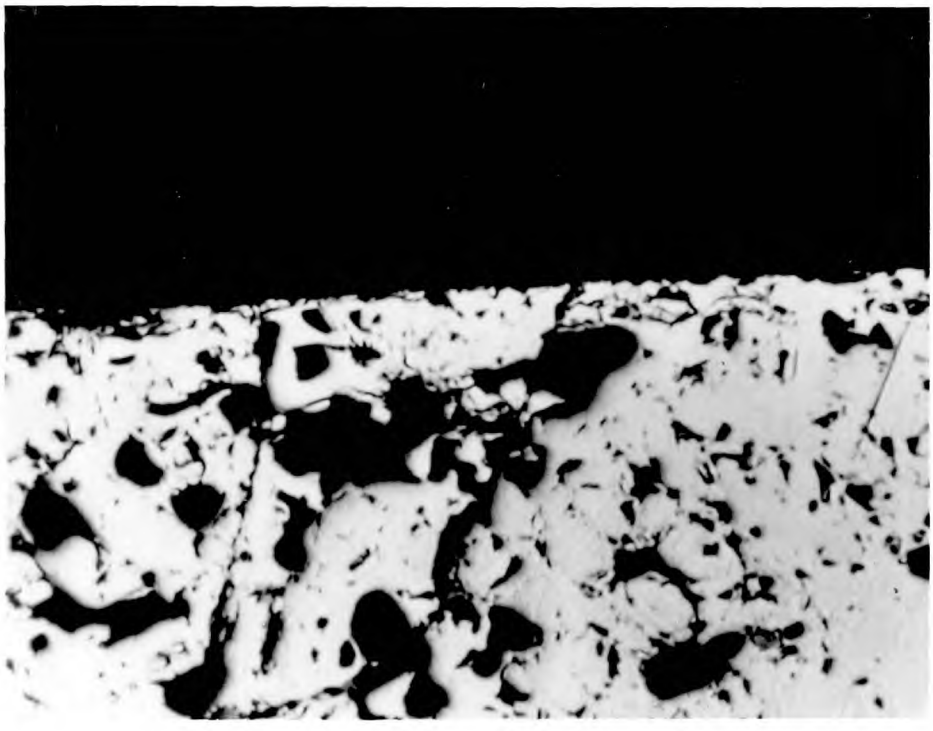

Fig. B-22 Same edge as shown in Fig. B-20 after leaching for 60 hours at 80°C with 0.01M Fe^{3+} (pH∿1) (x 300)

a) x 180

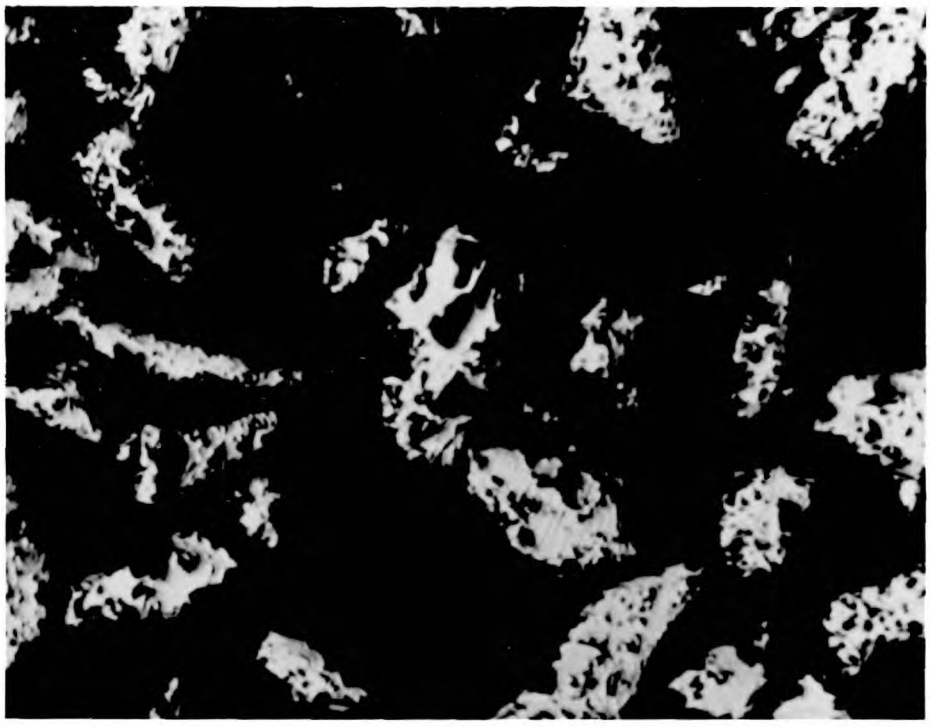

b) x 600

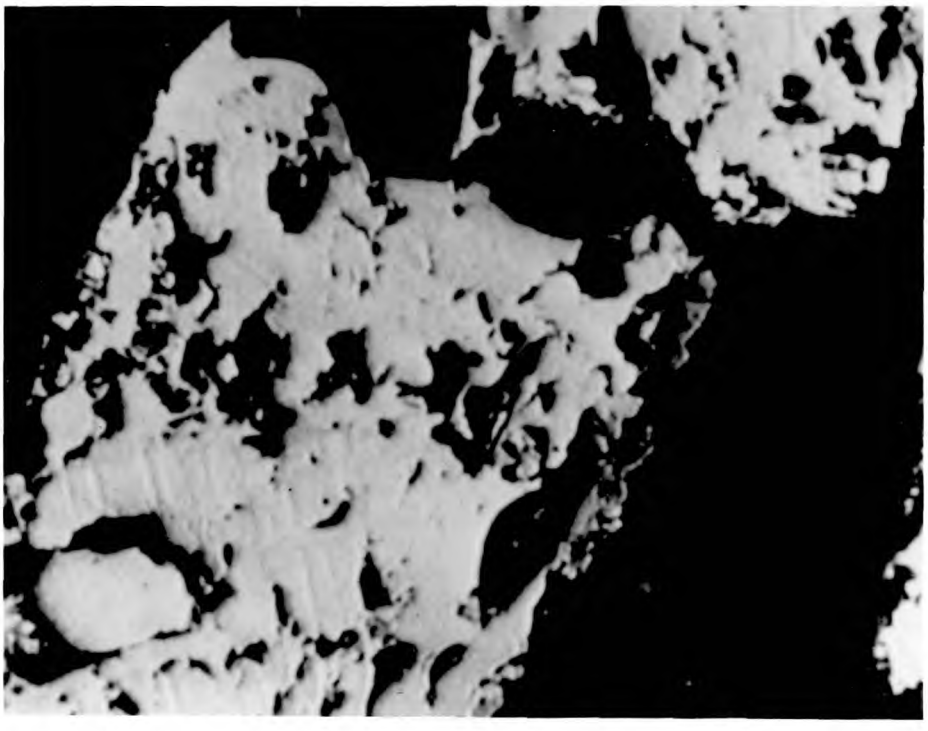

Fig.B-23 α-leach residue (24% Cu dissolved).

APPENDIX C

OPEN FURNACE AND PRESSURE FURNACE DESIGN

ABSTRACT

For the synthesis and recrystallisation of double sulphides both an open furnace and a pressure furnace were designed.

This design involved the following steps for both types of furnace:

i) Calculation of the thickness of the insulating material in order to obtain a required temperature gradient, knowing the approximate furnace tube diameter and the temperature on the winding, or calculation of the external temperature on the surface of the insulation knowing its thickness.

ii) Calculation of the number of turns in the winding to maintain the required temperature in the furnace tube and compensate for the heat losses.

and also for the pressure furnace:

iii) Calculation of the wall thickness for the pressure vessel, taking as the internal radius the sum of the value obtained from i) plus the furnace tube radius, for a required working pressure and temperature on the internal cylindrical shell.

iv) Correction for the pipe standard size for the pressure vessel and furnace tube.

v) Design of welded joints and of fittings.

C.1 Basic Relations

For the heat losses the calculations were based on the following relations (JAKOB[136]):

Heat conducted through insulation=Heat lost from outer surface by convection + Heat lost by radiation

i) Heat conducted through insulation:

$$q_{CD} = \frac{2\pi k\ (T_1 - T_2).\ L}{\ln \frac{r_2}{r_1}}$$

k - thermal conductivity of insulation ($BTU ft^{-2} hr^{-1} {}^oF^{-1} ft$)
T_1 - inner temperature (of the winding) (^oR)
T_2 - outer temperature (of the external surface) (^oR)
r_1 - inner radius (of the winding) (ft)
r_2 - outer radius (of the insulating material) (ft)
L - length of the tube (ft)

ii) Heat lost by convection

$$q_{CV} = 2\pi r_2\ h_c (T_2 - T_3).L$$

h_c - heat transfer coefficient ($BTU\ ft^{-2} hr^{-1} {}^oF^{-1}$)
r_2 - outer radius (of the insulating material) (ft)
T_2 - temperature on the external surface (^oR)
T_3 - atmospheric temperature (^oR)

with

$$h_c = 0.27 \left(\frac{T_2 - T_3}{2r_2}\right)^{0.25} \quad \text{if X between } 10^3\text{-}10^9$$

$$h_c = 0.18\ (T_2 - T_3)^{\frac{1}{3}} \quad \text{if X between } 10^9\text{-}10^{12}$$

The value X is initially assumed and later corrected

$$X = \frac{D_2^3\ \rho^2\ g\ \beta\ Cp\ (T_2 - T_3)}{\mu K}$$

T_2 - temperature on the external surface (^oR)
T_3 - atmospheric temperature (^oR)
$D_2=2r_2$ (outer diameter) (ft)
ρ - density of fluid (air) (lb ft^{-3})
g - gravitational acceleration (ft hr^{-2})
β - coefficient of thermal volume expansion of the fluid ($^oF^{-1}$)
Cp - specific heat of the fluid (BTU ft^{-1} hr^{-1} $^oF^{-1}$)
μ - dynamic viscosity of the fluid (lb hr^{-1} ft^{-1})
K - thermal conductivity of the fluid (BTU ft^{-1} hr^{-1} $^oF^{-1}$)

iii) Heat lost by radiation

$$q_r = 2\pi r_2 \sigma \varepsilon_2 \ (T_2^4 - T_3^4).L$$

σ - Stefan Boltzman's Constant (BTU ft^{-2} hr^{-1} $^oR^{-4}$)
ε_2 - emissivity
r_2 - outer radius (ft)
T_2 - temperature on the external surface (^oR)
T_3 - atmospheric temperature (^oR)

Graphical solution of the equation

$$\underset{(a)}{q_{CD}} = \underset{(b)}{q_{CV}} + q_r$$

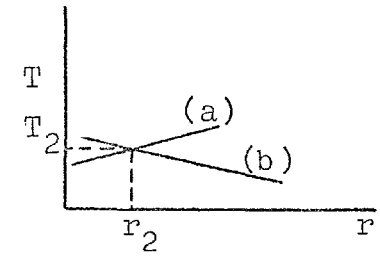

will give the value of T_2 or r_2 according to which was initially assumed.

Final iterations will lead to the true values of T_2 or r_2.

For the design of the pressure vessel, the following relations were used:

- Thickness of cylindrical shells under internal pressure (Perry(132))

$$t_s = \frac{PR}{SE-0.6P}$$

t_s - thickness (inches)
P - internal pressure (psi)
R - inside radius (inches)
S - maximum allowable stress (psi)
E - lowest efficiency of any joint in the head

- Thickness of the cover plates (Perry[132])

$$t_p = d\sqrt{\frac{CP}{S}}$$

t_p - thickness (inches)
d - diameter of bolt circle (inches)
C - constant
P - internal pressure (psi)
S - maximum allowable stress (psi)

C.2 Open Furnace

This furnace consisted of a 2" external diameter alumina tube, a Kanthal A_1 wire winding, Greenlite insulating fire bricks and a very thin sheet of asbestos.

C.2.1 Calculation of the External Surface Temperatures

Using the relations presented above it was possible to determine the heat losses for a certain thickness of the insulating material and the number of turns in the winding to keep the required temperature and compensate for the heat losses.

The values used for the calculation of the external surface temperature in order to have 950°C (1742°F) on the winding, using insulating material 4" thick, were as follows:

- For q_{CD}

$k = 2.9/_{12}$ BTU ft^{-2} hr^{-1} $^oF^{-1}$ ft (Greenlight insulating firebricks)
$T_1 = 2202^oR$ (1742°F)
T_2 = ? (outer temperature)
$r_1 = \frac{1}{12}$ ft
$r_2 = \frac{4}{12}$ ft

(the value of L is not necessary since it disappears during the calculations)

- For q_{CV}

i) X determined to be between 10^3 and 10^9 assuming the outer temperature $T_2 = 212^oF$, and using:

$T_2 = 77^oF$

$D_2 = 2r_2 = \frac{8}{12}$ ft

ρ (air) = 0.0808 lb ft^{-3} (77^oF)

$g = 4.17 \times 10^8$ ft hr^{-2}

β(air) = 2 030.6 x 10^{-6} $^oF^{-1}$ (77^oF)

Cp(air) = 0.2401 BTU lb^{-1} $^oF^{-1}$ (77^oF)

μ(air) = 0.0445 lb hr^{-1} ft^{-1} (77^oF)

K(air) = 0.0150 BTU hr^{-1} ft^{-1} $^oF^{-1}$ (77^oF)

ii) h_c was found to be 1.02 BTU hr^{-1} ft^{-2} $^oF^{-1}$ assuming $T_2 = 212^oF$:

iii) For q_{CV} the values used were

h_c = 1.02 BTU ft^{-2} hr^{-1} $^oF^{-1}$

$r_2 = \frac{4}{12}$ ft

T_2 = ? (outer temperature)

$T_3 = 537^oR$ (77^oF)

- For q_r

$\sigma = 0.174 \times 10^{-8}$ BTU ft^{-2} hr^{-1} $^oR^{-4}$

$\varepsilon_2 = 0.94$ (asbestos)

$r_2 = \frac{4}{12}$ ft

T_2 = ? (outer temperature)

$T_3 = 537^oR$ (77^oF)

The use of these values led to a relation

$$q_{CD} = q_{CV} + q_r$$

And the value obtained graphically for T_2 was about 753°R (293°F) corresponding to

{ Temperature on the winding: 950°C
Temperature on the external surface of the furnace: 150°C

Iterations using the new value for T_2 in the relations for X and h_c did not alter significantly the result obtained.

Experimental determinations showed a temperature on the external surface of about 100°C when the furnace was running at about 900°C.

C.2.2 Determinations of the Number of Turns in the Winding

Heat losses:

Using the expression for q_{CD} a value of 38.5 watt in^{-1} was found.

Considering rhe relations:

$$P = VI$$
$$V = RI$$
$$R = 2\pi r_1 n\rho$$

and using the following values:

$$P = 38.5 \text{ watt } in^{-1}$$
$$V = 220 \text{ V}$$
$$r_1 = 1"$$
$$\rho = \frac{0.63}{36} \Omega \text{ } in^{-1} \quad (A_1, \text{ 16 S.W.G. Kanthal wire})$$

the number of turns necessary was determined to be n = 9.

The furnace constructed according to the results obtained allowed the use of temperatures as high as 1100°C by taking the voltage to 240V.

C.3 Pressure Furnace

The pressure furnace was intended to consist of an alumina tube wound with A_1 Kanthal wire, Greenlite insulating firebricks and a stainless steel tube closed at both ends with blind flanges.

A transverse section of the pressure furnace can be represented schematically as

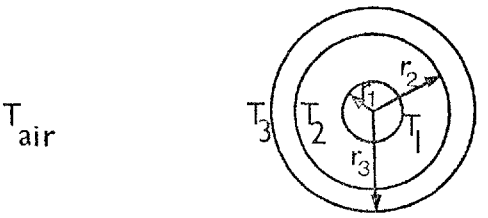

C.3.1 Calculation of the Thickness of the Insulating Layer

In order to facilitate the calculations, an infinitely thin wall was assumed initially for the stainless steel tube, and with the result obtained and using iterative methods, the actual values were determined. Thus, the following expression was used

$$\frac{K_{12}\,(T_1-T_2)}{\ln \frac{r_2}{r_1}} = r_2\, h_c\, (T_2-T_{air}) + r_2\sigma\varepsilon\, (T_2^4-T_{air}^4)$$

together with the following set of values for extreme working conditions:

T_1 = 2472°R (1100°C) - maximum required temperature for the winding

T_2 = 1392°R (500°C) - temperature on the inner shell of the pressure tube

$T_3 = T_2$ - assumed

T_{air} = 537°R (25°C)

$r_1 = \frac{1}{12}$ ft - approximate external radius for the alumina tube

r_2 = ? - radius for the inner shell of the pressure tube

$r_3 = r_2$ - assumed

$K_{12} = \frac{2.80}{12}$ BTU ft^{-2} hr^{-1} $^oF^{-1}$ ft - thermal conductivity of the firebrick assuming a mean temperature of 800°C

$\varepsilon_3 = 0.13$ - emissivity for the steel at 500°C

The result obtained for the value of r_2 showed that the internal radius of the stainless steel pipe should be

$$r_2 = 1.914"$$

Recalculations were made using the values found in the next section for the standard sizes of the tubes, and considering now the wall thickness for the stainless steel tube.

The relation considered for this case was

$$\frac{T_1 - T_3}{\frac{\ell n r_2/r_1}{k_{12}} + \frac{\ell n\ r_3/r_2}{k_{23}}} = r_3 h_c (T_3 - T_{air}) + r_3 \sigma \varepsilon_3 (T_3^4 - T_{air}^4)$$

where

T_3 = ? - temperature on the external surface of the pressure tube

$r_1 = \frac{1.181}{12}$ - radius of the winding assuming 59mm external diameter of the alumina tube and 16 gauge wire (1.626mmϕ)

$r_2 = \frac{1.913}{12}$ - radius of the inner shell of the standard size pressure tube

$r_3 = \frac{2.25}{12}$ - radius of the outer shell of a 4.5" standard size pressure tube

K_{23} = 14.0 BTU ft^{-2} hr^{-1} $^oF^{-1}$ ft - thermal conductivity of steel (high-chromium) assuming a mean temperature of 500°C.

The results obtained using these values confirmed the temperatures assumed for the extreme working conditions.

C.3.2 Calculation of the wall and Cover Plates Thickness for the Pressure Vessel

Using the relations mentioned in Section C-1, the approximate dimensions for the pressure vessel were obtained.

For the calculations, the following values were considered

Maximum Permissible Stress(*) (Perry(132))
for a stainless steel AISI 316 (18Cr, 10Ni,2Mo)

Temperature (^{o}F)	Max. Stress (psi)
800	16750
900	16000
950 (510°C)	15100
1000 ($\sim$538°C)	14000
1100 ($\sim$593°C)	10400
1150 ($\sim$621°C)	8500
1200	6800

P = 1500 psi - maximum working pressure required

R = 1.914 inches - radius of the internal shell of the pressure tube (calculated in the previous section)

S = 10 400 psi (593°C) - For safety reasons a higher temperature was considered for the maximum allowable stress

E = 1 - coefficient for the lowest efficiency of any joint in the head

d = 9.5 inches

C = 0.162 - constant for bolted blind flanges

With this set of values the results obtained were:

- thickness of the cylindrical shell = 0.302 inches
- thickness of the cover plates = 1.45 inches

(*) Values are supposed to be below 0.1% P.S.

It was therefore decided to use a seamless stainless steel pipe (AISI 316 - nominal composition 18 Cr, 10 Ni, 2Mo) with the following dimensions

Inside diameter	:	3.826"
Wall thickness	:	0.337"
Outside diameter	:	4.500"
length	:	26"

and cover plates according to the BS 1560:1958 for Class 1500 flanges:

Thickness	:	$2\frac{1}{8}$"
Diameter of bolt circle	:	$9\frac{1}{2}$"

The safety factors considered in these dimensions are therefore reasonably big since the maximum allowable stress considered was only 0.1% of the Proof Stress.

Recalculations using the standard values mentioned above showed that it will be possible to use pressures as high as 1670 psi providing that a temperature of 593°C at the inner surface of the pressure tube is not exceeded.

C-3.3 Design of Welded Connections and Fittings

The recommended welded connections for pressure vessels were used according to the BS1515: Part 2: 1968 and the dimensions of the ring-joint facings according to BS1560: 1958 as shown in detail on the attached workshop drawings.

These drawings also show other small details such as inlets and outlets.

Finally, the dimensions of suitable Purox recrystallized alumina tubes available are

	1st case	2nd case
External diameter	59mm	54mm
Internal diameter	50mm	45mm
length	600mm	600mm

and a winding was made on a 22" length of tube (2nd case) having 10 turns per inch.

It also should be noted that the stainless steel used is

acid, heat and rust-resistant.

Ultrasonic inspection of the constructed pressure furnace showed no major defects in the welded joints, and hydraulic pressure tests were carried out successfully to about 6000 psi at room temperature.

C-4 Workshop Drawings

PRESSURE VESSEL CONSISTS OF A 4" SEAMLESS STAINLESS STEEL PIPE (AISI 316 - NOMINAL COMPOSITION 18 Cr, 10 Ni, 2 Mo) and FOUR STAINLESS STEEL FLANGES, CLASS 1500, TWO OF THEM BEING BLIND FLANGES

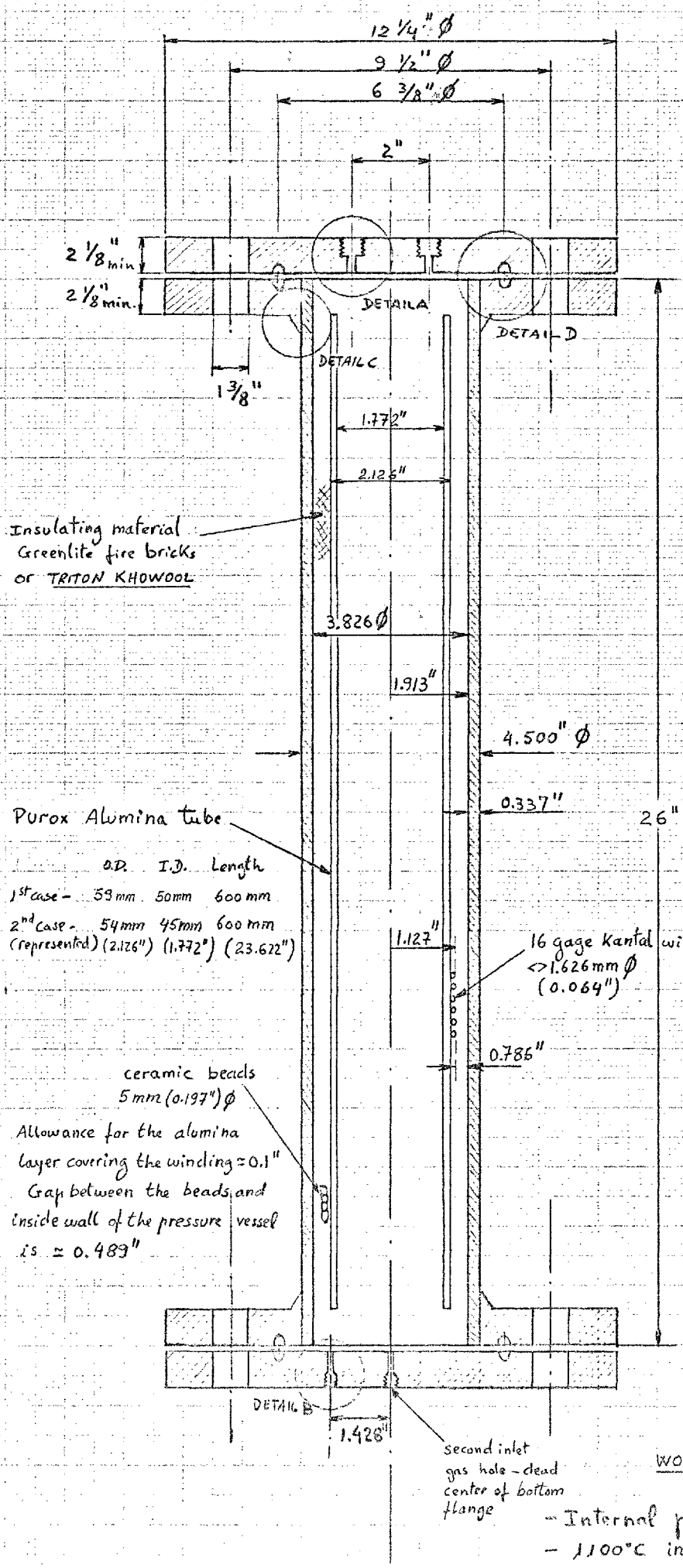

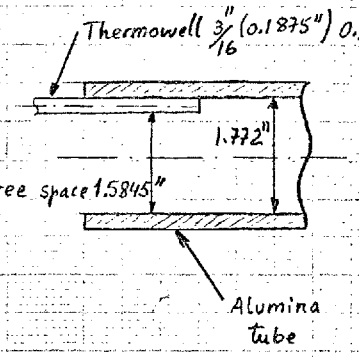

Winding: 22" lenght at 10 turns per inch

Total resistance ≃ 27Ω (25°C

220V → I = 8.1 A

240V → I = 8.9 A

WORKING CONDITIONS:

- Internal pressure = 1500 psi (max.)
- 1100°C in the center of the furnace (max.)

DIMENSIONS OF FLANGES CLASS 1500 (Austenitic chromium - nickel - molybdenum steel)

NOMINAL PIPE SIZE = 4"

Outside diameter of flange = 12 1/4"

Thickness of flange = 2 1/8" min

Diameter of Hub = 6 3/8"

Diameter of bolt circle = 9 1/2"

Nº of bolts 8 (High Tensile)

Diameter of bolts = 1 1/4"

Diameter of bolt holes = 1 3/8"

Lenght of stud-bolts = 7 3/4"

DETAILS FOR THE TOP BLIND FLANGE

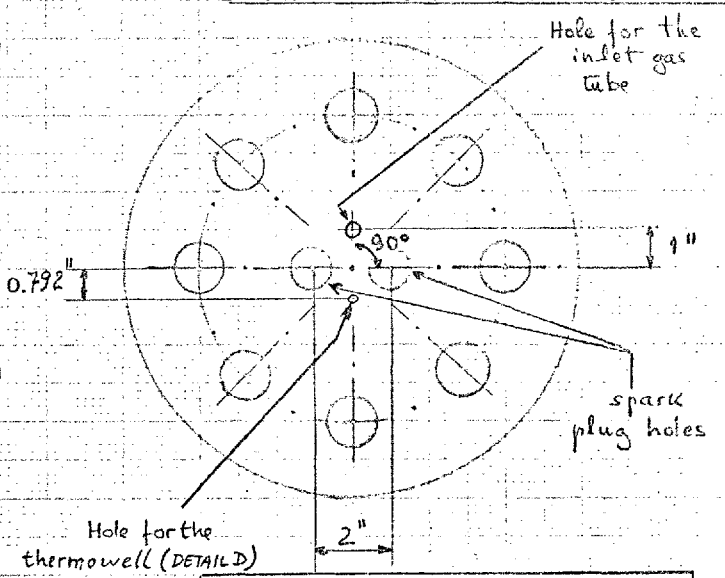

FOR THE INLET GAS HOLES ACCURATE MEASUREMENTS SEE W-125, AUTOCLAVE ENGINEERS: DRAWING 10-6891

DETAIL A

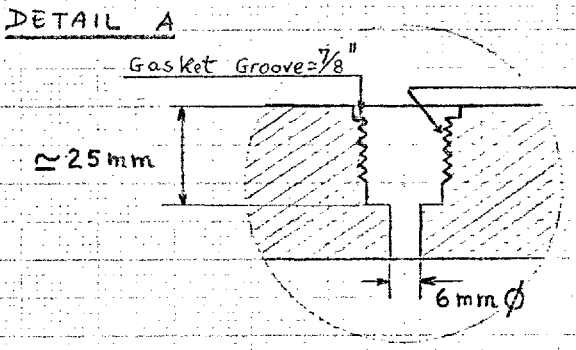

ACCURATE MEASUREMENTS TO BE TAKEN FROM N-9Y CHAMPION SPARK PLUG

DETAIL B

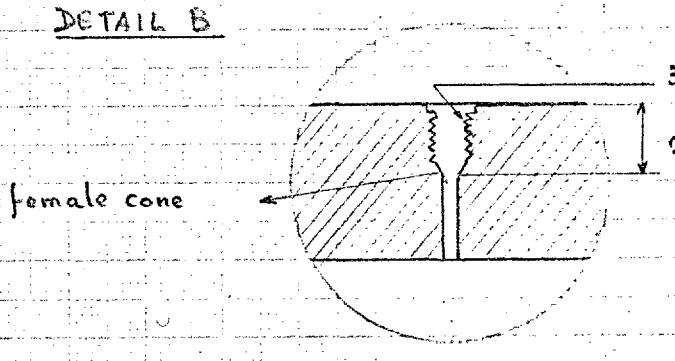

FOR THERMOWELL ACCURATE MEASUREMENTS SEE SW-187 AUTOCLAVE ENGINEERS: DRAWING 10-6891

DIMENSIONS OF RING-JOINT FACINGS (CLASS 1500)
(DETAIL D)

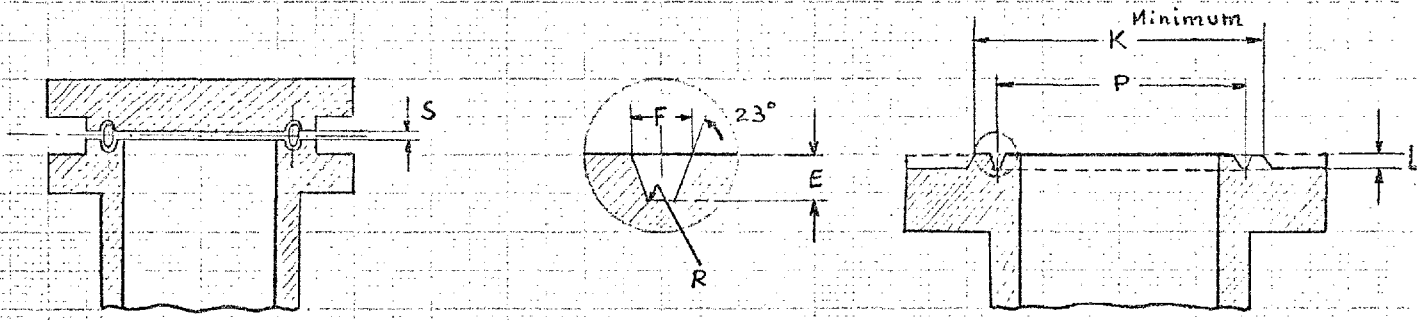

Nominal pipe size – 4"
Pitch diameter of groove P = 6 3/8"
Width of groove F = 15/32
Depth of groove E } 5/16"
Height of raised portion L }
Diameter of raised portion K = 7 5/8"
Radius at bottom of groove R = 1/32"
Ring number R.39
Approximate distance between flanges when ring is compressed S = 1/8"

TOLERANCES

E (Depth) $^{+\ 1/64}_{-\ 0}$ in
F (width) ± .008 in
P (Pitch Dia.) ± .005 in
R (Rad. at Bottom) Max.
On 23° (Angle) ± 1/2°

NOTE: Height L is equal to depth E but not subject to the tolerance on E

DIMENSIONS OF R.39 RING-JOINT GASKET (Stainless Steel) – Min. design seating stress 26 000 psi

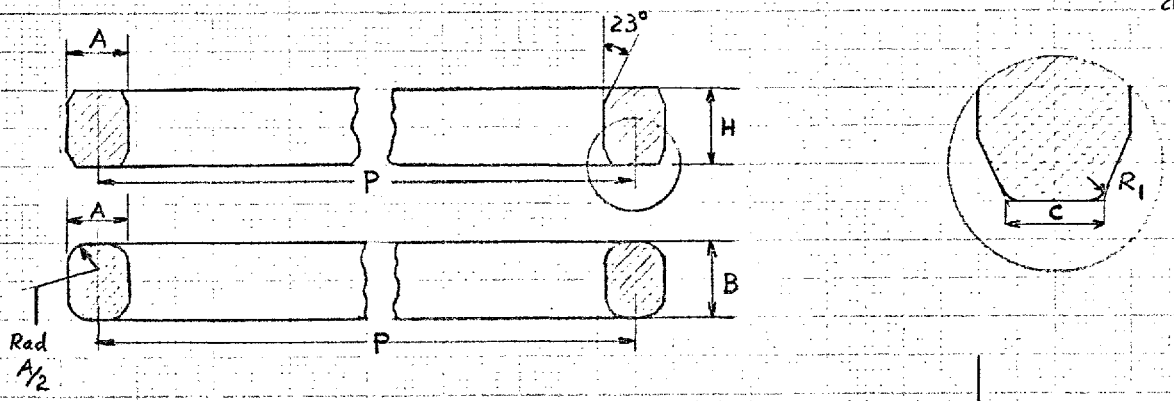

Pitch diameter P = 6 3/8"
width of ring A = 7/16"

Height of ring { oval – B = 11/16"
octagonal – H = 5/8"

Width on flat of octagonal rings C = 0.305"

R_1 = 1/16" for ring widths 7/8" and smaller and 3/32" for ring widths 1 in, and larger

TOLERANCES

P (Pitch Diam.) ± .007 in
A (Width of ring) ± .008 in
B and H (Height of ring) ± 1/64 in
C (width on flat of octagonal rings) ± .008 in
23° (Angle) ± 1/2°
R_1 ± 1/64 in

RECOMMENDED WELDED CONNECTIONS FOR PRESSURE VESSELS (DETAIL c)

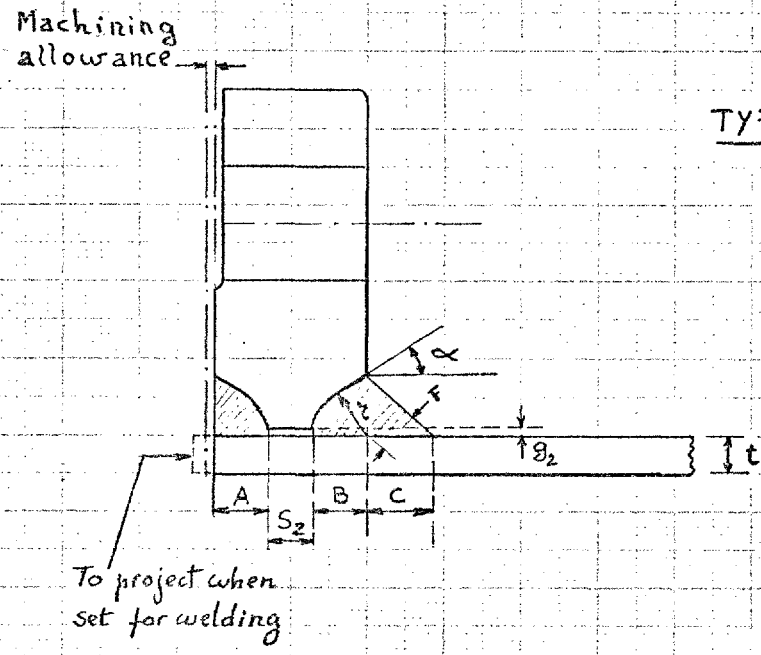

α = 15° to 35°
S_2 = 1/8 in to 3/16 in (3 mm to 4.5 mm)
g_2 = It is recommended that in no case should the gap between branch and shell exceed 1/8 in (3mm)
r = 1/4 in to 1/2 in (6 mm to 13 mm)
B + F = t = 0.337 in (8.56mm)
C = 1/4 in (6 mm) min. and 5/8 in (16 mm) máx.
A = t (min.) after machining flange to final thickness

B may be zero until t exceeds 5/8 in (16 mm)

Discretion must be used in applying the maximum and the minimum dimensions quoted which are subject to variation according to the welding procedure employed (e.g. size and type of electrodes) also the position in which the welding is carried out, and the welding process adopted.

ACKNOWLEDGMENTS

The author is greatly indebted to his supervisor, Dr. A.R. Burkin, for his invaluable help, continued advice and encouragement throughout the course of the present work.

In addition the author wishes to express his appreciation to all members of the Hydrometallurgy Group for their useful suggestions and help.

Thanks are due to Mr. J. Burgess for his practical advice and Mr. G.M. Steed of the Geology Department for the electron probe microanalyses.

Thanks are also due to the Photographic Section of the Metallurgy Department for the reproduction of the photographs.

The author is indebted to the Junta de Energia Nuclear (LFEN) - Portugal, and Comissão Portuguesa INVOTAN-Portugal, for making his studies at Imperial College possible.

Finally, the author wishes to express special thanks to his wife Maria José, for checking the manuscript and typescript.

REFERENCES

1. Warren, I.H. - Aust. J. app. Sci., 9, (1), 36-51 (1958)
2. Seraphim, D.P., and Samis, C.S. - Trans. metall. Soc. AIME, 206, 1096 (1956) - J. Metals 8 (8), 1096 (1956).
3. Jackson, K.J., and Strikland, J.D.H. - Trans. metall. Soc. AIME, 212, 373 (1958).
4. Dobrokhotov, G.N., and Maiorova, E.V. - Zh. prikl. Khim., 35 (8), 1702-1709 (1962).
5. Levich, V.G. - Physicochemical Hydrodynamics, Prentice Hall, Englewood Cliffs, N.J., (1962).
6. Stanczyk, M.H., and Rampacek, C. - Rep.Invest. U.S. Bur. Mines, No. 6193 (1963).
7. Björling, G., and Kolta, G.A. - VII International Mineral Processing Congress, 1, 127-38 (1964).
8. Klets, V.E., and Liopo, V.A. - Trudy Irkutsk. Politelch. Inst. No. 27, 123-130 (1966).
9. Stanczyk, M.H., and Rampacek, C. - Rep. Invest. U.S. Bur. Mines, No. 6808 (1966).
10. Nakahiro, Y. - Suiyowakai-Shi (Japan), 16 (2), 65-70 (1966).
11. Majima, H., and Peters, E.-Trans. metall. Soc. AIME, 236, 1409 (1966).
12. Vizsolyi, A., Veltman, H., Warren, I.H., and Mackiw, V.N. - J. Metals 19 (11), 52-59 (1967).
13. Uchida, T., Matsumcto, H., Omori, S., and Murayama, A. - Hakko Kyokaishi (Japan) 25 (4), 168-72 (1967).
14. Warren, I.H., Vizsolyi, A., and Forward, F.A. - Bull. Can. Inst. Min. Metall., May, 637 (1968).
15. Dutrizac, J.E., MacDonald, R.J.C., and Ingraham, T.R. - Trans. metall. Soc. AIME, 245, 955 (1969).
16. Björling, G., and Lesidrenski, P. - J. Metals, 20 (1), 149A (1968).
17. Prater, J.D., Queneau, P.B., and Hudson, T.J. - J. Metals, 22 (12), 23 (1970).
18. Wyckoff, R.W.G. - Bull. Soc.fr.Minér. Cristallogr., 93, 120-122 (1970).
19. Bruynesteyn, A., and Duncan, D.W. - Can. Met.Q., 10 (1), 57 (1971).

20. Haver, F.P., and Wong, M.M. - Rep.Invest. U.S. Bur. Mines, No. 7474 (1971).
21. Ermilov, V.V., Tkachenko, O.B., and Tseft, A.L. - Tr. Inst. Met. Obogashch, 30, 3-14 (1969).
22. Burdick, C.L., and Ellis, J.H. - J. Am. Soc., 39, 2518 (1917).
23. Gross, R., and Gross, N., - Neues Jb. Miner., 48, 113 (1923)
24. Pauling, L., and Brockway, L.O. - Z. Kristallogr., 82 188 (1932).
25. Donnay, G.,Corliss, L.M., Donnay, J.D.H., Elliott, N., and Hastings, J.M. - Phys. Rev., 112, 1917, (1958).
26. Pauling, L., and Huggins, M.L., - Z.Kristallogr., 87, 205-238 (1934).
27. Pauling, L. - The Nature of the Chemical Bond, Cornell University Press (1960).
28. Buerger, N.W., and Buerger, M.J. - Amer. Miner., 19, 289-303 (1934).
29. Kôzu, S., and Takané, K. - Proc. imp. Acad. Japan, Tokyo, 10, 498 (1934).
30. Boon, J.W. - Recl. Trav. chim. Pays-Bas Belg., 63, 69 (1944)
31. Cheriton, C.G. - Thesis, Harvard University, Cambridge, Massachusetts (1952)(unpublished).
32. Frueh, A.J. - Geochim, Cosmochim. Acta, 6, 79-89 (1954).
33. Austin, I.G., Goodman, C.H.L., and Pengelly, A.E. - Nature, 178, 433 (1956).
34. Hiller, J.E., and Probsthain, K., - Z. Kristallogr., 108, 108-129 (1956).
35. Donnay, G., and Kullerud, G. - Yb.Carnegie Instn. Wash., 57, 246 (1958) (Carnegie Institution of Washington, D.C., 1957-58).
36. Frueh, A.J. - J. Geol., 66, 218-23 (1958).
37. Shima, H. - Ganseki Kobutsu Kosho Gakkaishi, 47, 123-33 (1962).
38. Yund, R.A., and Kullerud, G. - J. Petrology, 7,454 (1966).
39. Aramu, F., and Bressani, T. - Nuovo Cim., B51 (2), 370-75 (1967).
40. Marfunin, A.S., and Mkrtchyan, A.R., - Geokhimiya, (10), 1094 (1967). (Geochem. Inter., 4 (5), 980 (1967)).
41. Zuev, V.V. - Zap.vses.miner. Obschch., 96 (6), 689-98 (1967)

42. Borshagovskii, B.V., Marfunin, A.S. et al. Izv. Akad. Nauk.SSSR, Ser. Khim., (6), 1267-71 (1968).
43. Raj, D., Chandra, K., Puri, S.P. - J. phys. Soc. Japan, 24 (1), 39-41 (1968).
44. Herzenberg, C.L. - Nuovo Cim., B53 (2), 516-17 (1968).
45. Buk'ko, I.A., and Kulagov, E.A. - Dokl. Akad. Nauk,SSSR, 152, 408-410 (1963).
46. Genkin, A.D., Filimonova, A.A., Shadlun, T.N., Soboleva, S.V. and Troneva, S.V. - Geol. Rudnykh Mestorzhdenii, 8, 41-54 (1966).
47. Cabri, L.J. - Econ. Geol., 62 (7), 910-25 (1967).
48. Bartholomé, P. - Studia Univ. Lovan. Faculté des Sciences, (Leopoldville), 4, 1 (1958).
48-a Barton, P.B.Jr., and Brian J. Skinner - Geochemistry of Hydrothermal Ore Deposits, Barnes, H.L., Holt, Rinehart and Winston, Inc., New York (1967).
49. Kullerud, G. - Yb. Carnegie Instn. Wash., 66, 404-9 (1966-67).
50. Merwin, H.E., and Lombard, R.H. - Econ. Geol., 32, 203-284 (1937).
51. Kullerud, G. - Yb. Carnegie Instn. Wash., 63, 200-2 (1964).
52. Schlegel, H., and Shüller, A. - Freiberger ForschHft., B,2 (1952).
53. Donovan, B., and Reichenbaum, G. - Br. J. appl. Phys., 9, 474-7 (1958).
54. Brett, R. - Econ. Geol., 59 (7), 1241-69 (1964).
55. Pankratz, L.B., and King. E.G. - Rep.Invest.U.S. Bur. q Mines, No. 7435 (1970).
56. Ruff and Graf - Z.Anorg. Allgem. Chem., 58, 209-211 (1908).
57. Stull, D.R. - Ind.Engng.Chem., 39, 517-50 (1947).
58. West, W.A., and Menzies, A.W.C. - J. phys. Chem., 33, 1880-92 (1929).
59. West, J.R. - Ind. Engng. Chem., 42, 713-8 (1950).
60. Rassow, H.-Z.Anorg.Allgem. Chem., 114, 117-50 (1920).
61. Loebel, R. - Handbook of Chemistry and Physics, p.D-143, 48thed., Weast, Cleveland: The Chemical Rubber Co. (1967-68)
62. Baker, E.H. - Trans. Instn. Min.Metall., C80, 93 (1971).
63. Isakova, R.A., Ugryumova, L.A., and Sapukov, I.A. - Trudy Inst. Metall.Obogashch., Akad.Nauk.Kaz.SSR,31,3-13 (1968).

64. Mayer, C.G. - quoted in Kelley, K.K. - Bull. U.S. Bur. Mines, (406), 120 (1937).
65. Joly - Phil. Mag. - 25, 856 (1913).
66. Volskii, A.N., and Agratcheva, R.A., - Collection of Papers, Moscow Inst. Non-ferrous Metals and Gold, (11), 29 (1945).
67. Isakova, R.A., Usanovich, M.I., Potanina, N.A., and Ugrumova, L.E. - Izv.Akad.Nauk. Kaz. SSR Ser. Khim., 19 (5), 78-81 (1969).
68. Chizhikov, D.M. - Metallurgiya Tyazholikh Metallov. M., p.648-71 (1948).
69. Svetrov, A.N., - Trudy Inst. Geol.Akad.Nauk.SSSR, part II, 30thEd. (1958).
70. Popoukina, L.A., and Okunev, A.N. - Trudy Inst. "Uniproned", 3rdEd. (1958).
71. Margulis, E.V., and Ponomarev, V.D., Vest.Akad.Nauk.Kaz. SSR, (11) (1959).
72. Golomzik, A.I. - Izv. Vysshikh Uchebn. Zavedenii, Tsvetn. Met., 7 (2), 47-8 (1964).
73. Gerasimov, A.I., Krestouńikov, A.N., and Shakhev, A.S. - Khimi. Termod Tsuetnoi Metall. Metallurgizdat (1961).
74. Karapet'yants, M. Kh. - Chemical Thermodynamics, Goskhimizdat (1953).
75. Tkachenko, O.B., et al. - Tr.Inst.Met. Obogashch., Akad. Nauk.Kaz., SSR, 19 (1965).
76. Young, P.A. - AMDEL Bull., (3). 1-19 (1967).
77. Mayer, C.G., and Kelley, K.K. - J. Am.chem. Soc., 54 3243 (1932).
78. Kelley, K.K. - Bull. U.S. Bur. Mines, (584) (1960).
79. Songina, O.A., Ospanov, Kh.K., and Rozhdestvenskaya, Z.B.-Zav.Lab., 32 (12), 1441-4 (1966).
80. Letnikov, F.A. - Isobarniye Potentziali Obrazovaniya Mineralov, Pub. NEDRA (1965).
81. King, J.A. - Ph.D. Thesis, Univ. of London (1966).
82. Cotton, F.A. and Wilkinson, G. - Advanced Inorganic Chemistry, 2nded., Interscience Publishers, London (1966).
83. Brown, J.B., - Can. Mineralogist., 10 (4), 696 (1970).
84. Brown, J.B. - Miner. Deposita (Berl.), 6,245-252 (1971).
85. Berner, R.A. - Geochim. Cosmochim. Acta 33, 267-273 (1969).
86. Latimer, W.M. - Oxidation Potentials, 2nded., Prentice Hall, New York (1952).

87. Kelley, K.K. - Bull. U.S. Bur. Mines. (406) (1937).
88. Kubaschewski, O., and Evans, E.LL. - Metallurgical Thermochemistry, 3rd ed., Permagon Press, Oxford (1958).
89. Ugarte-Alvarez, F.J.G. - Ph.D. Thesis, Univ. of London (1971).
90. Dana-Hurlbut - Dana's Manual of Mineralogy, 15th ed., John Wiley & Sons. Inc., New York.
91. Austin, I.G., Goodman, C.H.L., and Pengelly, A.E. - J. electrochem. Soc., 103, 609-10 (1956).
92. Richardson, F.D., and Jeffes, J.H.E. - J.Iron Steel Inst., 171, 167 (1952).
93. Ramdohr, P. - The Ore Minerals and their Intergrowths, Pergamon Press, London (1969).
94. Berry, L.G., and Thompson, R.M. - X-ray Powder Data for Ore Minerals - The Peacock Atlas, Geol. Soc. America Mem. (85) (1962) (Also A.S.T.M. file No.9 -423 - Ref.135).
95. Personal communication via Dr. A.R. Burkin.
96. Perkin-Elmer- Analytical Methods for Atomic Absorption Spectrophometry, Perkin-Elmer Corp., Norwalk, Connecticut, U.S.A. (1966-68-71).
97. Pantony, D.A. - A Laboratory Manual of Elementary Metallurgical Analysis, Part 2, Imperial College, London (1956).
98. Vogel, A.I. - Quantitative Inorganic Analysis, 3rd ed., Longmans, London (1961).
99. Handbook of Chemistry and Physics, 48th ed., Weast, Cleveland The Chemical Rubber Co. (1967-68).
100. Seidell, A. - Solubilities of Inorganic and Metal Organic Compounds, vol. 1., p. 1446, 3rd ed., D. Van Nostrand, N.Y. (1940).
101. Bradley, A.J., and Hope. A.H., Proc. R. Soc. (A), 136, 272 (1932).
102. Glocker, R., and Schafer - Naturwissenschaften, 21, 559 (1933); Z.Physik., 73, 289 (1932).
103. Rusterholz, A. - Z. Physik, 82, 538 (1933).
104. Disc Chart Integrator - Instruction Manual, Disc Instruments, Inc., Herts. England.
105. Rachinger, W.A. - J. scient. Instrum. 25, 254 (1948).

106. Burkin, A.R. - The Chemistry of Hydrometallurgical Processes, E.&F.N. Spon Ltd., London (1966).

107. Habashi, F. - The Principles of Extractive Metallurgy, vol. 2. (Hydrometallurgy), pag. 101, Gordon and Breach, London (1970).

108. Lipson, H., and Steeple, H. - Interpretation of X-ray Powder Diffraction Patterns, Macmillan, London (1970).

109. Ugarte-Alvarez - Unpublished work (1971).

110. Kametani, H. - Proceedings of the International Solvent Extraction Conference (ISEC 71), 1, 227 (1971) (Society of Chemical Industry, London).

111. Sullivan, J.D. - Trans. metall. Soc. AIME, 106, 531-33 (1933)

112. Dutrizac, J.E., MacDonald, R.J.C., and Ingraham, T.R. - Met. Trans. 1, (11), 3083-88 (1970).

113. Majima, H. - Can. Met. Q., 8 (3), 269 (1969).

114. Criss, C.M., and Cobble, J.W.-J.Am. chem.Soc., 86, 5385 - 5390 (1964).

115. Eggers, D.F., Gregory, N.W., Halsey, G.D., and Rabinovitch, B.S., - Physical Chemistry, p. 758, John Wiley and Sons, Inc., London (1964).

116. Cobble, J.W. - J. Am. chem. Soc., 86 5394-5401 (1964).

117. Lewis, G.N., and Randall, M. - Thermodynamics, pp643-658, 2nd.Ed., McGraw-Hill Book Co. New York (1961).

118. Robins, R.G., - Warren Spring Laboratory, LR 80 (MST) (1968).

119. Ashworth, V., and Boden, P.J. - Corros. Science, 10, 709-718 (1970).

120. D'yachkova, I.B., and Khodakovskiy, I.L. - Geokhimiya, (11), 1358-75 (1968) (Geochem.Inter., 5 (6), 1108-1125 (1968)).

121. Pryor, A. - J. Amer. chem. Soc., 82 (18) (1960).

122. Valensi, G. - Proceedings 2nd Meeting CITCE, Milano 1949, p. 51. Manfredi, Milano (1950).

123. Pourbaix, M. - Atlas of Electrochemical Equilibria in Aqueous Solution, Pergamon Press, Oxford, (1966).

124. Garrels, R.M., and Naeser, C.R. - Geochim. Cosmochim. Acta, 15, 113 (1958).

125. Barnes, H.L. - Yb. Carnegie Inst. Wash., 57, 234 (1957-58).

126. Barnes, H.L., and Kullerud, G. - Econ. Geol. 56 (4), 648 (1961).

127. Khodakovskiy, I.L., Ryzhenko, B.N., and Naumov, G.B. - Geokhimiya, (12), 1486-1503 (1968).

128. Wagman, D.D. et al. - Selected Values of Chemical Thermodynamic Properties, U.S. Department of Commerce. National Bureau of Standards, 270-3/4 (1969).

129. Biernat, R.J., and Robins, R.G. - Electrochim. Acta, 14 809-20 (1969).

130. Michard, G., and Allegre, C.J. - Miner. Deposita (Berl.) 4, 1-17 (1969).

131. Criss, C.M., and Cobble, J.W. - J.Am. chem. Soc., 86, 5390-5393 (1964).

132. Perry, J.H. - Chemical Engineer's Handbook, 4thEd., International Student Edition/McGraw-Hill.

133. Ellis, A.J., and Giggenbach, W. - Geochim. Cosmochim. Acta, 35, 247-260 (1971).

134. Connick, R.E., and Powell, R.E. - J. chem. Phys., 21, 2206 (1953).

135. A.S.T.M. X-ray Index Files
   a) α-chalcopyrite - File No. 9-423 (see also Ref. 94)
   b) Bornite - File No. 14-323 (see also Ref. 137).
   c) Pyrite (FeS_2) - File No. 6-0710.
   d) Pyrrhotite ($Fe_{1-x}S$;x=0.12) - File No. 17-200.
   e) Pyrrhotite ($Fe_{1-x}S$;x=0.094) - File No. 17-201.
   f) Sulphur (orthorhombic) - File No. 8-247.
   g) Goethite (Fe O.OH) - File No. 17-536.
   h) Halite (NaCl) - File No. 5-628.

136. Jakob, M., and Hawkins, G.A. - Elements of Heat Transfer 3rded., J. Chapman & Hall Ltd., London (1957).

137. Berry and Thompson, - Geol. Soc. Am. Mem., 85, 44 (1962).